Tripodal Inorganic 2-Pyridyl-phosphine Ligands and Unsymmetrical Analogues: Towards New Applications in Catalysis

---

M. Sc. Schirin Hanf

Gonville and Caius College

University of Cambridge

May 2019

This dissertation is submitted for the degree of

Doctor of Philosophy.

Für meine Eltern

Declaration

This thesis entitled “Tripodal Inorganic 2-Pyridyl-phosphine Ligands and Unsymmetrical Analogues: Towards New Applications in Catalysis” is submitted to the Degree Committee of Physics and Chemistry at the University of Cambridge. The work in this dissertation was carried out in the Department of Chemistry of the University of Cambridge under the supervision of Prof. Dominic S. Wright between April 2015 and April 2019. During this period, catalytic studies were undertaken at Leipzig University, Germany, in the group of Prof. Evamarie Hey-Hawkins.

This dissertation is the result of my own work and includes nothing, which is the outcome of work done in collaboration except where it is declared otherwise. Except where due reference is given, this thesis contains no material published or written by another person or presented for any other degree or diploma at a university. The dissertation does not exceed the prescribed word limit of 60,000 words.

Schirin Hanf

Cambridge, May 2019

Abstract

Although a range of phosphorus-based ligands are used extensively in homogeneous catalysis, 2-pyridyl-phosphines have been largely overlooked in this field. However, such ligands offer great potential for catalytic applications through the combination of two ligand sites with different donating and accepting properties.

In Chapter 1 previous studies of the structural and coordination chemistry of 2-pyridyl main group ligands are discussed, together with the applications of phosphine and tris-2-pyridyl ligands in catalysis which are relevant to the studies undertaken in the thesis. This chapter finishes with a statement of the aims of the thesis.

Chapter 2 focuses on sterically-constrained C_3-symmetric tris-2-pyridyl ligands and the effects of the substitution of the pyridyl rings at the 6-position on coordination to transition metal ions. The impact of such ligand modification is illustrated directly from the coordination studies of $P(6\text{-R-2-py})_3$ (R = H, Me) to iron(II). Whereas $P(2\text{-py})_3$ readily forms the cationic sandwich complex $[\{P(2\text{-py})_3\}_2Fe]^{2+}$, $P(6\text{-Me-2-py})_3$ forms only half-sandwich complexes of the type $[\{P(6\text{-Me-2-py})_3\}FeX_2]$ (X = Cl, OTf).

In addition to C_3-symmetric ligands, a range of unsymmetrical multidentate 2-pyridyl-phosphine ligands with tuneable electronic and steric character have been synthesised and are reported in Chapter 3. The stoichiometric reactions of $(R_2N)_xP(2\text{-py})_{3-x}$ (R = Me, Et, x = 1, 2) with alcohols result in the formation of (alkoxy)-2-pyridyl-phosphines $(RO)_xP(2\text{-py})_{3-x}$ (R = Me, 2-Bu, Ph, x = 1, 2). This synthetic procedure also allows the introduction of enantiomerically pure alcohols, and as such provides a very convenient two-step route to chiral 2-pyridyl-phosphine ligands. Coordination studies towards Cu^{I}, Ni^{II} and Rh^{I} have shown that both the pyridyl-N and bridgehead-P atoms can be involved in coordination to the metal centres. In the case of nickel, an interesting *in-situ* reduction of the metal centre was observed.

Different synthetic and computational approaches to quantify the donor properties of various 2-pyridyl-phosphines are presented in Chapter 4. The calculated Tolman electronic parameters give an overview of the donor properties of all investigated 2-pyridyl-phosphines with respect to PPh_3 and $P(^tBu)_3$.

In Chapter 5, the modification of the phosphorus bridgehead is reported. Air- and moisture-stable phosphorus(V) chalcogenides and fluorinated phosphines were synthesised. Also, a novel one-step procedure for the synthesis of fluorophosphonium salts was developed. Treatment of $(Et_2N)_2P(2\text{-py})$ with the bench-stable fluorinating reagent NFSI (*N*-fluorobenzenesulfonimide) leads to the selective formation $[FP(NEt_2)_2(2\text{-py})][N(SO_2Ph)_2]$.

Investigations of the applications of tris-2-pyridyl-phosphine complexes for hydrofunctionalisation reactions are explored in Chapter 6. Central to the study are the iron(II) complexes [{P(6-Me-2-py)$_3$}FeCl$_2$] and [{P(6-Me-2-py)$_3$}FeCl(OTf)]. *In-situ* reduction of the iron complex [{P(6-Me-2-py)$_3$}FeCl(OTf)] potentially results in the formation of Fe^0 species, which are active in hydrogenation reactions of minimally functionalised alkenes.

Acknowledgements

First of all, I would like to thank Prof. D. S. Wright for his supervision throughout my PhD studies. I really appreciated his support, creativity and openness. Thanks for many entertaining coffee breaks, Dom!

Secondly, I wish to thank Prof. E. Hey-Hawkins (Leipzig University) for the pleasant collaboration. I am very grateful for her support during my whole studies and for giving me the opportunity to get to know different fields in inorganic chemistry.

I would also like to express my gratitude to Dr. R. García-Rodríguez for his excellent support. His assistance and patience helped me a lot! Also, I would like to thank Dr. A. D. Bond for his help with X-ray crystallographic data.

I would also like to thank the members of the Wright group (and the rest of lab 301), who have made the duration of my PhD very enjoyable. The nice environment made lab work much easier. Especially, I would like to thank Peter Matthews, Evan Keyzer, Andy Peel, Lily Dixon, Robert Less and Thea Precht for their encouragement and their friendship.

I am very grateful to the whole Hey-Hawkins group in Leipzig, especially lab 312. Not only on an academic level but also personally the following persons supported me a lot: Peter Coburger, Benedikt Schwarze, Axel Straube, John Popp, Stefanie Märcker, Toni Grell, Reinhard Hoy and Sara Durini.

Many thanks to the following students for their help in the lab: Sascha Feldmann, Sara Lorimer, Philipp Stehr, Caroline Dorsch and Till Friedmann. For proof-reading I thank Dr. R. García-Rodríguez, Dr. A. Colebatch and Dr. L. Dixon.

Lastly, I would like to thank my family, especially my parents. Vielen Dank für eure stetige Motivation und Unterstützung. Ohne euch wäre das alles nicht möglich gewesen. Danke dafür! Vielen Dank auch an Felix. Obwohl mich deine Gelassenheit manchmal aufregt, hat sie mich in den letzten Jahren oft auf den Boden zurückgebracht. Ich bin dir unendlich dankbar dafür und freue mich auf die nächsten Jahre mit dir und unserem kleinen Mann Friedrich.

Financial support by the European Union, the Fonds der Chemischen Industrie and the Studienstiftung des deutschen Volkes was gratefully appreciated.

List of Publications

The following publications were published during the period from April 2015 to May 2019, and are directly related to this thesis:

1) *Sterically-constrained tripodal phosphorus-bridged tris-pyridyl ligands.*
   S. Hanf, R. García-Rodríguez, A. D. Bond, E. Hey-Hawkins, D. S. Wright, *Dalton Trans.* **2016**, *45*, 276–283.

2) *A non-chiral lithium aluminate reagent for the determination of enantiomeric excess of chiral alcohols.*
   R. García-Rodríguez, S. Hanf, A. D. Bond, D. S. Wright, *Chem. Commun.* **2017**, *53*, 1225–1228.

3) *Multidentate 2-pyridyl-phosphine ligands – towards ligand tuning and chirality.*
   S. Hanf, R. García-Rodríguez, S. Feldmann, A. D. Bond, E. Hey-Hawkins, D. S. Wright, *Dalton Trans.* **2017**, *46*, 814–824.

The following publications were published during the period from April 2015 to May 2019, and are not directly related to this thesis:

4) *Synthesis and Structures of Rare Earth 3-(4'-Methylbenzoyl)-propanoate Complexes – New Corrosion Inhibitors.*
   C. N. de Bruin-Dickason, G. B. Deacon, C. M. Forsyth, S. Hanf, O. B. Heilmann, B. R. W. Hinton, P. C. Junk, A. E. Somers, Y. Q. Tan, D. R. Turner, *Austr. J. Chem.* **2016**, *70*, 478–484.

5) *The influence of halides in polyoxotitanate cages; dipole moment, splitting and expansion of d-orbitals and electron-electron repulsion.*
   S. Hanf, P. D. Matthews, N. Li, H. K. Luo, D. S. Wright, *Dalton Trans.* **2017**, *46*, 578–585.

6) *Regioselective 1,4-hydroboration of pyridines catalyzed by an acid-initiated boronium cation.*
   E. N. Keyzer, S. S. Kang, S. Hanf, D. S. Wright, *Chem. Commun.* **2017**, *53*, 9434–9437.

7) *A $[HN(BH{=}NH)_2]^{2-}$ Dianion, Isoelectronic with a β-Diketiminate.*
   R. J. Less, S. Hanf, R. García-Rodríguez, A. D. Bond, D. S. Wright, *Organometallics* **2017**, *37*, 628–631.

8) *Synthesis of 1,2-Diphospholides Using a Main Group "Superbase".*
   L. S. H. Dixon, S. Hanf, J. E. Waters, A. D. Bond, D. S. Wright, *Organometallics* **2018**, *32*, 4465–4472.

Overview of Numbered Compounds

In the following section, the compounds described in this thesis are presented. Derivatives of listed compounds, for example, the tris-2-pyridyl-oxide **O=1**, are excluded.

Chapter 2

1 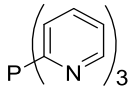	**2** 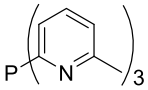
3 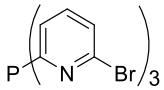	**4** 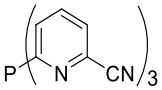
5 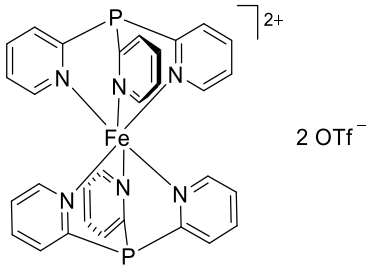	**6** 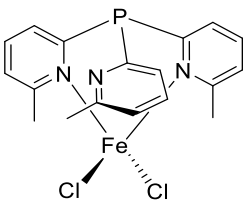
7 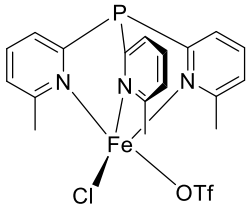	**8** 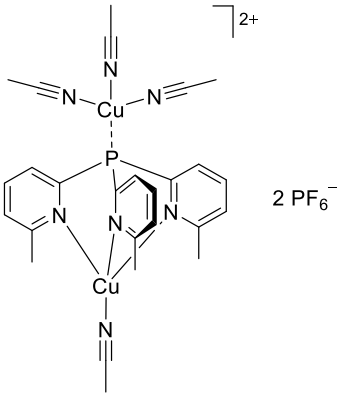
9 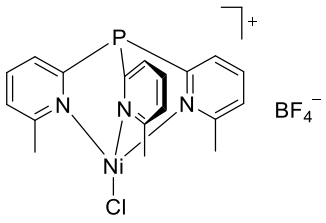	

Chapter 3

10 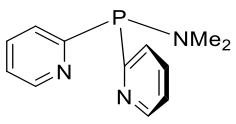	**11** 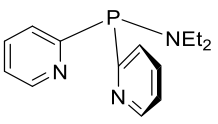
12 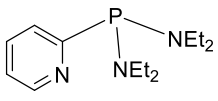	**13** 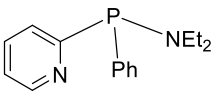

14 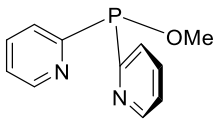	**15** 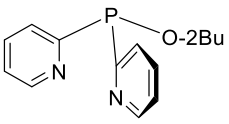
16 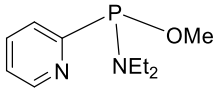	**17** 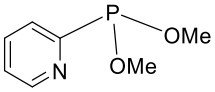
18 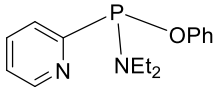	**19** 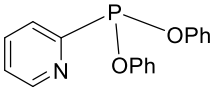
20 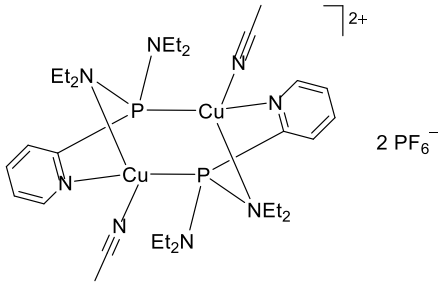	**21** 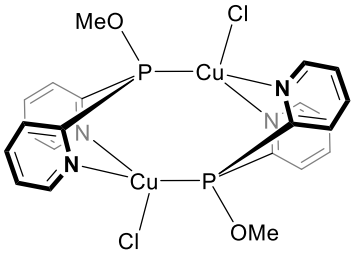
22 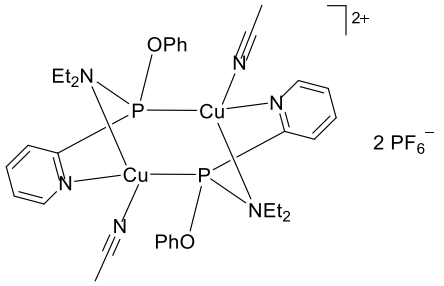	**23** 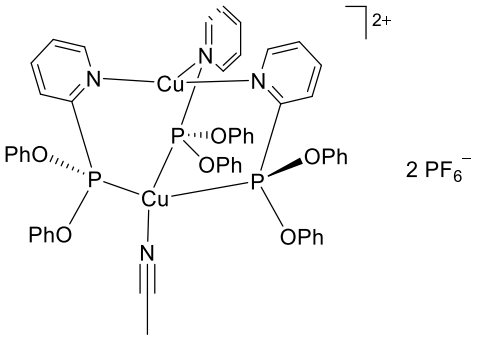
24 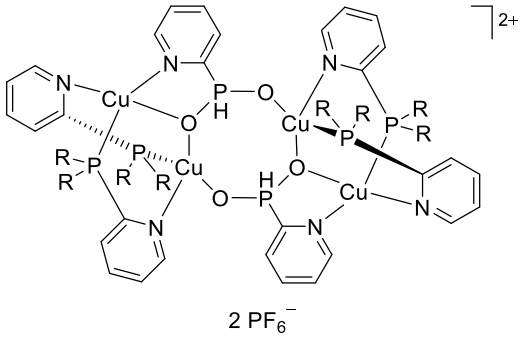	**25** 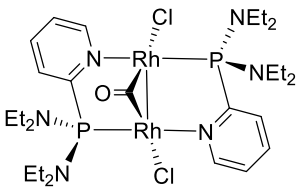
26 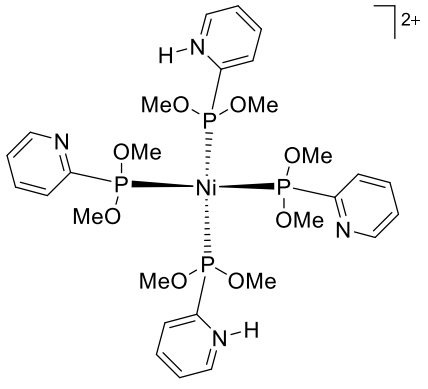	**27** 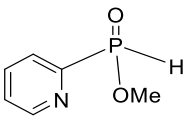

Chapter 4

28

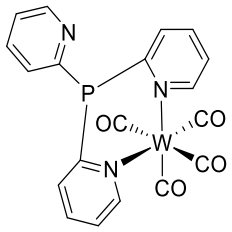

29

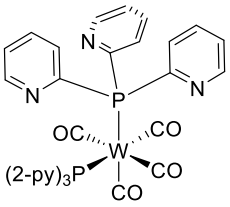

30

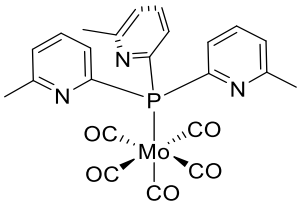

31

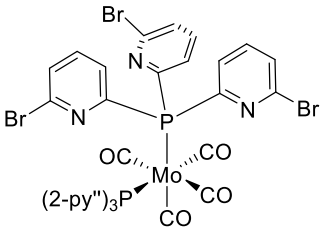

P(2-py'')$_3$ = P(6-Br-2-py)$_3$

Chapter 5

32

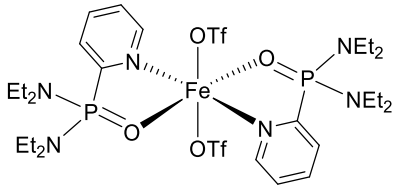

33

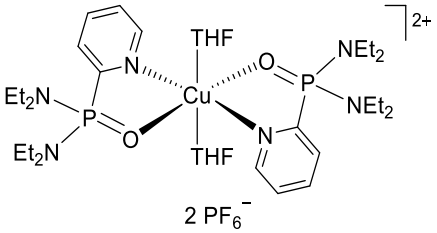

34

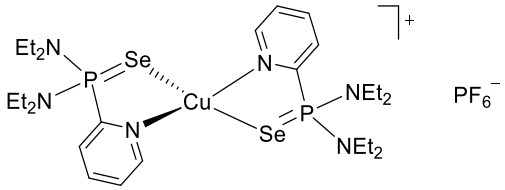

Chapter 6

35

36

37

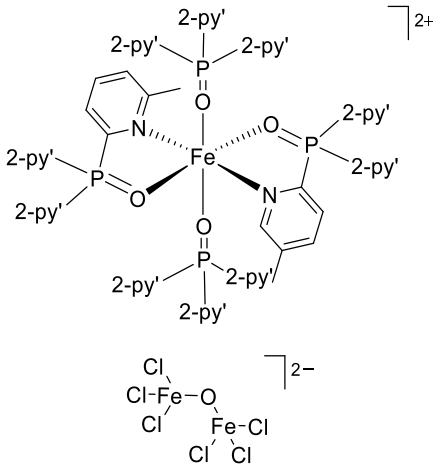

38

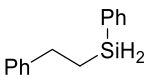

39 	**40** 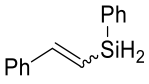
41 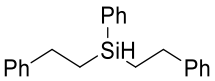	**42** 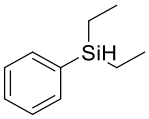

Colour Code for Solid State Structures

- Lithium
- Carbon
- Nitrogen
- Oxygen
- Fluorine
- Phosphorus
- Sulphur
- Chlorine
- Iron
- Nickel
- Copper
- Selenium
- Bromine
- Molybdenum
- Rhodium
- Tungsten

Abbreviations

Ar	Aryl
ATR	Attenuated total reflection
BINAP	2,2'-Bis(diphenylphosphino)-1,1'-binaphthyl
bipy	Bipyridine
b. p.	Boiling point
br	Broad
Bu	Butyl
ca.	*circa*
calcd.	Calculated
cat.	Catalyst
cf.	*confer*
CHELPG	Charges from electrostatic potentials using a grid-based method
COD	1,5-Cyclooctadiene
COSY	Correlation spectroscopy
Cp	Cyclopentadienyl
Cp*	1,2,3,4,5-Pentamethylcyclopentadienyl
Cy	Cyclohexyl
d	Doublet
Da	Dalton, unified atomic mass unit
DCM	Dichloromethane
dd	Doublet of doublets
DFT	Density functional theory
DIPAMP	Bis[(2-methoxyphenyl)phenylphosphino]ethane
DMAD	Dimethyl acetylenedicarboxylate
dppp	Propane-1,3-diylbis(diphenylphosphane)
DuPHOS	Diphosphine ligands, consisting of two phospholanes
E	Element
ECP	Electrophilic phosphonium cations
EDX	Energy dispersive X-ray spectroscopy
e.g.	*exempli gratia*
EI	Electron ionisation

ESI	Electrospray ionisation
Et	Ethyl
GC-MS	Gas chromatography-mass spectrometry
GGA	Generalised gradient approximation
HMBC	Heteronuclear multiple bond correlation
HMQC	Heteronuclear multiple-quantum correlation spectroscopy
HOMO	Highest occupied molecular orbital
HPLC	High-performance liquid chromatography
HR-MS	High-resolution mass spectrometry
HSQC	Heteronuclear single quantum coherence
IAO	Intrinsic atomic orbitals
i.e.	*id est*
IR	Infrared
J	Coupling constant
LUMO	Lowest unoccupied molecular orbital
m	Multiplet (NMR), medium (IR)
M	Metal, molecule (HR-MS)
Me	Methyl
MeCN	Acetonitrile
m. p.	Melting point
MS	Mass spectrometry
^{n}BuLi	*n*-Butyllithium
NAO	Natural atomic orbitals
NBD	2,5-Norbornadiene
NBO	Natural bond orbital
NFSI	*N*-fluorobenzenesulfonimide
NMR	Nuclear magnetic resonance
NOESY	Nuclear Overhauser effect spectroscopy
NP	Nanoparticles
OAc	Acetate
OMe	Methoxy
OPh	Phenoxy

OTf	Triflate
pE	Protonation enthalpy
Ph	Phenyl
pic	Picolyl
ppm	Parts per million
Pr	Propyl
py	Pyridyl
pypz	(6-Pyrazol-1-yl)pyridine
pz	Pyrazolyl
QALE	Quantitative analysis of ligand effects
QUINAP	1-(2-Diphenylphosphino-1-naphthyl)isoquinoline
RI	Resolution of identity
rt	Room temperature
s	Singlet (NMR), strong (IR)
SCF	Self-consistent field
SEM	Scanning electron microscopy
t	Triplet
td	Triplet of doublets
TEP	Tolman electronic parameter
THF	Tetrahydrofuran
tol	Toluene
UV-Vis	Ultraviole-visible
TS	Transition state
vs.	*versus*
VSEPR	Valence shell electron pair repulsion
w	Weak
δ	Chemical shift
λ	Wavelength
$\tilde{\nu}$	Wavenumber
ν	Frequency

Contents

1 Introduction

1.1 Tripodal Ligands

Tripodal ligands are facially-coordinating, polydentate (most often tri- or tetradentate) ligands with C_3-symmetry, which have shown remarkable potential in coordination, organometallic and bioinorganic chemistry in the past.[1] While tridentate C_3-symmetric ligand frameworks exhibit a central non-donor atom attached to three side groups, each of which contains at least one donor atom, tetradentate C_3-symmetric tripodal ligands comprise an additional donor atom at the bridgehead position. The success of these polydentate ligands can be attributed to the potential of these systems to act as chelate ligands and stabilise metal ions in a variety of oxidation states and geometries. A large number of these ligands contain mixed donor sets, such as N, S, O and P donor atoms, which provide the grounds for the synthesis of heterobimetallic complexes.[2,3]

Landmark studies carried by out S. Trofimenko on tris-pyrazolyl-borates (Figure 1.1a) have explored the breadth of applications of these types of frameworks, from ancillary ligands in catalysis to biomimetic model systems.[4–8] Closely related ligand systems based around pyridine moieties, such as the tris-2-pyridyl-methoxymethane ligand (Figure 1.1b), and aliphatic amines (Figure 1.1c) with acyclic and cyclic topologies have also been explored.[9–11]

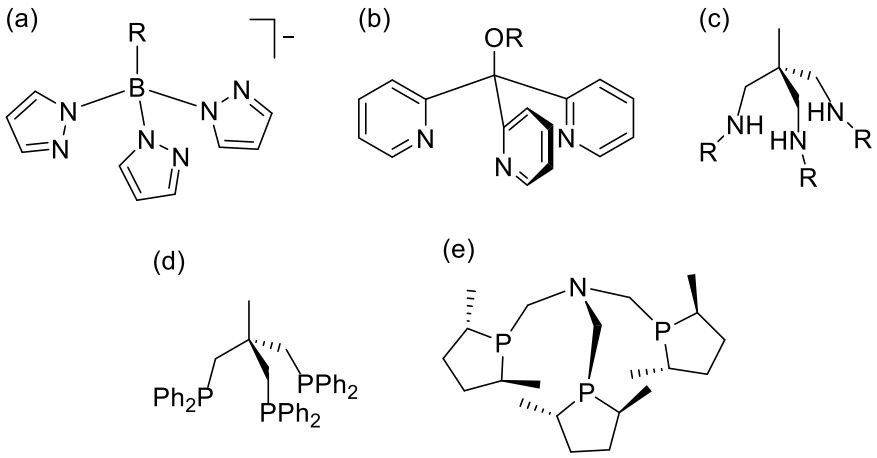

Figure 1.1: *Selected examples of tripodal ligands; (a) tris-pyrazolyl-borate, (b) tris-pyridyl-methoxymethane, (c) aliphatic amine, (d) triphos and (e) N-bridged phospholane ligand.*

Furthermore, various C_3-symmetric tripodal phosphines have been studied extensively and investigations into their catalytic activity have shown that triphos ligands (Figure 1.1d) are a particularly successful ligand family for a range of bridgehead atoms (for example carbon, phosphorus or nitrogen).[12,13] More recently, metal complexes of enantiomerically pure tripodal phosphines (Figure 1.1e) developed by M. J. Burk and co-workers have shown high activity in

asymmetric catalytic hydrogenation reactions, offering access to a diverse range of chiral compounds.[14–17]

1.1.1 Tris-2-pyridyl Ligands

Neutral tris-2-pyridyl ligands containing non-metallic bridgeheads E(2-py)$_3$ (2-py = 2-pyridyl, E = CX (X = H, OR, NH$_2$), N, P, P=O, As, Figure 1.2) have been known for at least three decades and are very closely related to the well-known family of tris-pyrazolyl-borates [RB(1-pz)$_3$]$^-$ (1-pz = pyrazolyl, R = H, alkyl, aryl, NR$_2$, SAr).[9]

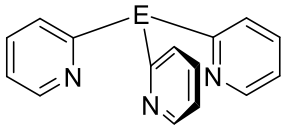

Figure 1.2: *The family of neutral tripodal tris-pyridyl ligands E(2-py)$_3$ (E = CX (X = H, OR, NH$_2$), N, P, P=O, As), containing non-metallic main group bridgehead atoms.*

The main difference between tripodal tris-pyridyl and tris-pyrazolyl-borate ligands is the charge of the systems. While most of the tris-pyridyl compounds are neutral (with some metallic and semi-metallic pyridyl ligands forming a unique exception), tris-pyrazolyl-borates are monoanionic. A second key distinction between tris-pyridyl and tris-pyrazolyl-borate ligands is that the p*K*a values of the conjugate acids (BH$^+$) of pyrazole (2.48) and pyridine (5.25) are very different, suggesting that pyridine is a better σ-donor than pyrazole.[9] Furthermore, pyridine-containing ligands have been reported to be better π-acidic ligands than pyrazole-based systems.[18] Hence, the properties of the corresponding transition metal complexes incorporating tris-pyridyl or tris-pyrazolyl-borate ligands can differ significantly in terms of their stability, charge, and redox behaviour as well as their solubility.

The nitrogen-bridged tris-2-pyridyl compound, N(2-py)$_3$, was first prepared by J. P. Wibaut and G. L. C. la Bastide in 1933 by the stepwise reaction of a 2-halopyridine with 2-aminopyridine (Scheme 1.1).[19] Modified synthetic approaches involving copper catalysis also enabled the synthesis of unsymmetrical versions of tris-2-pyridyl-amine.[20]

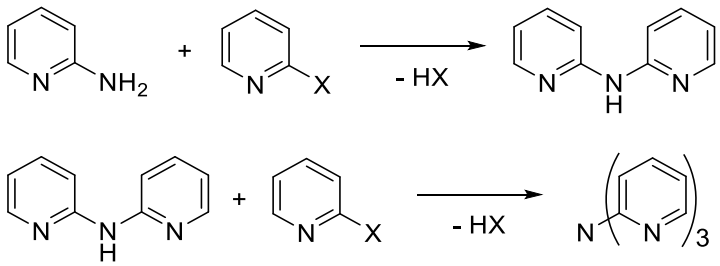

Scheme 1.1: *Synthesis of tris-2-pyridyl-amine via a two-step procedure.*

The first representative of a phosphorus-bridged tris-2-pyridyl ligand, namely, tris-2-pyridyl-phosphine P(2-py)$_3$, was synthesised by W. C. Davies and F. G. Mann in 1944 from the reaction of phosphorus trichloride with the Grignard reagent 2-pyridyl magnesium bromide in benzene.[21] Later, modified synthetic procedures involving a two-step synthesis were devised. The reaction of a 2-bromo- or 2-iodopyridine derivative with *n*-butyllithium forms the 2-lithiated pyridine species. Following this, the addition of phosphorus trichloride results in the formation of the tris-2-pyridyl-phosphine ligand (Scheme 1.2).[22–26] Newer approaches are based on one-pot reactions of 2-bromo-pyridine and elemental phosphorus at elevated temperatures.[27,28]

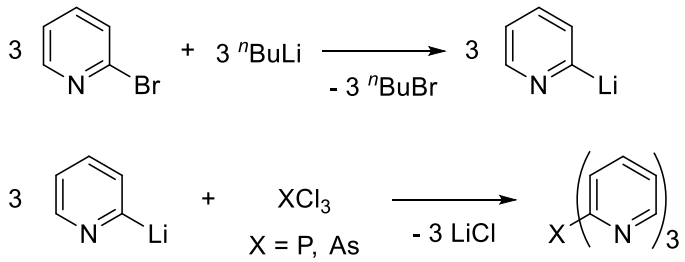

Scheme 1.2: *Synthesis of tris-2-pyridyl-phosphine and tris-2-pyridyl-arsine.*

Tris-2-pyridyl-arsine can be obtained in a manner similar to that described for the P counterpart, by the lithiation of 2-bromopyridine followed by reaction with arsenic trichloride.[23,29] There are fewer examples of heavier group 15 elements being employed as bridgeheads. This is probably the result of their perceived instability towards reductive elimination to generate elemental Sb or Bi, where unsubstituted 2-py ligands are present. However, the use of 2-lithio-6-methyl-pyridine gives access to antimony- and bismuth-bridged tripodal ligands of the form E(6-Me-2-py)$_3$ (E = Sb, Bi) in good yields. The increased stability of the latter can be ascribed to the electron-donating effect of the methyl group within the pyridyl substituent, which suppresses reductive elimination.[30]

The influence of the bridgehead atom on the reactivity of the pyridine groups in tripodal pyridyl ligands was initially investigated by F. G. Mann and J. Watson in 1948. It was found that while only two of the pyridyl-N atoms in tris-2-pyridyl-amine could be protonated with hydrochloric acid, all three pyridyl-N atoms were protonated in the phosphorus and arsenic counterparts.[31] This can be explained by the greater inductive effect of the nitrogen bridgehead atom relative to the P and As bridgeheads. This reduces the basicity of the remaining N atoms after the initial protonation.[32,33]

The synthesis of the carbon-bridged tris-2-pyridyl ligands, which was developed by J. P. Wibaut *et al.*, is based on the reaction of 2-lithiopyridine and dipyridyl ketone (Scheme 1.3).[34] Using tris-2-pyridyl-methanol as a starting material, J. W. Faller and D. L. White synthesised a variety of carbon-bridged tris-pyridyl ligands, such as tris-2-pyridyl-methane, tris-2-pyridyl-chloromethane and tris-2-pyridyl-ethoxymethane. The variability of a fourth substituent on the carbon atom lays the foundation for the synthesis of ligand frameworks with diverse physicochemical properties.[35] By

introducing chiral substituents in the 6-position, H. Adolfsson *et al.* were able to obtain chiral versions of tris-2-pyridyl-methanol.[36]

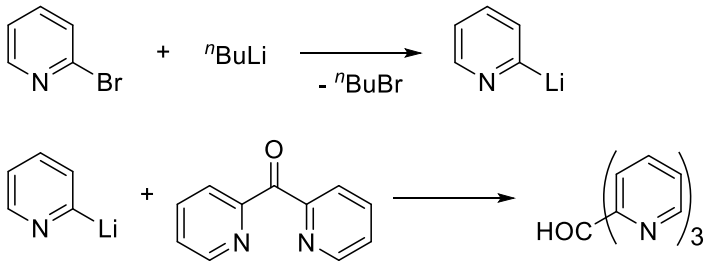

Scheme 1.3: *Synthesis of tris-2-pyridyl-methanol.*

More recently, ligands containing group 13 and 14 metallic or semi-metallic bridgeheads have been explored. The isoelectronic group 13 tris-2-pyridyl-aluminates $[RAl(2\text{-py})_3]^-$ (R = Me, Et, ^{n}Bu, 2-Bu, Figure 1.3) can be prepared from the reaction of $RAlCl_2$ with the *in-situ* generated 2-lithiopyridine.[37–42] These ligands are of special interest, as their donor properties can be easily manipulated through the introduction of substituents into the 6-position of the pyridyl ring[38,42] or by selective replacement of a pyridine arm by an alkoxide group.[38] The latter strategy can be used to introduce 3- and 4-alkoxymethylpyridyl groups, which facilitates applications of such systems in supramolecular chemistry.[43]

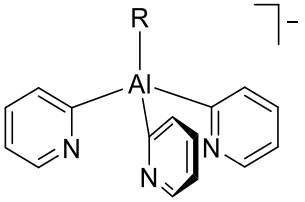

Figure 1.3: *The anionic tris-2-pyridyl-aluminate ligand $[RAl(2\text{-py})_3]^-$ (R = Me, Et, ^{n}Bu, 2-Bu).*

The metallic or semi-metallic group 14 analogues (Figure 1.4) can be divided into neutral element-IV ligands of the type $RE(2\text{-py})_3$ (E = Si, Sn, R = Me, ^{n}Bu)[44–46] and element-II anions of the type $[E(2\text{-py})_3]^-$ (E = Sn, Pb).[47–52] The different possible oxidation states of the bridgehead allow redox reactions to occur, often with concurrent pyridyl transfer.[53,54]

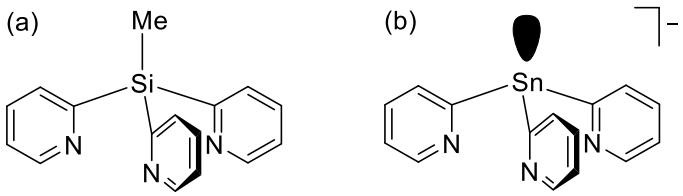

Figure 1.4: *(a) The neutral silicon(IV) tris-2-pyridyl ligand $[MeSi(2\text{-py})_3]$ and (b) the anionic tin(II) tris-2-pyridyl analogue $[Sn(2\text{-py})_3]^-$.*

Neutral element-IV ligands of the type RE(2-py)$_3$ with silicon and tin as bridgehead can be synthesised from chloro-precursors, such as MeSiCl$_3$ ^{n}BuSnCl$_3$, with the *in-situ* generated 2-lithio-pyridine.[45,46,55] The yield of the silicon-bridged tris-2-pyridyl ligand can dramatically be improved by the introduction of methyl substituents in the 6-position of the pyridyl ring.[56] The group 14 tris-2-pyridyl compounds [E(2-py)$_3$]$^-$ (E = Sn[44,45,48,50,52,57,58] and Pb[47,51]), where the metal is present in the +II oxidation state, can be obtained from the reactions of 2-lithiopyridine and suitable Sn and Pb precursors (*e.g.* SnCp$_2$, ^{n}BuSnCl$_3$, SnCl$_4$, PbCp$_2$). These compounds can bind to metal centres *via* both their pyridyl-nitrogen donor atoms and the lone pair of the bridgehead atom. This dual functionality makes them very versatile ligands for a variety of main group and transition metals.

1.1.2 Tris-2-pyridyl-phosphines

In 1988 R. Keene reported the crystal structure of P(2-py)$_3$, which revealed that two of the nitrogen donor atoms were oriented downwards away from the P bridgehead atom, with only one of the N atoms pointing in the direction of the P atom (Figure 1.5).[59]

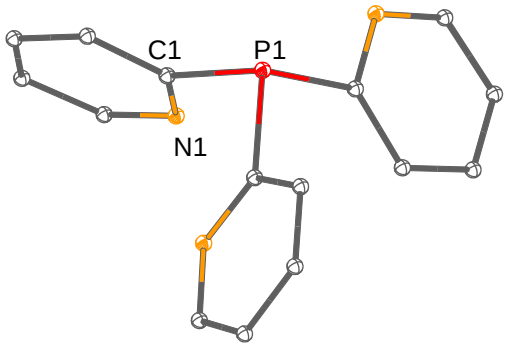

Figure 1.5: *Structure of the tripodal tris-2-pyridyl phosphine ligand.*[59] *Hydrogen atoms are omitted for clarity. Displacement ellipsoids are drawn at the 30 % probability level.*

In contrast to the nitrogen- and carbon-bridged pyridyl derivatives, 2-pyridyl-phosphines offer two different types of donor atoms. The combination of soft P and hard N atoms within one ligand framework gives these species diverse coordination behaviour. Their coordination chemistry towards a variety of metals, such as the main group metal Al,[60] transition metals, such as Cr,[61] Mn,[62–64] Co,[28,65] Ni,[66] Cu,[64,67–69] Zn,[69,70] Mo,[61,71,72] Tc,[73] Ru,[74–76] Rh,[72,77] Pd,[27] W,[61,71] Re[73] and Au,[78] as well as the lanthanoid Eu[79] has previously been examined.

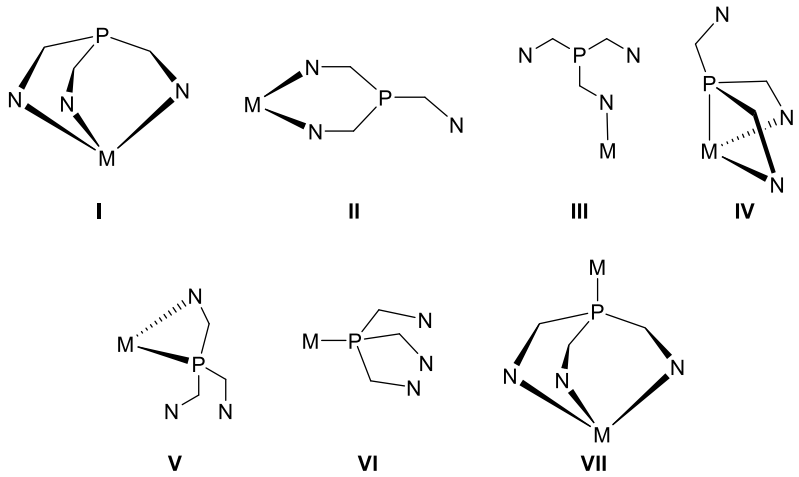

Figure 1.6: *Possible coordination modes of tripodal phosphorus-bridged tris-2-pyridyl ligands (M = metal).*

Due to the tripodal structure of the ligand and the presence of P and N donor atoms, various coordination modes can be adopted (Figure 1.6), with the *N*,*N*',*N*''-coordination mode (I) being most commonly found in the solid state structures of the P-bridged ligand systems.[28,61,74–76,79,80,62–65,68–71] Other exclusively *N*-coordination modes are the bidentate *N*,*N*'- (coordination mode II)[71,73] and the monodentate *N*-coordination mode (coordination mode III), which is found in a trimethylaluminium complex.[60] Coordination modes involving the soft P atom, such as *P*,*N*,*N*'[67] (coordination mode IV), *P*,*N*[72] (coordination mode V) or monodentate *P*-coordination[27,72,77,78] (coordination mode VI) have also been observed in a range of metal complexes. The *P*,*N*,*N*',*N*'' coordination mode (coordination mode VII), in which the 2-pyridyl-phosphine acts a tetradentate ligand, was observed as part of this thesis and will be discussed in depth in Chapter 2.[81] The afore-mentioned coordination modes (IV, V, VI, VII) are also known for some homobimetallic complexes, typically involving copper.[67,72,81,82] However, there are no reports in the literature of heterobimetallic tris-2-pyridyl-phosphine complexes.

Although the reactivity[83–85] and coordination chemistry[86] of C_3-symmetric P-bridged tripodal ligands have been extensively studied in the past, unsymmetrical congeners, as well as chiral derivatives, have been largely overlooked.[87] Of the few unsymmetrical ligands of this type to be explored to date, most have been based on the bidentate diphenyl-2-pyridyl-phosphine as an analogue of triphenylphosphine.[86,88,89]

1.2 Homogeneous Transition Metal Catalysis

The ability to mediate chemical reactions catalytically has dramatically influenced many branches of chemistry, from medicinal chemistry to petrochemistry.[90–92] Depending on the phases in which the reactants and catalysts are present, catalytic reactions can be classified as heterogeneous or homogeneous. In heterogeneous catalysis, the reactant and the catalysts are in different states of

matter, and the catalytic processes occur at the interface of two surfaces, typically a gas-solid interface. In contrast, in homogeneously-catalysed reactions, both the reactants as well as the catalysts are present in the same phase. Often, reactions occur in solution, but gas phase and solid state reactions can also be catalysed homogeneously.

In homogeneous catalysis, the breadth of catalysts applied so far for industrial processes is extremely varied, from simple protons to biologically complex systems such as enzymes. However, in the past few decades, the use of transition metal catalysts has been extensively investigated, due to the ability of these catalysts to mediate a diverse range of reactions *via* oxidative additions, reductive eliminations and β-hydride eliminations, among many other reactions.[93,94] The striking reactivity of transition metal catalysts can be attributed to their partially filled d orbitals, which enable facile ligand binding and switching between different oxidation states and electronic configurations (most commonly 16 and 18 valence-electron configurations) during the catalytic process.[95]

The mechanism of a large majority of homogeneously-catalysed reactions can be described by a simplified catalytic cycle (Scheme 1.4) in which the formation of an active catalyst species from the pre-catalyst (step I) is followed by the activation of the substrate *via* the formation of a metal-substrate complex (step II). This complex is then transformed into a metal-intermediate complex (step III), from which the product will be cleaved with the regeneration of the active catalytic species (step IV). During such a catalytic cycle, the metal centre can switch between different oxidation states, coordination numbers and electronic configurations.[94]

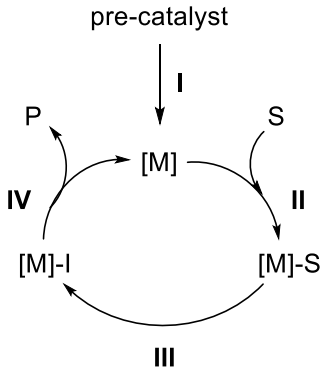

Scheme 1.4: *Schematic catalytic cycle (M = transition metal catalyst, S = substrate, I = intermediate, P = product).*

Although many transition metals are able to facilitate the individual steps in a catalytic reaction, some transition metals display greater activity than others for certain reactions, such as palladium for allylic substitutions and rhodium for hydroformylations of alkenes.[94]

1.2.1 Asymmetric Homogeneous Catalysis

Due to the significance of chiral compounds in areas ranging from medicine to materials science, enantioselective or asymmetric homogeneous catalysis has become one of the most active areas in current research.[96] Currently, approximately 80 % of active pharmaceutical compounds are chiral, with this number expected to rise in the future.[97] Despite the great importance of chiral compounds, obtaining enantiomerically pure materials remains challenging, and the investigation of the mechanism of asymmetric induction is of great interest.

The most widely-used strategy to induce chirality is based on the ability of a transition metal catalyst to differentiate the enantiotopic sites of a prochiral group within the substrate, such as a carbon–carbon or carbon–oxygen double bond.[96] Generally, the ligands used in asymmetric transition metal catalysis are not chemically modified during the catalytic cycle and are referred to as "spectator ligands". Although these types of ligands do not participate in chemical transformations, they influence the reactivity of the metal centre. The differentiation in enantioselective transition metal catalysis comes from the presence of chiral spectator ligands around the metal centre, which provide the possibility of multiplying molecular chirality.[98]

More recently, metal-ligand cooperation has become an important concept in transition metal catalysis. Here, both the metal and the ligand participate in the bond cleavage/formation, and the metal and the ligand can be chemically modified during bond activation. The concept of metal-ligand cooperation also refers to a change in the coordination mode of the cooperative ligand as a result of bond activation, as seen with hemilabile ligands.[99] The concept of hemilability was first introduced by T. B. Rauchfuss and refers to polydentate ligands that contain at least two different donor groups with distinct electronic properties, such as hard and soft donor atoms (Scheme 1.5).[100] The labile donor groups or ligands offer sites for substrate binding when removed during reaction from the pre-catalyst molecule and trigger the activity of the transition metal catalyst. In the absence of a substrate, the chelate effect of the multidentate ligand confers stability on the metal centre.

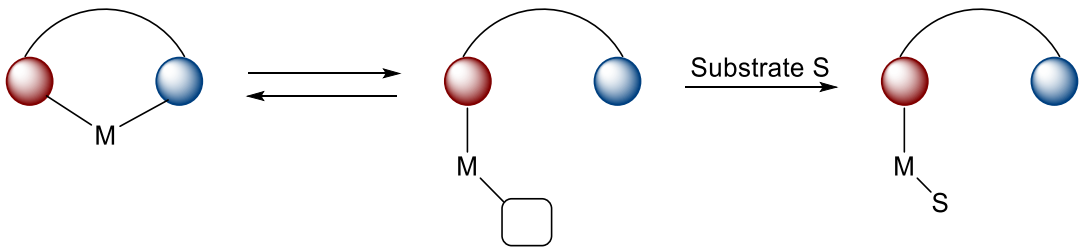

Scheme 1.5: *Concept of hemilabile ligands in homogeneous catalysis introduced by T. B. Rauchfuss.*[100]

1.2.2 Phosphine Ligands in Homogeneous Catalysis

The drive to optimise the stability and catalytic activity of transition metal complexes has led to the development of a diverse array of phosphine ligands.[90–92,101,102] Phosphorus has been one of the donor atoms of choice, as its coordination properties can often be predicted in terms of hard/soft acid and base theory and due to its easy traceability *via* ^{31}P NMR spectroscopy, which enables a more in-depth investigation into the mechanisms of catalytic reactions.[103] In order to tailor phosphine ligands for specific catalytic applications, a detailed knowledge of the factors that influence phosphine–metal bonding, and therefore the reactivity of the transition metal complexes, is necessary. Therefore, various quantitative ligand parameters have been developed.

One approach to determine the donor properties of phosphines, which was first established by W. Strohmeier in 1967, is called the electronic ligand parameter and describes the σ-donor and π-acceptor properties of a phosphine (Figure 1.7). Whereas σ-donation defines electron-donation from the P lone pair into the empty metal d orbitals, the π-accepting properties are related to the backdonation of electron density from the filled metal orbitals into the empty ligand orbitals (σ* orbitals of the phosphine ligand).[104] The electronic ligand parameter is based on the response of ligands (for instance CO) upon electronic changes on the metal centre caused by the coordination of the phosphine.[105]

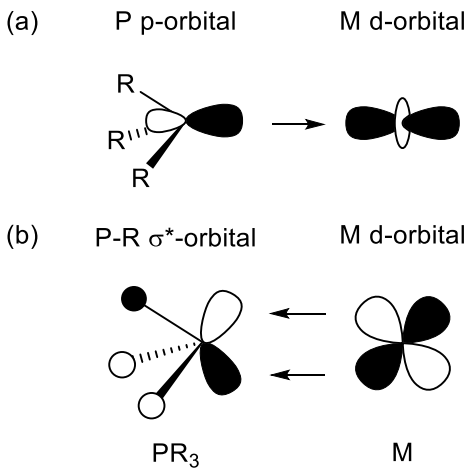

Figure 1.7: *(a) σ-Donation and (b) π-backdonation contributions within a transition metal phosphine complex.*

Later, C. A. Tolman devised the Tolman electronic parameter from the IR spectra of $[Ni(CO)_3L]$ complexes (L = phosphine ligand), using $P(^tBu)_3$ as the reference ligand.[106] With this method only the overall donor properties of a phosphine can be determined. However, sometimes it is necessary to have a deeper knowledge of the individual σ-donor and π-acceptor properties. The separation of these two entwined electronic parameters is of great importance but is not trivial. There are many studies based on computational methods and the symmetry of the orbitals of the nature of metal–phosphorus bonding.[103]

For the description of the steric ligand parameter of monodentate phosphines, the concept of the Tolman cone angle is most commonly used (Figure 1.8).[106] Originally, it was developed for a phosphine ligand bound to a nickel centre with an Ni–P bond length of 2.28 Å. More recently, computational methods have been employed, since ligands rarely form perfect cones, particularly when double coordination with two (different) ligands takes place and steric clash of the ligands occurs.[107]

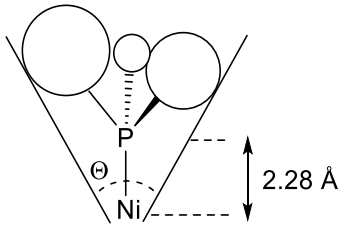

Figure 1.8: *Tolman's cone angle of an asymmetric monodentate phosphine.*

The most sophisticated approach so far, to describe the stereo-electronic properties of phosphine ligands is the so-called QALE model (quantitative analysis of ligand effects), which includes the Tolman cone angle, σ-donating and π-accepting properties, and other electronic effects. With the help of this model, information about the stereo-electronic factors, which influence the thermodynamics and kinetics of reactions, can be extracted.[108]

1.2.2.1 Development of Privileged Phosphines

Certain classes of asymmetric catalysts are known to catalyse a wide range of reactions with high enantioselectivities. Such species are known as "privileged structures" and their general applicability enables the synthesis of enantiomerically pure materials. Despite their very diverse structural features, most privileged homogeneous catalysts possess rigid ligand frameworks with multiple donor atoms that can strongly bind to a reactive metal centre.[109]

Often, privileged phosphines exhibit two-fold axes of symmetry within the ligand molecule.[109] The ligands in Figure 1.9 represent a small portion of those that have been successfully applied in asymmetric homogeneous catalysis. For example, Rh complexes of the chiral bidentate C_2-symmetric DIPAMP ligand (ethane-1,2-diylbis[(2-methoxyphenyl)phenylphosphane], Figure 1.9a) studied by W. S. Knowles and co-workers[101,110] have shown remarkable potential in enantioselective hydrogenation reactions, giving superior results compared to the monodentate derivatives. Rh and Ru complexes of the ligand BINAP (2,2′-bis(diphenylphosphino)-1,1′-binaphthyl, Figure 1.9b), a C_2-symmetric axial-chiral ligand framework developed by R. Noyori, have been extremely successful catalysts in hydrogenation reactions.[98] The ligand BINAP is employed in the industrial synthesis of menthol, or, more precisely, it is involved in the stereoselective hydrogenation of geraniol or nerol to (+)-(*R*)-citronellol.[111,112] Rh complexes of a

variety of ethane-bridged bis(phospholanes) and 1,2-bis(phospholano)benzene analogues (DuPHOS, Figure 1.9c) were studied by M. J. Burk and co-workers and have shown very high catalytic efficiencies and enantiomeric excesses in the asymmetric hydrogenation of various olefins.[14,15,17]

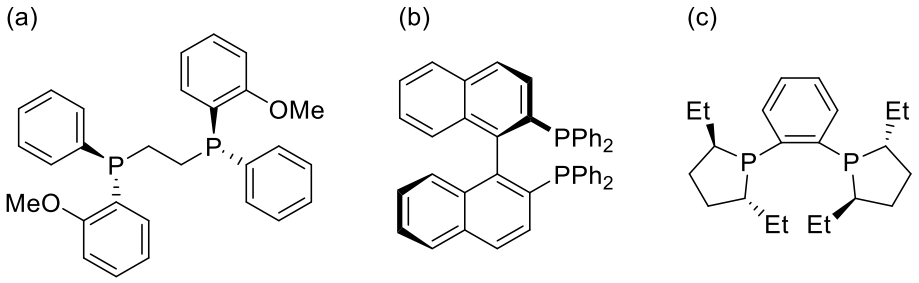

Figure 1.9: *Prominent examples of chiral C_2-symmetric phosphines applied in homogeneously-catalysed hydrogenation reactions.*

The remarkable success and wide application of C_2-symmetric ligands can be attributed to their induction of a high degree of stereo-control in asymmetric transition metal catalysis.[113,114] This is due to a reduction in the number of possible competing diastereomeric transition states of intermediate square-planar transition metal complexes (Figure 1.10a).[1]

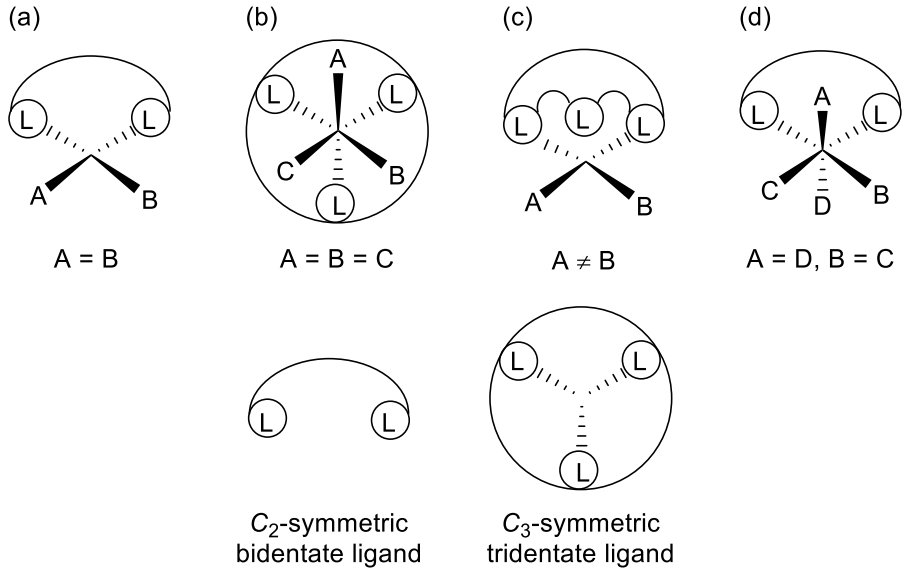

Figure 1.10: *Vacant coordination sites (A–D) in intermediate square-planar [(a) and (c)] and octahedral [(b) and (d)] transition metal complexes with C_2-symmetric bidentate and C_3-symmetric tridentate ligands. Graphic adapted from C. Moberg, Angew. Chem. Int. Ed., 1998.*[1]

In order to rationalise the relationship between the chirality of the ligand and asymmetric induction, the quadrant model (Figure 1.11), which is based on steric effects, can be utilised for C_2-symmetric phosphine ligands. In the case of DIPAMP, the crystal structure of the square-planar Rh precursor $[Rh(DIPAMP)(diene)]^+$ has shown that the enantioselectivity of the catalytic reaction is likely due

to the presence of two more sterically hindered sites (2nd and 4th quadrant), when the structure is divided into four quadrants. A prochiral olefin then might prefer to lie in the unhindered quadrants (1st and 3rd quadrant) and a prediction of the chirality of the product based on the chirality of the phosphine ligand is possible.[101] Similar assumptions based on steric effects were made for bis-phosphines, which contain stereogenic centres on the ligand backbone instead of P-chirality.[110]

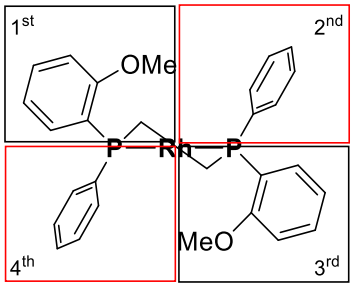

Figure 1.11: *Quadrant model for Rh-(R,R)-DIPAMP. Sterically hindered quadrants are shown in red. Additional ligands on the Rh centres and charges of the complexes are omitted for clarity.*

The quadrant model provides a very intuitive tool for the design of chiral bis-phosphine catalysts based on steric encumbrance. However, J. Halpern[115] and J. M. Brown[116] came to the conclusion that not only the preferred binding mode of the prochiral olefin, but also the differences in the reaction rates of subsequent reactions of the diastereomeric catalyst-substrate adducts, influence the enantioselectivity in asymmetric hydrogenation reactions (anti-lock-and-key behaviour).

While the properties of C_2-symmetric ligand systems have been extensively exploited for many industrial applications, compounds possessing ligands of higher symmetry have long been ignored. However, M. J. Burk and co-workers recently developed enantiomerically pure tripodal phosphines with C_3-symmetry (Figure 1.12).[14,16,17] The rigid character of C_3-symmetric ligands should also provide a high degree of stereo-chemical control, due to a reduced number of competing asymmetric environments[1,93,117] in intermediate octahedral transition metal species (Figure 1.10b). Chiral derivatives of such C_3-symmetric phosphines have been successfully applied in the asymmetric hydrogenation of methyl (*Z*)-α-acetamidocinnamate and dimethyl itaconate, although under high reaction temperatures.[16]

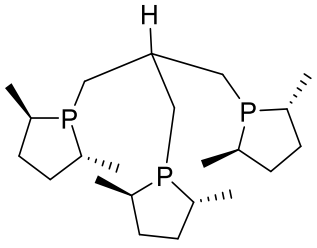

Figure 1.12: *Example of a chiral C_3-symmetric (R, R, R)-tris-phospholane ligand developed by M. J. Burk et al.*[16]

1.2.2.2 Mixed Donor Phosphine Ligands

Although symmetric multidentate phosphine ligands, such as DIPAMP, BINAP or DuPHOS, have long dominated the area of homogeneous asymmetric catalysis,[15,91,101] unsymmetrical ligands with two sterically- and electronically-distinct donor groups can also provide outstanding asymmetric induction in catalytic reactions.[103] The success of such mixed donor phosphines can be attributed to their hemilability, which enhances the reactivity of the corresponding transition metal complexes. K. Achiwa underscored this effect in 1992 with the isolation of unsymmetrical intermediates during the hydrogenation of olefins, using a Rh bis-phosphine complex. From these results, it was concluded that the steric and electronic properties of the two donor atoms can be altered individually in order to achieve optimal enantioselectivity.[118]

In the past, mixed donor ligand systems, especially P,N ligands, came to the fore due to the combination of a hard σ-donor N atom as well as the soft π-accepting phosphorus unit. In addition to the two very electronically different donor groups, the accessibility of P,N systems from chiral building blocks, such as chiral amino acids, makes these ligands very interesting. Moreover, P,N ligands can be easily separated from a homogeneous organic phase by protonation of the nitrogen atom(s) under acidic conditions, increasing the ease of isolation and purification compared to regular phosphine ligands.[119] The most prominent class of P,N-containing ligands are, arguably, the oxazoline-based P,N ligands, which were developed by A. Pfaltz[120] and G. Helmchen[121] (Figure 1.13a). These ligands have been applied in a range of asymmetric catalytic reactions, such as allylic substitutions, Heck reactions and hydrogenations.[122]

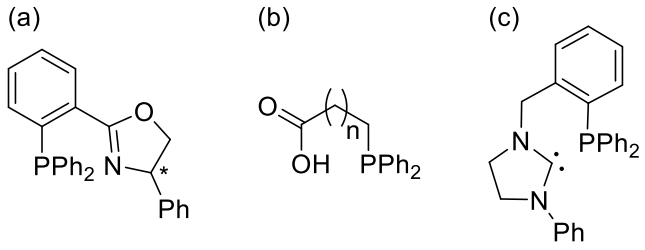

Figure 1.13: *(a) Chiral phosphinooxazoline ligand, (b) phosphinocarboxylic acid ligand (n = 1–3) and (c) a carbene-based phosphine ligand.*

Oxygen-containing mixed donor phosphines (*e.g.* phosphinites, phosphonites, and phosphites) are also very promising ligand candidates for asymmetric homogeneous catalysis. Compared to P,N ligands, these systems exhibit a decreased σ-donor contribution from the O atom and increased π-accepting properties of the P donor.[103] An example of the industrial application of such ligands is the use of a phosphinocarboxylic acid ligand (Figure 1.13b) in the Shell higher olefin process for the production of linear α-olefins from ethene.[103]

In addition to P,N- and P,O-containing ligands, P,C mixed ligand systems have been developed. N-heterocyclic carbene-based bidentate P,C ligands (Figure 1.13c) are of particular interest, as carbenes can act as π-acceptors as well as σ-donors. However, the pronounced σ-donor properties of the N-heterocyclic carbene units lead to more stable M–carbene bonds compared to the analogous M–P bonds. Therefore, the P donor group can dissociate from the metal centre and leave a vacant coordination site for substrate binding during a catalytic cycle. This unique feature makes P,C bidentate ligands attractive for Heck reactions, hydrogenations and Suzuki coupling reactions.[123]

1.2.3 Application of Pyridine-containing Phosphines in Homogeneous Catalysis

The development of multidentate mixed-donor ligands has become important because transition metal complexes of these hemilabile ligands can offer fascinating reactivity in homogeneous catalysis. In this context, pyridine-containing phosphines, also called pyr-phos ligands, have been employed in enantioselective catalytic reactions. These ligand systems combine σ-donor as well as π-acceptor properties, and as such are capable of stabilising metal centres during oxidative addition reactions, as well as metal centres in low-oxidation states. This dual functionality is considered to be very beneficial during catalytic reactions.[86]

Ruthenium complexes of the chiral P,N ligand 1-(diphenylphosphino)-2-ethoxy-l-(2-pyridyl)ethane (Figure 1.14a) have shown high activities with excellent turnover numbers in the transfer hydrogenations of ketones by 2-propanol.[124] Also, the hydroboration of several vinyl arenes can be catalysed using a chiral (*S*)-QUINAP [(*S*)-1-(2-diphenylphosphino-1-naphthyl)isoquinoline, Figure 1.14b] Rh complex to yield products with high chemoselectivity and enantioselectivity.[125] The bicyclic 2-(phosphinoaryl) pyridine (Figure 1.14c) has been used for palladium-catalysed asymmetric allylic substitutions,[126] and iridium complexes of the phosphinite (Figure 1.14d) have proven to be highly effective in hydrogenation reactions of purely alkyl-substituted alkenes.[127] Other catalytic transformations that utilise pyridine-based phosphine ligands include carbonylations and decarbonylation, hydroformylations, hydrosilylations, cross-coupling reactions and other catalytic transformations.[86,128]

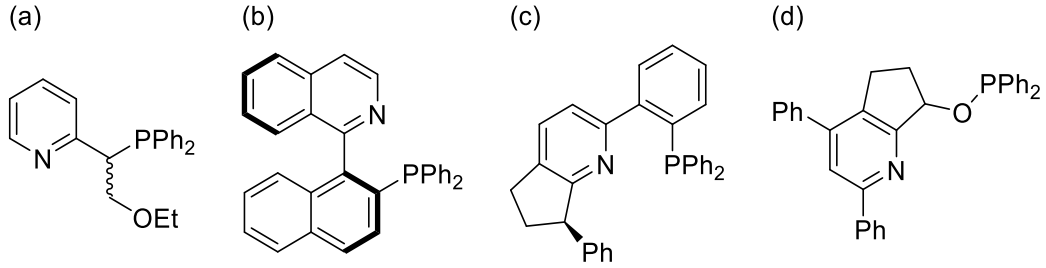

Figure 1.14: *Selected pyr-phos ligands that can be applied in diverse homogeneous asymmetric catalytic reactions.*

Although the versatility of these pyridine-containing P,N ligands has been demonstrated in numerous catalytic asymmetric syntheses, the application of 2-pyridyl-phosphines in catalysis, in which the phosphorus donor atom is directly connected to the pyridine moiety, has not been studied in great detail. This is possibly due to the fact that the pyridyl-nitrogen donor atoms in 2-pyridyl-phosphines, for example, $P(2\text{-py})_3$, bind strongly to metals such as Rh and Ru, rendering the complexes coordinatively saturated, leading to a low catalytic activity.[26] Also the potential formation of polymeric transition metal complexes of 2-pyridyl-phosphines *via* the coordination of the P and N atoms of the ligands to separate metal centres turned out to be a disadvantage.[129] There are, however, a few examples of the use of tris-2-pyridyl-phosphine ligands in homogeneously-catalysed reactions. Mn^{II}, Co^{II} and Ni^{II} complexes of the tripodal $P(2\text{-py})_3$ ligand are known to mediate the oxidation of tetralin,[62] and nitrile reduction can be promoted by a $P(2\text{-py})_3$ copper complex.[68] Also, rhodium complexes with 2-pyridyl-phosphines and sulfobetaine derivatives have been employed in the hydroformylation[26,130] and hydrogenation[129] of alkenes with moderate activities. Interestingly, transition metal complexes incorporating tris-2-pyridyl-phosphines have the potential to act as homogeneous catalysts in aqueous media, possibly because of partial protonation of the pyridyl-N atoms. The application of homogeneous catalytic systems in aqueous media is a cheaper alternative to using organic solvents, and enables easy separation of the catalysts and the products, especially in the case of biphasic systems.[82,131]

Other examples of catalysis mediated by so-called pyr-phos ligands are mainly based on phenyl derivatives of 2-pyridyl-phosphine.[88,89] For instance, rhodium complexes of $Ph_2P(2\text{-py})$ have been used for the hydroformylation of styrene,[132] and palladium complexes of this ligand have been employed in the carbonylation of propyne to afford methyl methacrylate with high turnover numbers.[133] The high activity and selectivity of the cationic palladium $Ph_2P(2\text{-py})$ catalysts towards the carbonylation of alkynes has been attributed to the ability of the 2-pyridyl-phosphine to act as a chelating ligand during the selectivity-determining step and as a monodentate ligand as well as a proton-shuttle to the active Pd centre in the rate-determining step of the catalytic cycle.[133] Transition metal complexes of the phenyl-bis(2-pyridyl)-phosphine ligand have been applied in Mitsunobu reactions of carboxylic acids.[134]

The previous studies in this area have shown that the two electronically distinct donor atoms within the ligand framework of 2-pyridyl-phosphines and the consequent potential hemilability of the phosphine can be beneficial during catalytic transformations. However, the very limited number of examples of 2-pyridyl-phosphines in homogeneous catalysis so far suggests that there is a great deal more potential for exploration in this area.

1.3 Project Aims

This thesis aims to enable facile access to a library of pyridine-containing P,N mixed donor ligands and their corresponding transition metal complexes. Towards this aim, the following design strategies will be pursued:

1. *Introduction of substituents into the pyridyl ring at the 6-position (i.e., adjacent to the N donor atom) of tris-2-pyridyl-phosphines.*

The introduction of substituents into the 6-position of the pyridyl ring should alter not only the steric properties of the C_3-symmetric ligands but also the electronic character of the neighbouring nitrogen donor atoms, influencing the coordination behaviour of the ligands.

2. *Synthesis of novel unsymmetrical derivatives of 2-pyridyl-phosphines.*

The investigation of unsymmetrical multidentate 2-pyridyl-phosphines provides an opportunity to introduce additional donor functionalities, such as amino or alkoxy groups. This strategy is an obvious way of introducing chirality *via* chiral donor groups or P-stereogenicity.

3. *Investigation of the donor properties of 2-pyridyl-phosphines.*

For the efficient design of suitable transition metal catalysts, it is important to understand the donor properties of the ligands used. Therefore, multiple experimental and computational approaches should be utilised.

4. *Modification of the phosphorus bridgehead atom.*

Through the modification of the bridgehead-P atom, for example, by oxidation of the phosphorus(III) atom to phosphorus(V), the electronic character of the phosphine bridgehead position can be dramatically altered. Depending on the transition metal used, the phosphine can be so hindered that it coordinates *via* its P donor atom to the metal centre.

The hope was that these developments would provide access to new and adaptable ligand sets for applications in single-site catalysis. In order to examine the catalytic activity of transition metal complexes of these ligands, hydrogenation and hydrosilylation reactions will also be a focus of this thesis.

2 Sterically-constrained Tris-2-pyridyl-phosphine Ligands

2.1 Preamble

As noted in the introduction to this thesis, the coordination chemistry[86] and reactivity[83–85] of C_3-symmetric phosphorus-bridged tris-pyridyl ligands of the type P(2-py)$_3$ have been studied extensively over the last few decades. Despite the breadth of these studies, there have been no systematic investigations into the substitution of the pyridyl ring at the 6-position (*i.e.*, adjacent to the N donor atom) of tris-2-pyridyl-phosphines. The introduction of substituents at the 6-position of tris-2-pyridyl-phosphines is of particular interest in this area as this should have a direct steric and electronic impact on the catalytic site.

D. S. Wright and co-workers have recently shown that the introduction of substituents within the pyridyl rings can have a large effect on the coordination characteristics of tris-pyridyl-aluminates.[39] For example, in the case of [RAl(2-py')$_3$]$^-$ (R = ^{n}Bu, 2-Bu, Et, py' = 2-py, 5-Me-2-py, 6-Me-2-py), the presence of the Me substituents in the 6-position of the pyridyl ring has a marked effect on the ability of the ligands to form sandwich arrangements of the type [{RAl(2-py')$_3$}$_2$M]. Scheme 2.1 shows the formation of a Mn sandwich complex using the [RAl(2-py)$_3$]$^-$ (R = ^{n}Bu, 2-Bu) ligand. In contrast, the introduction of a methyl group next to the pyridyl-N donor atoms leads to the formation of [{EtAl(6-Me-2-py)$_3$}Mn(μ-Cl)Li{(6-Me-2-py)$_3$AlEt}] under similar conditions, in which steric clash of the Me groups, which would occur in a sandwich-type compound in the case of relatively small Mn^{II}, is prevented by the formation of a Li–Cl–Mn bridge (Scheme 2.1).[39] Interestingly, neither the bridgehead group R nor the introduction of remote ring Me groups (for example, in the 5-position of the pyridyl ring) have any impact on the coordination behaviour of the aluminate ligands.

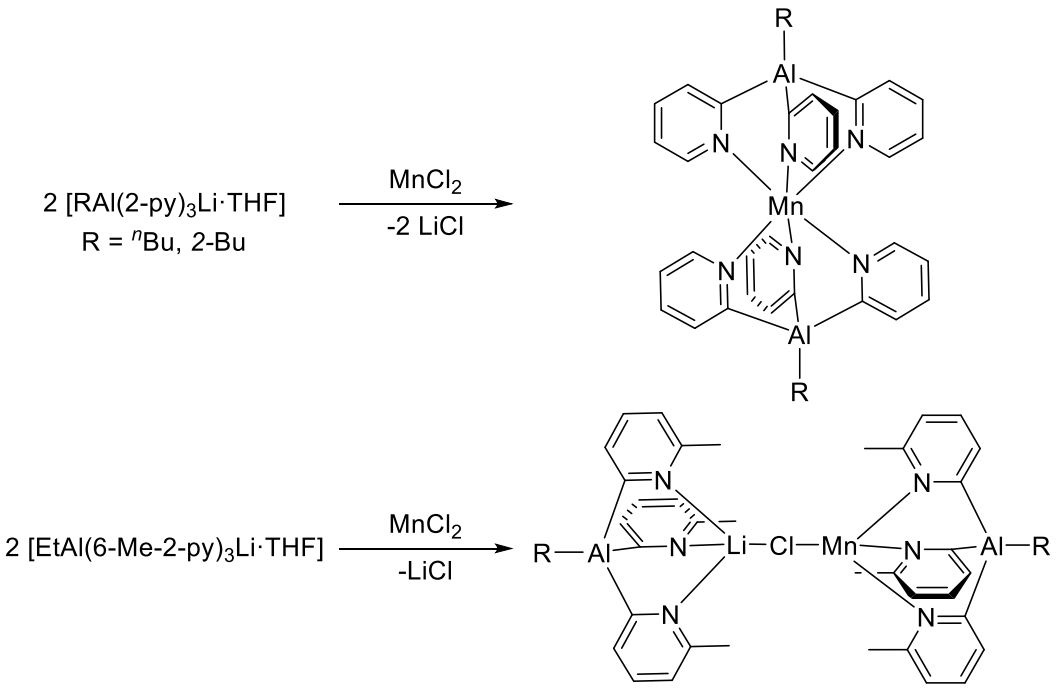

Scheme 2.1: *Reaction scheme showing the formation of tris-2-pyridyl-aluminate manganese complexes.*[39]

Recently, it has also been shown that sterically encumbered ligands, such as the precursor $[EtAl(6\text{-}Me\text{-}2\text{-}py)_3]^-$, are able to kinetically stabilise unusual metal oxidation states, such as Sm^{2+}, in a sandwich arrangement (Figure 2.1). When the unsubstituted lithium aluminate precursor $[EtAl(2\text{-}py)_3Li{\cdot}THF]$ was reacted with SmI_2 in a 2:1 ratio at room temperature, attempts to isolate the sandwich compound $[\{EtAl(2\text{-}py)_3\}_2Sm]$ always gave rise to the formation of the Al^{III}/Sm^{III} dimer $[\{EtAl(2\text{-}py)_3\}\{EtAl(2\text{-}py)_2O\}Sm]_2$, resulting from O_2 oxidation. The stability of the sandwich complex containing 6-Me-2-py ligands can be ascribed to the steric shielding of the samarium(II) ion which results in greater resistance towards molecular oxygen.[42]

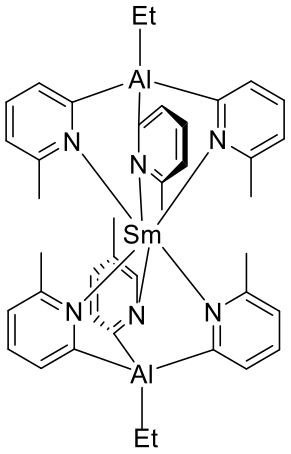

Figure 2.1: *Structure of the 6-substituted tris-2-pyridyl-aluminate omplex [{EtAl(6-Me-2-py)3}2Sm].*[42]

In addition to the steric influence of substitution within the pyridyl groups, its electronic effects have been investigated in the case of aluminium-bridged tris-pyridyl ligands.[37,38] For example, the

methyl-substituted aluminate $[EtAl(6\text{-}Me\text{-}2\text{-}py)_3]^-$ binds strongly to the divalent metal lanthanide ions europium(II) and ytterbium(II) to form sandwich complexes, whereas the bromine derivative $[EtAl(6\text{-}Br\text{-}2\text{-}py)_3]^-$ coordinates weakly and the CF_3 analogue $[EtAl(6\text{-}CF_3\text{-}2\text{-}py)_3]^-$ is unable to coordinate to lanthanide ions. Thus, the electron-withdrawing effect of the substituents has a clear impact on the electronic features of the neighbouring nitrogen donor atoms and therefore on the coordination behaviour of the ligand.[37]

Similar observations were made in regard to the introduction of methoxy groups into tris-2-pyridyl-methoxymethane ligands. Varying the number of methoxy groups in the 6-position of the pyridyl ring from zero to three has a considerable influence on the coordination geometry towards copper(I) as well as the ligand exchange behaviour. Whereas the unsubstituted $MeOC(2\text{-}py)_3$ ligand coordinates the copper metal centre *via* all of its pyridyl-nitrogen atoms, forming half- or full-sandwich complexes depending on the reaction stoichiometry, the trifunctionalised tris-pyridyl-carbinol derivative $MeOC(6\text{-}MeO\text{-}2\text{-}py)_3$ only forms the half-sandwich arrangement, due to its greater steric congestion.[24]

Spurred by the observation of the stabilising effect of 6-substitution of the pyridyl ring within the Al-based ligands and the dramatic effects of methoxy groups in the periphery of methoxymethane ligands on the coordination characteristics, one of the primary aims of this project was the synthesis of a variety of 6-substituted tris-2-pyridyl-phosphines (Figure 2.2). The steric and electronic properties of these ligands were investigated in a range of transition metal complexes. The introduction of chiral substituents in close proximity to the coordinating N donor atoms provides some indication of how tris-2-pyridyl-phosphines with chiral substituents at the 6-position may function in asymmetric homogeneous catalytic transformations.

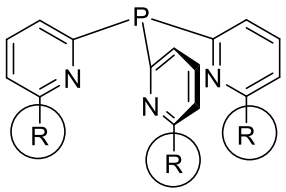

Figure 2.2: *The introduction of substituents into the 6-position of tris-2-pyridyl-phosphines.*

Some of the following sections were published in: S. Hanf, R. García-Rodríguez, A. D. Bond, E. Hey-Hawkins, D. S. Wright, *Dalton Trans.* **2016**, *45*, 276–283.

2.2 Ligand Design and Synthesis of P-bridged Tris-2-pyridyl Ligands

The unsubstituted tris-2-pyridyl ligand P(2-py)$_3$ (**1**) was prepared using a modified literature procedure,[74] in which 2-bromopyridine was lithiated using ^{n}BuLi at −78 °C, and the intermediate 2-lithio-pyridine was subsequently reacted with PCl_3 (in a 3 : 1 molar ratio, Scheme 2.2).

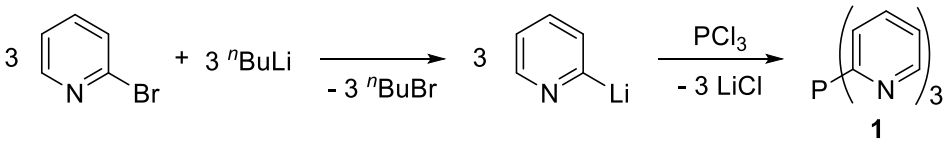

Scheme 2.2: *Synthesis of the unsubstituted tris-2-pyridyl-phosphine ligand **1**.*

The methyl- and bromine-substituted derivatives were obtained in an analogous way using 2-bromo-6-methylpyridine or 2,6-dibromopyridine, respectively. Low reaction temperatures are required in order to avoid the formation of any pyridyl-coupling products. Whereas P(2-py)$_3$ (**1**) and P(6-Me-2-py)$_3$ (**2**) can be obtained using an aqueous acidic workup (in 53 % and 62 % yield, respectively), the Br-substituted compound P(6-Br-2-py)$_3$ (**3**) could not be extracted from the crude reaction product in the same manner, possibly due to the lower basicity of the pyridyl-nitrogen atoms. Furthermore, the solubility of the three ligand systems varies significantly. While **1** and **2** are soluble in a variety of organic solvents, the bromine analogue **3** is largely insoluble, which limits its applications.

To investigate the differences in basicity of the three tris-2-pyridyl-phosphines **1**–**3**, their first free protonation enthalpies (pE) were calculated (Table 2.1) according to Equation 2-1 and 2-2[135] using DFT (density functional theory) methods at the BP86,[136–138] def2-TZVP[139,140] level of theory (see Chapter 8.4, page 134). The protonation energy is defined as the energy difference of the protonated ligand (E_{LH+}) minus the energy of the ligand (E_L).

$$L + H^+ \rightarrow LH^+ \tag{2-1}$$

$$pE = E_{LH^+} - E_L \tag{2-2}$$

Table 2.1: *Calculated protonation energies of the tris-2-pyridyl-phosphines **1**–**3**.*

Compound	First Free Protonation Enthalpy [kcal·mol^{-1}]
1	–248.40
2	–253.38
3	–239.30

While the Me-substituted ligand **2** has the most exothermic protonation enthalpy, due to the electron-donating effect of the Me groups on the pyridyl-nitrogen atoms, a significantly less

exothermic first protonation enthalpy was calculated for the bromine analogue **3**. This is consistent with the fact that the Br-substituted phosphine cannot be protonated under the same conditions as the unsubstituted or Me-substituted counterparts.

To emphasise the electronic effects of the introduction of substituents on the neighbouring pyridyl-nitrogen donor atoms, the distribution of the CHELPG charges (charges from electrostatic potentials using a grid-based method, developed by C. M. Breneman and K. B. Wiberg), within the ligands **1**–**3** were calculated and are shown in Figure 2.3.[141] The charges were calculated at the same level of theory as the first free protonation enthalpies and represent atomic charges, which are fitted to reproduce the molecular electrostatic potential at a number of grid points around the molecule. Whereas the charges on the pyridyl-nitrogen atoms in **1** and **2** are almost identical, there is a clear decrease in the negative charge on the N atoms in the bromine counterpart **3**. This again is in accordance with the experimental findings and the calculated first free protonation enthalpies, since lower electron density on the nitrogen donor atoms will lead to reduced basicity.

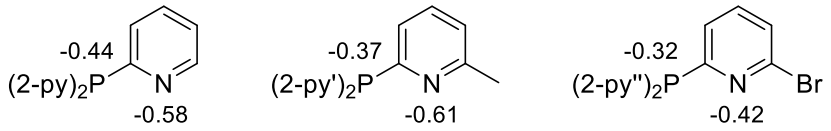

Figure 2.3: *CHELPG charges of the P and N donor atoms within the tris-2-pyridyl-phosphines **1**–**3**.*

The new substituted ligand sets **2** and **3** were fully characterised by NMR and IR spectroscopy, elemental analysis, and single-crystal X-ray crystallography (Figure 2.4). Both compounds crystallise in non-chiral space groups as racemic mixtures of the two possible rotamers.

The novel ligands **2** and **3** are of special interest, since they are much more sterically demanding than the unsubstituted counterpart **1**, which was crystallographically characterised by F. R. Keene *et al.* previously.[59] This is seen most obviously in the orientation of the N atoms in both ligands (upwards) towards the bridgehead-P atoms. In contrast, the unsubstituted ligand has two of the N atoms orientated downwards away from the P atom, with only one of the N atoms disposed in a similar alignment to that in **2** and **3**.[59] This difference is a consequence of avoiding steric clashing between the 6-Me and 6-Br substituents and an alteration of the s-character of the phosphorus lone pair. A more detailed comparison of the solid state structures of **1**, **2** and **3** (Table 2.2) also shows that the P–C_{py} bond lengths of **2** and **3** are about 0.02 Å longer than those in the unsubstituted **1**. Furthermore, the unsubstituted compound exhibits an uneven distribution of P–C_{py}–N_{py} bond angles, which vary between 111° and 120°, whereas the methyl- and bromine-substituted ligands have uniform angles of *ca.* 113°.

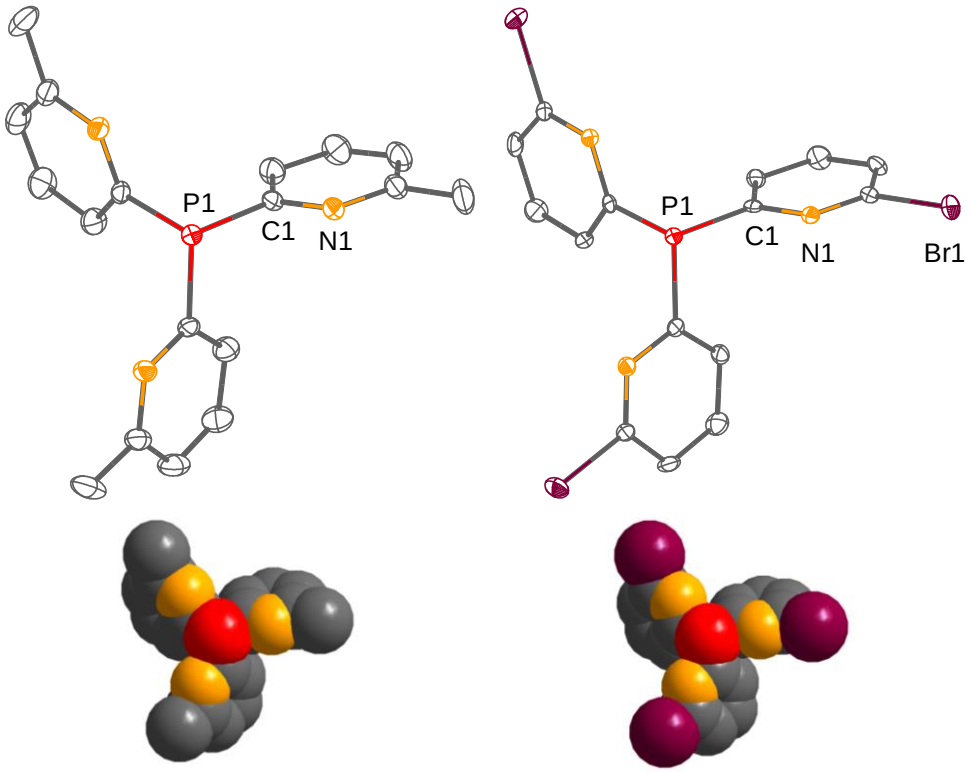

Figure 2.4: *Structures of ligands **2** (left) and **3** (right) and their space filling diagrams. Hydrogen atoms are omitted for clarity. Displacement ellipsoids are drawn at the 30 % probability level. Only one of the rotamers of each is shown.*

Table 2.2: *Selected bond lengths (Å) and angles (°) in the three ligands **1**–**3**.*

	1[59]	**2**	**3**
P(1)–C_{py}	1.824(3)–1.834(3)	1.847(2)–1.851(2)	1.852(8)
C_{py}–P(1)–C_{py}	101.0(1)–102.7(1)	99.2(1)–99.8(1)	99.0(3)
P(1)–C_{py}–N_{py}	111.6(2)–120.2(2)	113.0(2)–113.5(2)	112.9(5)

As part of the broader study of 6-substituted pyridyl ligands, the cyano-derivative **4** was also prepared in 70 % yield (Scheme 2.3).[142]

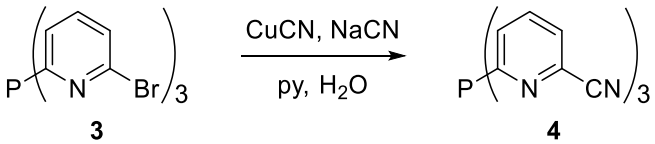

3 **4**

Scheme 2.3: *Synthesis of the CN-substituted P-bridged tris-2-pyridyl-phosphine P(6-CN-2-py)$_3$ (**4**).*[142]

The introduction of the nitrile functionality provides the possibility of post-functionalisation and the introduction of other organic substituents, such as carboxylic acids (*via* hydrolysis of the CN

group) or primary amines (*via* reduction). This may also offer the potential to introduce chiral substituents in the pyridyl rings.

2.3 Iron and Copper Complexes of Tris-2-pyridyl-phosphines

The coordination behaviour of **1**, **2** and **3** towards Fe^{II} and the softer Cu^{I} ion was explored in order to investigate the impact of the increased steric demand through substitution in the 6-position of the pyridyl rings.

Reactions of the three ligands **1**, **2** and **3** with iron(II) chloride were carried out in toluene at room temperature and under reflux conditions using different stoichiometries. No products could be isolated from the 2 : 1 stoichiometric reaction of the unsubstituted ligand **1** with $FeCl_2$. However, using $Fe(OTf)_2$ as the Fe^{II} source in acetonitrile (Scheme 2.4) resulted in the immediate formation of a dark red solution at room temperature, from which dark red crystals of the sandwich compound $[\{P(2\text{-}py)_3\}_2Fe](OTf)_2$ (**5**) were isolated after workup (in 73 % yield, powder). The observation of sharp resonances with no paramagnetic shift in the ^1H NMR spectrum of **5** (as well as the dark red colour of the complex) confirms the low-spin ($t_{2g}^6\ e_g^0$) electronic diamagnetic configuration of the compound. The coordination of the Fe^{II} ion by **1** result in a noticeable upfield shift in the $^{31}P\{^1H\}$ NMR resonance from −1.0 ppm ($CDCl_3$) for the uncoordinated ligand to −9.0 ppm (CD_3COCD_3) in **5**. Also obvious is the upfield shift of the ^1H NMR signal of H(6) (*i.e.*, the H adjacent to the N atoms, see Scheme 8.1). This resonance is found at 8.75 ppm (in $CDCl_3$) in the free ligand **1** but is shifted to 7.72 ppm (in CD_3COCD_3) in the transition metal complex **5**. This has been explained previously in terms of the effect of metal coordination on the aromatic ring current in 2 : 1 sandwich-type zinc complexes of tris-2-pyridyl-phosphine, tris-2-pyridyl-arsine,[143] and tris-2-pyridyl-COH ligands.[144]

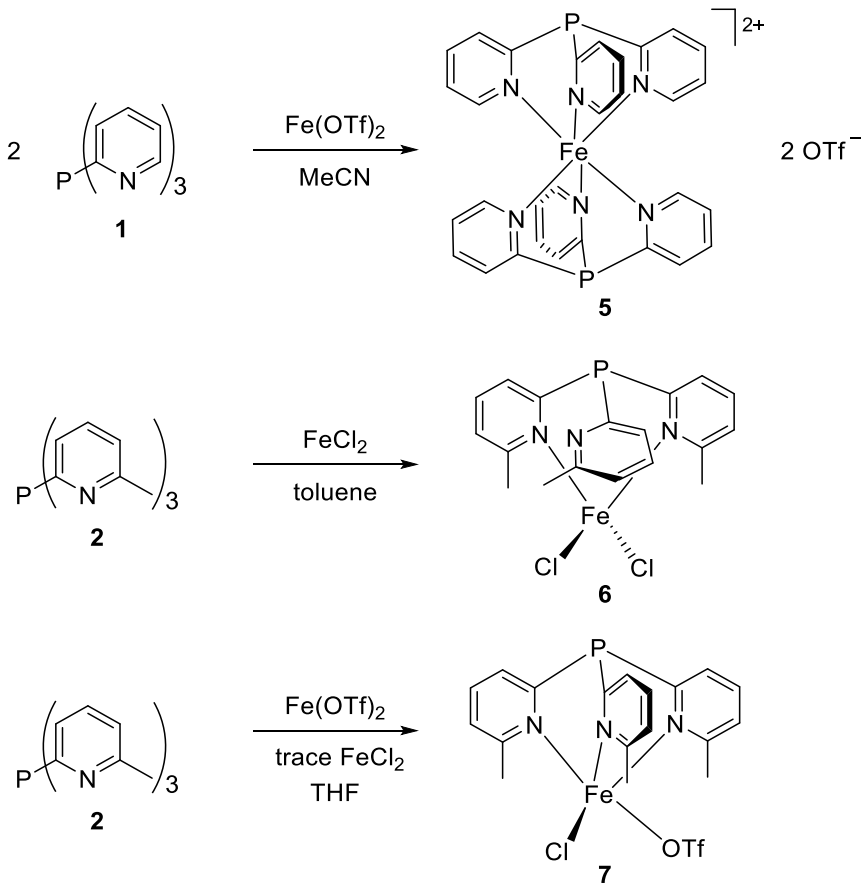

Scheme 2.4: *Reactions of phosphorus-bridged tris-2-pyridyl ligands with iron(II) chloride and iron(II) triflate.*

In contrast to the behaviour of **1** with $FeCl_2$, the reaction of the Me-substituted ligand **2** in 1 : 1 molar ratio with $FeCl_2$ gave pale yellow crystals of [{P(6-Me-2-py)$_3$}$FeCl_2$]·toluene (**6**·toluene) (Scheme 2.4). The colour as well as the very broad resonances in the NMR spectra suggested a paramagnetic character for the compound and a high-spin configuration of the Fe^{II} centre. Attempts to form the sandwich type compound [{P(2-py)$_3$}$_2$Fe]Cl_2 using a 2 : 1 reaction stoichiometry (ligand : $FeCl_2$) were not successful, and only the free ligand **2** was crystallised, possibly indicating that the ligand is too weak to replace the chlorine atoms on the Fe^{II} centre and/or that the steric shielding of the methyl groups in the 6-position of **2** prevents the coordination of Fe^{II} and the formation of a sandwich arrangement.

The reaction of the methyl-substituted ligand **2** with $Fe(OTf)_2$ in acetonitrile at room temperature (in a 1 : 1 and 2 : 1 molar ratio) resulted in the formation of a dark green reaction mixture, which then turned black after a few hours and from which no solid products could be isolated. However, when THF was used as the reaction solvent a clear yellow solution was produced, from which the only product that could be isolated was the half-sandwich compound [{P(6-Me-2-py)$_3$}FeCl(OTf)]·2THF (**7**·2THF) in low yield, in which all of the nitrogen atoms coordinate the Fe^{II} centre (Scheme 2.4). The unexpected presence of the Cl atom coordinated to Fe^{II} appears to result from the contamination of the commercially-supplied $Fe(OTf)_2$ with $FeCl_2$. The

yield was dramatically improved (to 38 %) by the deliberate addition of LiCl (one equivalent) as the Cl source. The main feature of this reaction is the formation of a half rather than full-sandwich complex with the 6-Me-substituted ligand, similarly to **6**·toluene, supporting the idea that the steric clashing of the Me groups precludes the formation of a full-sandwich complex.

Attempts to employ the 6-Br-substituted ligand **3** or the CN-substituted ligand **4** with Fe^{II} using various salts ($FeCl_2$, $Fe(OTf)_2$ and $Fe(PF_6)_2$) and reaction stoichiometries were unsuccessful. This was in part due to the very low solubility of the ligands in a broad range of organic solvents and also their apparently low donor ability resulting from the electron-withdrawing effect of the substituents. In the case of **3**, the reduced donor ability and the resulting limited reactivity was confirmed by charge distribution studies (see Chapter 2.2, page 20).

Additional coordination studies involved Cu^{I} (Scheme 2.5), by way of comparison with the harder behaviour of Fe^{II} which favours *N*- rather than *P*-coordination. The reaction of $[Cu(MeCN)_4]PF_6$ with the methyl-substituted tris-pyridyl ligand **2** in a 2 : 1 ratio at room temperature gave the immediate formation of a bright yellow solution, from which crystals of $[(MeCN)_3Cu\{P(6\text{-Me-2-py})_3\}Cu(MeCN)](PF_6)_2$ (**8**) were isolated in 68 % yield (powder) after workup. Similarly, to the diamagnetic complex **5**, the P resonance of the $P(6\text{-Me-2-py})_3$ ligand in **8** is shifted upfield in the $^{31}P\{^1H\}$ NMR spectrum from −1.0 ppm ($CDCl_3$) for the uncoordinated ligand to −15.6 ppm (CD_3CN) in the copper(I) complex.

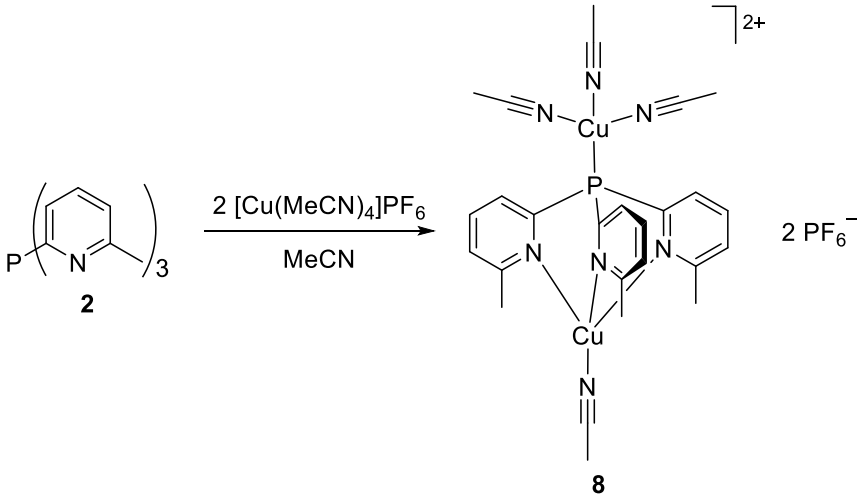

Scheme 2.5: *Synthesis of the copper(I) tris-2-pyridyl-phosphine complex **8**.*

The solution UV-Visible spectra of the 2-pyridyl-phosphine ligands **1** and **2** are presented in Figure 2.5 and show absorptions in the region of 250–340 nm. These transitions can most likely be attributed to π–π* transitions within the pyridine frameworks.

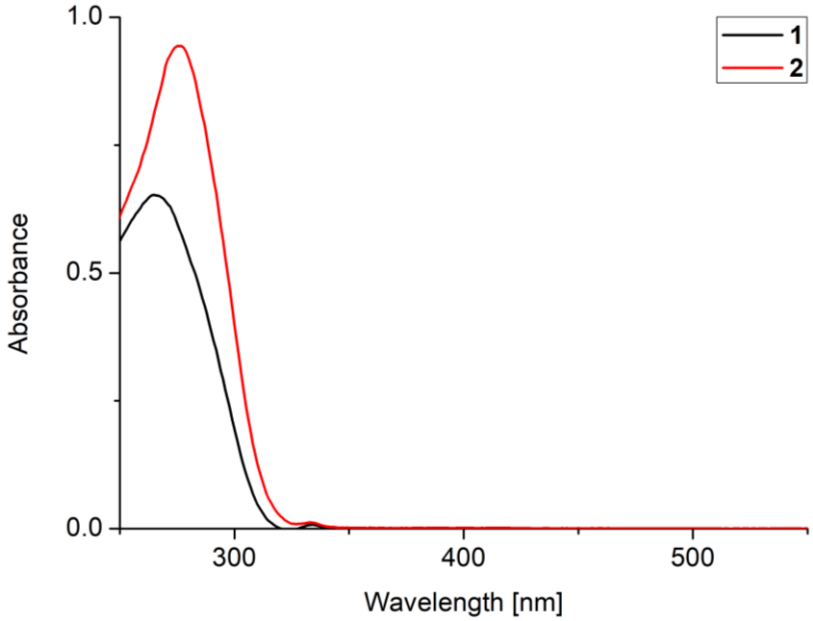

Figure 2.5: *UV-Vis spectra of the ligands **1** (black) and **2** (red). Spectra were recorded in DCM (both at a concentration of $5.0 \cdot 10^{-5}$ mol·L^{-1}). Background solvent corrections were applied.*

The iron and copper transition metal complexes **5**–**8** show a series of absorptions in the range 250–475 nm (Figure 2.6).

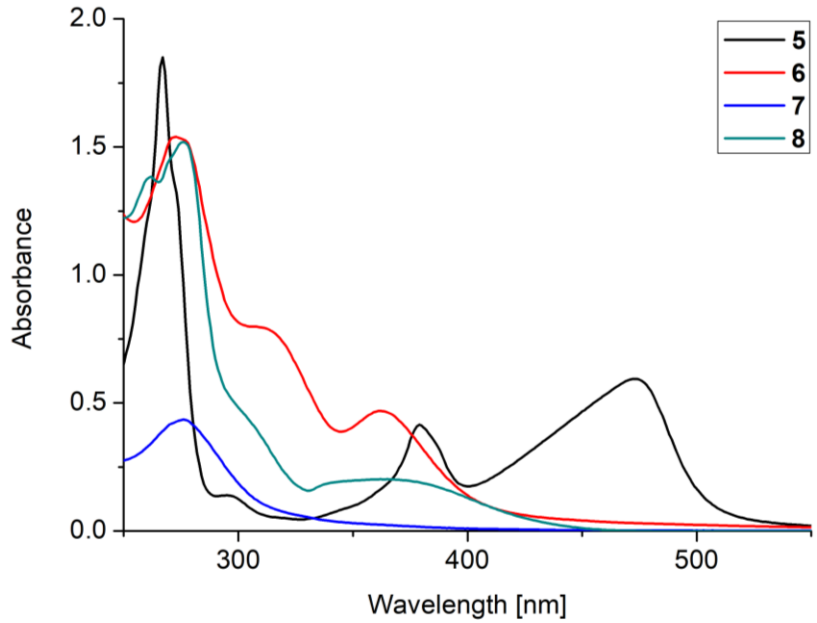

Figure 2.6: *UV-Vis spectra of **5** (black, in DCM), **6**·toluene (red, in DCM), **7**·2THF (blue, in MeOH) and **8** (green, in MeCN). All spectra were recorded at a concentration of $5.0 \cdot 10^{-5}$ mol·L^{-1}. Background solvent corrections were applied.*

The most intense transitions for all of the complexes are found at *ca.* 270–280 nm (ε = 30300–37000 L·cm^{-1}·mol^{-1}, Table 2.3) and are consistent with the absorption bands of ligands **1** and **2**. Therefore, these transitions are assigned as ligand centred transitions, such as π–π* transitions

within the pyridine frameworks. The remaining lower energy absorptions for the complexes **5**, **6**·toluene and **8** (ε = 3000–15000 $L \cdot cm^{-1} \cdot mol^{-1}$), which are responsible for the intense observed colours of the complexes, can be assigned to M–L charge transfer transitions. Similar observations were made for Cu^{I} complexes of tris-(2-pyridyl)-phosphine oxide.[29] Surprisingly, the iron(II) complex **7**·2THF does not exhibit any low-energy charge-transfer bands. Its pale yellow/orange colour therefore results entirely from the tail of the ligand-centred transition.

Table 2.3: *Molar extinction coefficients calculated from UV-Vis spectra (all at a concentration of $5.0 \cdot 10^{-5}$ mol·L^{-1}).*

Compound	Solvent	Wavelength λ [nm]	Absorbance	Molar ext. coefficient ε [$L \cdot cm^{-1} \cdot mol^{-1}$]
1	DCM	268.0	0.649	12976.5
2	DCM	281.0	0.905	18107.2
5	DCM	475.0	0.592	11834.3
		379.9	0.411	8227.6
		300.9	0.155	3091.5
		267.0	1.850	37003.1
6·toluene	MeCN	367.1	0.455	9102.5
		313.9	0.784	15682.3
		276.0	1.519	30379.6
7·2THF	MeOH	276.9	0.434	8685.3
8	MeCN	363.0	0.202	4036.6
		276.9	1.517	30344.8

2.3.1 Solid State Structures of the Transition Metal Complexes

The solid state structures of the new complexes [{P(2-py)$_3$}$_2$Fe](OTf)$_2$ (**5**), [{P(2-py)$_3$}FeCl$_2$]·toluene (**6**·toluene), [{P(2-py)$_3$}FeCl(OTf)]·2THF (**7**·2THF) and of [(MeCN)$_3$Cu{P(6-Me-2-py)$_3$}Cu(MeCN)](PF$_6$)$_2$ (**8**) were determined by single-crystal X-ray crystallography. Details of key bond lengths and angles found in these complexes are given in Table 2.4.

Table 2.4: *Selected bond lengths (Å) and angles (°) in the transition metal complexes* ***5–8*** *(M = Fe, Cu).*

	5	**6**·toluene	**7**·2THF	**8**
$P–C_{py}$	1.826(3)–1.837(3)	1.839(3)–1.845(3)	1.831(2)–1.840(3)	1.836(3)–1.840(3)
$M–N_{py}$	1.985(2)–2.008(2)	N(1/2)–Fe(1) 2.109(3)–2.117(2)	2.084(2)–2.257(2)	2.065(2)–2.079(3)
M···P	3.3339(8)–3.3693(8)	3.523(1)	3.3087(7)	Cu(1)···P(1) 3.1747(9) Cu(2)–P(1) 2.2022(9)
$C_{py}–P–C_{py}$	96.9(1)–101.6(1)	100.2(1)–107.3(1)	99.5(1)–107.2(1)	102.6(1)–104.1(1)
$P–C_{py}–N_{py}$	119.7(2)–121.1(2)	114.0(2)–123.3(2)	121.9(2)–122.4(2)	119.4(2)–120.5(2)
$N_{py}–M–N_{py}$	89.55(8)–92.94(9)	N(1)–Fe(1)–N(2) 102.91(9)	83.83(8)–103.26(7)	94.4(1)–97.5(1)

The structure of the cation of $[\{P(2\text{-py})_3\}_2Fe](OTf)_2$ (**5**) is shown in Figure 2.7. The two tris-2-pyridyl ligands of the cation coordinate the Fe^{II} centre using all three of the N atoms of each of the pyridyl ligands, forming a sandwich-type structure. The result is a distorted octahedral environment for the Fe centre. The relatively short $Fe–N_{py}$ bond lengths (1.985(2)–2.008(2) Å), are consistent with low-spin Fe^{II} as expected from the diamagnetic nature of **5**.[145] These bond lengths are similar to those found in the only other iron(II) sandwich cation of this type containing tris-2-pyridyl ligands, $[\{O=P(2\text{-py})_3\}_2Fe]^{2+}$ (2.007(3) Å,[146] 1.980(4)–1.984(3) Å).[147]

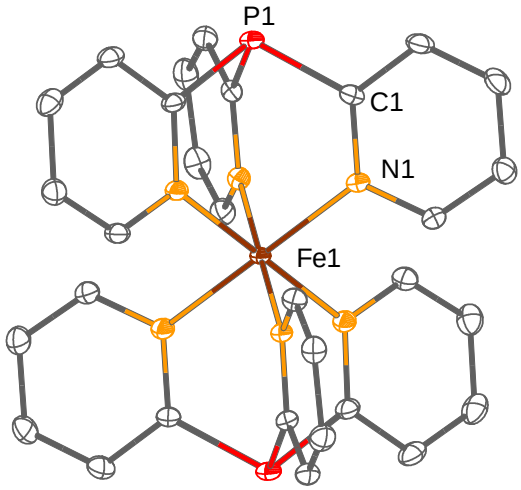

Figure 2.7: *Structure of the sandwich cation* $[\{P(2\text{-py})_3\}_2Fe]^{2+}$ *of* ***5****. Only one of the two molecules in the asymmetric unit is depicted. Triflate counterions and hydrogen atoms are omitted for clarity. Displacement ellipsoids are drawn at the 30 % probability level.*

The structure of **6**·toluene is shown in Figure 2.8. The Fe^{II} cation of the complex has a distorted tetrahedral geometry, being coordinated by two N atoms of the tris-2-pyridyl ligand and two Cl atoms. The Fe–N_{py} bond lengths are in the range 2.109(3)–2.117(2) Å and are noticeably longer than the Fe–N_{py} bonds in **5** despite the reduction in coordination number. The latter observation is consistent with the anticipated high-spin $t_2^3e^3$ configuration of the Fe^{II} centre. Interestingly, one of the pyridyl-nitrogen atoms does not coordinate to the iron(II) ion in the solid state structure and points away from the metal (Fe(1)···N(3) 4.266(3) Å).

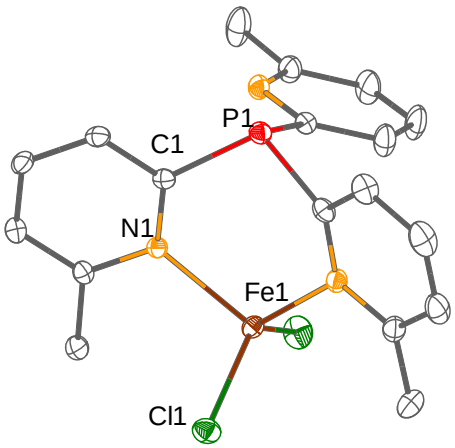

Figure 2.8: *Structure of [{P(6-Me-2-py)$_3$}FeCl$_2$]·toluene (**6**·toluene). Lattice-bound toluene molecules and hydrogen atoms are omitted for clarity. Displacement ellipsoids are drawn at the 30 % probability level.*

The formation of a half-sandwich type complex similar to **6**·toluene is also confirmed in the structure of **7**·2THF (Figure 2.9). Here, however, the presence of a more weakly coordinating OTf^- anion, which exhibits a long contact with the Fe^{II} ion (2.422(2) Å), leads to all three of the N atoms of the tris-2-pyridyl ligand engaging the Fe^{II} ion, so that the metal centre has a distorted trigonal-bipyramidal geometry. The weakness of the interaction of the triflate anion with the Fe^{II} centre is not only shown by the long Fe···O contact involved, but also from the fact that the Fe-coordinated Cl ligand is only marginally displaced from the P···Fe–Cl axis (18°). Associated with this is the elongation of the Fe–N_{py} bond *trans* to the Fe···O bond (Fe(1)–N(2) 2.257(2) Å; *cf.* Fe(1)–N(1) 2.117(2) Å, Fe(1)–N(3) 2.084(2) Å) in **7**·2THF.

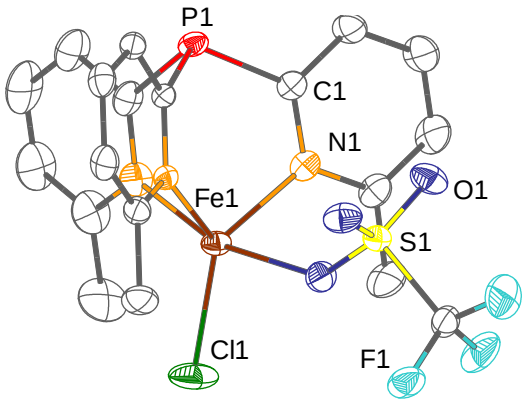

Figure 2.9: *Structure of [{P(6-Me-2-py)$_3$}FeCl(OTf)]·2THF (**7**·2THF). THF molecules and hydrogen atoms are omitted for clarity. Displacement ellipsoids are drawn at the 30 % probability level.*

The effect of the coordination of a softer Cu^{I} ion is illustrated in the structure of complex **8**, in which both the *N*- and *P*-coordinated sites are employed in metal coordination.

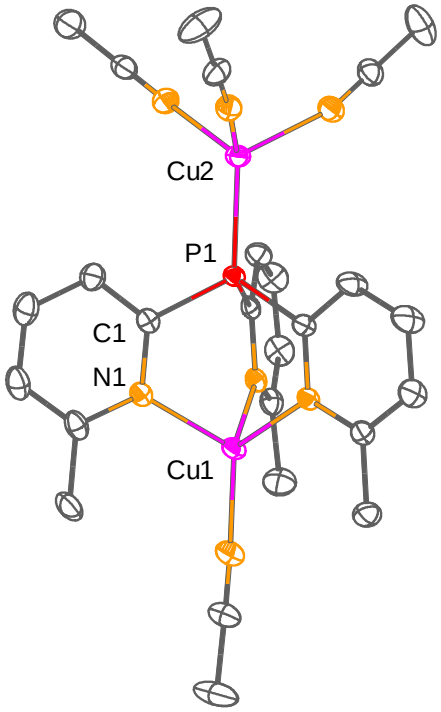

Figure 2.10: *Structure of the cation in [(MeCN)$_3$Cu{P(6-Me-2-py)$_3$}Cu(MeCN)](PF$_6$)$_2$ (**8**). Hydrogen atoms as well as the PF_6^- counterions are omitted for clarity. Displacement ellipsoids are drawn at the 30 % probability level.*

As shown in Figure 2.10, Cu(1) is coordinated by all three of the N atoms of the tris-2-pyridyl ligand as well as a MeCN ligand, while Cu(2) is coordinated by the bridgehead-P atom and by three MeCN ligands. Both Cu ions therefore attain distorted tetrahedral geometries. The ambidentate *N*,*N*′,*N*″-/*P*-coordination mode exhibited for the ligand in **8** is unprecedented for any tris-2-pyridyl ligand. Different ambidentate coordination modes have been found in the previously reported complexes

$[Mo_2(O_2CCF_3)_4\{P(2\text{-py})_3\}_2]$ (*N*-/*P*-),[72] $[Pd_2Cl_2(DMAD)\{P(2\text{-py})_3\}_2]$ (*N*-/*P*-) (DMAD = dimethyl acetylenedicarboxylate),[82] $[RuCl(PPh_3)_2\{P(2\text{-py})_3\}]$ (*N*,*N*′-/*P*-)[76] and $[CuCl_2\{P(2\text{-py})_3\}]_2$ (*N*,*N*′-/*P*).[67]

2.4 Attempted Synthesis of Heterobimetallic Tris-2-pyridyl-phosphine Complexes

As mentioned previously, 2-pyridyl-phosphines can adopt various coordination motifs with a range of different transition metals, which also include some homobimetallic complexes.[67,72,81,82] However, there are no reports in the literature concerning heterobimetallic tris-2-pyridyl-phosphine complexes, although phenyl-2-pyridyl [88,148] and (2-picolyl)-phosphine derivatives, such as $Ph_2P(2\text{-pic})$ or $PhP(2\text{-pic})_2$ (2-Pic = 2-picolyl, CH_2-2-py),[149,150] have proven to be suitable precursors for the synthesis of heterobimetallic transition metal compounds. The success of these phosphines can be attributed to their ability to act as Janus-head ligands that can coordinate *via* the pyridyl-nitrogen atoms as well as the phosphorus bridgehead. Due to the different electronic properties of the donor atoms, two different metals can be coordinated (Figure 2.11). The rigidity of the ligand frameworks induced by the small bite angle of the phosphines is also beneficial for this. Studies concerning the phenyl congener $Ph_2P(2\text{-py})$ have previously shown that this rigidity leads to the formation of interesting complexes containing M–M bonds.[151]

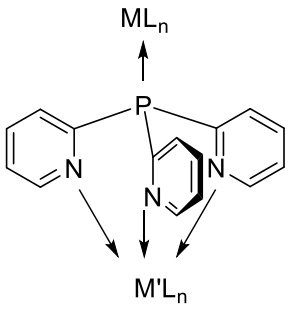

Figure 2.11: *Tris-2-pyridyl-phosphine has the potential to act as a Janus-head ligand and can potentially coordinate two different metals via the P and N donor atoms.*

Based on these previous results, the synthesis of heterobimetallic tris-2-pyridyl-phosphine complexes was attempted. The Fe^{II} sandwich complex **5** was reacted with $[Ni(MeCN)_6](BF_4)_2$ in acetonitrile. However, the desired heterobimetallic complex, in which the iron centre remains coordinated to the pyridyl-nitrogen atoms and the nickel(II) ion is coordinated to the P bridgehead, was not formed (Scheme 2.6). Only the pure complex **5** could be isolated from the reaction mixture, and ^{31}P NMR spectroscopy indicated no complexation *via* the phosphorus atom.

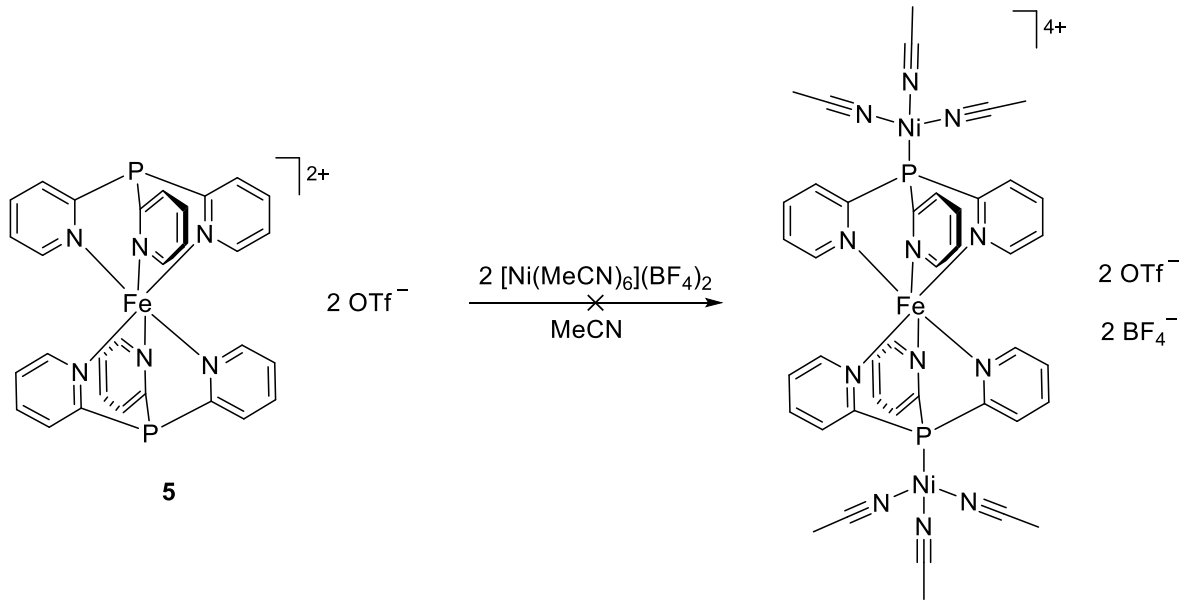

5

Scheme 2.6: *Attempted synthesis of a heterobimetallic 2-pyridyl-phosphine complex starting from complex* ***5****.*

Subsequently, the half-sandwich complex **6** was reacted with $[Ni(MeCN)_6](BF_4)_2$ in MeCN to obtain a Ni,Fe complex in which the Fe centre is coordinated to the pyridyl-N atoms and the Ni ion to the P bridgehead. The formation of a brown solution indicated a complexation reaction. However, instead of isolating the heterobimetallic species, red single-crystals of the nickel(II) tris-2-pyridyl-phosphine complex **9**, in which the nickel is tetrahedrally coordinated by the three pyridyl-N atoms and a chloride, were isolated. The chloro ligand originates from the iron(II) half-sandwich complex **6** (Scheme 2.7). The complex **9**·DCM represents the first solid state structure of a nickel(II) half-sandwich complex incorporating a tris-2-pyridyl-phosphine ligand. Previous work has only postulated the formation of $[\{P(2\text{-py})_3\}NiCl_2]\cdot H_2O$ on the basis of elemental analysis and mass spectrometry measurements.[131]

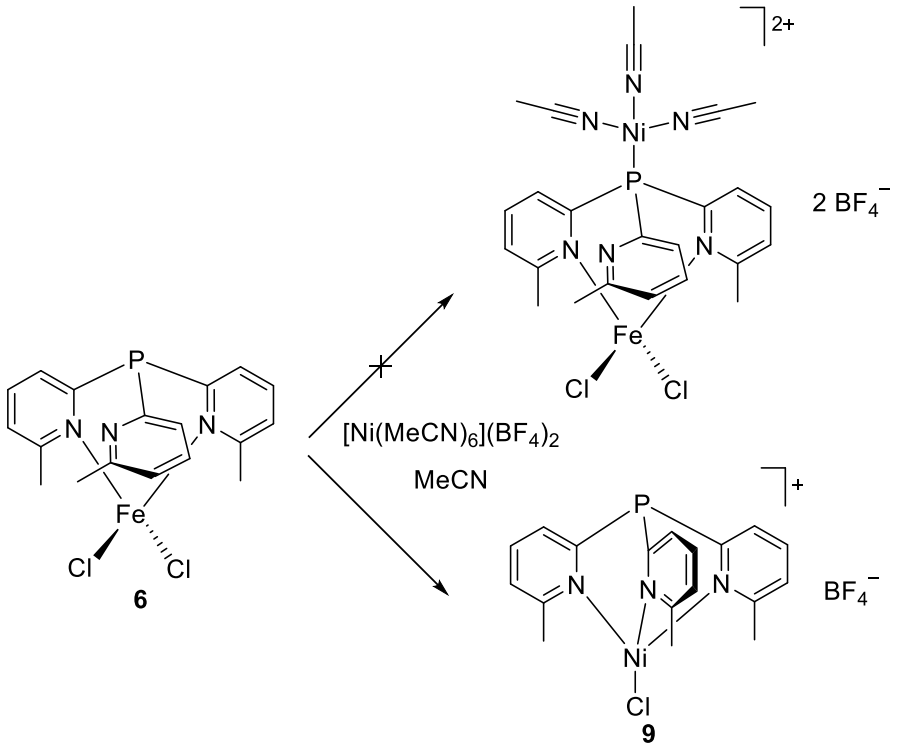

Scheme 2.7: *Formation of the nickel half-sandwich complex [{P(6-Me-2-py)$_3$}NiCl]BF$_4$·DCM (**9**·DCM).*

The paramagnetic complex **9**·DCM was characterised by single-crystal X-ray crystallography and its structure is shown in Figure 2.12.

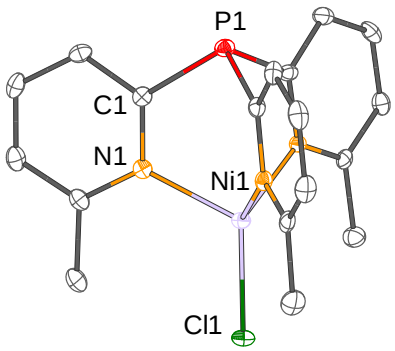

Figure 2.12: *Structure of the cation of [{P(6-Me-2-py)$_3$}NiCl]BF$_4$·DCM (**9**·DCM). The lattice-bound DCM molecule, the BF$_4^-$ anion, and the hydrogen atoms are omitted for clarity. Displacement ellipsoids are drawn at the 30 % probability level.*

Selected bond lengths and angles of the nickel(II) complex are listed in Table 2.5. The P–C$_{py}$ bond lengths of 1.829(4)–1.837(4) Å are in the same range as those observed for the iron(II) half-sandwich complexes **6**·toluene (1.839(3)–1.845(3) Å) and **7**·2THF (1.831(2)–1.840(3) Å), whereas the Ni–N$_{py}$ bond lengths of 2.020(3)–2.041(3) Å are slightly shorter than the Fe–N$_{py}$ bond lengths in the corresponding iron(II) complexes **6**·toluene (2.109(3)–2.117(2) Å) and **7**·2THF (2.084(2)–2.257(2) Å). This shortening of the M–N$_{py}$ bond lengths when the metal centre is changed from Ni^{II} to Fe^{II} is expected, since there is a decrease in ion radius. The smaller metal ion radius also results

in a shorter M···P contact. While the phosphorus bridgehead and the iron metal centres are 3.523(1) Å apart in **6**·toluene and 3.3087(7) Å in **7**·2THF, a Ni···P distance of only 3.238(1) Å was observed in the nickel complex **9**·DCM.

Table 2.5: *Selected bond lengths (Å) and angles (°) in the tris-2-pyridyl-phosphine nickel(II) complex* ***9****.*

	9·DCM
P–C_{py}	1.829(4)–1.837(4)
Ni–N_{py}	2.020(3)–2.041(3)
Ni···P	3.238(1)
C_{py}–P–C_{py}	100.4(2)–101.7(2)
P–C_{py}–N_{py}	120.4((3)–122.0(3)
N_{py}–Ni–N_{py}	94.9(1)–96.0(1)

2.5 Concluding Remarks

The current study of the effects of substitution at the 6-position of the pyridyl rings in P-bridged tris-pyridyl ligands of the type P(6-R-2-py)$_3$ (R = H, Me, Br, CN) illustrates a simple but nonetheless important result, namely, that such substitution does indeed limit the coordination of the ligands on steric grounds relative to the unsubstituted ligand. This is illustrated directly from the coordination studies of unsubstituted P(2-py)$_3$ (**1**) and P(6-Me-2-py)$_3$ (**2**) to Fe^{II}. Whereas **1** readily forms the cationic sandwich complex [{P(2-py)$_3$}$_2$Fe]$^{2+}$ (**5**), **2** forms only half-sandwich complexes of the type [{P(6-Me-2-py)$_3$}FeX_2] (**6** and **7**).

However, the enhanced steric encumbrance is not the only factor explaining the different behaviour of the ligands; the electronic effects of the substituents on the adjacent pyridyl nitrogen atoms also play a role. This can be seen from the fact that the ligand sets **1** and **2** can be easily protonated with hydrochloric acid, whereas the bromine-substituted derivative **3** cannot be purified from the crude reaction mixture by protonation, due to the lower basicity of the pyridyl-N atoms. This was confirmed by the calculation of the first free protonation enthalpies of the ligands and charge distribution studies. Consequently, the electron-withdrawing effect of the bromo- and cyano-substituents on the donor properties of the adjacent nitrogen donor atoms also alters the coordination behaviour of the ligands. While the tripodal ligands **2** and **3** coordinate easily to 3d transition metals, the ligand sets **3** and **4** show no coordination towards a variety of metal ions.

Unfortunately, no heterobimetallic complexes in which the tris-2-pyridyl-phosphines acted as Janus-head ligands could be synthesised starting from the sandwich complex **5** or the half-sandwich complex **6**. Instead, the nickel(II) tris-2-pyridyl half-sandwich complex **9** was isolated. In this

complex, the methyl-substituted 2-pyridyl-phosphine **2** chelates the metal centre *via* its three pyridyl-nitrogen atoms.

Although limited studies of the isovalent Al-ligand $[MeAl(6\text{-}Me\text{-}2\text{-}py)_3]^-$[37,39] and trifunctionalised tris-pyridyl-carbinol derivatives $MeOC(6\text{-}MeO\text{-}2\text{-}py)_3$[24] have been undertaken recently, to the best of our knowledge, this current study is the first in which the steric and electronic influence of substituents has been explored for any family of P-bridged neutral tris-pyridyl ligands. This is significant because these ligand systems, in contrast to the aluminate ligands, are significantly more robust and air stable than their metal-bridged counterparts and therefore easier to employ in Real-World settings. In particular, this feature makes ligands such as **2** potentially highly useful, 6-electron neutral capping ligands in single-site catalysis (in much the same way as formally anionic Cp* is employed).

3 Access to (Amino)- and (Alkoxy)-2-pyridyl-phosphines

3.1 Preamble

Although C_3-symmetric tris-2-pyridyl-phosphines have been studied in the last three decades,[9] unsymmetrical derivatives of 2-pyridyl-phosphines and chiral examples have been largely overlooked. The introduction of chirality into 2-pyridyl-phosphines is a logical extension of this area, since it is related to similar developments of other stereogenic phosphorus ligands, which have dominated the area of asymmetric catalysis, such as BINAP,[98] DuPHOS[14,15,17] and DIPAMP.[101,110]

To date, only a few unsymmetrical examples of 2-pyridyl-phosphines have been reported in the literature, most of which are based on phenyl analogues, such as diphenyl-2-pyridyl-phosphine, $Ph_2P(2\text{-py})$, and phenyl-bis(2-pyridyl)-phosphine, $PhP(2\text{-py})_2$.[66,89,152–157] Other derivatives, such as $(Me_2N)_2P(2\text{-py})$,[158] $(Et_2N)_2P(6\text{-O}^t\text{Bu-2-py})$,[159] $EtPhP(2\text{-py})$,[160] $CyP(2\text{-py})_2$,[161] lithiated phosphanylamine $[Li\{(2\text{-py})_2PNSiMe_3\}]_2$[162] or (2-picolyl)-phosphine derivatives, such as $Ph_2P(2\text{-pic})$, $PhP(2\text{-pic})_2$[149,163–165] and $Ph_2P(NSiMe_3)(2\text{-pic})$,[166,167] have been investigated but represent rare examples in this field. To the best of our knowledge, no enantiomerically pure 2-pyridyl-phosphine derivatives have been isolated and applied in asymmetric homogeneous catalysis.

Encouraged by the potential for new developments in this area, our focus was the exploration of simple synthetic routes to new multidentate 2-pyridyl-phosphine ligands, which possess another electronically different donor atom in addition to the pyridyl-nitrogen and the phosphorus bridgehead. This could be beneficial in terms of the hemilability of the ligands in corresponding transition metal catalysts during asymmetric organic transformations. For this purpose the focus was on the synthesis of (amino)-2-pyridyl-phosphines $(R_2N)_xP(2\text{-py})_{3-x}$ and (alkoxy)-2-pyridyl-phosphines $(RO)_xP(2\text{-py})_{3-x}$ (R = organic substituent, x = 1, 2, Figure 3.1).

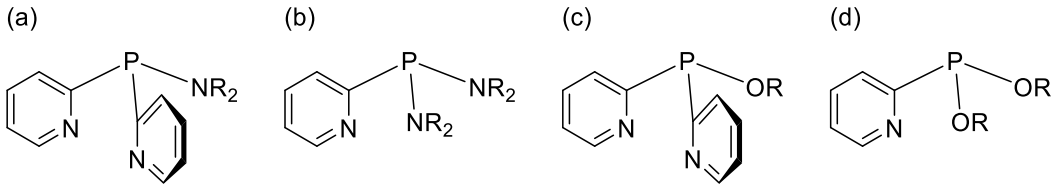

Figure 3.1: *Investigation of (a) (amino)-2-pyridyl- and (b) bis(amino)-2-pyridyl-phosphine ligands, as well as (c) (alkoxy)-2-pyridyl- and (d) bis(alkoxy)-2-pyridyl-phosphine ligands.*

Amino and alkoxy groups were selected as additional donor functionalities, since mixed P,N as well as P,O ligands have shown great success in asymmetric homogeneous catalysis, as mentioned in the introduction of this thesis.[103] (Amino)-2-pyridyl- and (alkoxy)-2-pyridyl-phosphines are also

potentially interesting precursors to other ligand frameworks, due to the greater polarity of the P–N[166] and P–O bonds compared to that of the P–C bond, which should render the ligand systems more reactive. For example, amino-phosphine precursors have previously been employed in the synthesis of (alkoxy)(amino)-phosphine ligands.[168–171]

The synthetic approach of the replacement of the pyridyl moieties in a 2-pyridyl-phosphine ligand framework is also an obvious way of introducing chirality (Figure 3.2). This can be achieved *via* the installation of an additional chiral donor group, for example chiral amines, amino acids or alcohols, since a large number of chiral amines and alcohols are commercially available. Chiral 2-pyridyl-phosphines can also be obtained through a P-stereogenic centre incorporating three chemically different substituents on the P bridgehead, since most phosphines are configurationally stable at room temperature with inversion barriers of more than 30 kcal·mol^{-1}.[172]

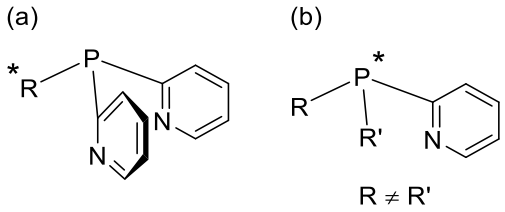

Figure 3.2: *Introduction of chirality via (a) a chiral donor group or (b) through a P-stereogenic centre.*

Some of the following sections were published in: S. Hanf, R. García-Rodríguez, S. Feldmann, A. D. Bond, E. Hey-Hawkins, D. S. Wright, *Dalton Trans.* **2017**, *46*, 814–824.

3.2 Synthesis of (Amino)-2-pyridyl-phosphines

In the current work, the (amino)-2-pyridyl-phosphines $(Me_2N)P(2\text{-py})_2$ (**10**) and $(Et_2N)P(2\text{-py})_2$ (**11**) were obtained from the reactions of the corresponding phosphorus chlorides $(Me_2N)PCl_2$[173] and $(Et_2N)PCl_2$,[174] (respectively) with *in-situ* generated 2-pyridyllithium at −78 °C in a 1 : 2 molar ratio (Scheme 3.1).

This synthetic approach was selected rather than the reaction of a chloro-2-pyridyl-phosphine precursor with an amine, since it is not possible to synthesise the key compound $Cl_xP(2\text{-py})_{3-x}$ (x = 1, 2) by variation of the stoichiometry in the reaction of PCl_3 with Li(2-py). This reaction leads exclusively to the formation of the tri-substituted compound $P(2\text{-py})_3$.[26] Only very recently has a route to $Cl_2P(2\text{-py})$ been introduced; this route involves the reaction of a 2-pyridyl organo-zinc intermediate with PCl_3 in a two-step synthesis.[175] Primary amino substituents (RNH) were not employed because the reactions of primary amines (RNH_2) with PCl_3 normally produce P–N ring compounds.[176]

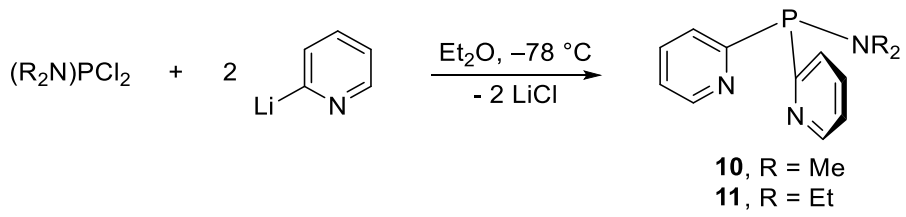

Scheme 3.1: *Synthesis of the (amino)-2-pyridyl-phosphines **10** and **11**.*

The reaction of $(Me_2N)PCl_2$ and Li(2-py) produced a mixture of compound **10** and other unidentified P-containing products (86 % product, 14 % side products according to $^{31}P\{^1H\}$ NMR spectroscopy, in addition to LiCl). Pure samples of $[\{(Me_2N)P(2\text{-py})_2\}(LiCl)_3\cdot 2THF]_2$ ($[\mathbf{10}(LiCl)_3\cdot 2THF]_2$) could be obtained by crystallisation. Single-crystal X-ray analysis of $[\mathbf{10}(LiCl)_3\cdot 2THF]_2$ shows that the two $(Me_2N)P(2\text{-py})_2$ ligands in the molecular structure chelate two separate Li^+ cations using their two pyridyl-nitrogen atoms (Figure 3.3, left), with the NMe_2 groups of each ligand remaining uncoordinated. A dimeric structure containing a central hexameric $(LiCl)_6$ core (Figure 3.3, right) is formed, in which two $(LiCl)_2$ ring units are bridged by two $(Me_2N)P(2\text{-py})_2$-chelated Li^+ and two Cl^- ions. To the best of our knowledge, the $(LiCl)_6$ core arrangement is unprecedented among previously reported Li-salt complexes. Interestingly, the NMe_2 group of the $(Me_2N)P(2\text{-py})_2$ ligand in $[\mathbf{10}(LiCl)_3\cdot 2THF]_2$ is almost planar (sum of RNR angles is 360°). This is similar to the situation found in the tungsten(0) complex $[W(CO)_4\{(Me_2N)_2P(2\text{-py})\}]$, in which one of the NMe_2 groups is again almost planar.[158]

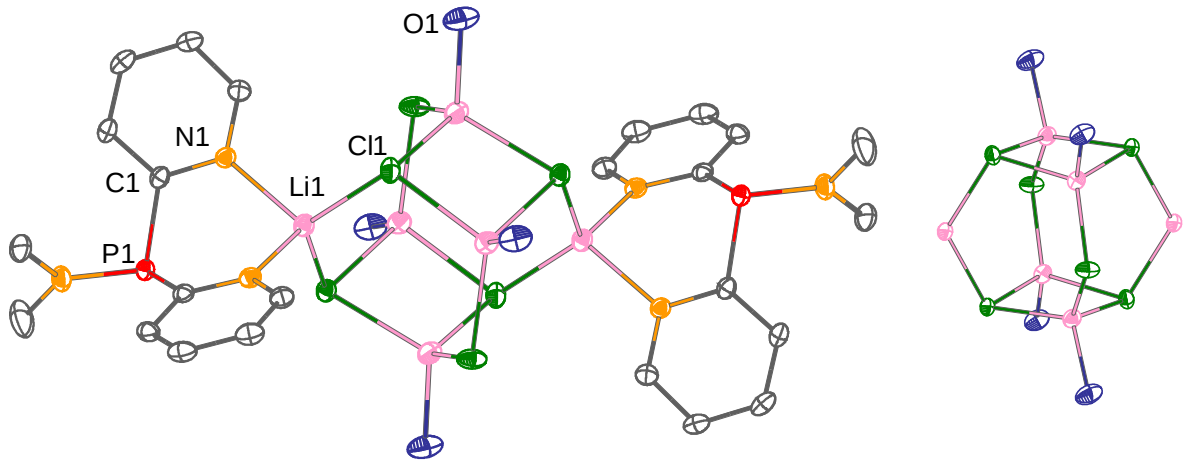

Figure 3.3: *Structure of $[\{(Me_2N)P(2\text{-py})_2\}(LiCl)_3\cdot 2THF]_2$ ($[\mathbf{10}(LiCl)_3\cdot 2THF]_2$, left) and the $(LiCl)_6$ core (right). Hydrogen atoms and carbon atoms of the THF moieties are omitted for clarity. Displacement ellipsoids are drawn at the 30 % probability level.*

The reaction of $(Et_2N)PCl_2$ and Li(2-py) leads to the formation of a mixture of $[\{(Et_2N)P(2\text{-py})_2\}LiCl]_2$ ($[\mathbf{11}\cdot LiCl]_2$) and another unidentified P-containing product, as well as LiCl. The pure product could be isolated by crystallisation using THF and *n*-hexane. Again, as seen in the case of

[**10**(LiCl)$_3$·2THF]$_2$, X-ray crystallography revealed the presence of two (amino)-2-pyridyl ligands, which coordinate to Li^+ cations *via* their two pyridyl-nitrogen donor atoms (Figure 3.4). Neither the phosphorus bridgehead nor the amino-nitrogen atom are involved in any coordination. In contrast to the hexameric LiCl core in [**10**(LiCl)$_3$·2THF]$_2$, only one (LiCl)$_2$ ring unit is present in the structure of [**11**·LiCl]$_2$.

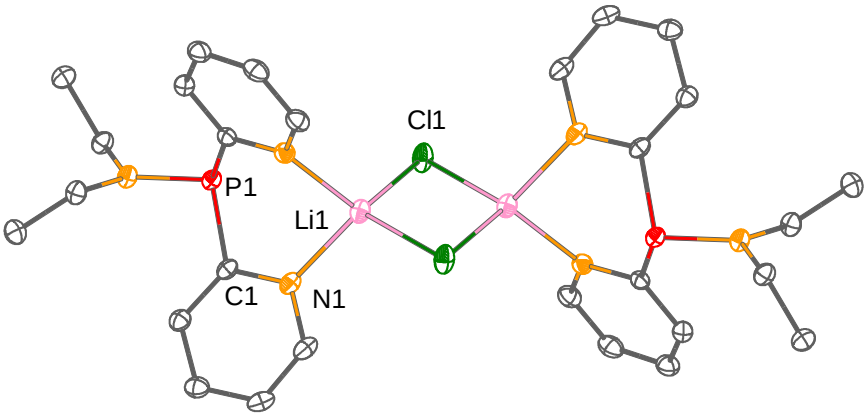

Figure 3.4: *Structure of [{(Et$_2$N)P(2-py)$_2$}LiCl]$_2$ ([**11**·LiCl]$_2$). Hydrogen atoms are omitted for clarity. Displacement ellipsoids are drawn at the 30 % probability level.*

As observed in [**10**(LiCl)$_3$·2THF]$_2$, the NEt$_2$ group of the (Et$_2$N)P(2-py)$_2$ ligand is planar (sum of RNR angles is 360°). DFT calculations (BP86,[136–138] def2-TZVP,[139,140] see Chapter 8.4, page 134) on [**11**·LiCl]$_2$ and the isolated ligand **11** (without the LiCl core) show that the HOMO–4 and the HOMO involve significant electron-donation from the N lone-pair of the NEt$_2$ group into one of the P–C(2-py)σ* orbitals (Figure 3.5). NBO[177] and second-order perturbation analyses of [**11**·LiCl]$_2$ and **11** (at the same level of theory) support this conclusion. Donor-acceptor interactions between the amino-nitrogen lone pair and the two P–C(2-py)σ* orbitals were calculated to have stabilisation energies of 5.54 and 6.0 kcal·mol^{-1} for [**11**·LiCl]$_2$ and 4.44 and 5.72 kcal·mol^{-1} for **11**. This explains the nearly planar geometry of the N atom of the NEt$_2$ group observed in the solid state structure of [**11**·LiCl]$_2$.

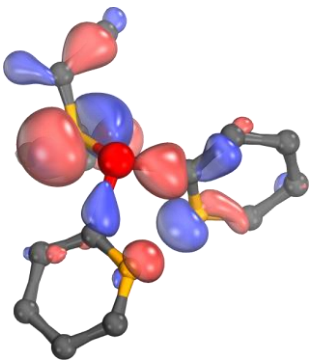

Figure 3.5: *HOMO of the free ligand (Et$_2$N)P(2-py)$_2$ (**11**, BP86,[136–138] def2-TZVP[139,140]). Plotting-threshold: 70 %.*

The reaction of $(Et_2N)_2PCl$[178] and Li(2-py) in a 1 : 1 molar ratio gives the bis(amino)-2-pyridyl-phosphine $(Et_2N)_2P(2\text{-py})$ (**12**, Scheme 3.2). After fractional distillation, compound **12** can be obtained as a pale yellow oil (in 57 % yield).

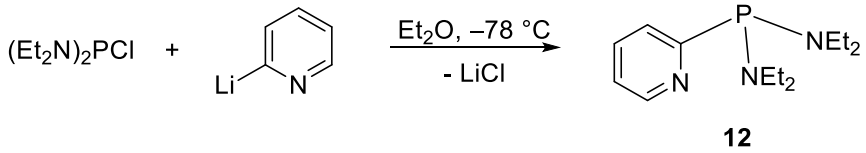

12

Scheme 3.2: *Synthesis of the bis(amino)-2-pyridyl-phosphine **12**.*

As part of this study, the related ligand $Ph(Et_2N)P(2\text{-py})$ (**13**) was synthesised from the reaction of Li(2-py) with $Ph(Et_2N)PCl$[179] (Scheme 3.3, in 33 % yield). Since **13** has three different organic substituents, the phosphine is P-stereogenic, although it is obtained as a racemic mixture.

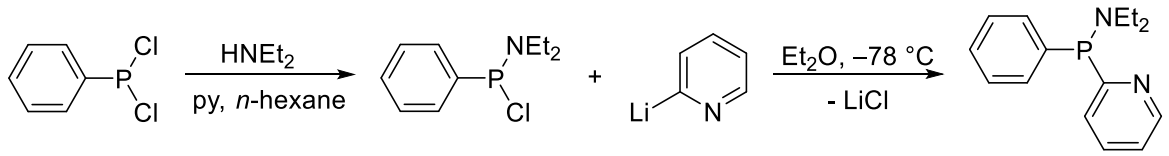

13

Scheme 3.3: *Synthesis of the (amino)-2-pyridy-phosphine **13**, which is obtained as racemic mixture.*

3.3 Synthesis of (Alkoxy)-2-pyridyl-phosphines

The extension of the previous synthetic methodology for (amino)-2-pyridy-phosphines to alkoxy-substituted 2-pyridyl-phosphines was a logical next step. Unfortunately, the reaction of $(RO)_xPCl_{3-x}$ (x = 1, 2) and Li(2-py) only resulted in the formation of an intractable mixture of products. However, the reaction of the (amino)-2-pyridyl-phosphines [**10**$(LiCl)_3 \cdot 2THF]_2$ and **12** with various alcohols has proven to be a straightforward strategy to the desired (alkoxy)-2-pyridyl-phosphines (Scheme 3.4). The crude compound **10** (including LiCl and some minor P-containing impurities), instead of the more easily assessable ethyl congener **11** was selected as the precursor, since the bulk purity of **10** could be improved. This synthetic method gives access to the rarely studied ligand class[159,180,181] of multidentate (alkoxy)-2-pyridyl-phosphines, which were previously not readily accessible, due to the synthetic challenges involved in the synthesis of the key precursors $Cl_xP(2\text{-py})_{3-x}$ (x = 1, 2).[26,175]

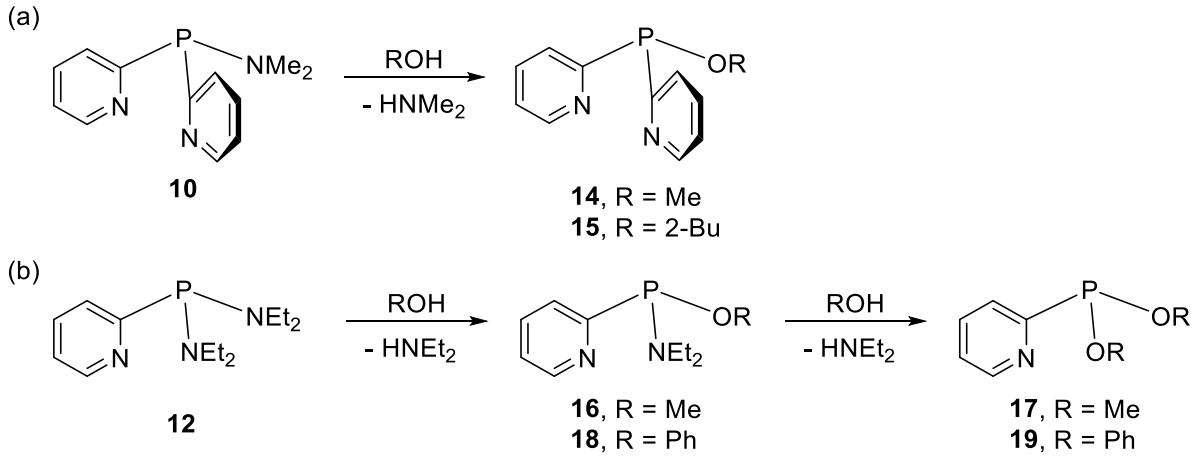

Scheme 3.4: *Synthesis of (a) (alkoxy)-2-pyridyl- and (b) bis(alkoxy)-2-pyridyl-phosphines (R = Me, 2-Bu, Ph).*

The NMe_2 group in the (amino)-2-pyridyl-phosphine [**10**$(LiCl)_3 \cdot 2THF]_2$ can easily be replaced by a variety of alcohols. The reaction of MeOH with crude **10** gives the dimeric LiCl complex $[\{(MeO)P(2\text{-}py)_2\}LiCl]_2$ ([**14**$\cdot LiCl]_2$) after crystallisation (Figure 3.6).

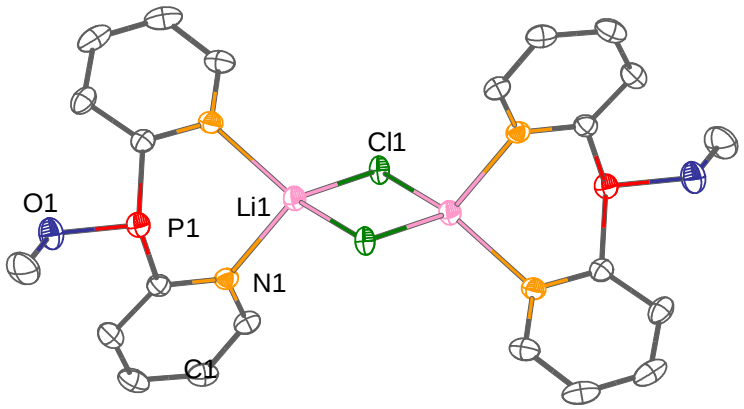

Figure 3.6: *Structure of* $[\{(MeO)P(2\text{-}py)_2\}LiCl]_2$ ([**14**$\cdot LiCl]_2$). *Hydrogen atoms are omitted for clarity. Displacement ellipsoids are drawn at the 30 % probability level.*

This method was readily extended to the more sterically demanding 2-butanol. The reaction of crude **10** with racemic 2-butanol results in the formation of $(2\text{-BuO})P(2\text{-py})_2$ (**15**). The solid state structure of **15** (Figure 3.7) also consists of a dimeric lithium chloride complex [**15**$\cdot LiCl]_2$, with a similar molecular structure to [**14**$\cdot LiCl]_2$.

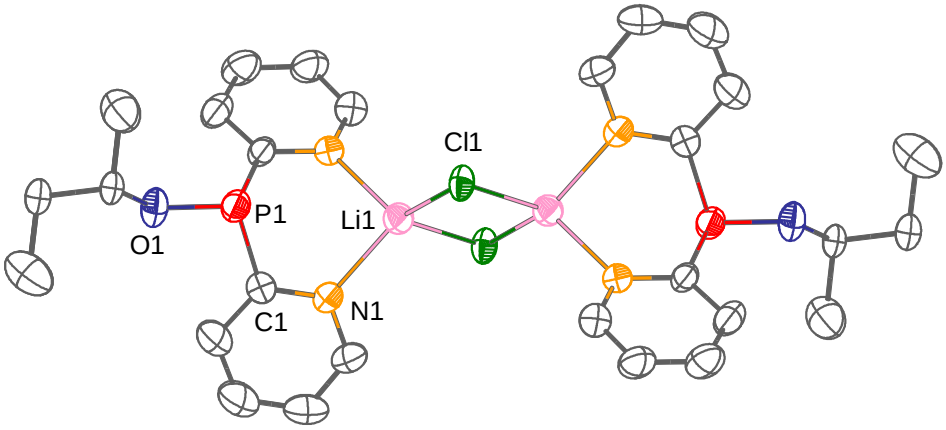

Figure 3.7: *Structure of [{(2-BuO)P(2-py)$_2$}LiCl]$_2$ ([**15**·LiCl]$_2$). Hydrogen atoms are omitted for clarity. Displacement ellipsoids are drawn at the 30 % probability level.*

This strategy allows the facile introduction of chirality using the commercially available (*S*)- and (*R*)-enantiomers of 2-butanol. *In-situ* ^{31}P NMR spectroscopic studies employing the chiral alcohols in place of racemic 2-butanol indicate *ca.* 90 % conversion to the corresponding chiral phosphines (**15**-*S* and **15**-*R*) under the same conditions, which were not further isolated.

A comparison of the phosphine ligands in the structures of [**10**(LiCl)$_3$·2THF]$_2$, [**14**·LiCl]$_2$ and [**15**·LiCl]$_2$ shows that those of the alkoxy-substituted ligands are more pyramidal, with the sum of the bond angles about the P atoms being 309° in [**10**(LiCl)$_3$·2THF]$_2$, 296° in [**14**·LiCl]$_2$ and 298° in [**15**·LiCl]$_2$ (despite the increase in the steric congestion in [**15**·LiCl]$_2$ compared to that in [**10**(LiCl)$_3$·2THF]$_2$). This trend can be interpreted in terms of VSEPR theory, since there is less bonding-pair/bonding-pair repulsion in the (alkoxy)-2-pyridyl-phosphines.

The reaction of (Et$_2$N)$_2$P(2-py) (**12**) with different alcohols allows the stepwise introduction of alkoxy groups, depending on the nucleophilicity of the alcohol used. In the case of the more nucleophilic MeOH, the isolation of the mono-substituted product (Et$_2$N)(MeO)P(2-py) (**16**) did not prove to be possible at room temperature, since the di-substituted product (MeO)$_2$P(2-py) (**17**) is formed simultaneously even in the 1 : 1 stoichiometric reaction of **12**. *In-situ* ^{31}P NMR spectroscopic studies revealed that after the formation of *ca.* 30 % of **16**, the formation of di-substituted **17** begins to occur. Di-substituted (MeO)$_2$P(2-py) (**17**) is obtained from the reaction of **12** in MeOH as the solvent. In contrast, an *in-situ* ^{31}P NMR spectroscopic study of the reaction of PhOH with **12** in toluene at reflux shows that the 1 : 1 reaction produces mono-substituted (Et$_2$N)(PhO)P(2-py) (**18**), while the addition of a second equivalent gives the di-substituted product (PhO)$_2$P(2-py) (**19**) (Figure 3.8). The new ligands **17**, **18** and **19** can be obtained easily from the preparative scale reactions as pale yellow oils (in 73 % [**17**], 86 % [**18**], 44 % [**19**] yield).

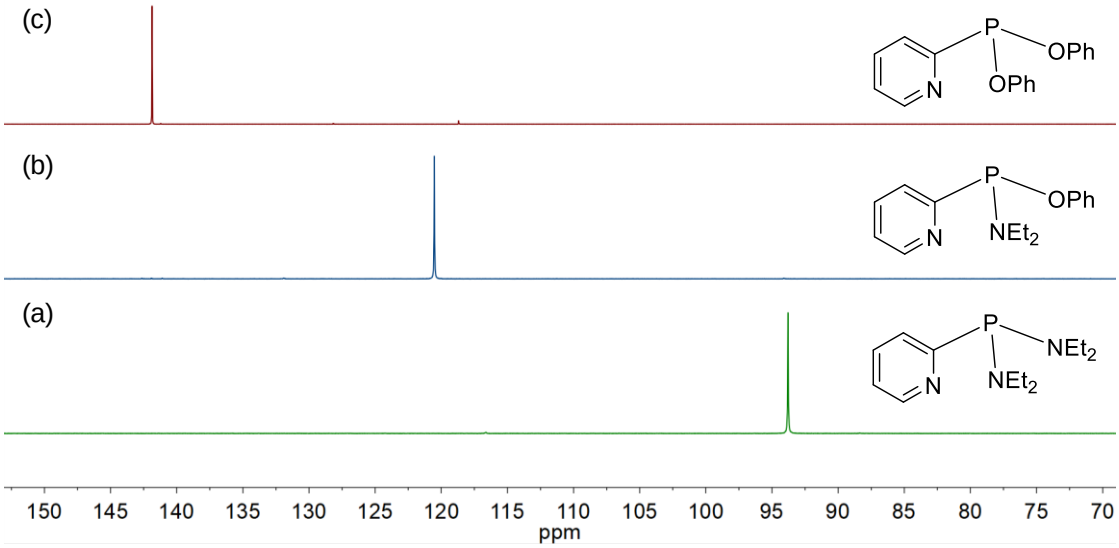

Figure 3.8: *$^{31}P\{^{1}H\}$ NMR spectra showing the progress of the reaction of **12** with PhOH; (a) the pure starting material, (b) addition of 1 equivalent of PhOH at reflux in toluene, (c) addition of a further equivalent of PhOH.*

3.4 Chiral (Amino)- and (Alkoxy)-2-pyridyl-phosphines

Unlike their amine counterparts, most P-stereogenic phosphines are stable at room temperature and can therefore be isolated as enantiomerically pure compounds.[172] The enhanced configurational stability of phosphines can be explained by rehybridisation, which must occur during the inversion process. During the configurational transformation, a trigonal-planar transition state is adopted, in which the hybridisation of the inverting centre, in this case the P atom, changes from sp^3 to sp^2. At the same time, the P lone pair occupies a p orbital in the transition state (TS, Figure 3.9). Since phosphorus is less electronegative than nitrogen, the s-character of the lone pair is enhanced, which leads to a higher inversion barrier for the rehybridisation.[182] The inversion barrier of trivalent group 15 compounds is also often related to a second-order Jahn-Teller effect.[183] The transformation of the pyramidal C_{3v}-symmetric ground state to the planar D_{3h}-symmetric transition state is associated with an activation energy, which is caused by the increase in the HOMO energy due to the loss of HOMO-LUMO orbital mixing. This activation energy is more significant for phosphines than for amines due to the larger ground-state HOMO-LUMO mixing.[182]

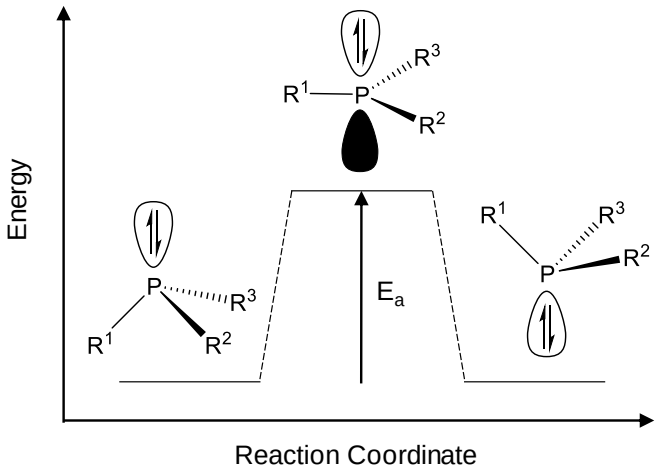

Figure 3.9: *Inversion of tertiary tetrahedral phosphines via a trigonal-planar transition state.*

It has been shown that there is a strong dependence of the inversion barrier on the nature of the substituents attached to the phosphorus atom.[184] For example, increasing the bulk of the substituents lowers the inversion barrier, since the steric encumbrance destabilises the pyramidal phosphine ground state. π-Delocalisation of the lone pair into neighbouring orbitals also decreases the inversion barrier, since the ground state is already flattened. In contrast, heteroatom substituents tend to lead to an enhanced inversion barrier, due to the presence of non-bonded electron pairs on the substituents.[184]

Although the phosphines **13** and **18** contain unsymmetrical substituted P atoms, with three different organic substituents attached to the phosphorus bridgehead (Figure 3.10), they were obviously obtained as a racemic mixture and not as stereogenically pure phosphines.

13 **18**

Figure 3.10: *Potentially P-chiral 2-pyridyl-phosphine ligands **13** and **18**.*

The inversion barriers of the phosphines were calculated using DFT methods, employing the PWPB95[185] functional in conjunction with the def2-QZVP[139,140] basis set (see Chapter 8.4, page 134). Figure 3.11 depicts the pyramidal ground states of the phosphines and the trigonal-planar transition states. The sum of the R–P–R angles in the pyramidal ground state of **13** is 306.8°, whereas the sum of these angles is 301.1° in the ground state of **18**. This observation leads to the conclusion that **13** most likely exhibits a smaller inversion barrier than **18**, since the pyramidal ground state is slightly flattened. The sum of the R–P–R angles in the planar transition states was found to be 360°.

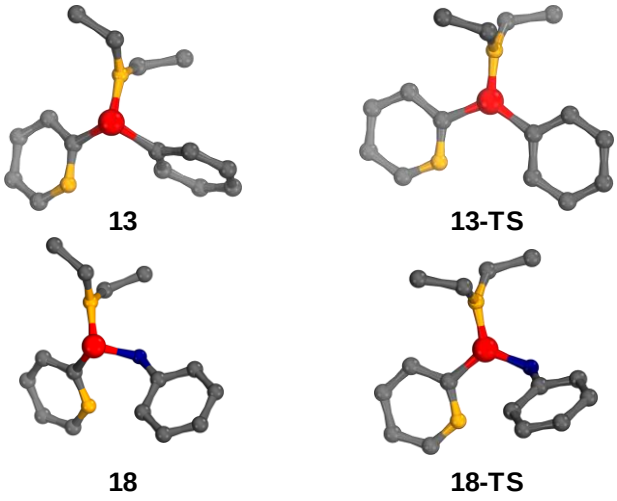

Figure 3.11: *Calculated ground and transition states for the inversion of* ***13*** *and* ***18****.*

The calculated inversion barrier for compound **13** amounts to E_a = 28.55 kcal·mol^{-1} (119.46 kJ·mol^{-1}), whereas the inversion activation energy of **18** is significantly higher with E_a = 46.51 kcal·mol^{-1} (194.61 kJ·mol^{-1}). This is somewhat expected, since the electron-withdrawing effect of the phenoxy group increases the s-character of the P lone pair, which increase the energy of the rehybridisation process of the P lone pair during the inversion.

The localised molecular orbitals of the P lone pair for **13** (HOMO–12) and **18** (HOMO–11) are depicted in Figure 3.12. Loewdin population analyses of these two molecular orbitals show that the s-orbital contribution of the phosphorus atom in **13** is 14.91 %, which is slightly lower than that of the phenoxy-phosphine **18** at 17.79 %. This agrees with the observed lower sum of the R–P–R angles and the higher inversion barrier of **18**.

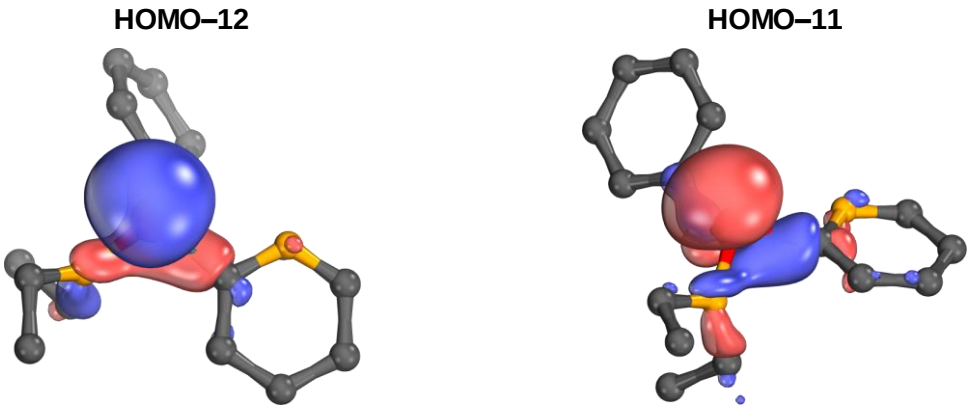

P: 9.8 % s, 4.2 % p_x, 46.8 % p_y 4.9 % p_z
N_{Et}: 1.5 % p_y, 1.8 % p_z
C_{py}: 3.7 % p_x, 1.7 % d_{xy}
C_{Ph}: 2.3 % p_y

P: 10.6 % s, 3.1 % p_x, 42.9 % p_y, 3.0 % p_z
N_{Et}: 1.6 % p_y
C_{py}: 5.8 % p_x
O: 6.2 % p_y

Figure 3.12: *Localised molecular orbitals of (Et_2N)(Ph)P(2-py) (**13**, left) and (Et_2N)(PhO)P(2-py) (**18**, right), including Loewdin population analyses (≥1.5 %). Plotting-threshold: 70 %.*

Using the Eyring equation (Equation 3-1), the half-life of the inversions of the P-stereogenic phosphines can be calculated.

$$k_{rac} = \frac{k_B T}{h} e^{\frac{-\Delta G}{RT}} \quad (3\text{-}1)$$

$$t_{1/2} = \frac{\ln 2}{k_{rac}} \quad (3\text{-}2)$$

For phosphine **18**, $t_{1/2} = 1.7 \cdot 10^{16}$ days, whereas the $t_{1/2}$ is 1122.8 days for phenyl-2-pyridyl-phosphine **13**, which has a lower inversion barrier. These half-lives, as well as the quite high inversion barriers, should allow the isolation of the individual enantiomers, which could then be employed as chiral ligands in asymmetric homogeneous catalysis.

In order to acquire enantiomerically pure phosphines, the compounds can either be stereoselectively synthesised using stoichiometric amounts of a chiral auxiliary or prepared by asymmetric catalysis.[186–188] Moreover, P-stereogenic phosphines can be obtained by resolution of a racemic mixture using chemical resolution methods (by the use of chiral auxiliaries or cyclometallated Pd compounds) or by direct resolution employing preparative HPLC (high-performance liquid chromatography) methods.[187,188] Since phosphines **13** and **18** were obtained as racemic mixtures, direct resolution by HPLC was attempted. The phosphines were borane-protected using $BH_3 \cdot SMe_2$ to avoid any oxidation of the P bridgehead during the separation process (Scheme 3.5).

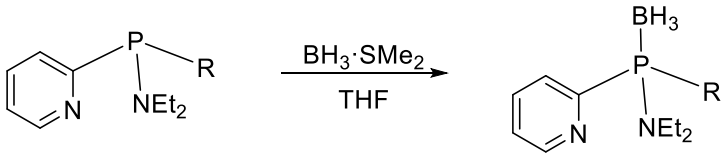

13, R = Ph
18, R = OPh

BH$_3$-13, R = Ph
BH$_3$-18, R = OPh

Scheme 3.5: *Borane-protection of the (amino)- and (alkoxy)-2-pyridyl-phosphines **13** and **18**.*

Chiral screening on an analytical scale was carried out by the company Phenomenex. The samples were screened in reverse and polar organic mobile phase conditions with seven different stationary phases. For the phenyl-2-pyridyl-phosphine **BH$_3$-13**, the best separation of the racemate was achieved with a cellulose-based column (Lux Cellulose-3) in reverse phase conditions (Figure 3.13). A mixture of ammonium bicarbonate:acetonitrile:diethylamine (40:60:0.1) was used as the eluent and a resolution of 5.76 was obtained. The results suggest that the two peaks represent enantiomers, as their peak-area ratios remain constant at multiple wavelengths and their absorption spectra overlap well. Their peak-area ratios are approximately 1:1, as expected. The separation of the racemic mixture was also possible in polar organic conditions on the same column using

ethanol:isopropanol:diethylamine (90:10:0.1) as the eluent. However, a slightly worse resolution of 2.96 was obtained.

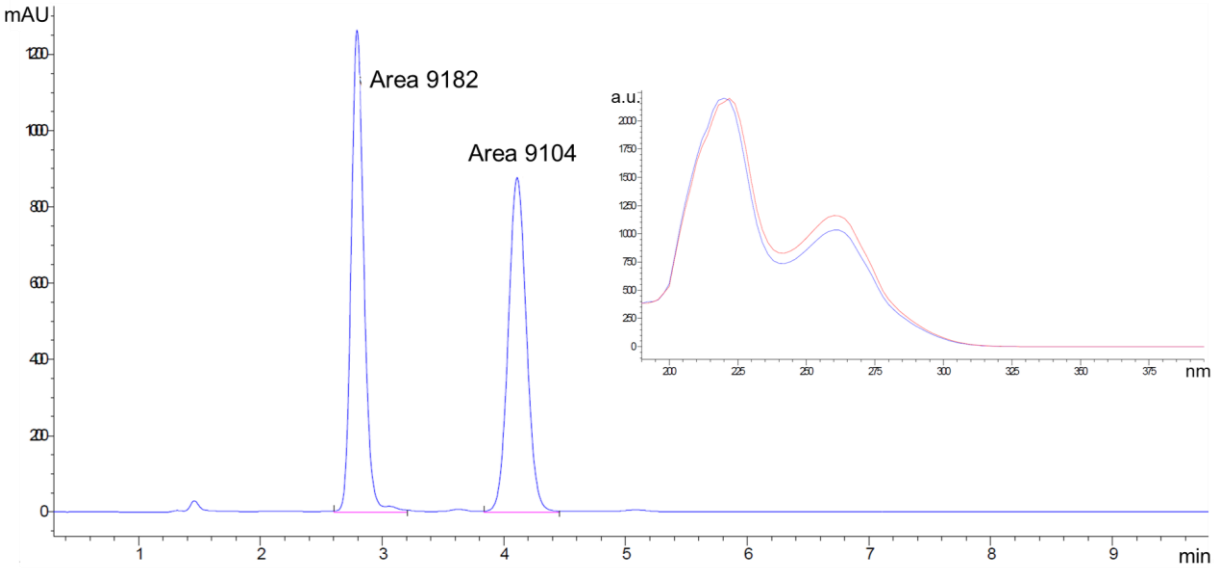

Figure 3.13: *HPLC chromatogram of* ***BH_3-13*** *(stationary phase: Cellulose-3 100 mm x 4.6 mm, mobile phase: 20 mM ammonium bicarbonate:acetonitrile:diethylamine 40:60:0.1). Insert: UV-Vis spectrum (detection: 254 nm).*

The racemic mixture of **BH_3-18** could also be separated using the same cellulose-based column in reverse phase conditions (Figure 3.14). A mixture of ammonium bicarbonate, acetonitrile and diethylamine in a 46:54:0.1 ratio was used, and a resolution of 2.67 was achieved. Again, it is logical to assume that the two main peaks represent enantiomers, as their peak-area ratios remain constant at multiple wavelengths, their absorption spectra overlap well, and their peak-area ratios are approximately 1:1, as expected. The smaller peaks at retention times of about 2 min probably represent some hydrolysis products, since the compounds are not stable under air over a prolonged amount of time.

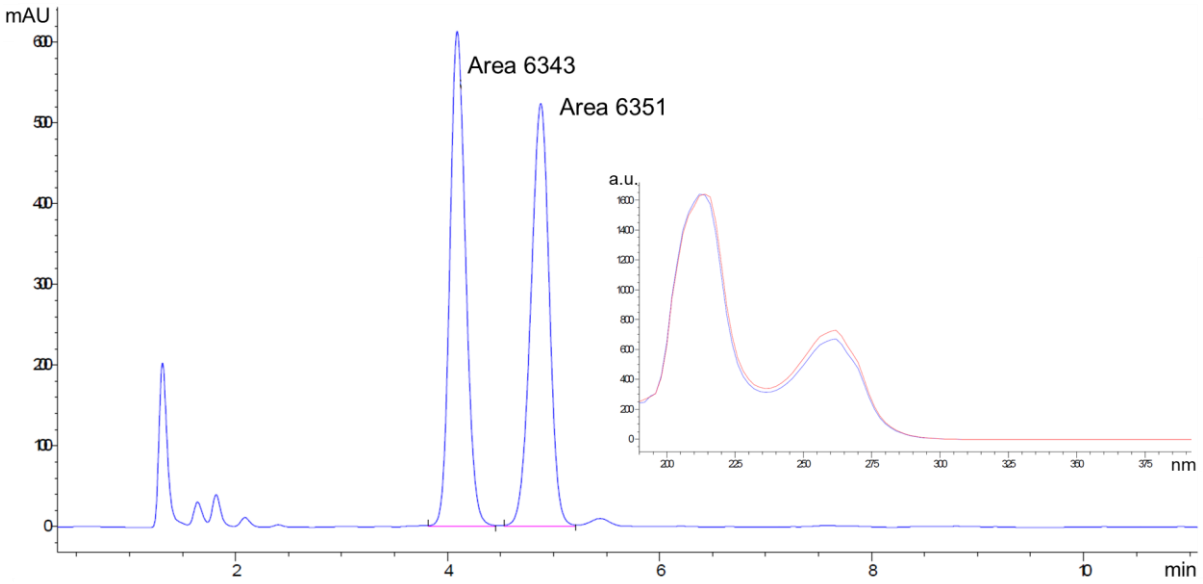

Figure 3.14: *HPLC chromatogram of* ***BH$_3$-18*** *(stationary phase: Cellulose-3 100 mm x 4.6 mm, mobile phase: 20 mM ammonium bicarbonate:acetonitrile:diethylamine 46:54:0.1). Insert: UV-Vis spectrum (detection: 254 nm).*

Although the chiral screening and the separation of the phosphine enantiomers was done on an analytical scale, upscaling to a preparative scale will enable the isolation of the enantiopure materials in quantities sufficient for the synthesis of chiral transition metal catalysts, which can then be applied in asymmetric homogeneous catalysis.

3.5 Copper(I) Complexes of (Amino)- and (Alkoxy)-2-pyridyl-phosphines

In the past, copper(I) 2-pyridyl-phosphine complexes have been of interest in catalysis[68,128] and for their photo-optical properties.[189–193] Therefore, the coordination chemistry of the synthesised (amino)- and (alkoxy)-2-pyridyl-phosphine ligands was studied with the soft transition metal ion Cu^I.

Attempts to employ the mono-substituted ligands $(Me_2N)P(2\text{-py})_2$ ([**10**$(LiCl)_3 \cdot 2THF]_2$) and $(Et_2N)P(2\text{-py})_2$ ([**11**$\cdot LiCl]_2$) with Cu^I (and also with other transition metal precursors) using various reaction conditions were unsuccessful. However, the reaction of $(Et_2N)_2P(2\text{-py})$ (**12**) with $[Cu(MeCN)_4]PF_6$ in MeCN results in the formation of a bright yellow solution, from which the bimetallic copper(I) complex $[(MeCN)Cu\{(Et_2N)_2P(2\text{-py})\}]_2(PF_6)_2$ (**20**, Scheme 3.6) could be isolated in 19 % crystalline yield. Similarly to the earlier reported diamagnetic iron(II) and copper(I) complexes of $P(2\text{-py})_3$ and $P(6\text{-Me-2-py})_3$, the P resonance of the $(Et_2N)_2P(2\text{-py})$ ligand in **12** is shifted upfield in the $^{31}P\{^1H\}$ NMR spectrum from 93.9 ppm ($CDCl_3$) for the uncoordinated ligand **12** to 84.0 ppm (CD_3COCD_3) in **20**. Also, the $^{31}P\{^1H\}$ NMR signal of the P atom, which directly coordinates to the copper centre, in **20** is clearly broadened in contrast to the free ligand **12**. This is

due to the coupling to the quadrupole cores (I = 3/2) of ^{63}Cu (natural abundance: 69.2 %) and ^{65}Cu (natural abundance: 30.8 %).[194]

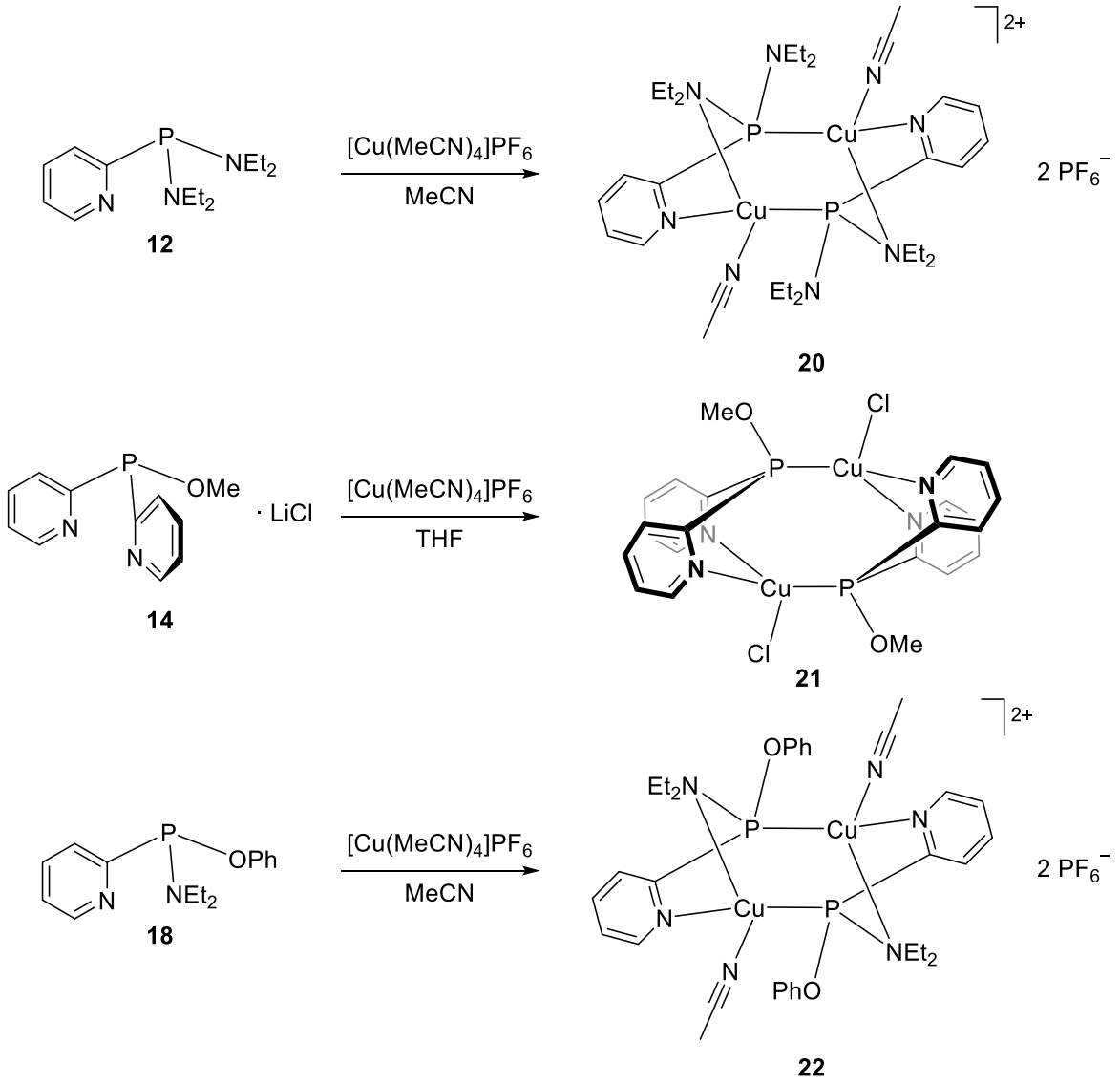

Scheme 3.6: *Synthesis of the dimeric copper(I) 2-pyridyl-phosphine complexes* ***20–22****.*

The different coordination behaviour of **10** and **11** compared to that of **12** is similar to that of di-2-picolylphenylphosphane ligands, which have been investigated in greater detail by electron density studies.[150] Whereas the lithium chloride-free ligand PhP(2-pic)$_2$ can be coordinated to metals by the nitrogen donor atoms,[165] the dimeric compound [PhP(2-pic)$_2$LiCl]$_2$ exhibits a reduced tendency towards metal coordination. This behaviour is somewhat unexpected, since the lithium salt should be easily replaced by other metal cations in polar solvents. D. Stalke and co-workers explained the limited reactivity of the LiCl-containing 2-picolyl-ligand through the enhanced shielding of the nitrogen donor atoms by the LiCl moiety.[150]

To investigate this shielding effect, the distribution of the CHELPG charges within the ligands **11**, [**11**·LiCl]$_2$ and **12** was calculated, and is shown in Figure 3.15.[141] The charges were calculated at

the BP86,[136–138] def2-TZVP[139,140] level of theory (see Chapter 8.4, page 134). There is a clear difference between the charge distribution of the LiCl-free ligand **11** and the LiCl-containing complex, which was optimised as dimeric structure [**11**·LiCl]$_2$. Whereas the pyridyl-nitrogen donor atoms in **11** exhibit a much more negative charge, the corresponding N atoms in [**11**·LiCl]$_2$ are more electropositive and therefore shielded by the bridging LiCl moiety. The charge of the pyridyl-nitrogen atom within the di-substituted ligand **12** is similar to that of the LiCl-free ligand **11**. These observations are in accordance with the finding of D. Stalke and co-workers and could explain the limited coordination ability of [**11**·LiCl]$_2$ compared to that of ligand **12**.[150] The CHELPG charge distribution also demonstrates that the diethylamino-nitrogen atoms are much more electropositive in comparison with the pyridyl-nitrogen, which is the cause of their diminished donor properties.

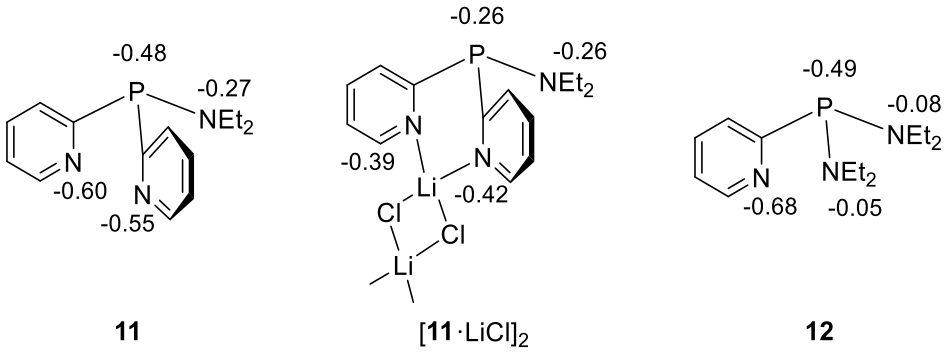

Figure 3.15: *CHELPG charges of the phosphorus and nitrogen donor atoms within the (amino)-2-pyridyl-phosphines **11**, [**11**·LiCl]$_2$ and **12**.*

No indication of a reaction between the (alkoxy)-2-pyridyl-phosphine [**14**·LiCl]$_2$ and [Cu(MeCN)$_4$]PF$_6$ in THF at room temperature was observed, with an almost colourless solution being formed. However, after the mixture was brought to reflux overnight, a yellow solution was produced and a few crystals of [ClCu{(MeO)P(2-py)$_2$}]$_2$·MeOH (**21**·MeOH, Scheme 3.6) could be obtained after workup from a saturated methanol solution. Unfortunately, **21**·MeOH could not be isolated in significant yield, despite repeated attempts. This transition metal complex is the first example of a metal complex of an (alkoxy)-bis(2-pyridyl) ligand and is very similar to the dimeric complex **20** incorporating the bis(amino)-2-pyridyl-phosphine ligand **12**.

The copper(I) complex [(MeCN)Cu{(Et$_2$N)(PhO)P(2-py)}]$_2$(PF$_6$)$_2$ (**22**) was obtained from the reaction of (Et$_2$N)(PhO)P(2-py) (**18**) with [Cu(MeCN)$_4$]PF$_6$ in MeCN under reflux conditions. Again, as observed for **20**, the ^{31}P{^{1}H} singlet for **22** is broadened and shifted upfield to 107.8 ppm (CD$_3$CN) relative to the free ligand **18** (120.2 ppm, CDCl$_3$).

Ligands **12**, [**14**·LiCl]$_2$ and **18**, which contain at least two nitrogen atoms, produce very similar structural arrangements with Cu^I, in which the phosphorus bridgehead and either two pyridyl-nitrogen atoms or one pyridyl-nitrogen and an amino-nitrogen donor atom are involved in the

coordination. Interestingly, however, when only one nitrogen atom is present for coordination to the soft Cu^{I} centre, as in $(PhO)_2P(2\text{-py})$ (**19**), a completely different type of complex in which only the phosphorus bridgehead and the pyridyl-nitrogen are involved in the coordination is formed (Scheme 3.7).

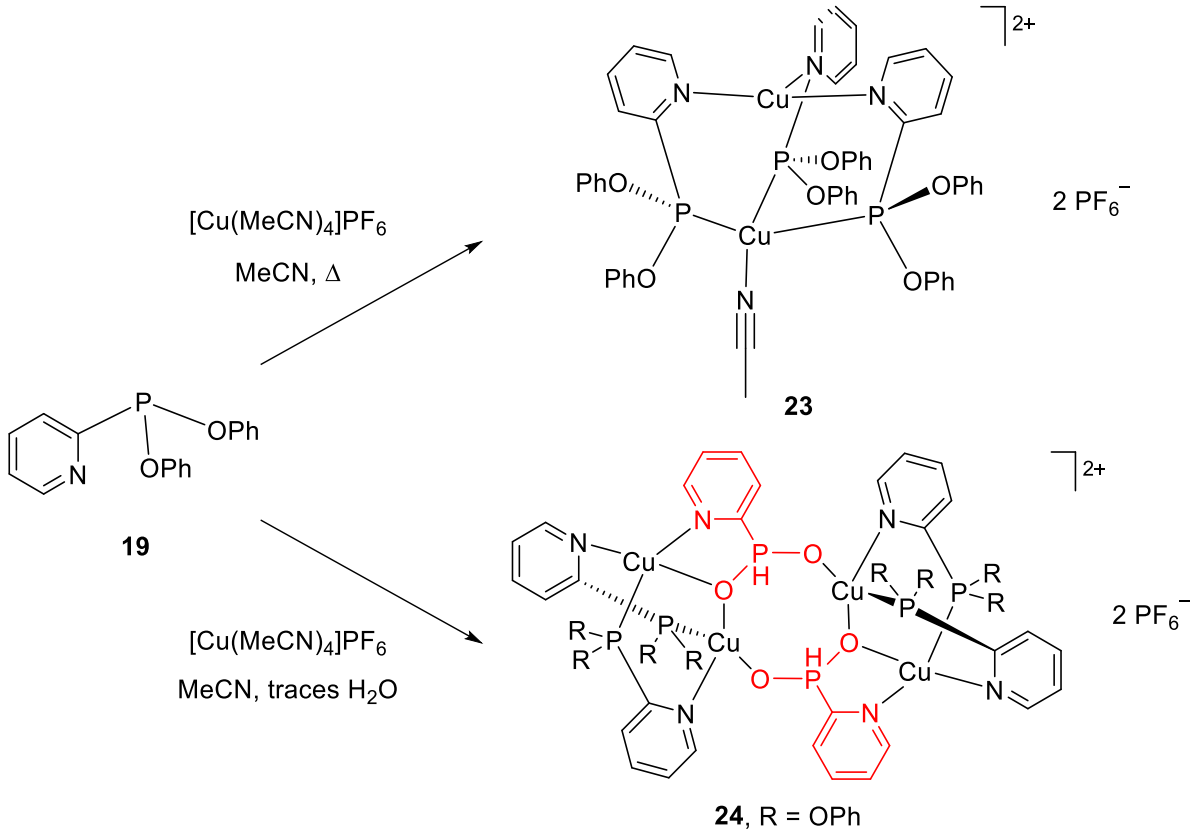

Scheme 3.7: *Formation of the copper(I) complexes* ***23*** *and* ***24****, depending on the reaction conditions.*

The reaction of **19** with $[Cu(MeCN)_4]PF_6$ in MeCN under reflux conditions gives $[(MeCN)Cu_2\{(PhO)_2P(2\text{-py})\}_3](PF_6)_2 \cdot 3THF$ (**23**·3THF, Scheme 3.7). As observed previously, the $^{31}P\{^{1}H\}$ NMR signal of the phosphorus bridgehead in **23** is shifted upfield from 142.8 ppm (CD_3CN) to a broad signal at 120.7 ppm (CD_3CN), due to the complexation. When the reaction of **19** with $[Cu(MeCN)_4]PF_6$ in MeCN was carried out at room temperature (instead of at reflux), in addition to the broad signal at 120.7 ppm (in CD_3CN) for **23,** a sharp singlet at 21.6 ppm was repeatedly observed in the $^{31}P\{^{1}H\}$ NMR spectrum. This signal splits into a doublet ($^{1}J_{PH}$ = 597.2 Hz) in the proton-coupled ^{31}P spectrum, suggesting the formation of a P–H containing species (Figure 3.16).

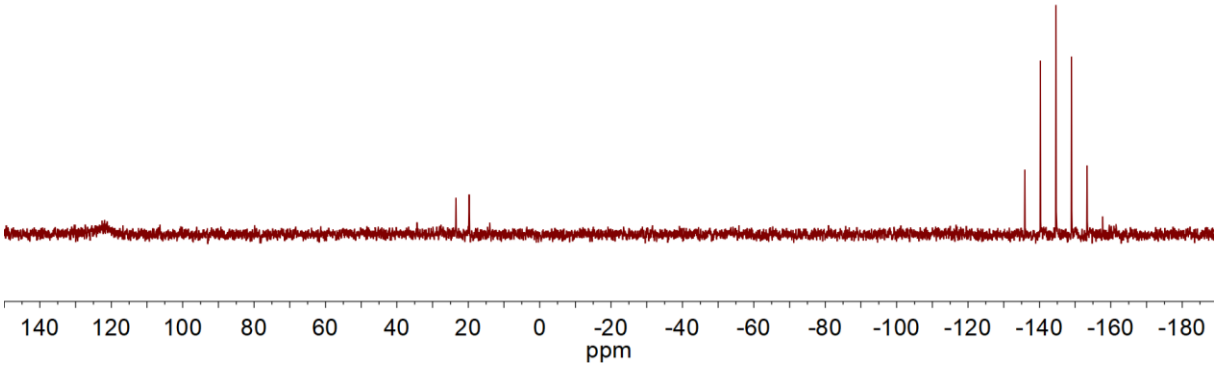

Figure 3.16: *^{31}P NMR (CD_3CN, 161.98 MHz) spectrum of [{OP(O)(H)(2-py)}Cu_2{$(PhO)_2$P(2-py)}$_2$]$_2$$(PF_6)_2$ (**24**·2THF).*

The copper complex [{OP(O)(H)(2-py)}Cu_2{$(PhO)_2$P(2-py)}$_2$]$_2$$(PF_6)_2$·2THF (**24**·2THF) contains $(PhO)_2$P(2-py) (**19**) and $[OP(O)(H)(2\text{-py})]^-$ ligands (Scheme 3.7, marked in red). The latter ligand apparently results from the hydrolysis of **19** by adventitious water. The formation of the $[OP(O)(H)(2\text{-py})]^-$ ligand accounts for the observation of a P–H resonance in the $^{31}P\{^1H\}$ NMR spectrum. Such pyridyl phosphonic acid derivatives are not unknown, and have usually been prepared by the hydrolysis of diethyl pyridine-2-phosphonate with hydrochloric acid.[195] The potassium salt of pyridyl phosphonic acid exhibits a ^{31}P NMR shift of 9.2 ppm, which agrees with our findings, since an downfield shift of the signal is expected upon coordination to copper(I).[196] *In-situ* ^{31}P NMR spectroscopic studies of a solution of crystals of **24**·2THF dissolved in MeCN show that the $[OP(O)(H)(2\text{-py})]^-$ ligand completely decomposes after reflux (72 h), leaving only the resonance for $(PhO)_2$P(2-py) (**19**). This observation explains why **23**·3THF is formed exclusively in the reaction at reflux, with the hydrolysis product **24**·2THF being absent.

3.5.1 Solid State Structures of the Copper(I) Complexes

The solid state structures of the new Cu^I complexes [(MeCN)Cu{$(Et_2N)_2$P(2-py)}]$_2$$(PF_6)_2$ (**20**), [ClCu{$(MeO)_2$P(2-py)}]$_2$·MeOH (**21**·MeOH), [(MeCN)Cu{(Et_2N)(PhO)P(2-py)}]$_2$$(PF_6)_2$ (**22**), [(MeCN)Cu_2{$(PhO)_2$P(2-py)}$_3$]$(PF_6)_2$·3THF (**23**·3THF) and [{OP(O)(H)(2-py)}Cu_2{$(PhO)_2$P(2-py)}$_2$]$_2$$(PF_6)_2$·2THF (**24**·2THF) were determined by single-crystal X-ray crystallography. Details of key bond lengths and angles found in these complexes are given in Table 3.1 and Table 3.2.

Table 3.1: *Selected bond lengths (Å) and angles (°) in the transition metal complexes* ***20*****–*****22*****.***

	20	**21**·toluene	**22**
P(1)–C_{py}	1.833(3)	1.833(3), 1.839(2)	1.824(2)
P(1)–N_{Amino}	1.658(3), 1.740(2)	-	1.676(2)
P(1)–O_{Alkoxy}	-	1.616(2)	1.636(1)
Cu(1)–N_{py}	2.072(2)	2.078(2), 2.072(3)	2.055(2)
Cu(1)–N_{Et}	2.334(3)	-	2.543(2)
Cu(1)···P(1)	2.9234(8)	3.2108(7)	2.9613(6)
Cu(1')–P(1)	2.2137(8)	2.1641(8)	2.1974(6)
P(1)–C_{py}–N_{py}	113.2(2)	115.2(2), 115.7(2)	112.9(1)
P(1)–Cu(1')–N(1')$_{py}$	118.74(7)	118.78(7), 119.76(7)	119.60(5)

The solid state structure of **20** (Figure 3.17) is that of a centrosymmetric dimer, in which the NEt_2 groups of each of the ligands **12** do not coordinate Cu^I, with each Cu^I ion being chelated by the N atoms of the remaining NEt_2 group and the 2-py group of each ligand. The dimeric structure comes about by the formation of inter-monomer Cu–P bonds of 2.2137(8) Å to the P atom of **12**.

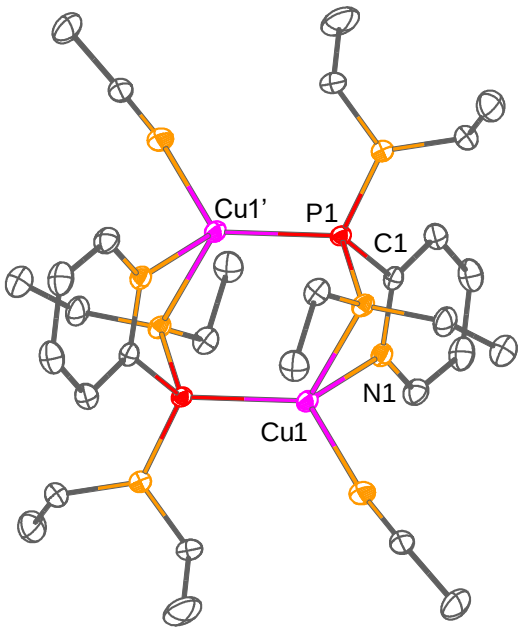

Figure 3.17: *Dimeric structure of the cation of* $[(MeCN)Cu\{(Et_2N)_2P(2\text{-}py)\}]_2(PF_6)_2$ ***(20).*** *Hydrogen atoms and the* PF_6^- *counterions are omitted for clarity. Displacement ellipsoids are drawn at the 30 % probability level.*

The copper complex $[ClCu\{(MeO)P(2\text{-}py)_2\}]_2$·MeOH (**21**·MeOH) is very similar to **20** and again consists of a centrosymmetric dimer, in which each Cu^I atom is chelated by the two pyridyl-N atoms

of one of the two ligands **14** and by the P bridgehead atom of the other ligand (Figure 3.18). The inter-monomer Cu–P bonds of 2.1641(8) Å are about 0.05 Å shorter than in complex **20**. The OMe groups of the ligands **14** are not coordinated to Cu^{I}, as might be expected on the basis of hard-soft concepts.

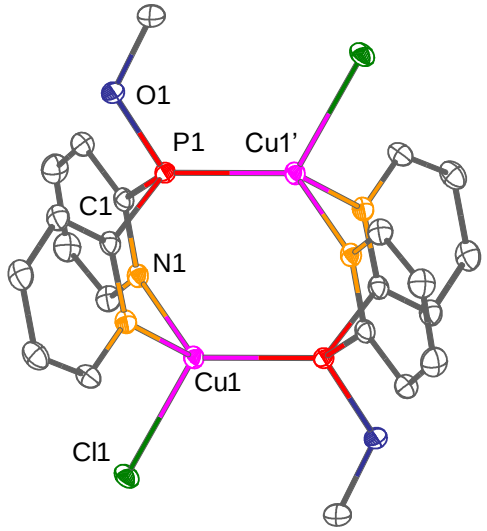

Figure 3.18: *Structure of [ClCu{(MeO)$_2$P(2-py)}]$_2$·MeOH (**21**·MeOH). Hydrogen atoms and the MeOH molecule are omitted for clarity. Displacement ellipsoids are drawn at the 30 % probability level.*

The reaction of $(Et_2N)(PhO)P(2\text{-py})$ (**18**) with $[Cu(MeCN)_4]PF_6$ in MeCN yielded crystals of $[(MeCN)Cu\{(Et_2N)(PhO)P(2\text{-py})\}]_2(PF_6)_2$ (**22**, Figure 3.19). In the dimeric structure, the Cu^{I} atoms are chelated by the N atoms of the NEt_2 and 2-py groups, with Cu(1)–N_{py} bond lengths of 2.055(2) Å and Cu(1)–N_{Et} bond lengths of 2.543(2) Å, of one of the ligands **18** as well as the P bridgehead of the second ligand molecule. The inter-monomer Cu–P bonds of 2.1974(6) Å are in same region as found in **20** and **21**·MeOH. The OPh groups of both ligand molecules remain uncoordinated.

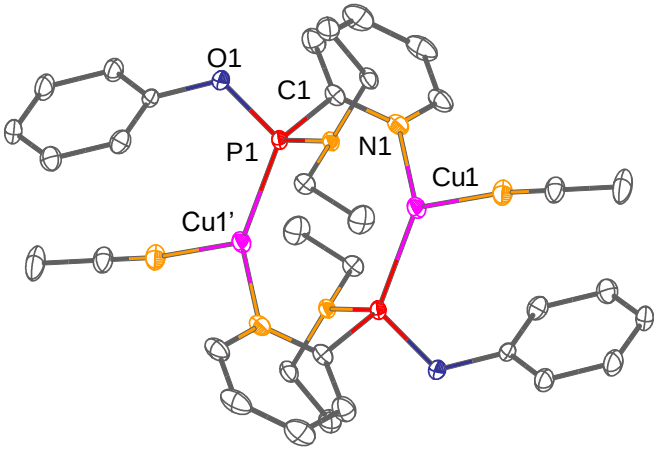

Figure 3.19: *Dimeric structure of the cation of [(MeCN)Cu{(Et$_2$N)(PhO)P(2-py)}]$_2$(PF$_6$)$_2$ (**22**). Hydrogen atoms and the PF_6^- counterions are omitted for clarity. Displacement ellipsoids are drawn at the 30 % probability level.*

As mentioned before, ligand arrangements, which contain at least two nitrogen donor atoms show a very similar coordination behaviour towards copper(I). In the cases of the complexes **20**–**23** the phosphorus atom as well as two nitrogen atoms (either from two pyridyl moieties or from a pyridyl ring and an amino functionality) are involved in the coordination and cause the formation of centrosymmetric dimeric structures.

Table 3.2: *Selected bond lengths (Å) and angles (°) in the transition metal complexes **23** and **24**.*

	23·3THF	**24**·2THF
P–C_{py}	1.816(3)–1.827(3)	1.815(6)–1.824(6)
P–OPh	1.601(3)–1.614(2)	1.614(4)–1.631(4)
P–O	-	1.474(4)–1.490(4)
Cu–P	Cu(1)–P 2.2594(9)–2.2924(8) Cu(2)···P 3.062(1)–3.180(1)	Cu(2')–P(1) 2.128(2) Cu(1')– P(3) 2.148(2)
Cu(2)–N_{py}	1.983(2)–2.034(3)	-
P–C_{py}–N_{py}	111.2(2)–114.3(3)	116.0(4), 116.8(4)

In contrast, the bis(phenoxy)-2-pyridyl-phosphine ligand **19** forms the homobimetallic complex **23**·3THF (Figure 3.20) with copper(I) under reflux conditions, in which one of the Cu^{I} centers [Cu(2)] is coordinated by three pyridyl-N atoms of three separate ligands **19** (Cu(2)–N_{py} 1.983(2)–2.034(3) Å), as well being loosely coordinated by the F atom of a PF_6^- anion (Cu···F 2.90(1) Å, the other of which, balancing the +2 charge, is not coordinated). Similar Cu···F interactions have been seen in two-dimensional Cu^{II} coordination polymers of the type $\{[Cu(PF_6)(4,4'\text{-bipy})_2(MeOH)]\cdot PF_6\cdot 3MeOH\}_n$, in which Cu···F distances of 2.306(3)–2.614(3) Å have been observed.[197] The remaining Cu^{I} centre in **23**·3THF is bonded to the three P atoms of the three ligands **19** and to a MeCN molecule, resulting in a pseudo-tetrahedral geometry. The bridging of the two Cu^{I} centers in **23**·3THF results in a short Cu···Cu distance of 2.9431(7) Å. Similar Cu···Cu distances were observed in dinuclear Cu^{I} complexes of Ph_2P(2-pypz) (2-pypz = (6-pyrazol-1-yl)pyridine)[198] and Ph_2P(2-py)[190] but cannot be considered as significant metallophilic interactions. As seen before in the structures of **21** and **22**, the OPh groups of **19** are not bonded to Cu^{I}. Again, this is due to the hardness of the O atoms relative to the soft N and P ligand set.

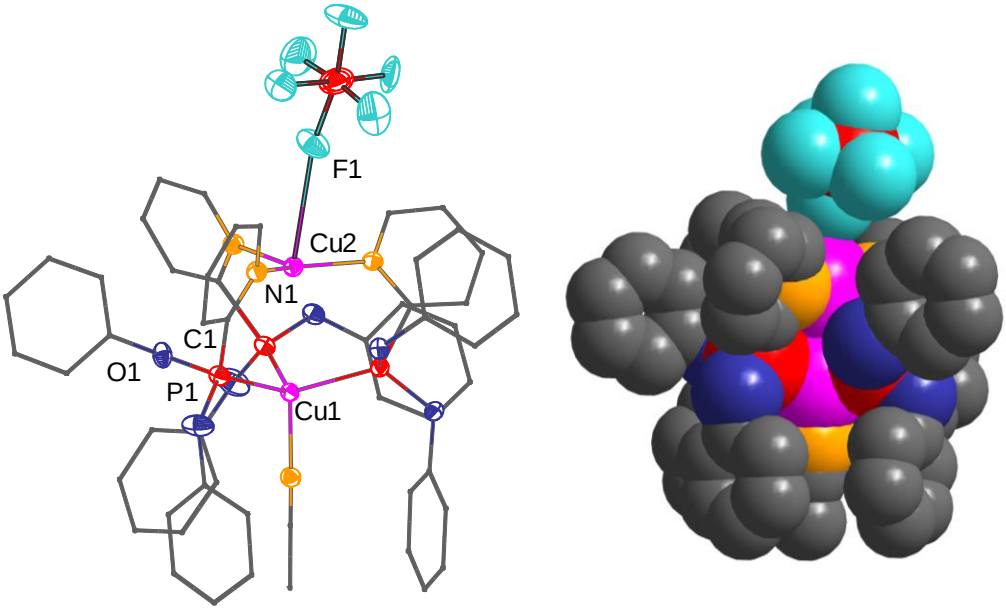

Figure 3.20: *Structure of [(MeCN)Cu$_2${(PhO)$_2$P(2-py)}$_3$](PF$_6$)$_2$·3THF (**23**·3THF) (left) and its space filling diagram (right). Hydrogen atoms, one PF$_6^-$ counterion, and the THF molecules are omitted for clarity. Carbon atoms are represented as sticks and displacement ellipsoids are drawn at the 30 % probability level.*

When the reaction of the bis(phenoxy)-2-pyridyl-phosphine ligand **19** and [Cu(MeCN)$_4$]PF$_6$ was carried out at room temperature, NMR spectroscopy provided evidence for the formation of a new species. Further confirmation of the new species comes from X-ray crystallography and indicates that the new complex is [{OP(O)(H)(2-py)}Cu$_2${(PhO)$_2$P(2-py)}$_2$]$_2$(PF$_6$)$_2$·2THF (**24**·2THF, Figure 3.21), which contains (PhO)$_2$P(2-py) (**19**) and [OP(O)(H)(2-py)]$^-$ ligands. The later ligand apparently results from hydrolysis of **19** by adventitious water. The complicated centrosymmetric structural arrangement of **24**·2THF contains a central Cu$_2$P$_2$O$_4$ ring unit with Cu–O bond lengths between 2.049(4)–2.117(4) Å and P–O bond lengths in the range of 1.474(4)–1.490(4) Å. The four Cu^I ions have pseudo-tetrahedral geometries, and are coordinated by the [OP(O)(H)(2-py)]$^-$ ligands (using the two O and the pyridyl-N atoms) and by the ligand **19** (using one of the pyridyl-N atom and the bridgehead-P atom) with phosphorus–copper bond lengths in the region of 2.128(2)–2.148(2) Å.

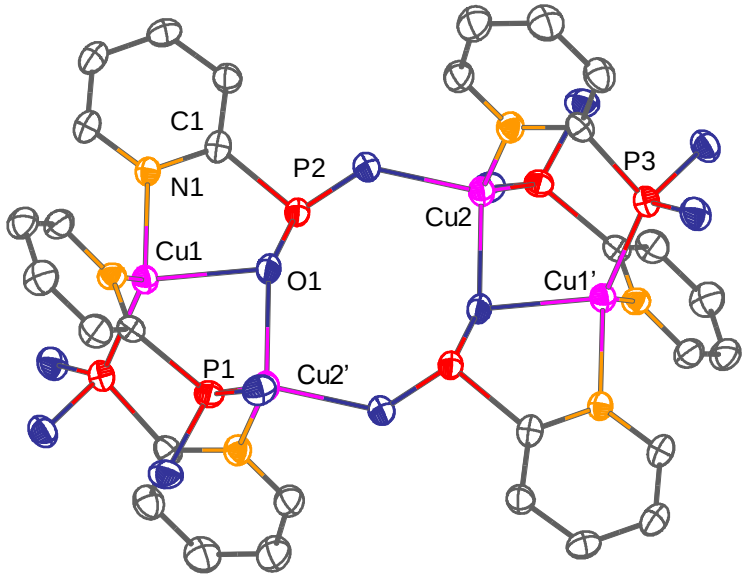

Figure 3.21: *Structure of the cation of [{OP(O)(H)(2-py)}Cu$_2${(PhO)$_2$P(2-py)}$_2$]$_2$(PF$_6$)$_2$·2THF (**24**·2THF). Carbon atoms of the phenoxy groups, hydrogen atoms, PF_6^- counterions, and the THF molecules are omitted for clarity. Displacement ellipsoids are drawn at the 30 % probability level.*

3.6 A Dinuclear Rhodium (Amino)-2-pyridyl-phosphine Complex

In the past, most studies concerning homo- and heterobimetallic complexes of 2-pyridyl-phosphines have been concerned with Ph$_2$P(2-py), since this ligand set has proven to be a useful building block due to its small bite angle. The resulting rigidity of the ligand enabled the synthesis of bimetallic complexes and can support the formation of M–M bonds.[88,153,199–201]

A dinuclear rhodium 2-pyridyl-phosphine complex [Rh$_2$Cl$_2$(μ-CO){(Et$_2$N)$_2$P(2-py)}$_2$] (**25**) was synthesised from the reaction of the bis(diethylamino)-2-pyridyl-phosphine **12** and di-μ-chloro-tetracarbonyldirhodium(I) in DCM (Scheme 3.8). The mixture turned brown immediately and a colourless gas was produced, which indicated the loss of CO ligands from the Rh precursor. Brown single-crystals of **25** could be grown by layering a saturated DCM solution with *n*-hexane (in 40 % yield).

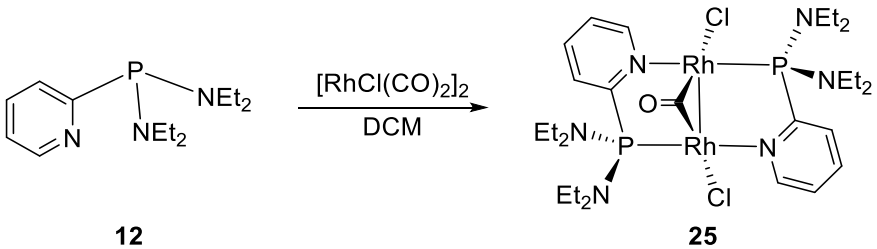

12 **25**

Scheme 3.8: *Synthesis of the dinuclear rhodium 2-pyridyl-phosphine complex **25**.*

Single-crystal X-ray crystallography (Figure 3.22) revealed the formation of a homobimetallic rhodium complex in which the two rhodium(I) centres are each coordinated to a P atom of one ligand (2.2004(6) and 2.2026(6) Å) and a pyridyl-N atom (2.148(2) and 2.153(2) Å) of the other ligand. Additionally, each Rh atom is attached to a chlorine atom, with Rh–Cl bond lengths of 2.3651(8) and 2.3727(6) Å, and to a CO ligand that bridges the two metal centres. The presence of a bridging CO ligand was also confirmed by IR spectroscopy (IR, KBr, ν [cm^{-1}] = 1786). The rhodium–carbon bond lengths were found to be 1.941(2) and 1.950(2) Å with a Rh–CO–Rh bond angle of 84.15(7)°. Furthermore, a Rh–Rh bond of 2.6073(6) Å is formed, leading to a very distorted square-pyramidal coordination environment for each rhodium centre. The complex has an approximate C_2-symmetry with a two-fold axis passing along the carbonyl C=O bond. In complex **25**, each rhodium possesses 16 valence-electrons.

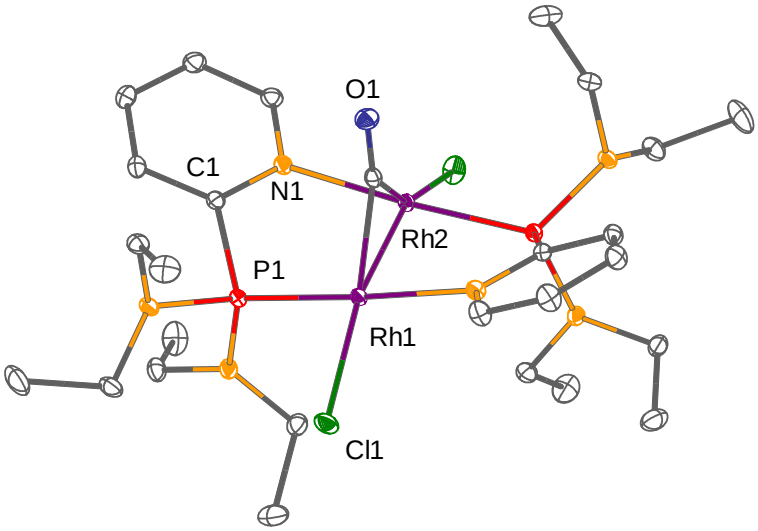

Figure 3.22: *Structure of [Rh_2Cl_2(μ-CO){$(Et_2N)_2$P(2-py)}$_2$] (**25**). Hydrogen atoms are omitted for clarity. Displacement ellipsoids are drawn at the 30 % probability level.*

A very similar A-frame complex [Rh_2Cl_2(μ-CO){Ph_2P(2-py)}$_2$] was synthesised by A. L. Balch and co-workers and contains the phenyl-derived ligand Ph_2P(2-py). This complex was obtained from the reaction of the monomeric Rh complex [RhCl(CO){Ph_2P(2-py)}] with half an equivalent of [RhCl$(CO)_2]_2$. The Rh–Rh bond length in this complex is 2.612(1) Å, which is in the same range as observed in **25**.[199] The term A-frame complex was introduced by R. Eisenberg and describes coordination complexes of the form [M_2(μ-X)$(L)_2L'_2$] (M = Rh, Pt, X = CO, SO, NO, H^-, Cl^-, L = bidentate ligand, L'= CO, Cl^-) that comprise two bridging ligands which are at least bidentate, and a single atom bridge (Figure 3.23).[202,203] In general, A-frame complexes comprising unsymmetrical bridging ligands are chiral if the ligands are present in a head-to-tail orientation towards each other.

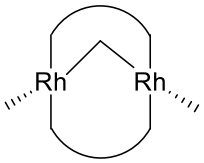

Figure 3.23: *A-frame type structure of a dinuclear rhodium complex.*

In the $^{31}P\{^{1}H\}$ NMR spectrum of **25**, a multiplet at 113.9–112.2 ppm is observed, which can be attributed to an AA'XX' spin system (Figure 3.24). Through simulation of the spin system using SpinWorks,[204] the coupling constants could be determined ($^{1}J_{P–Rh}$ = 164.8 Hz, $^{2}J_{P–Rh}$ = –7.9 Hz, $^{1}J_{Rh–Rh}$ = ±14.7 Hz and $^{3}J_{P-P}$ = ±14.7 Hz). Very similar coupling constants were obtained for the complex incorporating the diphenyl-2-pyridyl-phosphine ligand ($^{1}J_{P–Rh}$ = 144.0 Hz, $^{2}J_{P–Rh}$ = –7.4 Hz $^{1}J_{Rh–Rh}$ = 12.0 Hz and $^{3}J_{P–P}$ = 16.0 Hz).[199]

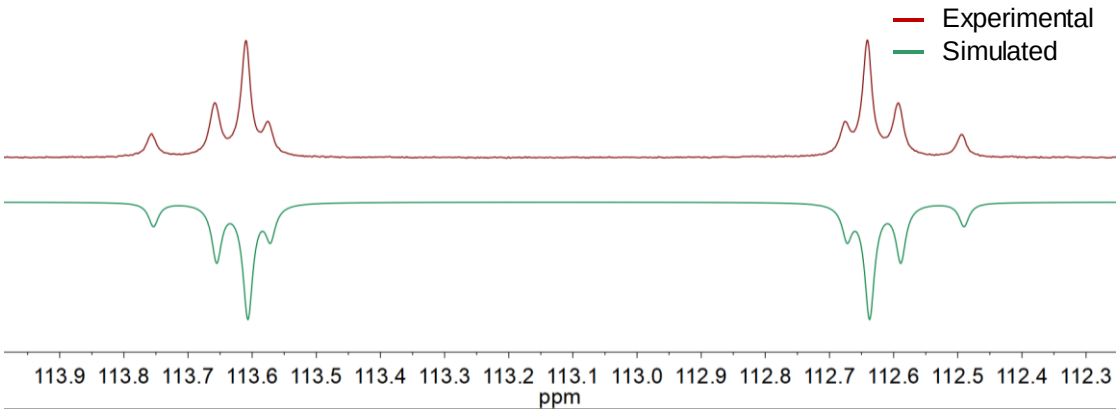

Figure 3.24: *$^{31}P\{^{1}H\}$ NMR ($CDCl_3$, 161.99 MHz) spectra (experimentally obtained and simulated) of* ***25****. The spectrum was simulated using SpinWorks.*[204]

To investigate the nature of the Rh–Rh bond, DFT calculations at the BP86,[136–138] old-ZORA-def2-TZVP[139] level of theory were utilised (see Chapter 8.4, page 134). These calculations were performed because it has been shown that in some Rh-complexes, the steric and packing effects play a much more significant role than the electronic effects in terms of the coordination geometry of the complexes and the formation of M–M bonds.[205,206] In order to determine the most suitable DFT functional for the description of the electronic properties of **25**, the experimentally observed CO stretching frequency in the IR spectrum was used as reference point (IR, KBr, ν [cm^{-1}] = 1786).

From the Wiberg bond index of the Rh–Rh bond (0.43), it is obvious that there is an electronic interaction between the rhodium centres. To further quantify this interaction, Figure 3.25 depicts a more detailed representation of the frontier molecular orbitals (HOMO–2 and –6). According to Loewdin population analyses, these two orbitals show significant contributions from the Rh centres and a clear interaction between the d orbitals.

HOMO–2

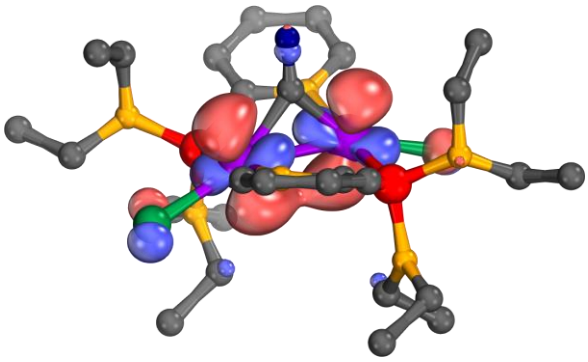

Rh1: 3.2 % s, 9.4 % d_{xz}, 1.4 % d_{xy}, 2.8 % d_{yz}, 19.0 % d_{z2}, 1.9 d_{x2-y2}
Rh1: 3.2 % s, 9.4 % d_{xz}, 1.4 % d_{xy}, 2.9 % d_{yz}, 18.9 % d_{z2}, 1.9 d_{x2-y2}
Cl1: 3.2 % p_y
Cl2: 3.2 % p_y

HOMO–6

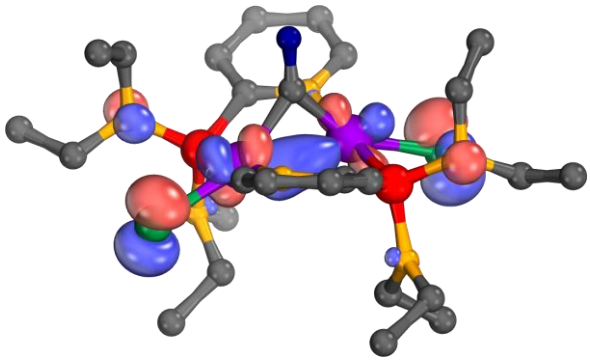

Rh1: 7.9 % d_{xz}, 4.0 % d_{xy}, 2.4 % d_{z2}, 1.7 % d_{x2-y2}
Rh1: 7.9 % d_{xz}, 4.0 % d_{xy}, 2.4 % d_{z2}, 1.7 % d_{x2-y2}
N_{Et}1: 2.4 % p_x , 2.5 % py
N_{Et}2: 2.4 % p_x , 2.5 % py
Cl1: 2.1 % p_x ,14.3 % p_z
Cl2: 2.1 % p_x ,14.3 % p_z

Figure 3.25: *Molecular orbitals of [Rh_2Cl_2(μ-CO){$(Et_2N)_2$P(2-py)}$_2$] (**25**), including Loewdin population analyses (≥1.5 %). Plotting-threshold: 70 % (HOMO-2) and 55 % (HOMO-6).*

These findings can also be confirmed using the intrinsic bond orbitals (Figure 3.26).[207,208] Intrinsic atomic orbitals (IAOs) are a relatively new method to connect quantitative self-consistent field wave functions to a qualitative picture without any empirical input. This novel technique allows the computation of the nature and shape of chemical bonds and the simple representation of a realistic *ab initio* electronic wave function.[207,208] In contrast, other techniques, such as F. Weinhold's natural atomic/bond orbital analyses (NAO/NBO)[209,210] are quite complicated and are based on various nontrivial assumptions, such as the hypothesis that atomic orbitals have spherical symmetry and can be obtained by a complex series of transformations.[209] The NBO model also assumes that a Lewis-like bonding pattern for each molecule exists and only has to be found.[177] These assumptions can lead to major errors in the interpretation of unusual bonding situations. The application of unbiased IAOs should therefore facilitate the interpretation of the chemical valence of molecules in difficult cases. This is achieved by defining an intrinsic minimal basis,[211] a set of perturbed core and valence atomic orbitals, which can exactly describe the occupied molecular orbitals of a previously computed SCF wave function.[207] The intrinsic bond orbitals (IBOs), derived from that, can then be utilised to describe the bonding situation within a molecule and can also be used to follow chemical reactions, since only a minimal number of IBOs change their nature or connectivity during a reaction.[207,208]

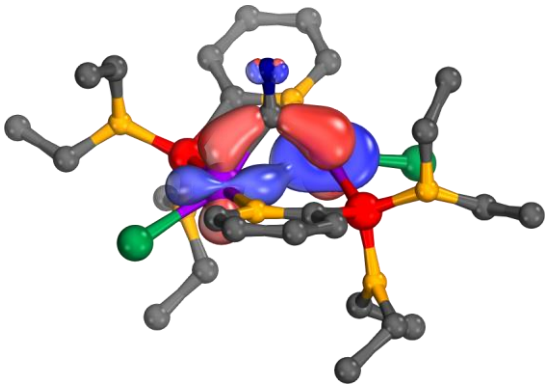

Figure 3.26: *Intrinsic bond orbital of [$Rh_2Cl_2(\mu$-CO){$(Et_2N)_2P(2$-py)$\}_2$] (**25**). Plotting-threshold: 80 %.*

Looking at an IBO of the complex **25**, a clear interaction between the two rhodium metal centres is obvious and gives rise to the assumption that the Rh–Rh bond is formed due to not only steric effects but also electronic factors, such as compensation of the electron-deficiency of the metal centres and the formation of a 16 valence-electron count on each of the Rh atoms. An attempted NBO analysis gave no clear indication of this, possibly due to the delocalisation within the system.

3.7 Unexpected Behaviour of a Bis(alkoxy)-2-pyridyl-phosphine Ligand towards Nickel

Commonly, tetracoordinate nickel(0) complexes of the form NiL_4 (P = trialkyl-, triaryl-, alkyl-aryl-phosphines) can be by synthesised from labile Ni^0 precursors, such as $[Ni(COD)_2]$ (COD = 1,5-cyclooctadiene) or nickel carbonyl complexes, *e.g.* $[Ni(CO)_2(COD)]$.[212] In order to avoid these very reactive and unstable nickel(0) species, an alternative path to tetrakisphosphine nickel(0) complexes comprises the *in-situ* reduction of a nickel(II) precursor, such as $NiCl_2$ or $[NiX_2L_2]$ (X = Cl, Br, L = phosphine), with Zn,[213,214] Na,[212] $NaBH_4$[215] or KC_8[216] in the presence of a phosphine. It was also found that nickel(II) halides can be reduced by triethyl phosphite in the presence of an amine and water to form tetrakis(triethyl phosphite)nickel(0) complexes. This reaction yields the corresponding ammonium salt and phosphine oxide in addition to the nickel complex (Equation 3-3).[217,218]

$$NiX_2 + 5\ P(OEt)_3 + 2\ NR_3 + H_2O \rightarrow [Ni\{P(OEt)_3\}_4] + 2\ HNR_3X + O{=}P(OEt)_3 \qquad (3\text{-}3)$$

Later on it was shown that $NiCl_2$ and triethyl phosphite produce tetrakis(triethyl phosphite)nickel(0) at elevated temperatures. This was the first example of a direct nickel(II) to nickel(0) reduction by an organic phosphite in the absence of other reducing agents or amines.[219] Although the reaction mechanism of this *in-situ* reduction was not further investigated, it can be speculated that the phosphite ligand is “non-innocent” and the reaction is probably accompanied by the oxidation of the ligand and the consequent formation of phosphorus(V) derivatives, for example the corresponding phosphine oxide.

Such redox transformations of certain late transition metals (*e.g.* Ni, Cu, Rh, Pd, Ir, Pt) in the presence of a phosphorus donor compound are typically promoted by hard ligands (*e.g.* O^{2-}, F^{-}, OH^{-}, ^{-}OAc, and H_2O) and are most often observed for Pd^{II}.[217,220–229] In the case of Pd, the coordination of a hard anion X^{-} to the Pd centre is followed by P–X reductive elimination, which results in the reduction of palladium(II) to palladium(0) and the simultaneous oxidation of a tertiary phosphine to P^{V} species, such as phosphine oxides or difluorophosphoranes.[220,225,229,230] For example attempts to prepare $[Pd(dppp)_2][BF_4]_2$ [dppp = propane-1,3-diylbis(diphenylphosphane)] from the reaction of $[Pd(MeCN)_4](BF_4)_2$ and dppp resulted in the formation of the zerovalent complex $[Pd(dppp)_2]$ and a difluorophosphorane *via* a fluoride-induced redox reaction. Attempts to extend this palladium redox chemistry to nickel were not successful in the past.[220] The tetrafluoroborate anion, which has previously been shown to be a suitable fluoride source for transition metal complexes,[231,232] was identified as the fluoride source in the case of the Pd^{II} to Pd^{0} reduction reaction.

In general, such BF_4^{-} decomposition reactions were observed for heterocyclic ligands, such as cyclic amines,[233] pyrazoles,[234–236] imidazoles,[237] and pyridines,[238] and are most likely to occur *via* coordination of the BF_4^{-} anion to the metal ion. This metal complex, which is suspected to initiate the decomposition, may then further react with the available ligands to yield various decomposition products, from monomeric, dimeric and tetrameric species to chain- and cubane-type F-containing species (Scheme 3.9).[232]

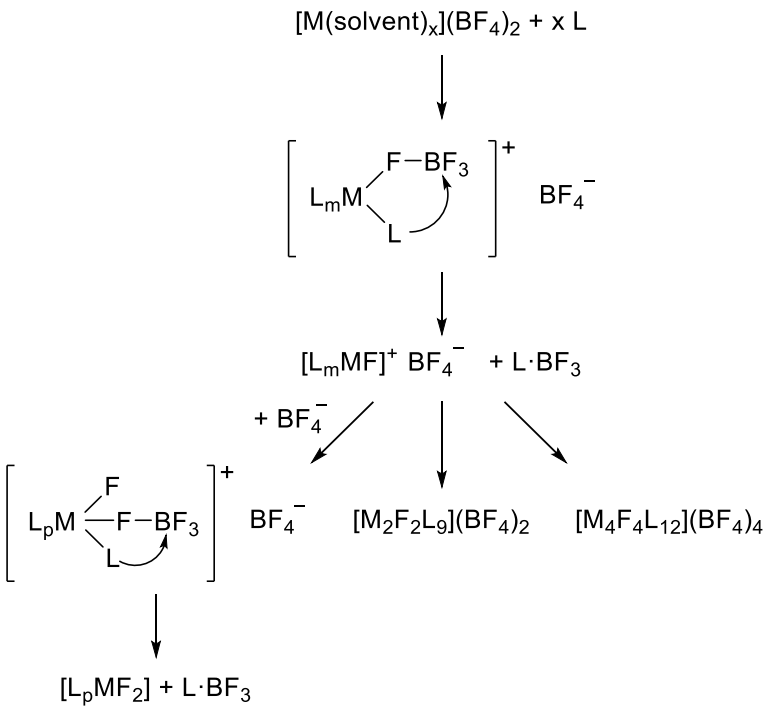

Scheme 3.9: *Proposed mechanism for the decomposition of the tetrafluoroborate anion and the formation of monomeric, dimeric and tetrameric M–F species.*[232]

Similar redox behaviour as described for the Pd complexes above was observed as part of this thesis from the reaction of $[Ni(MeCN)_6](BF_4)_2$ with four equivalents of bis(methoxy)-2-pyridyl-phosphine (**17**) in acetonitrile. Upon addition of the ligand to the nickel precursor, a dark orange/brown solution was formed immediately. The mixture was stirred overnight and after removal of the solvent, a brown oil was obtained. From a saturated MeOH solution dark red crystals of a nickel(0) complex (**26**) could be isolated (Scheme 3.10). The isolation of a nickel(0) complex, despite the use of a well-known nickel(II) precursor, which is not known to exhibit this type of reactivity on its own, points towards an *in-situ* reduction of the metal centre.

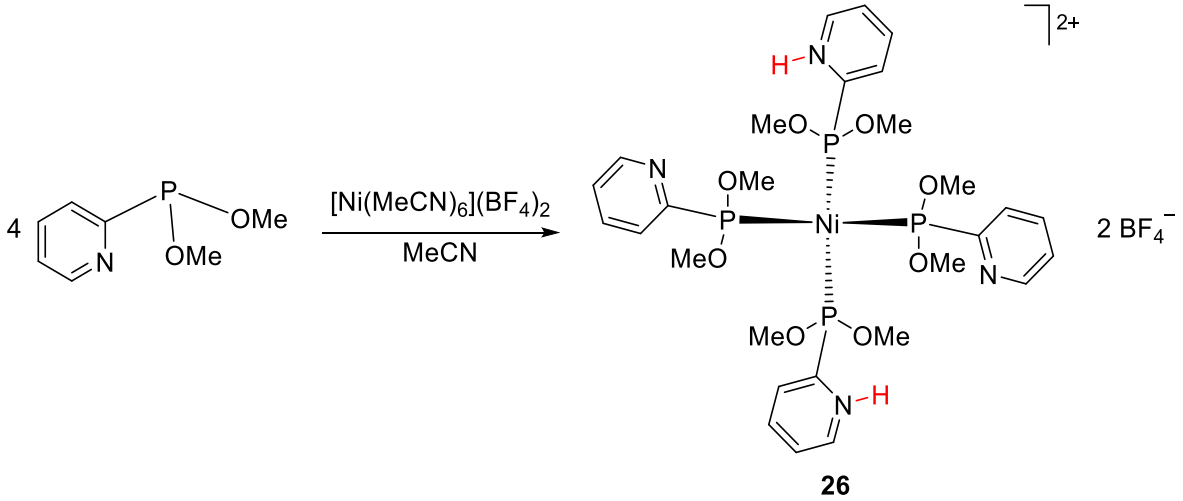

26

Scheme 3.10: *Synthesis of a nickel(0) bis(methoxy)-2-pyridyl-phosphine complex* ***26****.*

The solid state structure of the nickel complex is shown in Figure 3.27. Within the complex, the nickel centre is tetrahedrally coordinated by four bis(alkoxy)-2-pyridyl-phosphine ligand molecules *via* the phosphorus bridgehead atoms with Ni–P bond lengths of 2.1006(6)–2.1234(7) Å. Similar Ni–P bond lengths are found in other tetrahedral nickel(0) complexes, developed by D. L. DuBois and co-workers.[239,240] A slight distortion of the tetrahedral coordination geometry is obvious from the P–Ni–P bond angles, which are in the range 106.16(2)–111.63(2)°.

Interestingly, two of the pyridyl ligands are protonated and form H-bonds to the unprotonated pyridine nitrogen atoms (N···N 2.647(3)–2.688(3) Å, $N_{py}H–N_{py}$ 1.76(3)–1.80(3) Å). Similar short N···N distances were found in bis(4-methylpyridine)hydrogen tetraphenylborate (2.608 Å).[241] The presence of two protonated ligand molecules and two tetrafluoroborate anions within the unit cell, further supports the assumption that the nickel centre is present in an oxidation state of 0.

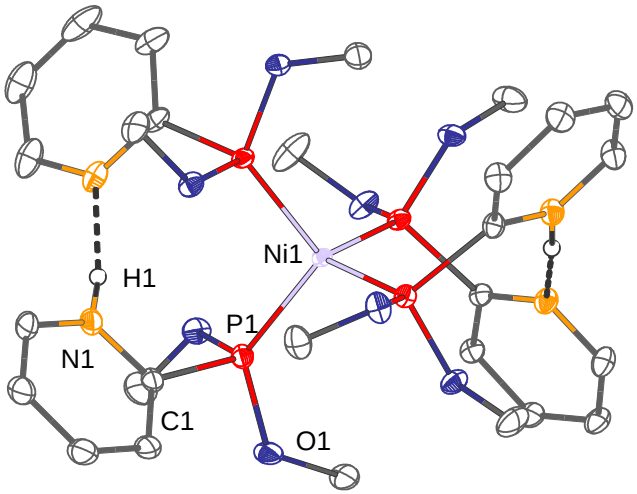

Figure 3.27: *Structure of the dication of [{(MeO)$_2$P(2-py-H)}$_2${(MeO)$_2$P(2-py)}$_2$Ni](BF$_4$)$_2$·MeOH (**26**·MeOH). Hydrogen atoms, BF$_4^-$ counterions and the MeOH molecule are omitted for clarity. Displacement ellipsoids are drawn at the 30 % probability level.*

NMR spectroscopic analyses of crystals of **26**·MeOH strongly suggest the diamagnetic character of the complex, with sharp peaks being observed in the ^{1}H and ^{31}P NMR spectra. In addition, an upfield shift of the ^{31}P{^{1}H} NMR signal to 154.5 ppm (CD_3CN) is observed upon complexation of the phosphine ligand (free ligand **17**, 150.1 ppm, $CDCl_3$). The potential alternative formulation as a diamagnetic tetrahedral nickel(II) complex is not possible, although the isomerism of **26** to a square-planar structure in solution cannot be excluded on this basis. So far, low-spin ground states were only found in tetrahedral nickel(IV) tetraalkyl complexes.[242]

Since the NH proton could not be unambiguously assigned in the ^{1}H NMR spectrum, IR measurements in the solid state were carried out (Figure 3.28). The very short distances between the pyridyl-nitrogen atoms involved (N···N 2.645(2)–2.688(3) Å) point towards a strong hydrogen bonding, which usually causes NH stretching vibrations to appear as very broad absorptions at around 2500 cm^{-1}.[241,243] Indeed a very broad absorption at 1900–2250 cm^{-1} can be observed in the IR spectrum of **26**·MeOH. The OH stretching vibration of **26**·MeOH can be found as broad absorption around 3400 cm^{-1}.

To verify the experimentally observed NH stretching frequency, a geometry optimisation and frequency analysis of the dication [{(MeO)$_2$P(2-py-H)}$_2${(MeO)$_2$P(2-py)}$_2$Ni]$^{2+}$ on the TPSS,[244] def2-TZVP[139,140] level of theory was conducted (see Chapter 8.4, page 134). From these calculations N···N distances of 2.72 Å and NH stretching frequencies of 2210 and 2206 cm^{-1} were obtained and showed a good agreement with the experimental values.

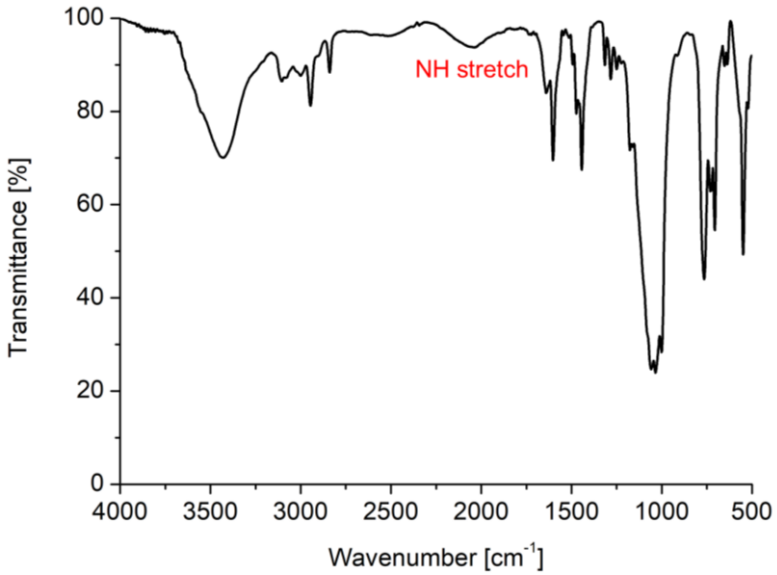

Figure 3.28: *IR spectrum of* ***26****·MeOH, measured as a KBr pellet in the solid state.*

3.7.1 Investigation of the Reduction Mechanism

As mentioned before, nickel(II) halides can be reduced in the presence of triethyl phosphite and water with the formation of the phosphine oxide.[217,219] A similar *in-situ* reduction of the metal centre can be seen from the reaction of $[Ni(MeCN)_6](BF_4)_2$ with the good π-accepting ligand bis(methoxy)-2-pyridyl-phosphine (**17**) yielding the nickel(0) complex **26**. However, in the case of **26** the oxidation product of the reaction is not easily identified since there is no water added to the reaction mixture. In order to clarify the reduction mechanism *in-situ* NMR spectroscopic measurements were carried out. The key question in this regard is also whether a fluoride-assisted redox reaction is a possible reaction path, similar to that observed in the formation of Pd^0 phosphine complexes.[220,225,229]

The $^{31}P\{^1H\}$ NMR spectrum of the reaction mixture of bis(methoxy)-2-pyridyl-phosphine (**17**) and $[Ni(MeCN)_6](BF_4)_2$ in CD_3CN is shown in Figure 3.29, with the main signal at 154.5 ppm corresponding to the nickel(0) complex **26**. Besides this singlet, other resonances of unidentified P-containing species are detected, indicating that several different transformations of the ligand took place. Some of the observed signals are also broadened, which could probably be due to a possible coordination to a paramagnetic Ni^{II} centre. No further splitting of the resonances in the proton-coupled ^{31}P NMR spectrum is obvious and therefore, the presence of P–H species can be excluded.

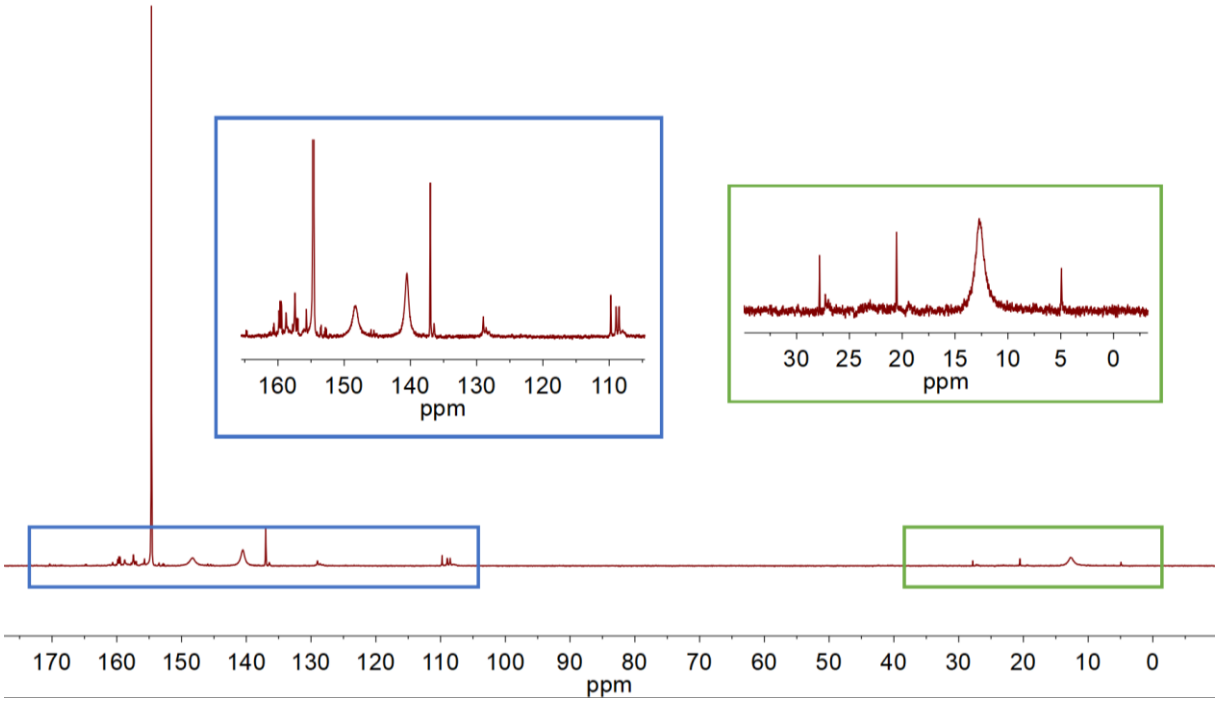

Figure 3.29: *$^{31}P\{^{1}H\}$ NMR (CD_3CN, 161.99 MHz) spectrum of the reaction mixture of **17** and $[Ni(MeCN)_6](BF_4)_2$ in CD_3CN.*

Since signals in the typical range for P^V phosphine oxide derivatives[228,245,246] were detected in the $^{31}P\{^{1}H\}$ NMR spectrum of the reaction mixture (around 15 ppm), test reactions of **17** with air and water were performed to determine whether a water-induced $P^{III} \rightarrow P^V$ redox reaction[217] was responsible for the reduction of the metal in complex **26**. However, the reactions of **17** with air or water led almost exclusively to the formation of the secondary phosphine oxide (MeO)P(O)H(2-py) (**27**, Scheme 3.11), which is identified by a singlet at 24.6 ppm in the $P\{^{1}H\}$ NMR spectrum that splits into a doublet with a coupling constant of 581.6 Hz in the proton-coupled ^{31}P NMR spectrum due to P–H coupling (for comparison, the phenyl counterpart methyl phenyl phosphinate (MeO)P(O)H(Ph) appears at 27.8 ppm in the $P\{^{1}H\}$ NMR spectrum in $CDCl_3$).[247] Since no such secondary phosphine oxide signal was detected in the ^{31}P NMR spectrum of the reaction mixture of **17** and $[Ni(MeCN)_6](BF_4)_2$, the potential role of water and oxygen in the formation of **26** can be excluded.

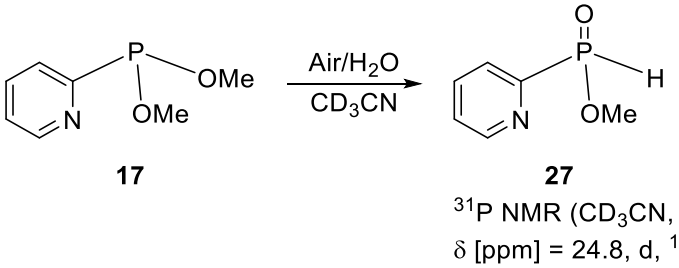

Scheme 3.11: *Reactions of phosphine **17** with air or water yield the secondary phosphine oxide **27**.*

No further information could be gleaned from the ^{31}P NMR spectrum of the reaction mixture, as none of the remaining resonances could be identified. Therefore, a $^{19}F\{^{1}H\}$ NMR spectrum was recorded (Figure 3.30). As seen for the ^{31}P NMR spectrum, the main signal, a singlet at –151.9 ppm, can be attributed to the tetrafluoroborate anions of the nickel(0) complex **26**.

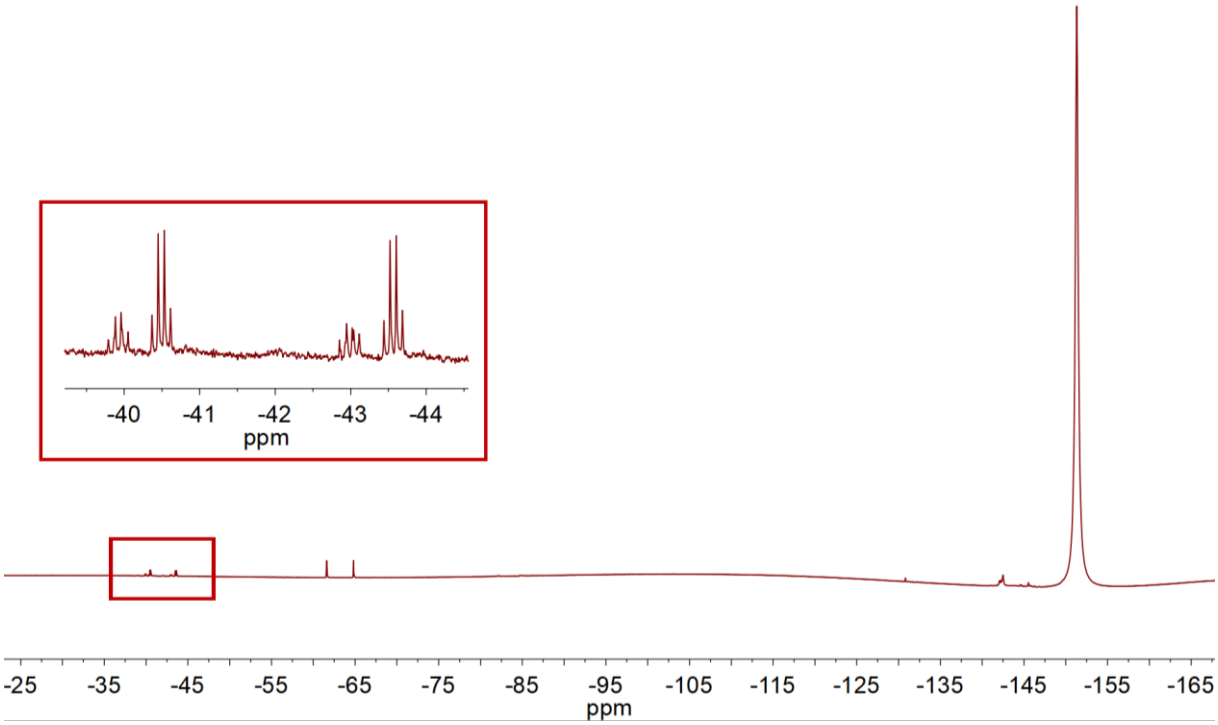

Figure 3.30: *$^{19}F\{^{1}H\}$ NMR (CD_3CN, 376.49 MHz) spectrum of the reaction mixture of* ***17*** *and $[Ni(MeCN)_6](BF_4)_2$ in CD_3CN.*

Additionally, two low-intensity doublets of (binomial) quartets (–41.4 and –41.9 ppm) are observable in the $^{19}F\{^{1}H\}$ spectrum. Both signals comprise one large coupling constant of 1155.8 Hz, which is in the typical range of a one-bond P–F scalar coupling.[248] The smaller coupling constants of 35.0 and 30.9 Hz presumably arise from the long range coupling to magnetically-equivalent P atoms. The possible origin of these signals could be nickel complexes which comprise fluorinated and unfunctionalised ligand molecules. However, the precise nature of which remains open to speculation. Besides these two signals, a doublet at –63.2 ppm with a coupling constant of 1203.2 Hz can be detected in the spectrum, which similarly indicates the presence of an F species with a directly bonded P atom. Furthermore, signals in the region of –130 up to –150 ppm, showing no distinct fine structure, are observable. The proton-coupled ^{19}F NMR spectrum does not indicate further splitting. These data are insufficient to allow any structural assignment of the species involved but do indicate that a complicated series of reactions appears to be occurring.

To further investigate the possibility of a fluoride-induced redox activity, **17** was reacted with NFSI (*N*-fluorobenzenesulfonimide) as a fluorinating reagent in CD_3CN. The $^{31}P\{^1H\}$ NMR spectrum of the reaction mixture showed a doublet at 9.0 ppm with a $^1J_{PF}$ coupling constant of 1055.3 Hz, which can be attributed to $[(MeO)_2PF(2\text{-py})][N(SO_2Ph)_2]$ (**F-17-NSI**, Scheme 3.12). Besides the main signal, two other doublets were observed in the $^{31}P\{^1H\}$ and $^{19}F\{^1H\}$ NMR spectra of the reaction mixture. Since the signals of the fluorophosphonium cation **F-17**$^+$ cannot be detected in the $^{31}P\{^1H\}$ NMR or in the $^{19}F\{^1H\}$ NMR spectrum of the reaction of **17** with $[Ni(MeCN)_6](BF_4)_2$, it can be speculated that, instead of **F-17**$^+$, nickel complexes of other P,F-containing derivatives are formed.

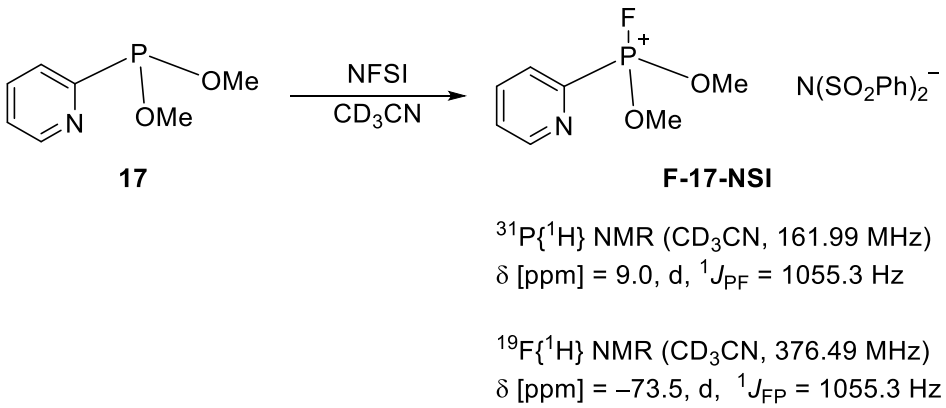

Scheme 3.12: *Fluorination of the bis(methoxy)-2-pyridyl-phosphine (**17**) using NFSI as fluorination reagent.*

Although no definite conclusions can be drawn from the NMR spectroscopic analyses as far as the detailed mechanism of formation of **26** is concerned, the appearance of further signals in the ^{31}P and ^{19}F NMR spectra of the reaction mixture suggest that the reaction mechanism involves decomposition of the tetrafluoroborate anion and the associated formation of F^-. Subsequently, a fluoride-assisted redox reaction could take place and potentially lead to $P^{III} \rightarrow P^V$ transformation followed by the transfer of two electrons from phosphorus to nickel to form the zerovalent nickel complex **26**. Whether a nucleophilic attack of a fluoride ion on to a coordinated phosphine ligand or a coordination of the fluoride to the nickel centre occurs first, remains presently uncertain. Nevertheless, similar observations have been made for Pd phosphine complexes, and the driving force of the fluoride-induced redox activity is suspected to be the formation of strong P–F bonds.[220,225,229]

3.7.2 Investigation of the Proton Source

In order to investigate the proton source for the protonation of two of the four pyridyl moieties within complex **26**, *in-situ* high-resolution mass spectrometry (HR-MS) analyses with electrospray ionisation was carried out. Analysis of the reaction mixture containing four equivalents of the bis(methoxy)-2-pyridyl-phosphine ligand (**17**) and one equivalent of the metal precursor

$[Ni(MeCN)_6](BF_4)_2$ in acetonitrile shows the presence of more than one nickel-containing species in the negative ion mode, with the main species being the doubly-protonated Ni^0 complex with three BF_4^- anions [**26**+BF_4]$^-$ (1005.1412 Da, calcd. 1005.1400 Da, 1.2 ppm error). The assignment of this peak to the nickel(0) complex **26** was confirmed by HR-MS analysis of the pure isolated crystals of **26**·MeOH, which showed the same peak in negative mode. A very small amount of a species with the m/z of 1003.1574 Da was also detected and most likely corresponds to a nickel(II) complex with three BF_4^- anions, in which the ligand molecules are not protonated. In addition, a peak with m/z of 1093.1638 Da was observed and arises most likely from a nickel complex with either three protonated ligands and four BF_4^- anions or a nickel complex with two protonated ligands and a hydride attached to the nickel centre as well as four BF_4^- anions. In the first case, the nickel centre would be present in the oxidation state 0, whereas in the latter case an oxidation state+2 would have to be assumed.

If the reaction is carried out with six equivalents of the ligand **17** with respect to the nickel precursor, instead of four, only the formation of the double protonated Ni^0 complex is observed and not the unprotonated nickel(II) complex. Furthermore, the unidentified peak with m/z ratio 1093.1638 Da is again observable in the mass spectrum (negative ion mode) of the acetonitrile reaction mixture. In the positive ion mode, HR-MS measurements indicated the presence of free ligand **17** as well as the corresponding phosphine oxide **O=17** (most likely due to air exposure during the measurement). No 2,2′-bipyridine was detected, although oxidative C-C coupling reactions of pyridyl compounds can be observed in the presence of metal-organic compounds.[249] These observations point again towards the fact that the (alkoxy)-2-pyridyl-phosphine ligand **17** is involved in the *in-situ* reduction of the metal centre.

To pinpoint the proton source for the protonation of the pyridyl groups, the reaction of $[Ni(MeCN)_6](BF_4)_2$ with four equivalents of **17** was carried out in the aprotic solvent C_6F_6. The reaction results in the formation of a brown precipitate, which was then analysed by HR-MS in acetonitrile. Again, the formation of the double protonated Ni^0 complex is observed, leading to the assumption that the protons of the pyridinium groups result either from ligand scrambling during the reaction or from the MeCN molecules within the nickel(II) precursor and not from the solvent on its own. In connection with this, it is a well-known phenomenon that upon coordination to a M^{2+} cation increase in the acidity of protons within various ligands can occur.[250] In the case of zerovalent nickel bis(dialkylphosphino)ethane fragments, the formation of η^2-nitrile complexes and the subsequent cleavage of the C–H or the C–CN bonds has been reported by W. D. Jones and co-workers (although the C–H activation product was only observed at low temperatures).[251–253]

To further elaborate the role of protons in the reaction, protonation as well as deprotonation experiments were carried out and monitored *via* HR-MS analyses. For this purpose, the complex **26** was dissolved in methanol and treated with two equivalents of tetrafluoroboric acid solution (50 wt% in diethyl ether) or triethylamine. In the case of the protonation experiment, a species was detected which can be assigned to a nickel(0) complex with three protonated ligands and four tetrafluoroborate anions indicating that double protonation of the complex is possible. However, a nickel(II) hydride species $[\{(MeO)_2P(2\text{-py-H})\}_2\{(MeO)_2P(2\text{-py})\}_2NiH]^{3+}$ presents a further possibility and in fact, E. S. Wiedner *et al.* have shown that depending on the acid used for the protonation, either double protonation of the amino groups or hydride formation in similar complexes can take place.[254] Unfortunately, NMR spectroscopic investigations of the reaction of **26** with acid could not rule out either possibility and also showed that decomposition of the complex is occurring. For the deprotonation experiment, small amounts of a monoprotonated Ni complex were detected besides the starting material which indicates that the complex can at least partially be deprotonated.

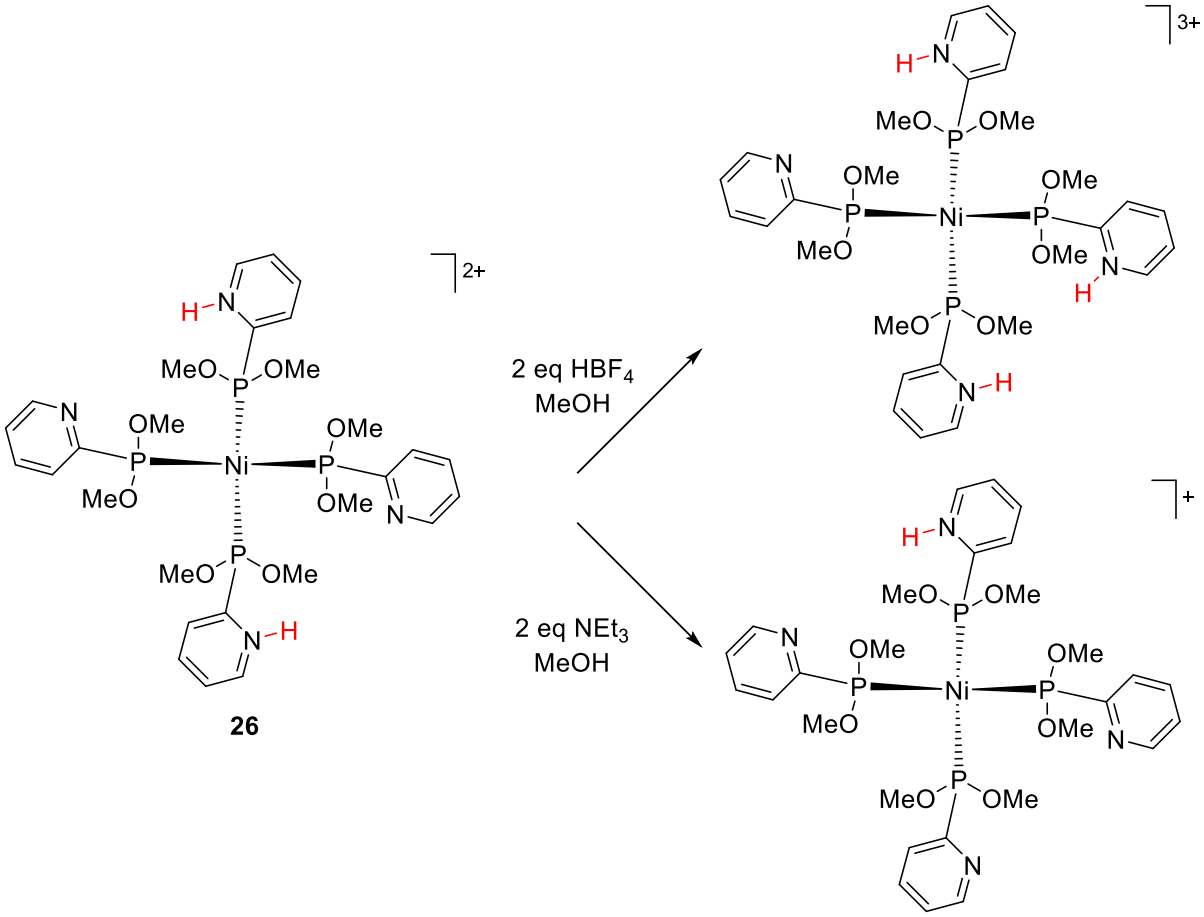

Scheme 3.13: *Attempted protonation and deprotonation experiments of the nickel(0) complex* ***26****.*

From the *in-situ* HR-MS measurements it can be concluded that the reduction process is probably triggered by the "non-innocent" bis(methoxy)-2-pyridyl-phosphine ligand **17** and that the protons

of the protonated pyridinium moieties do not originate from the solvent but from the coordinated MeCN molecules within the nickel(II) precursor or from ligand scrambling. Complex **26** can also be partly protonated and deprotonated.

3.8 Concluding Remarks

2-Pyridyl-phosphine ligand sets can be extensively elaborated using a simple set of synthetic approaches. (Amino)-2-pyridyl-phosphines $(R_2N)_xP(2\text{-py})_{3-x}$ (R = Me, Et, x = 1, 2) can be obtained from the reactions of amino-chloro-phosphines with 2-pyridyllithium. (Alkoxy)-2-pyridyl-phosphines $(RO)_xP(2\text{-py})_{3-x}$ (R = Me, 2-Bu, Ph, x = 1, 2) can be easily derived by direct reactions of the (amino)-2-pyridyl-phosphines with alcohols.

The developed synthetic approach for the easy modification of the 2-pyridyl-phosphine ligand framework provides the potential means for the introduction of chirality through the introduction of chiral amino or alkoxide groups or by creating stereogenic P bridgeheads. For example, the step-wise reaction of alcohols with (amino)-2-pyridyl-phosphines can be used to obtain multidentate (alkoxy)(amino)-2-pyridyl-phosphines $(R_2N)(RO)P(2\text{-py})$, which contain three different organic substituents. These mixed P,N,O ligands were obtained as racemic mixtures, but enantiomerically pure phosphines can be obtained *via* direct resolution using chiral HPLC methods. DFT calculations have shown that the optically pure phosphines should be stable towards racemisation over a prolonged amount of time.

The coordination chemistry of a range of these new ligand systems was investigated for the first time, showing that both the pyridyl-N and bridgehead-P atoms can be involved in coordination to the soft Cu^I centres. Different coordination behaviours were observed for ligands of this type, depending on the number of N donor atoms. While 2-pyridyl-phosphines containing two or more N donor atoms form dimeric Cu^I complexes in which the phosphorus bridgehead and two nitrogen donor atoms (amino- or pyridyl-N atoms) are involved in the coordination, ligands with only one N donor atom form a structural arrangement in which only the phosphorus bridgehead as well as the pyridyl-nitrogen are involved in the coordination.

(Amino)- and (alkoxy)-2-pyridy-phosphines coordinate to metals, such as nickel or rhodium. The 2-pyridyl-phosphine **12** forms a dinuclear A-type complex with Rh^I in which a Rh–Rh bond is present. The reaction of the bis(methoxy)-2-pyridyl-phosphine **17** with $[Ni(MeCN)_6](BF_4)_2$ leads to an unexpected *in-situ* reduction of the metal centre and the formation of a tetrahedral nickel(0) complex **26**. The redox activity is probably induced by the decomposition of the tetrafluoroborate anion and therefore a fluoride-assisted oxidation of the phosphorus atom and reduction of the nickel centre potentially explains the experimental findings. Complex **26** could find application in the field

of electrocatalysts, since similar nickel bis-phosphine complexes with noncoordinating pendant amine bases in the second coordination sphere of the ligand backbone have proven to be very efficient electrocatalysts for hydrogen oxidation and proton reduction.[255–258]

4 Investigation of the Donor Properties of 2-Pyridyl-phosphines

4.1 Preamble

In the development of synthetic organometallic catalysts, variation of the surrounding ligand molecules can lead to enhanced or reduced catalytic activity. It is therefore essential to carefully evaluate ligand characteristics and predict the impact of the ligand framework on the properties of the corresponding transition metal catalyst.[259] In this regard, the steric and electronic effects of the ligands are the most crucial factors to consider, since the key properties of metal complexes, such as their absorption or redox properties, are greatly affected by these parameters.

As mentioned in the introduction of this thesis, the Tolman electronic parameter (TEP) is widely used to quantify the electronic effects of phosphines.[106] In this context, electronic effects describe the net donor ability of a phosphine ligand, and comprise its electron-donating as well as electron-accepting properties. For tertiary phosphines, the TEP is an empirical value, and can be derived from the IR spectrum of the corresponding $[Ni(CO)_3L]$ (L = phosphine) complexes. The concept is based on a simple model: if the ligand donates electron density towards the nickel centre, the nickel can then transfer a certain amount of this electron density to the antibonding π* orbitals of the three remaining CO groups (Figure 4.1). This so-called backdonation to the carbonyl moiety induces a weakening of the C–O bond and a red shift of the corresponding symmetric carbonyl stretching frequency in the IR spectrum. Based on the symmetric A_1 CO stretching frequency in the IR spectrum, the combined σ-donor and π-acceptor properties of phosphines can then be derived. Often, however, the misleading assumption is made, that, due to quite similar σ-donor abilities of tertiary phosphines, the TEP only describes the π-acceptor strength of the ligands.

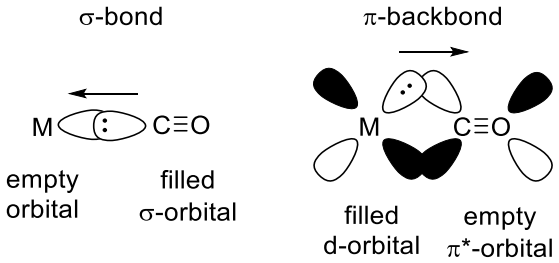

Figure 4.1: *Molecular orbitals involved in the M–CO coordinative bond. Left: σ-bond, right: π-backbond.*

The correlation between the donor properties of the phosphine and the CO ligands as a probe for the electron density on the nickel centre is illustrated in Equation 4-1, where νCO_{Ni} refers to the A_1 CO vibration of $[Ni(CO)_3L]$, 2056.1 cm^{-1} is the A_1 CO vibration of $[Ni(CO)_3\{P(^tBu)_3\}]$ and χ describes the effect of the phosphine ligand on the frequency of the A_1 CO stretch of the corresponding $[Ni(CO)_3L]$ complex. Here, $P(^tBu)_3$ is used as a very simple reference ligand due to

its strong σ-donor character. According to the literature, the symmetric A_1 carbonyl stretching frequency of $[Ni(CO)_3L]$ complexes is designated as the Tolman electronic parameter and is given in cm^{-1}.

$$\nu CO_{Ni} = 2056.1 cm^{-1} + \sum \chi \tag{4-1}$$

The Tolman electronic parameter has shown to have a good linear correlation with the CO stretching frequencies of many other metal carbonyl complexes, incorporating tertiary phosphines (Equation 4-2, where a and b are linear coefficients).[106,260,261]

$$\nu CO_{Metal} = a \cdot \nu CO_{Ni} + b \tag{4-2}$$

Despite the very good correlation between the TEP and experimentally measured data, electron-deficient phosphines with good π-acceptor properties often follow a different correlation than more electron-rich phosphines, which are known to be poor π-acceptors. Consequently, most equations that relate various transition metal complexes to the TEP scale are only accurate for poor π-acceptor ligands.[261] The binding properties of ligands have also shown a certain dependence on the choice of transition metal[262] and the comparison of different ligand types, *e.g.* carbenes and phosphines, *via* the TEP, is questionable.[259]

In addition to the use of the CO moiety as probe for the electronic properties of a phosphine metal fragment, other methods, such as certain $^1J_{PE}$ coupling constants (E = element), have been employed to predict and evaluate the donor properties of phosphines ligands. Especially, for multidentate phosphines with heteroatom-containing substituents, the direct phosphorus-31 selenium-77 spin–spin coupling constant ($^1J_{PSe}$) of the phosphine selenide has proven to be a very useful approach. This is due to the fact that in such multitopic ligand sets, not only the phosphorus atom, but also other heteroatoms, can be involved in coordination to a metal carbonyl fragment, which complicates the determination of the TEP.[263]

The $^1J_{PSe}$ coupling constant values of phosphine selenides depend on the nature of the substituents on the phosphorus atom and are known to reflect the σ-donating ability of the corresponding phosphine: the more pronounced the σ-donor character of the phosphine, the smaller the absolute value of the coupling constant. The coupling constant is sensitive towards the hybridisation, or more precisely the s-character, of the lone pair of the phosphorus atom. In general, the spin-spin coupling constant increases with the introduction of more electron-withdrawing substituents and an enhanced s-character of the phosphorus lone pair.[263] In this context, it should be kept in mind that in addition to the electronic properties of the phosphine, its steric effects influence the $^1J_{PSe}$ coupling constant, since the presence of bulky substituents results in a decrease in s-character of the P lone pair caused by the widening of the R–P–R bond angles.[264] The $^1J_{PSe}$ coupling constants of phosphorus selenides

are also known to correlate with the Brønsted basicity (pK_B) of the corresponding phosphines, or to be more precise, of the phosphorus atom.[264]

Since the evaluation and prediction of the donor properties of phosphines are crucial for the rational design of transition metal catalysts, the donor abilities of 2-pyridyl-phosphines were investigated. Therefore, the Tolman electronic parameters derived from experimental and computational data, as well as donor properties derived from the $^1J_{PSe}$ coupling constants of the corresponding phosphine selenides were utilised. This data can provide grounds for the classification of novel 2-pyridyl-phosphines with regard to the classic tertiary phosphines used in homogeneous transition metal catalysis.

4.2 Experimental Determination of the Donor Properties of 2-Pyridyl-phosphines using W and Mo Carbonyl Complexes

Originally, nickel carbonyl complexes of the form $[Ni(CO)_3L]$ (L = phosphine), in which the phosphine only coordinates the metal *via* the phosphorus atom, were used to determine the Tolman electronic parameter and describe the intrinsic electronic properties of various ligand systems.[106] However, due to the toxicity of the nickel tetracarbonyl precursor, the CO stretching frequencies of other metal carbonyl complexes incorporating tertiary phosphines have been a topic of interest. In this regard, tungsten and molybdenum carbonyl complexes have shown excellent correlation with the TEPs obtained from $[Ni(CO)_3L]$ complexes.[260,261] The advantage of using molybdenum and tungsten carbonyl compounds for the determination of the TEP lies in their easy synthetic manageability as well as the diamagnetic character of the Mo^0/W^0 carbonyl species, which enables facile NMR spectroscopic analysis. Therefore, 2-pyridyl-phosphines were reacted with tungsten(0) and molybdenum(0) carbonyl precursors to determine the CO stretching frequencies and convert these into the TEP.

Preliminary reactions of $P(6\text{-Me-2-py})_3$ (**2**) and $(Et_2N)_2P(2\text{-py})$ (**12**) with tungsten and molybdenum hexacarbonyl were carried out in acetonitrile at room temperature and under reflux conditions. However, these reactions resulted in very slow and unspecific conversions and no products other than starting materials could be isolated. Therefore, the acetonitrile derivatives $[M(CO)_5(MeCN)]$ (M = W, Mo),[265] which were obtained from the reaction of the corresponding metal hexacarbonyl with trimethylamine *N*-oxide in acetonitrile, were selected as carbonyl precursors.

The reaction of tris-2-pyridyl-phosphine $P(2\text{-py})_3$ (**1**) with $[W(CO)_5(MeCN)]$ in a 1 : 1 stoichiometric reaction resulted in the formation of a brown solution. $^{31}P\{^1H\}$ NMR spectroscopy revealed the presence of various phosphorus-containing tungsten complexes, probably due to the various possible coordination modes (*e.g. via* the phosphorus as well as the nitrogen donor atoms).

For example, the signal at 33.9 ppm with $^{1}J_{PW}$ = 116.8 Hz in the $^{31}P\{^{1}H\}$ NMR spectrum can most likely be attributed to a tungsten carbonyl complex in which the phosphine coordinates to W *via* the phosphorus bridgehead, whereas the more upfield shifted signals in the range of –5.0 and –10.0 ppm point towards coordination of the phosphine *via* the pyridyl-nitrogen donor atoms. Layering a saturated DCM solution with *n*-hexane produced dark red crystals of the tungsten tris-2-pyridyl-phosphine complex **28** as well as colourless crystals of complex **29** (Scheme 4.1). Within complex **28**, the tungsten atom is coordinated by two pyridyl-nitrogen atoms of the ligand in a *cis* arrangement and four remaining carbonyl ligands. A similar complex, [Cl{P(2-py)$_3$}W≡CPh(CO)$_2$], in which only two of the three pyridyl-nitrogen atoms are involved in the coordination to the tungsten centre was previously reported in the literature by C.-M. Che and co-workers.[71] Complex **29** contains a tungsten centre that is coordinated by two phosphorus atoms of two ligand molecules and four carbonyl ligands. Unfortunately, since **28** and **29** could not be separated, no conclusions about the donor strength of the phosphine can be drawn. However, very similar results were obtained from the reaction of [Mo(CO)$_4$(NBD)] (NBD = norbornadiene, bicyclo[2.2.1]hepta-2,5-diene) and P(2-py)$_3$ or PhP(2-py)$_2$. *In-situ* NMR and IR spectroscopic analyses have shown that initially, the *N*,*N*'- (analogous to **28**) and the *P*,*P*'-coordinated (analogous to **29**) complexes are formed in equimolar amounts, but then decomposition of the *N*,*N*'-coordinated complex occurs.[266,267]

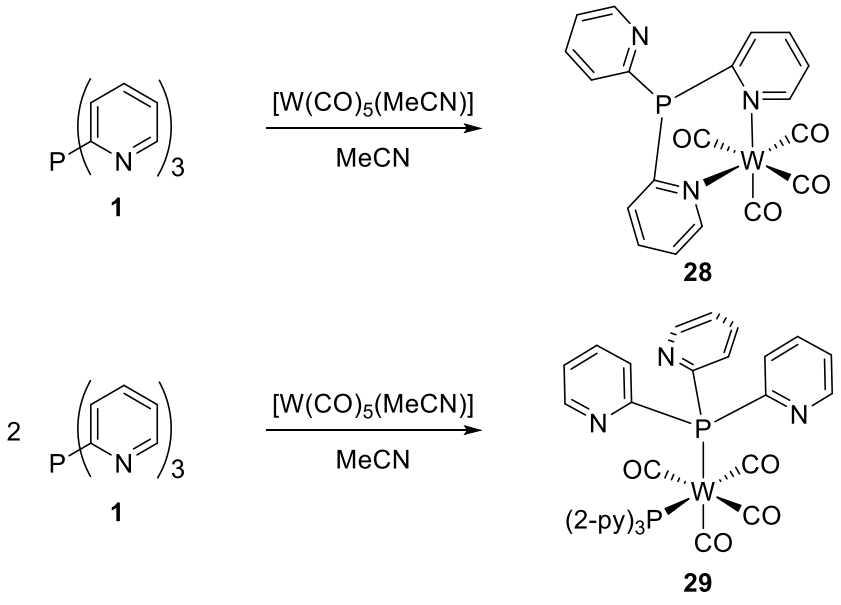

Scheme 4.1: *Reaction of the phosphorus-bridged tris-2-pyridyl ligand **1** with [W(CO)$_5$(MeCN)] to afford complex **28** and **29**.*

Attempts to employ the 6-Me- or 6-Br-substituted ligands P(6-Me-2-py)$_3$ (**2**) and P(6-Br-2-py)$_3$ (**3**) with [W(CO)$_5$(MeCN)] were unsuccessful, and only the tungsten precursor was isolated after workup. However, $^{31}P\{^{1}H\}$ NMR spectroscopic analyses of the reaction mixtures indicated a

downfield shift of the signals with respect to those of the free ligands and the appearance of tungsten satellites. These findings point towards the presence of tungsten phosphine complexes in which *P*-coordination of the ligand takes place. No pure products could be isolated from the reactions of the (amino)- and (alkoxy)-2-pyridyl-phosphines $(Et_2N)_2P(2\text{-py})$ (**12**), $(MeO)_2P(2\text{-py})$ (**17**) and $(Et_2N)(PhO)P(2\text{-py})$ (**18**) with $[W(CO)_5(MeCN)]$, and NMR spectroscopic analyses gave no clear indication of what kind of tungsten complexes have been formed. This is probably due to the presence of a variety of different donor atoms and dynamic complexation behaviour in solution. Additionally, the acetonitrile tungsten precursor may not have been an ideal starting material, since the tungsten complex $[W(CO)_5\{(Me_2N)_2P(2\text{-py})\}]$ has been prepared previously from the reaction of the phosphine with $[W(CO)_5(THF)]$.[158]

The reaction of tris-2-pyridyl-phosphine **1** with the *in-situ* generated $[Mo(CO)_5(MeCN)]$ resulted in the formation of different P-containing species, which exhibited downfield as well as upfield shifted signals in the $^{31}P\{^1H\}$ NMR spectrum with respect to the free ligand. Layering a saturated DCM solution with *n*-hexane gave single-crystals of the literature-known Mo-complex $[\{P(2\text{-py})_3\}Mo(CO)_3]$ in which the ligand binds the metal at the facial position of an octahedron *via* all three pyridyl-nitrogen atoms.[61] The upfield shift of the $^{31}P\{^1H\}$ NMR signal to –4.3 ppm in $CDCl_3$ indicates that this *N*,*N*',*N*''-coordination is retained in solution.

The molybdenum(0) complex $[Mo(CO)_5\{P(6\text{-Me-2-py})_3\}]$ (**30**) was cleanly obtained from the reaction of **2** with $[Mo(CO)_5(MeCN)]$ in acetonitrile at room temperature (Scheme 4.2). **30** represents the first Mo complex in which a 2-pyridyl-phosphine coordinates to the Mo metal centre only *via* the P bridgehead. Other 2-pyridyl-phosphine Mo complexes usually involve *N*,*N*',*N*''-coordination, such as in the case of $[\{P(2\text{-py})_3\}Mo(CO)_3]$,[61] or *P*,*N*-coordination, as found in *trans*-$[Mo_2(O_2CCF_3)_4\{P(2\text{-py})_3\}_2]$.[72] Again, crystals could be grown by layering a DCM solution with *n*-hexane (crystalline yield: 18 %). The $^{31}P\{^1H\}$ spectrum of **30** contains a singlet, which is shifted downfield to 45.3 ppm (CD_3CN) relative to the free ligand **2** (–3.2 ppm, $CDCl_3$). Since only *P*-coordination to the Mo centre occurred, the CO stretching frequencies in **30** can be utilised to calculate the TEP.

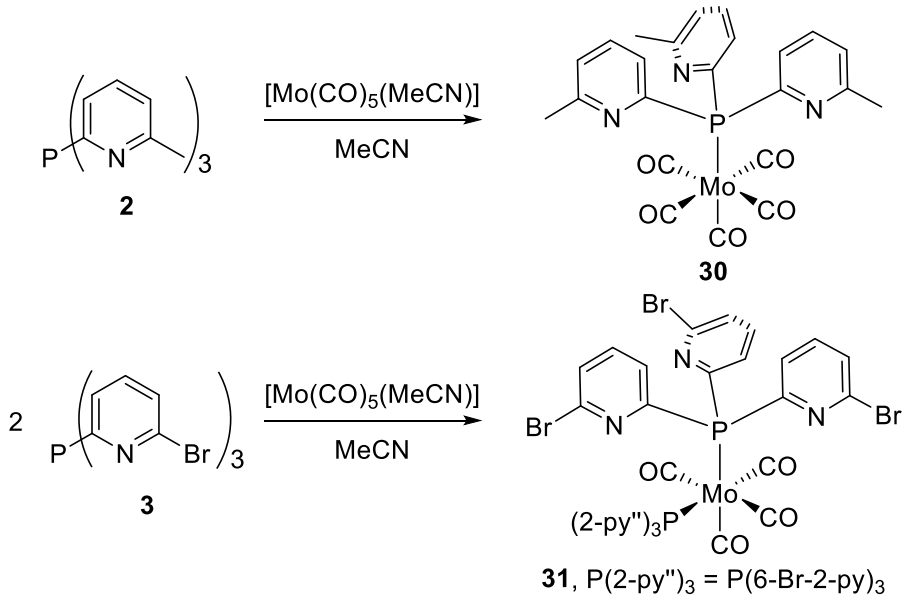

Scheme 4.2: *Reactions of the tripodal ligands **2** and **3** with in-situ generated [Mo(CO)$_5$(MeCN)].*

Figure 4.2 shows the IR spectrum of **30** and the presence of at least four carbonyl stretching frequencies in the range of 1913–2070 cm^{-1}. Based on the ideal C_{4v}-symmetry of the complex, only three bands would be expected. However, due to the local C_3-symmetry of the ligand the molecular symmetry of the complex is reduced, and geometry optimisations and subsequent frequency analysis (TPSS,[244] def2-TZVP,[139,140] see Chapter 8.4, page 136) revealed the presence of five different CO stretching frequencies, out of which three are very similar in energy. Also it has been shown that the symmetry in the solid state tends to be lower than the molecular symmetry.[45] Thus, for the evaluation of the donor strength, only the A_1 stretch at *ca.* 2070 cm^{-1} will be used, owing to the overlapping and unresolved nature of the lower-energy bands.[268]

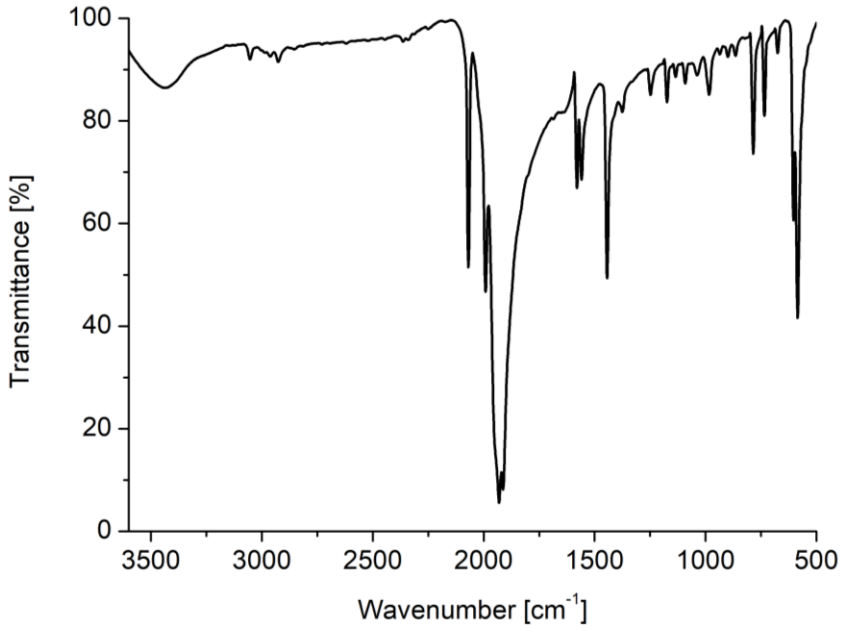

Figure 4.2: *IR spectrum of [Mo(CO)$_5${P(6-Me-2-py)$_3$}] (**30**), measured as a KBr pellet in the solid state.*

Based on the correlation between the TEP and the experimentally measured data, the A_1 CO vibration in $[Mo(CO)_5L]$ complexes can be converted into the TEP (Equation 4-3).[261]

$$\nu CO_{Ni} = 1.116 \cdot \nu CO_{Mo} - 243;\ R = 0.858 \qquad (4\text{-}3)$$

From Equation 4-3, the A_1 stretch at 2070 cm^{-1} for complex **30** was calculated to correspond to an A_1 stretch of 2067 cm^{-1} in the corresponding nickel complex $[Ni(CO)_3\{P(6\text{-Me-2-py})_3\}]$.

In the case of the reaction of the 6-Br-substituted tripodal phosphine **3** with $[Mo(CO)_5(MeCN)]$, the disubstituted complex *cis*-$[Mo(CO)_4\{P(6\text{-Br-2-py})_3\}_2]$ (**31**) was isolated as crystals in 13 % yield (Scheme 4.2). Interestingly, two ligand molecules, instead of one, coordinate to the metal *via* their phosphorus bridgehead atoms in a *cis* fashion. In the $^{31}P\{^1H\}$ NMR spectrum a downfield shift to 50.3 ppm in $CDCl_3$ with respect to the free ligand (–0.9 ppm, CD_3COCD_3) was again observed, as seen in complex **30**. The IR spectrum of **31** is shown in Figure 4.3 and exhibits three carbonyl bands in the 1880–2030 cm^{-1} region. In theory, four stretching frequencies would be expected from the ideal C_{2v}-symmetry of the complex, which was also confirmed by frequency analysis of **31** (TPSS,[244] def2-TZVP,[139,140] see Chapter 8.4, page 136). However, due to the broadness of the bands, the fourth one is likely obscured by the remaining bands.

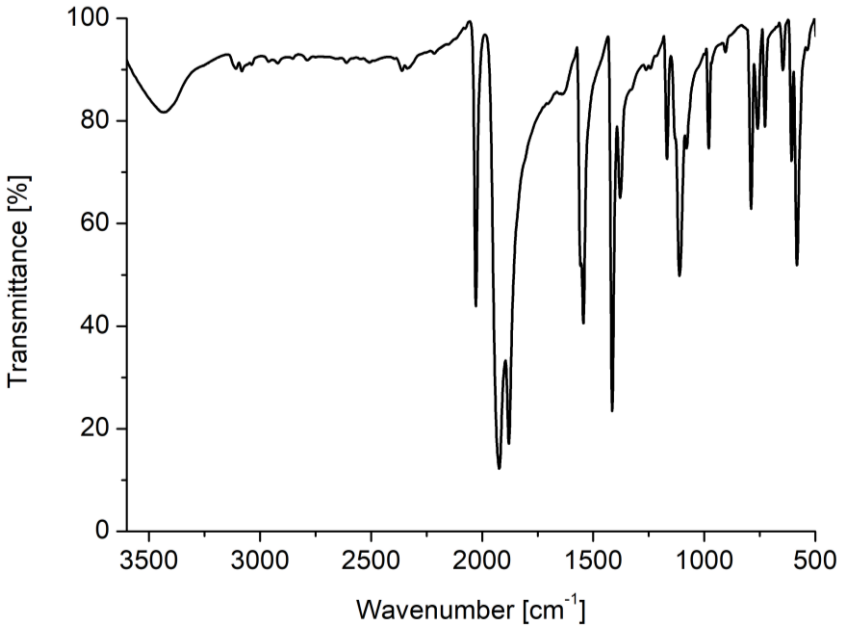

Figure 4.3: *IR spectrum of cis-[Mo(CO)$_4${P(6-Br-2-py)$_3$}$_2$] (**31**), measured as a KBr pellet in the solid state.*

For the conversion of the A_1 CO stretch at approximately 2029 cm^{-1} in **31** into the corresponding Tolman parameter, the so-called Crabtree scale can be used. R. H. Crabtree showed that the carbonyl stretching frequency of *cis*-$[Mo(CO)_4(L–L)]$ complexes, in which L–L can be a bidentate phosphine ligand or two monodentate phosphines, correlates very well (R = 0.996) with the TEP using Equation 4-4.[260]

$$\nu CO_{Ni} = 0.593 \cdot \nu CO_{Mo} + 871;\ R = 0.996 \qquad (4\text{-}4)$$

An A_1 νCO absorption at 2074 cm^{-1} was calculated for the corresponding nickel complex $[Ni(CO)_3\{P(6\text{-Br-2-py})_3\}]$; this frequency is slightly larger than the one calculated for $[Ni(CO)_3\{P(6\text{-Me-2-py})_3\}]$. This indicates decreased metal–CO backbonding and a progressively stronger C–O bond in the case of the $P(6\text{-Br-2-py})_3$ ligand. Therefore, **3** exhibits a lower net donor strength than **2**, which is plausible, since the introduction of electron-withdrawing substituents in the 6-position of the pyridyl rings, like the Br-substituent, should lead to reduced σ-donor strength and enhanced π-acceptor capability. In comparison, the triphenylphosphine nickel complex $[Ni(CO)_3(PPh_3)]$ shows an A_1 νCO absorption at 2070 cm^{-1}.[261] From this it can be concluded that **2** has a slightly higher net donor strength than PPh_3, whereas the bromine-substituted ligand **3** comprises the lowest net donor strength, due to its better π-accepting properties.

As seen in the case of the reactions with tungsten carbonyl, no pure products could be isolated from the reactions of the (amino)- and (alkoxy)-2-pyridyl-phosphines **12**, **17** and **18** with Mo^0, despite several purification and crystallisation attempts. However, in all cases downfield shifts of the singlets in the $^{31}P\{^1H\}$ NMR spectra were observed, suggesting that coordination *via* the phosphorus atoms probably occurred.

4.2.1 Solid State Structures of the W and Mo Complexes

The solid state structures of the new tungsten(0) and molybdenum(0) complexes $[\{P(2\text{-py})_3\}W(CO)_4]\cdot$DCM (**28**·DCM), *cis*-$[W(CO)_4\{P(2\text{-py})_3\}_2]$ (**29**), $[Mo(CO)_5\{P(6\text{-Me-2-py})_3\}]$ (**30**) and *cis*-$[Mo(CO)_4\{P(6\text{-Br-2-py})_3\}_2]$ (**31**·2 *n*-hexane) were determined by single-crystal X-ray crystallography (Table 4.1).

Table 4.1: *Selected bond lengths (Å) and angles (°) in the transition metal complexes* ***28*****–*****31*** *(M = W, Mo).*

	28·DCM	**29**	**30**	**31**·2 *n*-hexane
P–C_{py}	1.835(3)–1.848(4)	1.843(2)–1.851(2)	1.835(2)–1.838(2)	1.804(3)–1.853(3)
P–M	-	2.5050(7)–2.5253(6)	2.5064(6)	2.493(1)–2.5290(8)
M–N_{py}	2.268(2)–2.278(2)	-	-	-
C_{py}–P–C_{py}	100.1(1)–103.7(1)	99.0(1)–103.1(1)	101.74(8)–103.01(8)	97.7(2)–105.2(1)
P–C_{py}–N_{py}	112.0(2)–120.8(2)	110.7(2)–118.0(2)	111.8(1)–113.1(1)	112.7(2)–120.9(2)
M–CO	C_{cis} 2.032(3)–2.058(3) C_{trans} 1.953(3)–1.959(3)	C_{cis} 2.036(3)–2.038(2) C_{trans} 1.975(3)–1.995(2)	C_{cis} 2.037(2)–2.061(2) C_{trans} 2.001(2)	C_{cis} 2.010(4)–2.071(4) C_{trans} 1.987(3)–1.988(5)
C–O	C_{cis} 1.141(4)–1.151(4) C_{trans} 1.169(4)–1.172(4)	C_{cis} 1.143(3)–1.146(4) C_{trans} 1.149(3)–1.162 (3)	C_{cis} 1.136(3)–1.141(2) C_{trans} 1.145(3)	C_{cis} 1.128(5)–1.156(4) C_{trans} 1.147(7)–1.154(4)

Figure 4.4 depicts the crystal structure of the W^0 complex [{P(2-py)$_3$}W(CO)$_4$]·DCM (**28**·DCM). The tris-2-pyridyl-phosphine coordinates the tungsten centre using two of the three pyridyl-nitrogen donor atoms. The third pyridyl-N atom is not involved in any coordination in the solid state and points away from the metal. In addition, four carbonyl ligands coordinate to the tungsten centre, resulting in a distorted octahedral coordination environment. The W–N_{py} bond lengths (2.268(2)–2.278(2) Å) are slightly longer than those found in [Cl{P(2-py)$_3$}W≡CPh(CO)$_2$] (2.254(5)–2.255(5) Å[71]), which is consistent with the difference in oxidation state between the two complexes. Furthermore, the N–W–N bond angles are in the range 82.07(8)–82.76(8)° and are therefore considerably smaller than the ideal octahedral angle of 90°, due to the chelation of the W centre *via* the two nitrogen atoms of one ligand. The W–CO bond lengths in *cis* positions with respect to the N-donor atoms of the ligand are in the range 2.032(3)–2.058(3) Å and therefore larger than the two W–CO bond lengths in *trans* position, which were found to be 1.953(3)–1.959(3) Å. For the C–O bond lengths, the reverse trend is be observed. The *cis* C–O bond lengths (1.141(4)–1.151(4) Å) are shorter than the *trans* ones (1.169(4)–1.172(4) Å). This can be attributed to the *cis*-effect of the coordinated phosphine ligand.[269,270] The *cis*-labilising ability of phosphine ligands in group 6 carbonyl compounds, which is found to be opposite to the *trans*-effect, influences the ground state properties (*e.g.* the *cis*-M–CO bond length) as well as the thermodynamic and kinetic

properties.[271] The *cis*-effect of a ligand on the ground state properties of other bonds within a transition metal complex is generally referred to as the *cis*-influence.[269]

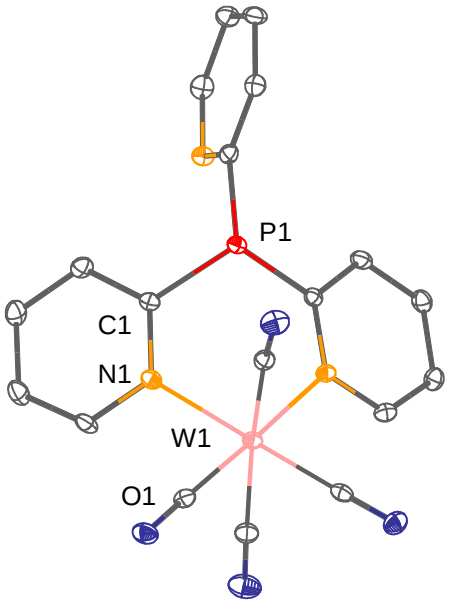

Figure 4.4: *Structure of [{P(2-py)$_3$}W(CO)$_4$]·DCM (**28**·DCM). Only one of the two molecules in the asymmetric unit is depicted. The DCM solvent molecule and hydrogen atoms are omitted for clarity. Displacement ellipsoids are drawn at the 30 % probability level.*

The tungsten complex **29**, in which two ligand molecules are involved in the coordination *via* their P bridgeheads, is shown in Figure 4.5. In addition to the two phosphine molecules in *cis* positions, four CO groups coordinate the metal, resulting in a distorted octahedral coordination. Due to the steric clash between the phosphine ligands, the P–W–P angle is slightly widened (98.77(2)°). The P–W bond lengths are in the range 2.5050(7)–2.5253(6) Å and therefore slightly shorter than those found in [W(CO)$_4${Ph$_2$P(2-py)}$_2$] (2.5562(4) Å[272]), which could be due to the better π-accepting properties of P(2-py)$_3$ compared to that of Ph$_2$P(2-py). The lengths of the W–CO in *cis* position to both phosphine ligands are in the range 2.036(3)–2.038(2) Å and therefore longer than the ones in a *trans* arrangement, which were found to be 1.975(3)–1.995(2) Å, which agrees with the *cis*-influence. The C–O bond lengths found in **29** (C_{cis}–O 1.143(3)–1.146(4) Å, C_{trans}–O 1.149(3)–1.162(3) Å) are almost identical with those in the diphenyl-2-pyridyl-phosphine tungsten complex [W(CO)$_4${Ph$_2$P(2-py)}$_2$] (C_{cis}–O 1.141(2) Å, C_{trans}–O 1.163(2) Å).[272]

Interestingly, the *cis*/*trans*-isomerisation in diphenyl-2-pyridyl-phosphine tungsten carbonyl complexes was found to be affected by intramolecular, or more precisely intraligand, hydrogen bonding and cation π-interactions, and can therefore be switched by the deliberate protonation or deprotonation of the 2-pyridyl-phosphine derivatives.[272,273] Also, the solid state structure of **29** shows an intramolecular face-to-face π-stacking interaction between the two pyridyl moieties of the

two phosphine ligands with the shortest distance between the rings being 3.617(3) Å (C–C distance between *ipso* carbon atoms, Figure 4.5 right). The angle between the planes formed by the pyridyl rings was found to be 20.71°. The attractive π-π interactions and the compression of the C_{py}–P–C_{py} angles from the expected 109.5° to 99.0(1)–103.1(1)° reduce the repulsion between the phosphine ligands and can probably play a role in the formation of a *cis* arrangement of the 2-pyridyl-phosphines. However, since the π-interaction between the two pyridyl moieties exceeds the sum of the van der Waals radii of the carbon atoms and there is significant tilting of the pyridyl rings, the *cis*-influence and the therewith associated kinetically controlled substitution of the second phosphine could also explain the unexpected *cis* arrangement of the ligands found in **29**.

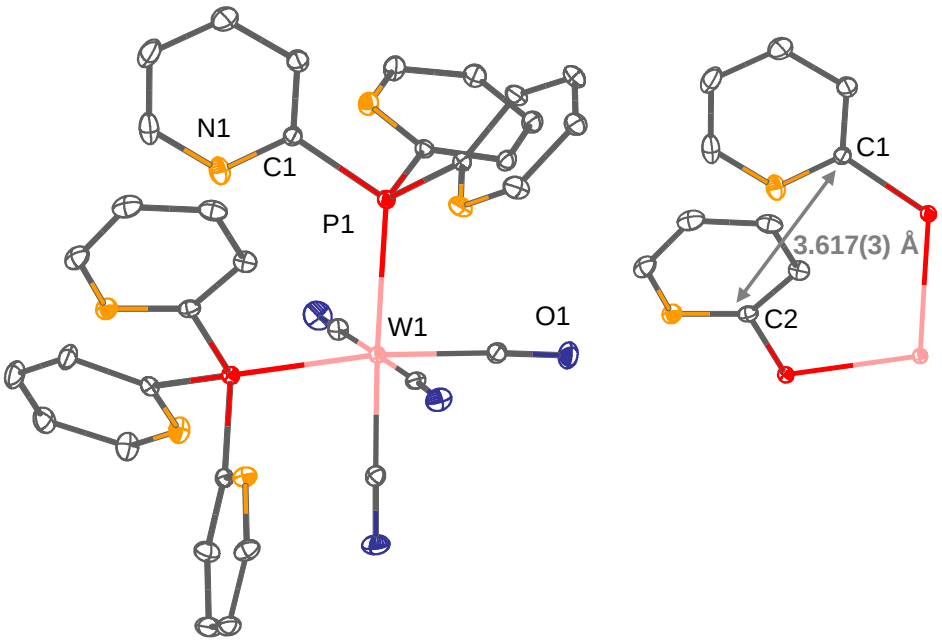

Figure 4.5: *Structure of cis-[W(CO)$_4${P(2-py)$_3$}$_2$] (**29**, left) and face-to-face π-stacking interaction between the two pyridyl rings of the phosphine ligands (right). Hydrogen atoms are omitted for clarity. Displacement ellipsoids are drawn at the 30 % probability level.*

When Mo^0, more precisely [Mo(CO)$_5$(MeCN)], was employed, complex **30** was isolated, in which only coordination *via* the phosphorus bridgehead, rather than the harder nitrogen donor atoms, was observed (Figure 4.6). The Mo^0 centre again has a distorted octahedral coordination environment and is coordinated by the P atom of phosphine **2** with a Mo–P bond length of 2.5064(6) Å, and by five carbonyl ligands. The Mo–P bond length in **30** is shorter than in its triphenylphosphine counterpart [Mo(CO)$_5$(PPh$_3$)] (2.560(1) Å[274]), suggesting a different ligand donor strength. The Mo–CO bond lengths *cis* to the ligand are in the range 2.037(2)–2.061(2) Å, whereas again a shorter Mo–CO bond length for the *trans* CO ligand was observed (2.001(2) Å). The C–O bond lengths in *cis* and *trans* position to the ligand in complex **30** are the same within the error (C_{cis}–O 1.136(3)–1.141(2) Å, C_{trans}–O 1.145(3) Å). Similar Mo–C and C–O bond lengths were found in the

corresponding complex [Mo(CO)$_5$(PPh$_3$)] (Mo–C$_{cis}$ 2.030(4)–2.067(4) Å, Mo–C$_{trans}$ 1.995(3) Å[274]). Therefore, no detailed conclusions about the σ-donating and π-accepting properties of **2** in comparison to PPh$_3$ can be drawn from the single-crystal X-ray crystallographic structures of both compounds. However, the determination of the TEP *via* the IR spectrum of **30** leads to the conclusion that the methyl-substituted tris-2-pyridyl-phosphine **2** has a higher net donor strength and therefore better σ-donor properties than PPh$_3$, due to the electron-donating properties of the methyl substituents.

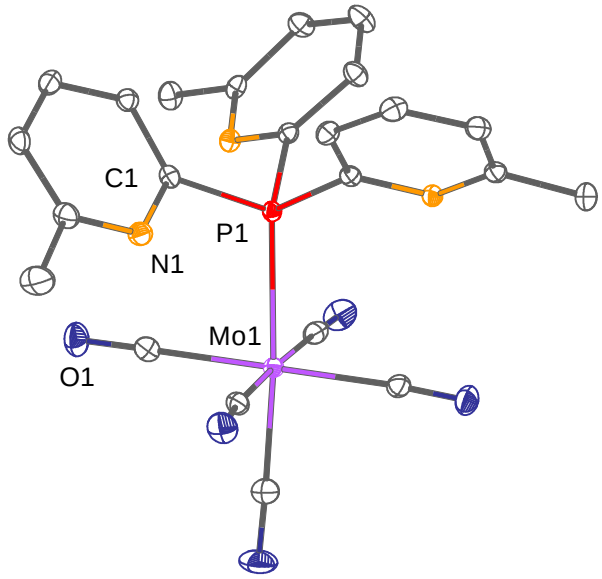

Figure 4.6: *Structure of [Mo(CO)$_5${P(6-Me-2-py)$_3$}] (**30**). Hydrogen atoms are omitted for clarity. Displacement ellipsoids are drawn at the 30 % probability level.*

The structure of *cis*-[Mo(CO)$_4${P(6-Br-2-py)$_3$}$_2$] (**31**) is shown in Figure 4.7. Two bromo-substituted tris-2-pyridyl-phosphine ligands coordinate the metal with their phosphorus bridgeheads (Mo–P 2.493(1)–2.5290(8) Å) in addition to four carbonyl ligands. Again, the phosphine ligands are *cis* to each another, which was unexpected based on the steric congestion. However, the repulsion is reduced by the compression of the C$_{py}$–P–C$_{py}$ angles from the expected 109.5° to 97.7(2)–105.2(1)° and the slight opening of the P–Mo–P angle to 95.13(3)°. Additionally, the solid state structure revealed intramolecular π–π interactions between the pyridyl rings of the two ligands, like those seen in the W complex **29**. The distance between the *ipso* carbon atoms of the two pyridyl rings was found to be 3.354(4) Å, and the angle between the pyridyl planes is 5.29°. The Mo–P bond lengths found in **31** are shorter than those in its counterpart *cis*-[Mo(CO)$_4$(PPh$_3$)$_2$] (2.576(2)–2.577(2) Å[275]), which can probably be attributed to the greater π-acceptor strength of P(6-Br-2-py)$_3$ in comparison to triphenylphosphine. Again, as seen in the complexes before, the Mo–CO bond lengths at the *cis* position with respect to both ligands are longer and in the range 2.010(4)–2.071(4) Å, whereas the Mo–CO bond lengths of the mutually *trans* carbonyl ligands are slightly shorter (1.987(3)–1.988(5) Å). The C–O bond lengths in **31** are with C$_{cis}$–O 1.128(5)–1.156(4) Å and C$_{trans}$–

O 1.147(7)–1.154(4) Å similar to the ones observed in the triphenylphosphine derivative *cis*-$[Mo(CO)_4(PPh_3)_2]$ (C_{cis}–O 1.136(8)–1.137(8) Å, C_{trans}–O 1.149(8)–1.158(8) Å[275]). Although the C–O bond lengths point towards a very similar donor strength of the tris-2-pyridyl-phosphine P(6-Br-2-py)$_3$ (**3**) and triphenylphosphine, the previously determined TEP values show the enhanced π-acceptor character of **3**, in comparison to PPh_3.

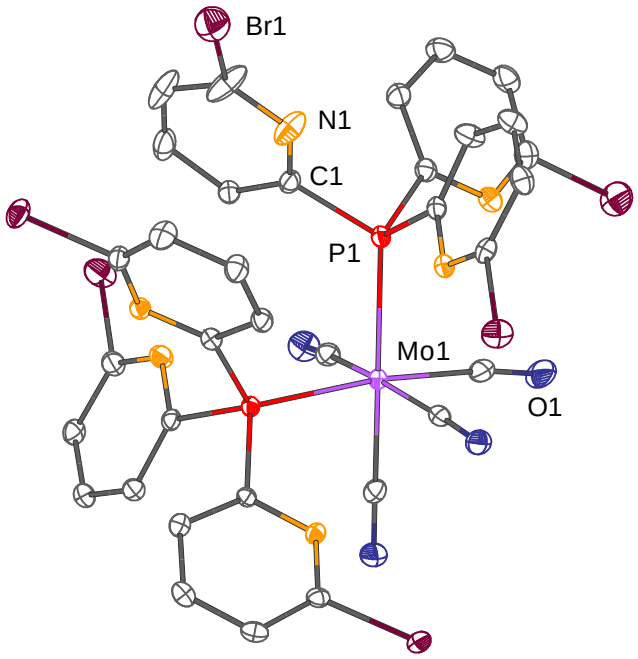

Figure 4.7: *Structure of cis-[Mo(CO)$_4${P(6-Br-2-py)$_3$}$_2$]·2 n-hexane (**31**·2 n-hexane). Hydrogen atoms, solvent molecules and the split valence of one of the Br atoms are omitted for clarity. Displacement ellipsoids are drawn at the 30 % probability level.*

4.3 Experimental Determination of the Donor Properties using Phosphine Selenides

2-Pyridyl-phosphines are multidentate ligands, which possess at least phosphorus and nitrogen donor atoms. The presence of additional donor atoms other than phosphorus within the ligand framework complicates the experimental determination of the donor ability of such phosphines *via* the Tolman electronic parameter, since atoms other than phosphorus can be involved in the coordination to a metal carbonyl fragment. This has already been demonstrated in the previous discussion of the tungsten and molybdenum complexes of 2-pyridyl-phosphines. As an alternative the $^1J_{PSe}$ coupling constant of organophosphorus selenides can be utilised, since this direct spin-spin coupling constant depends on the nature of the substituents on the phosphorus atom and is known to reflect the σ-donor properties of phosphine ligands.[263]

2-Pyridyl-phosphines were easily converted into the corresponding phosphine selenides by the reaction of the relevant phosphine with grey selenium at elevated temperatures (Scheme 4.3).

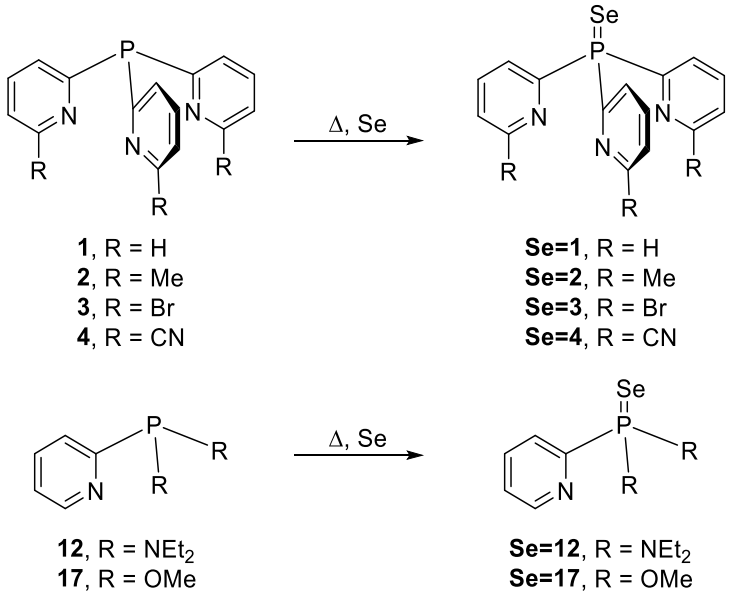

Scheme 4.3: *Oxidation of the 2-pyridyl-phosphines with grey selenium at elevated temperatures.*

The reaction progress was monitored by $^{31}P\{^{1}H\}$ NMR spectroscopy, and a shift of the phosphine selenide with respect to the free phosphine, as well as the appearance of selenium satellites, could be observed (Table 4.2). The selenium satellites in the $^{31}P\{^{1}H\}$ NMR spectrum are due to the coupling with the spin 1/2 ^{77}Se nucleus, which has a natural abundance of only 7.63 %.[276] In the following discussion, the phosphine selenides derived from **1**, **2**, **3**, **4**, **12** and **17** are denoted as **Se=1**, **Se=2**, **Se=3**, **Se=4**, **Se=12** and **Se=17**, respectively. All reactions were carried out in D_8-toluene, since $^{1}J_{PSe}$ values can differ in various solvents, especially if an interaction between the solvent and the selenium atom occurs.[264]

Table 4.2: *$^{31}P\{^{1}H\}$ NMR chemical shifts of the free ligands and their corresponding selenides (L = phosphine).*

Ligand	$^{31}P\{^{1}H\}$ NMR [ppm] of L in $CDCl_3$	$^{31}P\{^{1}H\}$ NMR [ppm] of Se=L in D_8-toluene	$^{1}J_{PSe}$ [Hz] of Se=L in D_8-toluene
$P(2\text{-py})_3$ (**1**)	–1.0	30.7	782.4
$P(6\text{-Me-2-py})_3$ (**2**)	–3.2	30.1	756.4
$P(6\text{-Br-2-py})_3$ (**3**)	–0.6	28.1	782.4
$P(6\text{-CN-2-py})_3$ (**4**)	1.3	31.2	759.7
$(Et_2N)_2P(2\text{-py})$ (**12**)	93.9	71.9	787.2
$(MeO)_2P(2\text{-py})$ (**17**)	150.1	89.3	886.0
PPh_3	–5.4	35.2	759.7

A downfield shift of the $^{31}P\{^{1}H\}$ NMR signals was observed for the tris-2-pyridyl-phosphine selenides **Se=2**, **Se=3** and **Se=4** in comparison with the free phosphines. This deshielding effect is

in line with the behaviour of many other organophosphorus selenides.[277] In contrast, the selenides of the (amino)-2-pyridyl-phosphine **Se=12** and the (alkoxy)-2-pyridyl-phosphine **Se=17**, appear further upfield from the corresponding phosphines **12** and **17**. NBO and second-order perturbation analyses of **Se=12** and **Se=17** (TPSSh,[244,278,279] def2-TZVP,[139,140] see Chapter 8.4, page 136), indicated that this could be due to electron-donation from the amino-nitrogen and alkoxy-oxygen lone pairs into the antibonding P–C_{py} and P=Se orbitals. This leads to enhanced electron density around the phosphorus atom and a shielding effect.

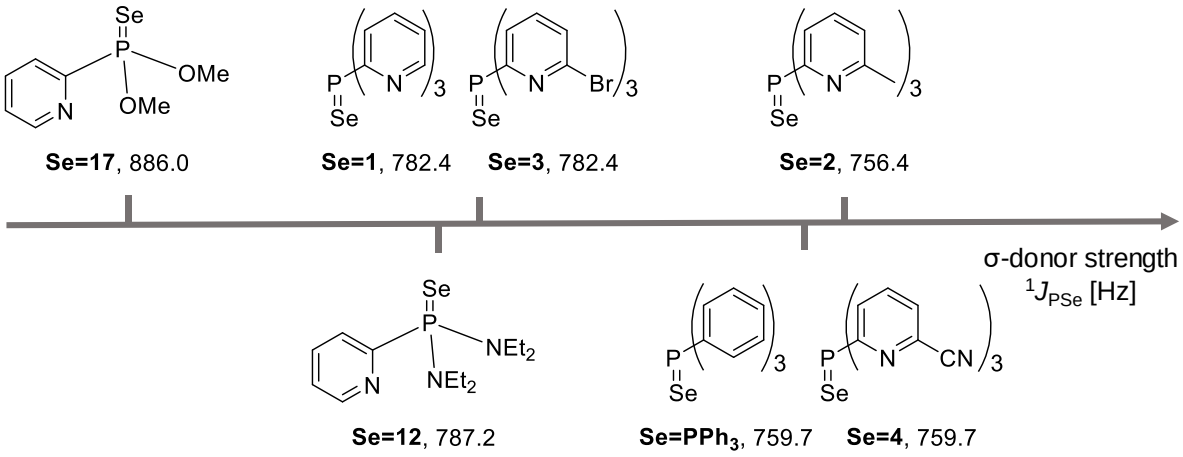

Figure 4.8: *Experimentally obtained $^1J_{PSe}$ coupling constants (in Hz) of some 2-pyridyl-phosphine selenides.*

The $^1J_{PSe}$ coupling constants of the different 2-pyridyl-phosphine selenides are distributed very widely (Figure 4.8). The largest spin-spin coupling constant by far of $^1J_{PSe}$ = 886.0 Hz was obtained for the (alkoxy)-2-pyridyl-phosphine **Se=17**. Since the $^1J_{PSe}$ coupling constant is inversely proportional to the σ-donor strength of phosphines, **17** exhibits the lowest σ-donating properties among the investigated 2-pyridyl-phosphines. The second largest coupling constant with 787.2 Hz was observed for the amino-phosphine **Se=12**. This is in line with the general trend that the reduction of the net electron-withdrawing ability of the groups attached to the P atom, and the associated reduction of the s-character of the P lone pair, causes the $^1J_{PSe}$ values to decrease.[263]

The phosphine selenides **Se=1** and **Se=3** exhibit similar $^1J_{PSe}$ coupling constants of 782.4 Hz. Surprisingly, for the CN-substituted ligand **Se=4** an even smaller $^1J_{PSe}$ coupling constant was observed, despite the electron-withdrawing nature of the cyano groups. In theory, the electron-withdrawing substituents should lead to enhanced s-character of the P lone pair and an increase in the $^1J_{PSe}$ coupling constant. However, not only electronic properties of the phosphine influence the $^1J_{PSe}$ coupling constant but also steric effects. One possible explanation for this anomaly is that the steric influence of the Br and CN groups is the dominant effect in this case, and results in a decrease in s-character of the P lone pair caused by the widening of the R–P–R bond angles, which leads to smaller $^1J_{PSe}$ coupling constant values.[264]

When **Se=4** is compared to its 6-Me-substituted counterpart **Se=2**, a large decrease of the coupling constant from 759.7 Hz to 756.4 Hz can be observed. This can be attributed to the electron-donating effect of the methyl group. Based on the $^1J_{PSe}$ coupling constants, **Se=2** exhibits the highest σ-donor strength among the 2-pyridyl-phosphines investigated in this thesis. For comparison, the triphenylphosphine selenide exhibits a $^1J_{PSe}$ coupling constant of 759.7 Hz and therefore a comparable σ-donor strength to the tris-2-pyridyl-phosphine **2**.

4.4 Calculation of the Tolman Electronic Parameters of 2-Pyridyl-phosphines

Since the experimental determination of the TEP of 2-pyridyl-phosphines from W and Mo carbonyl complexes has proven to be difficult due to the presence of a variety of different donor atoms, DFT calculations were utilised to evaluate their net donor abilities. The advantage of using accurate DFT methods is that a variety of ligands can be assessed in a short amount of time.[259,280]

Table 4.3: *Relevant geometrical parameters (bond lengths in Å and angles in °) and A_1 CO stretching frequencies (in cm^{-1}) for the optimised [Ni(CO)$_3$L] complexes (L = phosphine).*

Ligand	Ni–P	Ni–C[a]	C–O[a]	P–Ni–CO	A_1 νCO
P(2-py)$_3$ (**1**)	2.211	1.808	1.152	103.46–106.07	2058
P(6-Me-2-py)$_3$ (**2**)	2.220	1.808	1.152	105.12–105.37	2053
P(6-Br-2-py)$_3$ (**3**)	2.203	1.812	1.150	104.81–105.25	2064
P(6-CN-2-py)$_3$ (**4**)	2.208	1.812	1.150	103.85–106.29	2064
(Me$_2$N)P(2-py)$_2$ (**10**)	2.224	1.807	1.153	103.11–108.81	2056
(Et$_2$N)$_2$P(2-py) (**12**)	2.232	1.806	1.153	102.27–110.99	2051
(Et$_2$N)(Ph)P(2-py) (**13**)	2.232	1.805	1.153	102.88–109.49	2051
(MeO)P(2-py)$_2$ (**14**)	2.203	1.807	1.152	103.74–106.27	2057
(2-BuO)P(2-py)$_2$ (**15**)	2.197	1.809	1.152	103.14–106.49	2056
(MeO)$_2$P(2-py) (**17**)	2.189	1.808	1.152	103.08–107.33	2061
(Et2N)(PhO)P(2-py) (**18**)	2.208	1.809	1.152	104.74–108.15	2057
(PhO)$_2$P(2-py) (**19**)	2.177	1.811	1.151	103.92–108.34	2064
PPh$_3$	2.236	1.806	1.153	104.93–105.12	2053
P(^{t}Bu)$_3$	2.294	1.801	1.155	107.85–107.92	2042

[a] Average bond lengths.

Geometry optimisations and frequency analyses of nickel carbonyl complexes of the form [Ni(CO)$_3$L] (L = phosphine) were carried out employing the TPSS[244] functional in conjunction

with the def2-TZVP[139,140] basis set (see Chapter 8.4, page136). In these complexes, coordination only *via* the phosphorus bridgehead atom is assumed (Figure 1.8). To define a spectrochemical series, the calculated symmetric A_1 carbonyl stretching frequencies of the nickel complexes were examined, and the tri-*tert*-butylphosphine and triphenylphosphine complexes were used as reference points (Table 4.3, Figure 4.9).

All of the optimised nickel complexes show red-shifted symmetric carbonyl stretching frequencies in comparison to free CO (2143 cm^{-1}). This is also accompanied by larger C–O bond lengths with respect to free CO (1.128 Å) and indicates a weakening of the C–O bond. However, there are only very small deviations in the C–O bond lengths, whereas the ν̃CO values appear more wide-ranging.

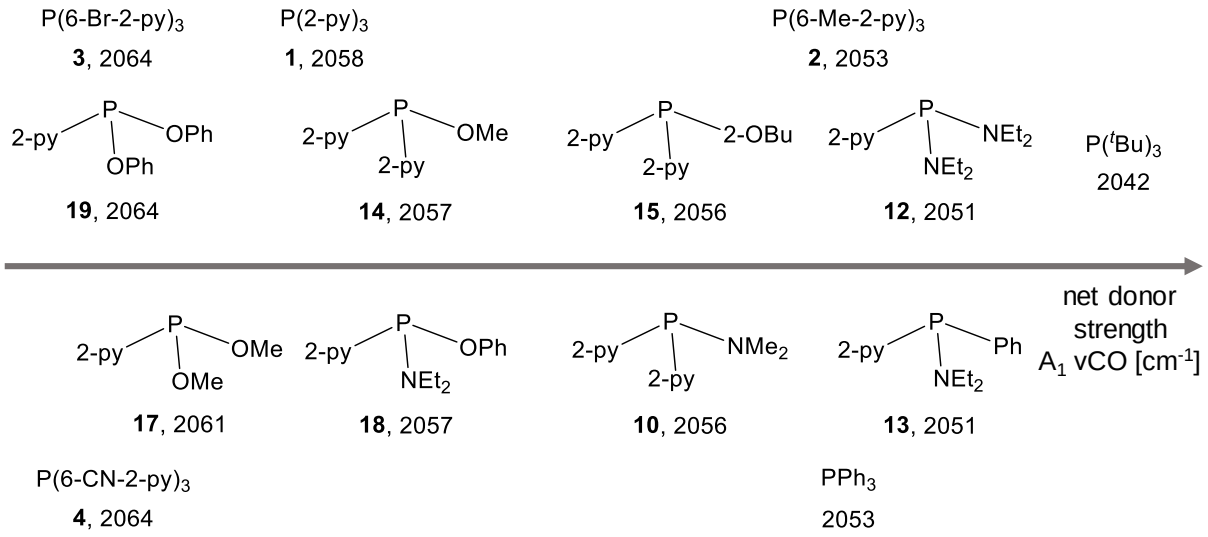

Figure 4.9: *Calculated symmetric A_1 CO stretching vibrations of a range of complexes $[Ni(CO)_3L]$ containing various 2-pyridyl-phosphine ligands. The stretching vibrations for PPh_3 and $P(^tBu)_3$ are included as references.*

Since the Tolman electronic parameter represents the overall donor ability of a ligand, which consists of the σ-donor minus the π-acceptor contributions, rough conclusions can be made about the donor nature of the ligand. From the DFT calculations, it is obvious that the Ni carbonyl complexes of 2-pyridyl-phosphines incorporating electron-withdrawing substituents in the 6-position of the pyridyl groups, such as those of the ligand sets **3** and **4**, exhibit the highest ν̃CO values and therefore the smallest net donor strength compared to the other phosphines. This finding indicates that **3** and **4** are poor σ-donors and exhibit greater π-accepting character, which would make them good coordination partners for electron-rich metals.

The nickel carbonyl complexes of the bis(alkoxy)-substituted 2-pyridyl-phosphines **17** and **19** show very similar symmetric carbonyl stretching frequencies to those calculated for the tris-2-pyridyl-phosphine complexes $[Ni(CO)_3$**3**$]$ and $[Ni(CO)_3$**4**$]$. Again, the relatively low overall donor ability of **17** and **19** can most likely be attributed to the presence of two electron-withdrawing alkoxy

substituents within the ligand sets, which lead to a reduction in the energy of the P–R σ* orbitals, allowing more efficient metal-phosphine backbonding.

The incorporation of amino groups into the ligand framework, for example when comparing **19** to **18**, results in a red shift of the νCO and therefore an increase in the net donor ability. The same effect can be observed for ligands with two pyridyl substituents rather than one. While [Ni(CO)$_3$**17**] exhibits a νCO of 2061 cm^{-1}, the A_1 CO stretching frequency of [Ni(CO)$_3$**14**] was calculated to be 2057 cm^{-1}. Similarly, the introduction of electron-donating groups in the 6-position of the pyridyl moiety, such as in the case of **2**, leads to an enhanced donor strength of the phosphine. The net donor ability of ligand **2** is therefore comparable with that of triphenylphosphine.

The highest net donor strength among the investigated 2-pyridyl-phosphine ligands was found for the bis(amino)-2-pyridyl-phosphine **12**. This finding can be explained by its reduced π-accepting properties, since π-donation from the nitrogen lone pair into the P-N' σ* orbital competes with backdonation from the metal centre to the phosphine. [280]

The smallest symmetrical CO stretching frequency of the nickel carbonyl complexes is found for P(^{t}Bu)$_3$. The very high net donor strength of the trialkyl-phosphine is due to the fact that the phosphine acts almost exclusively as a σ-donor, with little π-accepting ability.

4.4.1 Correlation of the TEP with Other Geometrical Parameters

D. G. Gusev showed that the calculated carbonyl stretching frequencies within [Ni(CO)$_3$L] complexes correlate very well with the calculated average C–O bond lengths for a variety of two-electron donor ligands.[259] The elongation of the C–O bond due to a more strongly donating auxiliary ligand set can be attributed to electron-donation from the ligand into the metal d orbitals and the subsequent transfer of electron density into the π* orbitals of the CO moieties. This induces a decrease in the bond order, and an elongation of the weakened C–O bond can be observed. Figure 4.10 shows the relationship between the average calculated C–O bond lengths within the nickel carbonyl complexes of various 2-pyridyl-phosphines with the calculated A_1 νCO value. A good linear correlation with $R^2 = 0.90$ is observed.

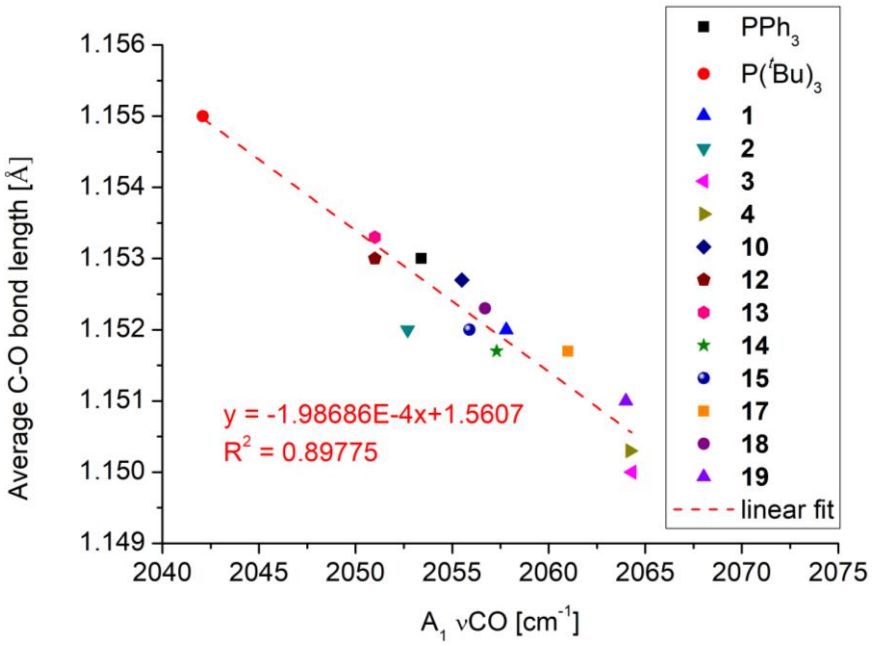

Figure 4.10: *Correlation of the calcd. average C–O bond lengths and the calcd. A_1 νCO for [Ni(CO)$_3$L].*

In principle, the average Ni–C bond lengths in [Ni(CO)$_3$L] complexes should also correlate with the symmetric A_1 CO stretching frequencies, since a good donor ligand renders the Ni centre more electron-rich and induces a contraction of the Ni–C bond length. Figure 4.11 shows that this is indeed the case, with the observed linear regression (albeit with a moderate R^2 value of 0.87) demonstrating that the Ni–C bond lengths can be used as an indicator of the overall donor properties of a phosphine. In the case of P(^{t}Bu)$_3$ the shortest average Ni–C bond length is observed. In contrast, the nickel complexes of the good π-acceptors **3**, **4** and **19** exhibit the longest Ni–C bond lengths.

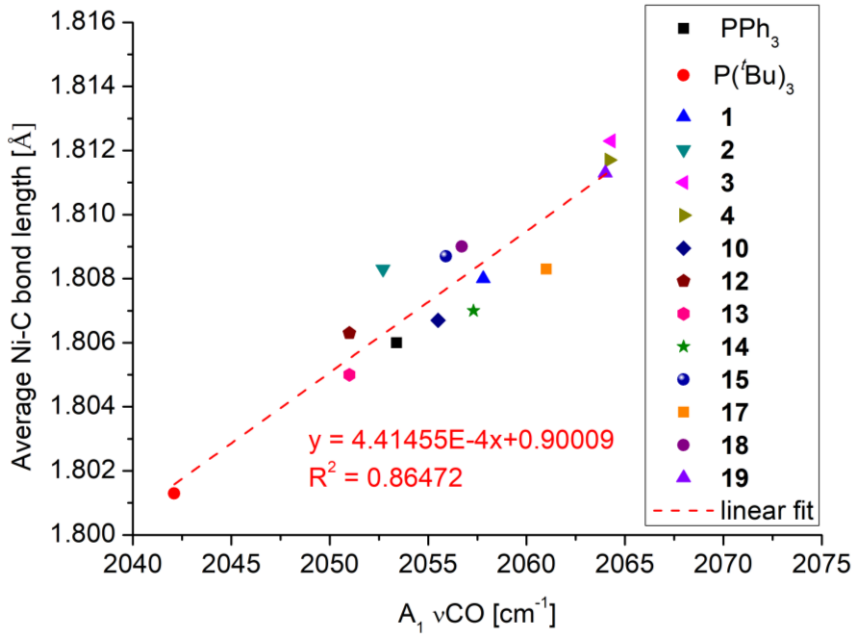

Figure 4.11: *Correlation of the calcd. average Ni–C bond lengths and the calcd. A_1 νCO for [Ni(CO)$_3$L].*

The variation in the donor strength of phosphines should also have an influence on the Ni–P bond lengths in the corresponding nickel tricarbonyl complexes. Here, increased σ-donor and π-accepting character of the phosphine should lead to shorter Ni–P bond lengths.

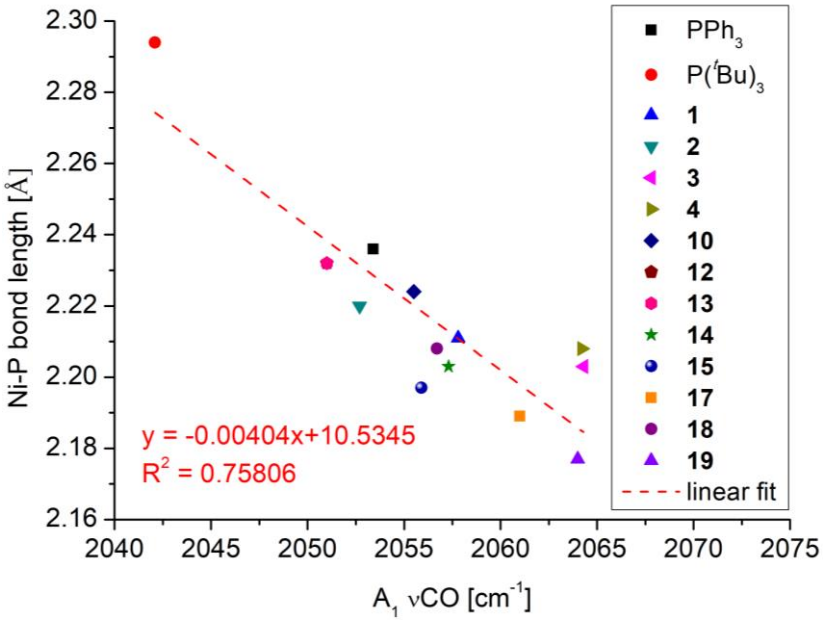

Figure 4.12: *Correlation of the calcd. Ni–P bond lengths and the calcd. A_1 νCO for [Ni(CO)$_3$L].*

Owing to the complicated interplay between the σ-donor and the π-acceptor character of the phosphines and the effect on Ni–P bond length, it is not surprising that the correlation of the bond length with the symmetric CO stretching frequency, depicted in Figure 4.12, is fairly weak (R^2 = 0.76). In addition, there are other factors, most obviously the steric character of the phosphines, that may also come into play. This is seen, for example, in the case of tri-*tert*-butylphosphine where the Ni–P bond length is longer than expected on the basis of the best-fit line.

4.5 Experimental *versus* Calculated Donor Properties

For the detailed investigation of the donor properties of various 2-pyridyl-phosphines, two experimental strategies and one computational approach were utilised.

The experimental approaches included the synthesis of tungsten and molybdenum carbonyl complexes and the determination of the symmetric A_1 carbonyl stretching frequency (Chapter 4.2, page 75). However, the synthesis was quite problematic due to different coordination modes that can be adopted by the multidentate 2-pyridyl-phosphines. Therefore, only two relevant exclusively P-molybdenum bonded complexes, [Mo(CO)$_4${P(6-Me-2-py)$_3$}] (**30**) and *cis*-[Mo(CO)$_4${P(6-Br-2-py)$_3$}$_2$] (**31**), were isolated and completely characterised. IR spectroscopy and subsequent conversion into the corresponding Tolman parameter, which was necessary due to the different substitution patterns of the two complexes, revealed that the 6-methyl-substituted ligand **2** has a

higher overall donor strength than its bromine counterpart **3**. This is not surprising, since the methyl group in the 6-position has an electron-donating effect, whereas the Br-substituents have electron-withdrawing character, as already been shown by the CHELPG charge distribution on the phosphorus bridgeheads.

Since the synthesis of W and Mo tris-2-pyridyl-phosphine complexes proved to be difficult, the corresponding phosphine selenides were easily synthesised and analysed *in-situ* by $^{31}P\{^{1}H\}$ NMR spectroscopy (Chapter 4.3, page 85). From the J_{PSe} values, conclusions could be drawn about the σ-donor strength of the phosphines (Figure 4.8). It was obvious that the introduction of electron-withdrawing substituents, such as those in the (alkoxy)-2-pyridyl-phosphine Se=P(OMe)$_2$(2-py) (**Se=17**), gave very large J_{PSe} values, which indicate enhanced s-character of the P lone pair and therefore reduced σ-donor strength. The introduction of more electron-donating substituents, for example, when comparing Se=P(2-py)$_3$ (**Se=1**) to Se=P(6-Me-2-py)$_3$ (**Se=2**), revealed a decrease in J_{PSe} and indicated better σ-donor properties. The relatively small $^{1}J_{PSe}$ coupling constant of the CN-substituted ligand Se=P(6-CN-2-py)$_3$ (**Se=4**) was surprising, since the electron-withdrawing CN groups should lead to a reduced σ-donor strength. However, this finding could be caused by a widened C–P–C angle due to the steric effect of the CN groups.

Although the $^{1}J_{PSe}$ values correspond to the σ-donor strength of a phosphine, whereas the TEP represents the overall donor ability, both values are proportional to each other, since the overall net donor strength is calculated as the σ-donor contribution minus the π-acceptor contributions. Therefore, the comparison of the experimentally obtained $^{1}J_{PSe}$ coupling constants and the calculated TEP values should give an indication of the σ-donor and π-acceptor character of the 2-pyridyl-phosphine ligands.

The large $^{1}J_{PSe}$ coupling constant for Se=P(MeO)$_2$(2-py) (**Se=17**) and the associated low σ-donor strength of **17** are in agreement with the calculated TEP values, which indicated a low net donor ability and the fact that **17** is a better π-acceptor than σ-donor ligand. However, the order of the $^{1}J_{PSe}$ coupling constants for the remaining phosphine selenides does not completely agree with the order of the TEP values obtained from DFT studies. According to the νCO values of the corresponding nickel complexes [Ni(CO)$_3$L] (L = phosphine), (Et$_2$N)$_2$P(2-py) (**12**) exhibits the highest net donor strength, followed closely by P(6-Me-2-py)$_3$ (**2**), whereas the net donor ability of P(2-py)$_3$ (**1**) was calculated to be much lower. In contrast, the investigations of the selenides indicate similar σ-donor properties for **12** and **1**.

From Figure 4.13, it is obvious that there is no clear correlation between the experimentally obtained $^{1}J_{PSe}$ values and the calculated TEP values, probably due to very different (donor, acceptor and steric character) 2-pyridyl-phosphines investigated. Similar studies by R. Starostra *et al.* also suggested

that linear relationships can only be obtained for certain phosphines. The correlation depends very strongly on the ligand family, and ligands with amino substituents do not follow any correlation.[277] D. W. Allen *et al.* also observed some discrepancies between the Tolman electronic parameter and the $^{1}J_{PSe}$ coupling constants of heteroaryl phosphines due to the different degrees of covalency of the metal–ligand bond for different ligands.[263] Furthermore, the $^{1}J_{PS}$ value strongly depends on the steric properties of the phosphine, since bulky substituents result in a decrease in the s-character of the P lone pair as a result of the widening of the R–P–R bond angles.[264] Obviously, due to the limited number of examples investigated in this thesis, this correlation cannot be discussed in detail.

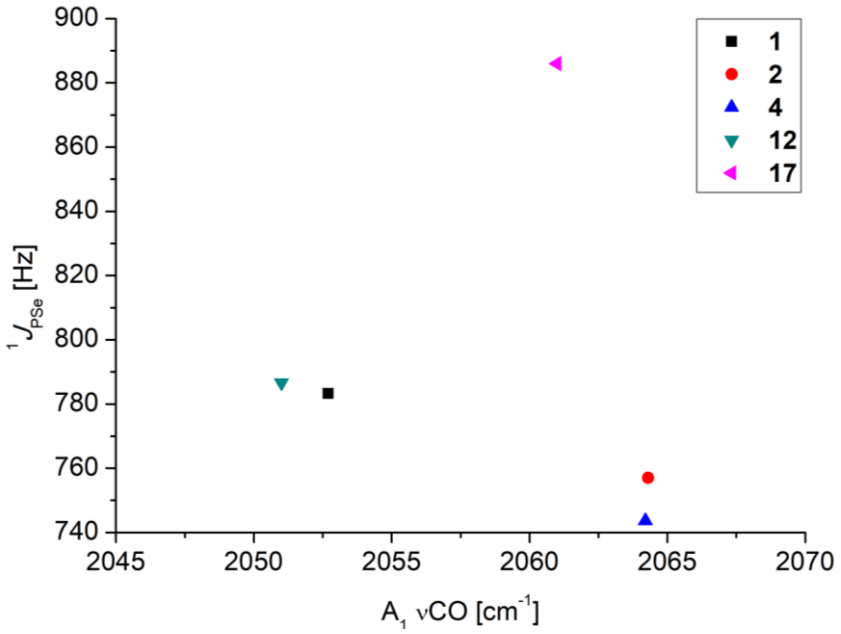

Figure 4.13: *Correlation of the experimentally obtained $^{1}J_{PSe}$ values with the calcd. Tolman electronic parameter.*

4.6 Concluding Remarks

In order to quantify the donor properties of various 2-pyridyl-phosphines, tungsten and molybdenum complexes, as well as phosphine selenides, were synthesised. However, the assessment of the donor properties of the metal complexes was not straightforward due to the multidentate character of the phosphines and the different coordination modes that can be adopted. Therefore, only two comparable Mo complexes containing exclusively P–metal bonding, **30** and **31**, were useful. From the conversion of the carbonyl stretching frequency into the corresponding Tolman parameter, it was obvious that P(6-Me-2-py)$_3$ (**2**) has a higher net donor strength than P(6-Br-2-py)$_3$ (**3**).

The synthesis of the phosphine selenides was readily achieved, and conclusions regarding the σ-donor properties of the ligands were drawn from the $^{1}J_{PSe}$ coupling constants. It was obvious that

the introduction of electron-withdrawing substituents (*e.g.* Br-substituents) leads to a lower σ-donor strength, whereas the introduction of electron-donating groups (*e.g.* Me groups) increases the σ-donor strength. However, the high net donor strength of the CN-substituted tris-2-pyridyl-phosphine P(6-CN-2-py)$_3$ (**4**) seems counterintuitive and probably steric effects play a further role.

In addition to the experimental work, the Tolman electronic parameters of twelve different 2-pyridyl-phosphines were calculated, along with those of P(^{t}Bu)$_3$ and PPh$_3$ as reference points. The Tolman parameter proved valuable for the investigation of the overall donor properties of phosphines and, by computing this parameter, many synthetic limitations could be avoided. The calculated TEPs confirmed the conclusions drawn from the synthesised Mo complexes, and showed that the introduction of substituents into the 6-position of tris-2-pyridyl-phosphines has a considerable effect on the overall donor properties of the phosphine. However, there was no clear correlation between the $^1J_{PSe}$ coupling constants and the calculated TEP values, probably largely due to the fact that no conclusions could be drawn from the coupling constant regarding the π-accepting properties. Steric effects also play a role in this context and complicate the interpretation and correlation of the experimentally obtained $^1J_{PSe}$ coupling constants and the calculated TEP values.

Studies of the correlation between the calculated Tolman electronic parameter, or more precisely, the symmetric A_1 stretching frequency of [Ni(CO)$_3$L] complexes, with other calculated geometric parameters of the nickel carbonyl complexes showed that the C–O bond lengths correlate best with the TEP (R^2 = 0.90). The Ni–C and Ni–P bond lengths can also be considered; less satisfactory correlation coefficients were observed (Ni–C: R^2 = 0.87 and Ni–P: R^2 = 0.76). Due to the changes in geometrical parameters between the different nickel carbonyl complexes (in particular, the steric character of the phosphines), the vibrational frequency is probably the most sensitive parameter.

Overall, this study showed that obtaining a detailed understanding of the electronic properties of ligands remains challenging, and that the exact determination of σ-donor and π-acceptor contributions is not possible. However, the overall donor properties can be described very well from experiments and calculations in the case of the few phosphines for which exclusive P–metal bonding is observed.

5 Modifications of the Phosphorus Bridgehead

5.1 Preamble

Trivalent phosphorus compounds containing a phosphorus atom in the +3 oxidation state are often sensitive towards air and moisture. Thus, when handling or storing such phosphines, special equipment and synthetic experience are required, which can be quite problematic on an industrial scale. To overcome these problems, the phosphorus compounds, or more precisely, the phosphorus atom, can be temporarily protected with BH_3 or oxidised with chalcogenides to afford air- and moisture stable phosphorus(V) compounds.[281,282] Due to their enhanced stability, phosphorus(V) compounds have received a great deal of attention as ligands in transition metal catalysis, for example, in cross-coupling reactions[283] and in the electrocatalytic oxidation of water.[284]

More recently, the focus has been on the development of highly Lewis-acidic electrophilic phosphonium cations (EPCs).[285–288] The Lewis acidity of such cations, especially fluorophosphonium cations, derives from a low energy P–F σ* orbital[286] and can be exploited in a variety of catalytic transformations, such as the hydrosilylation of alkenes,[289] the isomerisation of olefins[290] and the deoxygenation of ketones.[291] Interestingly, the Lewis acidity of EPCs, for example, $[FP(C_6F_5)Ph_2]^+$, is comparable to that of well-known Lewis acids such as $B(C_6F_5)_3$, despite the fact that the Lewis acidity of Group 13 compounds is classically derived from the presence of a vacant p orbital.

Electrophilic fluorophosphonium cations can be synthesised starting from electron-deficient phosphines, which are oxidised with xenon difluoride to give the difluorophosphoranes. The corresponding fluorophosphonium salts (Figure 5.1) can then be obtained by fluoride abstraction with Me_3SiOTf.

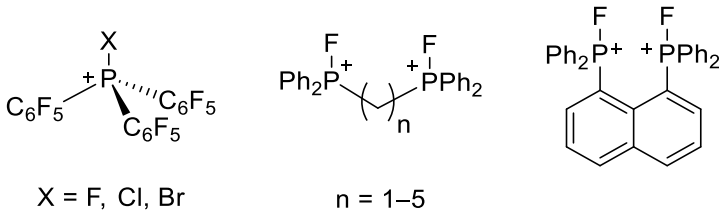

Figure 5.1: *Examples of electrophilic phosphonium cations and dications.*

The coordination chemistry of EPCs is very interesting with respect to the possibility of forming transition metal complexes in which the Lewis-acidic ligands, also known as Z-type ligands,[292] act as a σ-acceptor. In such complexes, the metal behaves as a Lewis base and therefore participates in covalent donor-acceptor interactions.[293] Boron-based ligands have often been employed as Z-type

ligands (Figure 5.2) due to the presence of a vacant p orbital on the boron centre.[294] However, recently D. Bourrisou and co-workers have demonstrated Z-type interactions between Pd and a phosphorus(V) centre,[295] and C. Tan *et al.* have shown that this combination can provide cooperative substrate activation, like that employed in carbonylative Sonogashira reactions.[296]

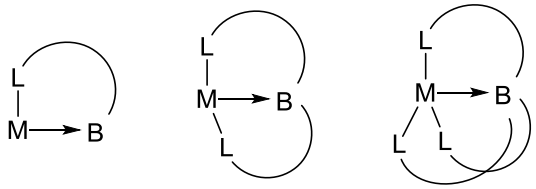

Figure 5.2: *Bonding motifs in boron-based Z-type complexes (M = Fe, Co, Ni, Cu, Ru, Pd, Os, Ir, etc., L = thione, imine, phosphine).*[294]

Building on these previous studies, the possibility of bridgehead modification of the tripodal C_3-symmetric 2-pyridyl-phosphines and their unsymmetrical derivatives was investigated. The focus was on the simple oxidation of the phosphorus(III) bridgehead atom with oxygen, sulphur and selenium to afford air- and moisture stable phosphorus(V) 2-pyridyl-phosphines. Consequently, the electronic properties of the bridgehead change dramatically, which leads to variation in the coordination characteristics of the ligands. In addition to the oxidation of the phosphorus atom using chalcogenides, the fluorination of the 2-pyridyl-phosphines was attempted with the aim of the synthesis of difluorophosphoranes and electrophilic phosphonium cations. These EPC ligand sets do not only contain a Lewis-acidic bridgehead but also provide additional donor functionalities, such as pyridyl or/and amino moieties. The potential of these ligands to act as ambidentate Z-type ligands was then investigated towards various transition metals.

5.2 Chalcogenides of 2-Pyridyl-phosphines

In the case of tris-2-pyridyl-phosphine, the solid state structure of the oxidised analogue was first reported in 2004 by M. Lahy and co-workers,[297] although a few metal complexes of this ligand had previously been structurally characterised.[146,147,298] The tris-2-pyridyl-phosphine oxide ligand has mainly been prepared by the oxidation of $P(2\text{-py})_3$ (**1**) with hydrogen peroxide.[298] A few years later, A. N. Kharat *et al.* reported the synthesis of tris-2-pyridyl-phosphine sulphide and selenide by reacting the tripodal ligand **1** with elemental sulphur or selenium at elevated temperatures.[299] Due to the loss of the electron-donating properties of the phosphorus bridgehead after oxidation, the introduction of chalcogenides can prevent the phosphorus atom from metal coordination.[146] Depending on the nature of the metal and the hardness/softness of the group 16 element, the chalcogenide atom can be utilised for metal complexation instead.[300]

The oxidation reaction used for the unsubstituted 2-pyridyl-phosphine can also be utilised in the synthesis of the chalcogenide derivatives of the Me- and Br-substituted ligands P(6-Me-2-py)$_3$ (**2**) and P(6-Br-2-py)$_3$ (**3**) (Scheme 5.1). The oxide O=P(6-Me-2-py)$_3$ (**O=2**) was prepared by the reaction of the methyl-substituted ligand **2** with XeF_2 in DCM. Originally, this synthetic approach was chosen for the fluorination of the bridgehead-P atom. However, the oxide **O=2** was formed instead, possibly due to residual water in the ligand from the aqueous workup. The sulphur and selenium analogues of the Br-substituted ligand S=P(6-Br-2-py)$_3$ (**S=3**) and Se=P(6-Br-2-py)$_3$ (**Se=3**) could be isolated from the reactions of **3** with an excess of sulphur or grey selenium, respectively, in toluene under reflux conditions.

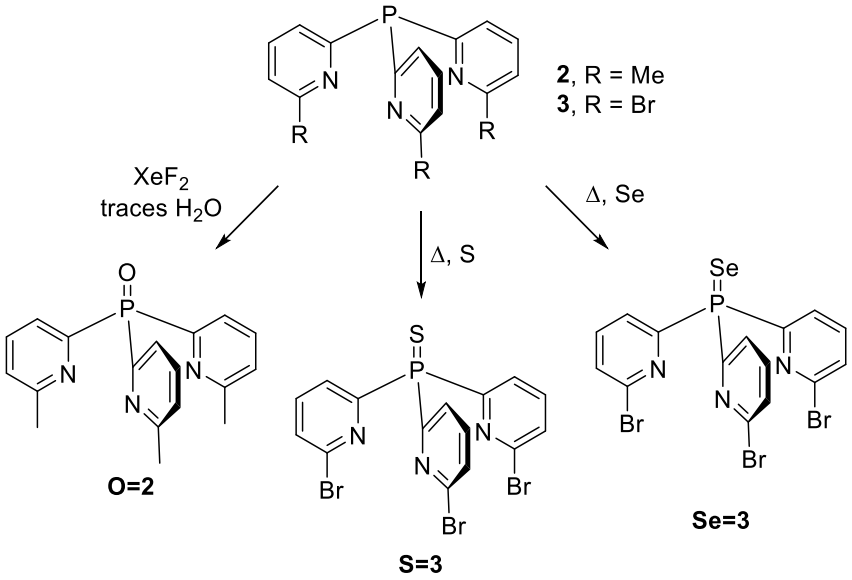

***Scheme 5.1**: Further modifications of the phosphorus bridgehead of the tris-2-pyridyl-phosphines **2** and **3**.*

The solid state structures of the chalcogenide derivatives of **2** and **3** were determined by single-crystal X-ray crystallography (Figure 5.3, Table 5.1). The chalcogenides **O=2**, **S=3** and **Se=3** exhibit shorter P–C_{py} bonds than the free phosphines **2** and **3**. Whereas in **2** and **3**, phosphorus–carbon bond lengths of 1.847(2)–1.851(2) Å and 1.852(8) Å were found, respectively, the P–C_{py} bonds in the oxygen derivative **O=2** are in the range of 1.819(2)–1.823(2) Å. Shortening of the bonds was also obvious in the sulphur and selenium derivatives of **3**, in which P–C_{py} bond lengths of 1.827(4)–1.837(4) Å for **S=3** and 1.827(4)–1.835(4) Å for **Se=3** were found. The introduction of the oxygen atom results in the biggest decrease in the P–C_{py} bond lengths. Additionally, from the crystal structures of the chalcogenides, an enlargement of the C–P–C bond angles with respect to those of the free phosphines becomes obvious. While C_{py}–P–C_{py} bond angles of 99.2(1)–99.8(1)° and 99.0(3)° were found in **2** and **3**, bond angles of 102.29(7)–106.15(7)° in **O=2**, 104.8(2)–106.5(2)° in **S=3** and 105.1(2)–106.8(2)° in **Se=3** were observed.

Table 5.1: *Selected bond lengths (Å) and angles (°) in the three chalcogenide phosphines* ***O=2***, ***S=3*** *and* ***Se=3*** *(X = O, S, Se).*

	O=2	**S=3**	**Se=3**
P(1)–C_{py}	1.819(2)–1.823(2)	1.827(4)–1.837(4)	1.827(4)–1.835(4)
P(1)=X	1.481(1)	1.942(2)	2.094(1)
C_{py}–P(1)–C_{py}	102.29(7)–106.15(7)	104.8(2)–106.5(2)	105.1(2) –106.8(2)
P(1)–C_{py}–N_{py}	113.7(1)–115.4(1)	112.8(3)–115.8(3)	113.1(3)–115.7(3)

A systematic increase in the P=X (X = O, S, Se) bond lengths going from oxygen to sulphur and then selenium, from 1.481(1) Å in **O=2**, to 1.942(2) Å in **S=3** and 2.094(1) Å in the selenide **Se=3**, is observed. Interestingly, in the 6-substituted X=P(6-R-2-py)$_3$ derivatives, two of the pyridyl-N atoms point towards the bridgehead-P atom and one N atom is orientated downwards away from the P atom, whereas in the unsubstituted oxide and sulphide, only one nitrogen is directed towards the phosphorus atom.[297,299] Although this difference is probably largely a consequence of avoiding steric clash between the Me and Br substituents, other factors are involved. For instance, in the structure of unsubstituted Se=P(2-py)$_3$, all the N donor atoms of the py groups point in the same direction as the Se atom, which has been attributed to the higher polarisability of Se in comparison to the S atom.[299]

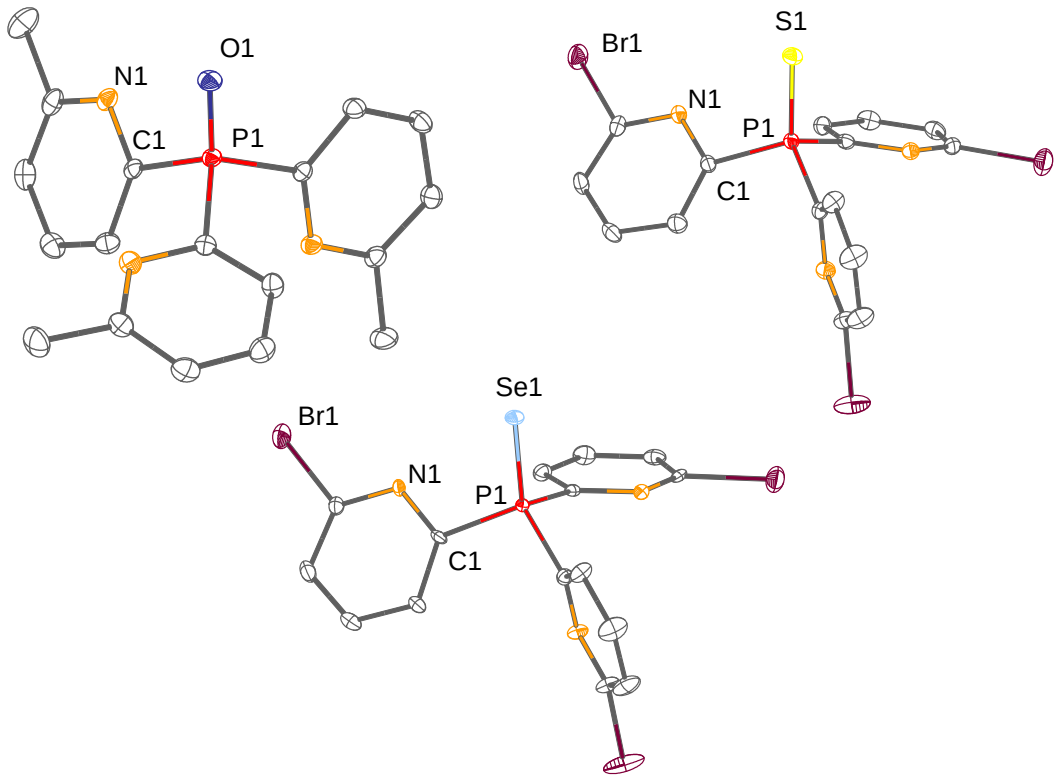

Figure 5.3: *Structures of O=P(6-Me-2-py)$_3$* ***(O=2)***, *S=P(6-Br-2-py)$_3$* ***(S=3)*** *and Se=P(6-Br-2-py)$_3$* ***(Se=3).*** *Hydrogen atoms are omitted for clarity. Displacement ellipsoids are drawn at the 30 % probability level.*

Also, the P bridgehead position of the (amino)- and (alkoxy)-2-pyridyl ligand frameworks can be modified (Scheme 5.2). For example, treatment of the (amino)- or (alkoxy)-2-pyridyl-phosphines $(Et_2N)_2P(2\text{-py})$ (**12**) and $(MeO)_2P(2\text{-py})$ (**17**) with grey selenium leads to the formation of the corresponding selenides **Se=12** and **Se=17** (see Chapter 4.3, page 85).

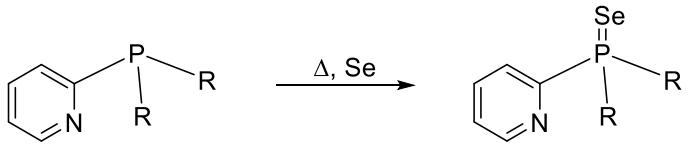

12, R = NEt_2 **Se=12**, R = NEt_2
17, R = OMe **Se=17**, R = OMe

Scheme 5.2: *Selenation of the bis(amino)-2-pyridyl-phosphine and the bis(alkoxy)-2-pyridyl-phosphine.*

5.3 Fluorination of 2-Pyridyl-phosphines

So far, studies of fluorophosphonium cations have mainly focused on phosphines containing phenyl substituents (*e.g.* C_6F_5).[286,289,290,301] On the one hand, this limits the coordination ability of the EPCs, but on the other hand, the replacement of C_6F_5 substituents with less electron-withdrawing substituents has been shown to result in diminished Lewis acidity.[302] To overcome this problem, dications have been synthesised, for example *via* the methylation of pyridyl substituents and the subsequent formation of pyridinium cations.[248,303] Therefore, the focus of the work in this section was the fluorination of C_3-symmetric tripodal tris-2-pyridyl-phosphines and unsymmetrical (amino)- and (alkoxy)-2-pyridyl-phosphine derivatives.

For the synthesis of the fluorinated tris-2-pyridyl-phosphine, carefully dried $P(2\text{-py})_3$ (**1**) was reacted with XeF_2 at –78 °C in DCM (Scheme 5.3).

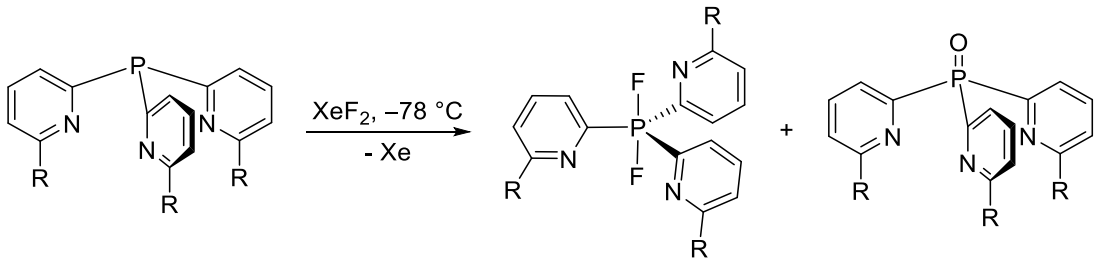

1, R = H **F_2-1**, R = H **O=1**, R = H
2, R = Me **F_2-2**, R = Me **O=2**, R = Me

Scheme 5.3: *Synthesis of the tripodal difluorophosphoranes* ***F_2-1 and F_2-2****.*

The formation of the difluorophosphorane $F_2P(2\text{-py})_3$ (**F_2-1**) was followed by NMR spectroscopy. The $^{31}P\{^1H\}$ NMR spectrum of the reaction mixture showed a triplet at –63.2 ppm ($CDCl_3$) along with a doublet at –42.0 ppm ($CDCl_3$) in the $^{19}F\{^1H\}$ NMR spectrum, with a one-bond coupling constant of $^1J_{PF}$ = 704.3 Hz (Figure 5.4). The very large upfield shift of **F_2-1** in the $^{31}P\{^1H\}$ NMR,

in contrast to the signal of **1** which appears as a singlet at –1.0 ppm ($CDCl_3$), is consistent with the oxidation of the P^{III} centre to P^{V}. Similar chemical shifts were observed for the difluorophosphoranes developed by D. W. Stephan. For example, the fluorinated phosphine F_2PPh_2(2-py) exhibits a triplet in the $^{31}P\{^1H\}$ NMR spectrum at –52.7 ppm and a doublet at –36.4 ppm in the $^{19}F\{^1H\}$ NMR spectrum with a one-bond coupling constant ($^1J_{PF}$) of 670.0 Hz (CD_2Cl_2).[248]

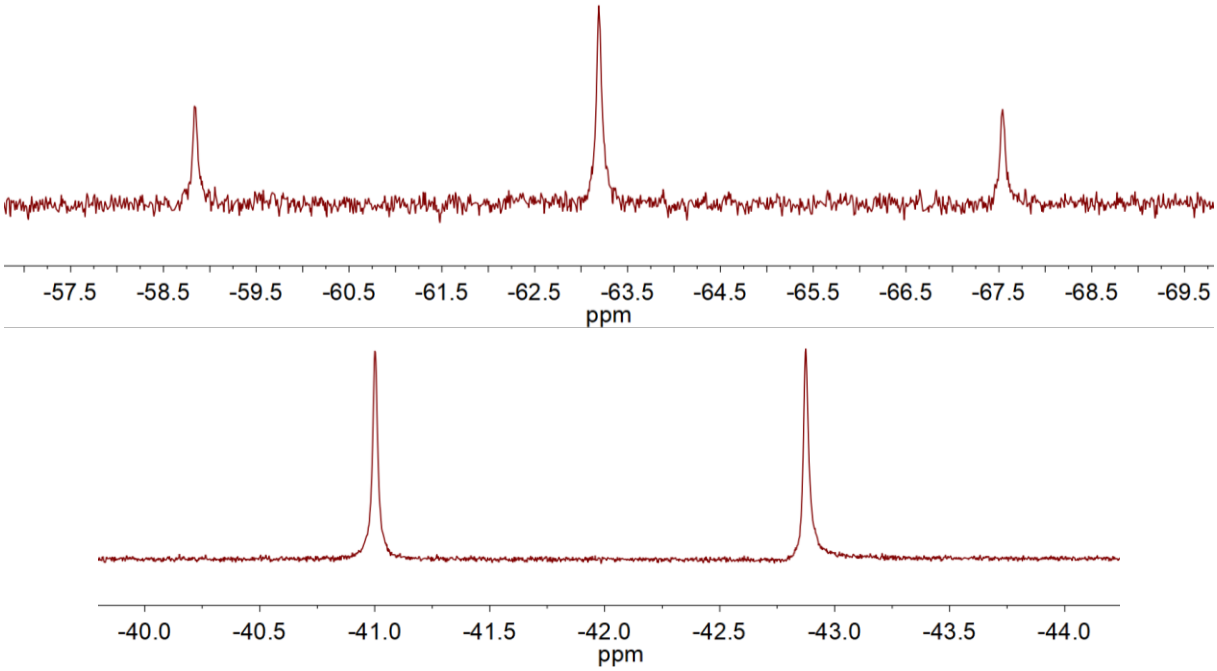

Figure 5.4: *Sections of the $^{31}P\{^1H\}$ (top, 161.98 MHz) and $^{19}F\{^1H\}$ NMR (bottom, 376.45 MHz) spectra of compound* ***F_2-1*** *in $CDCl_3$.*

Despite several synthetic attempts and modifications, compound **F_2-1** is only obtained in 84 % purity according to $^{31}P\{^1H\}$ NMR spectroscopy, and the presence of the oxidised phosphine O=P(2-py)$_3$ (**O=1**,14.2 ppm, $CDCl_3$, lit.: 14.8 ppm[304]) is also observed. Purification attempts only resulted in the decomposition of the fluorinated ligand **F_2-1**. Very similar observations were made during the fluorination of the 6-methyl-substituted ligand P(6-Me-2-py)$_3$ (**2**, Scheme 5.3), in which the formation of F_2P(6-Me-2-py)$_3$ (**F_2-2**) along with the oxidised phosphine O=P(6-Me-2-py)$_3$ (**O=2**, 14.6 ppm, $CDCl_3$) was observed. **F_2-2** exhibited a triplet at –61.7 ppm in the $^{31}P\{^1H\}$ NMR with a coupling constant of $^1J_{PF}$ = 688.2 Hz and a characteristic doublet at –38.68 ppm in the $^{19}F\{^1H\}$ NMR spectrum. The formation of the oxidised phosphines is probably due to traces of water resulting from the aqueous workup during the synthesis of the ligands **1** and **2**.

The fluorination of bis(amino)-2-pyridyl-phosphine $(Et_2N)_2$P(2-py) (**12**) with XeF_2 at –78 °C in DCM is less problematic than that of the previous tripodal 2-pyridyl-phosphines, and results exclusively in the formation of the difluorophosphorane (Scheme 5.4). F_2P$(NEt_2)_2$(2-py) (**F_2-12**) was obtained as a pale yellow oil in 71 % yield. In the room temperature $^{31}P\{^1H\}$ NMR spectrum

of **F_2-12** a triplet at –61.6 ppm is observed, and a doublet is present in the $^{19}F\{^1H\}$ NMR at –52.3 ppm ($^1J_{PF}$ = 730.0 Hz, $CDCl_3$). Again, the $^{31}P\{^1H\}$ NMR signal of the difluorophosphorane **F_2-12** is shifted considerably upfield with respect to **12** (93.9 ppm, $CDCl_3$). In order to obtain the fluorophosphonium cation, **F_2-12** can be treated with trimethylsilyl trifluoromethanesulfonate in DCM at –78 °C (Scheme 5.4). After the solvent was removed *in vacuo*, $[FP(NEt_2)_2(2\text{-py})]OTf$ (**F-12-OTf**) was obtained in 93 % purity according to $^{31}P\{^1H\}$ NMR spectroscopy.

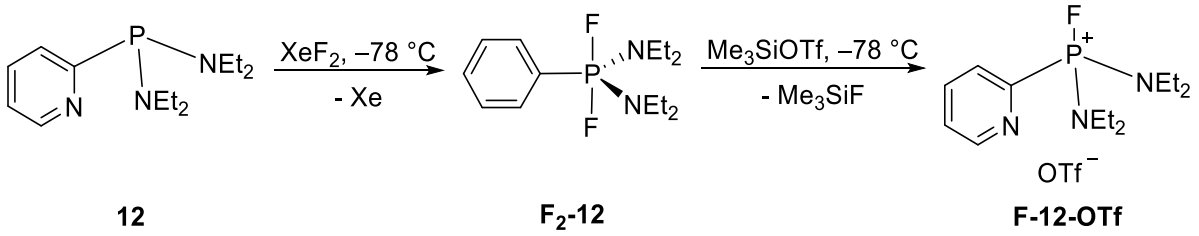

Scheme 5.4: *Synthesis of the difluorophosphorane* ***F_2-12*** *and the fluorophosphonium cation* ***F-12-OTf****.*

The electrophilic fluorophosphonium cation can also be obtained *via* a one-step procedure starting from **12**. Treatment of **12** with the fluorinating reagent *N*-fluorobenzenesulfonimide (NFSI) at room temperature in THF results in the direct formation of the salt $[FP(NEt_2)_2(2\text{-py})][N(SO_2Ph)_2]$ (**F-12-NSI**, Scheme 5.5). NFSI is an electrophilic fluorinating reagent, which has recently been used for site-selective mono-fluorinations of organic substrates.[305] Mechanistically, NFSI does not generate a F^+ cation, but acts as a fluorine transfer reagent to a nucleophile. This transfer reaction occurs *via* a single-electron transfer reaction or an S_N2 mechanism, depending on the reaction conditions and the nucleophile.[306]

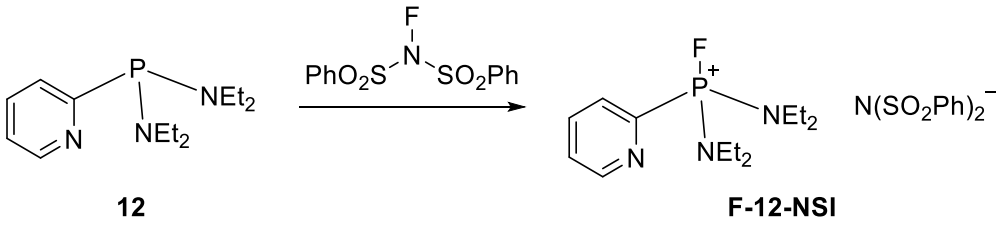

Scheme 5.5: *Synthesis of the fluorophosphonium salt* ***F-12-NSI*** *via a one-step procedure.*

The salt **F-12-NSI** exhibits a characteristic doublet at 44.5 ppm in the room temperature $^{31}P\{^1H\}$ NMR spectrum as well as a doublet in the $^{19}F\{^1H\}$ NMR at –91.0 ppm ($^1J_{PF}$ = 1050.1 Hz, $CDCl_3$). Again, similar resonances have been reported in the literature (*e.g.* for $[FPPh_2(2\text{-py})]OTf$, $^{31}P\{^1H\}$ NMR: 80.1 ppm, $^{19}F\{^1H\}$ NMR: –136.8 ppm, $^1J_{PF}$ = 1004.0 Hz, CD_2Cl_2).[248] This one-pot approach allows the isolation of **F-12-NSI** in 90 % yield as a colourless oil in 100 % purity. A great advantage of this method is the air-stability of crystalline NFSI in contrast to the very reactive and unstable xenon difluoride.

This synthetic procedure could also be applied to the C_3-symmetric tris-2-pyridyl-phosphines. However, in the case of P(6-Me-2-py)$_3$ (**2**), the fluorophosphonium salt [FP(6-Me-2-py)$_3$][N(SO$_2$Ph)$_2$] (**F-2-NSI**) could only be obtained in 50 % purity according to ^{31}P{^{1}H} NMR spectroscopy, and the formation of the oxidised phosphine as well as another unknown by-product was also observed.

To investigate the Lewis acidity of the fluorophosphonium cation **F-12**$^+$, geometry optimisations at the BP86,[136–138] def2-TZVP[139,140] level of theory were carried out (see Chapter 8.4, page 136). As clearly shown in Figure 5.5, the lowest unoccupied molecular orbital LUMO+4 is mainly concentrated opposite the P–F bond, indicating the Lewis acidity of the electrophilic cation (*via* the P–F σ* orbital). Smaller contributions of the LUMO+4 can be found within the pyridyl ring and at the fluorine atom.

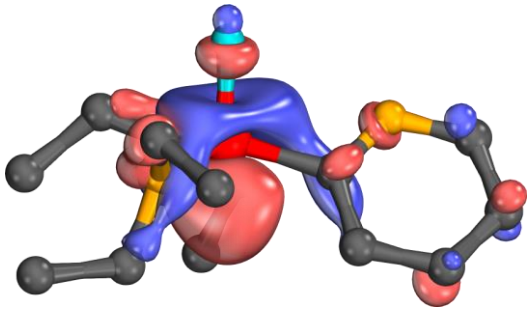

Figure 5.5: *LUMO+4 of the cation [FP(NEt$_2$)$_2$(2-py)]$^+$ (**F-12**$^+$). Plotting-threshold: 50 %.*

Recently, electrophilic fluorinating reagents, such as NFSI or Selectfluor [1-chloromethyl-4-fluoro-1,4-diazoniabicyclo[2.2.2]octane bis(tetrafluoroborate)], have been used not only as fluorinating reagents, but also as oxidants, for example, for the efficient oxidation of phosphorus(III) compounds with water as the oxygen source.[282] The addition of water to the fluorophosphonium salt **F-12-NFSI** in THF results cleanly in the conversion to the phosphine oxide, which can be monitored using *in-situ* ^{31}P{^{1}H} NMR spectroscopy (Scheme 5.6, **O=12**, 21.8 ppm, THF). This reaction probably occurs *via* the nucleophilic attack of water on the electrophilic P bridgehead, the formation of a reactive R$_3$PFOH intermediate, and subsequent HF elimination.[282]

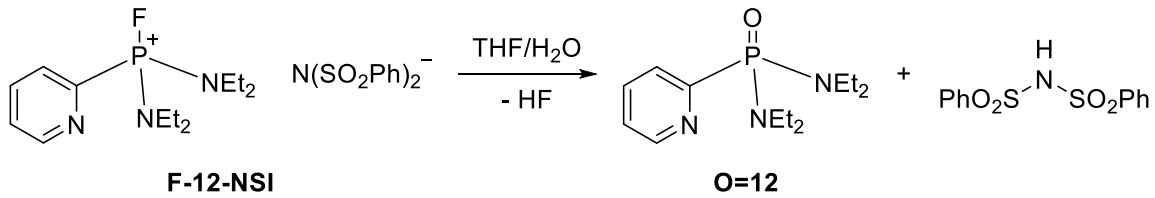

F-12-NSI **O=12**

Scheme 5.6*: Conversion of the fluorophosphonium salt **F-12-NSI** into the phosphine oxide **O=12**.*

5.4 Transition Metal Complexes of Bridgehead-modified 2-Pyridyl-phosphines

As discussed previously, alteration of the bridgehead position of 2-pyridyl-phosphines, for example, by oxidising the phosphorus atom, leads to completely different electronic properties of the ligand frameworks. This greatly influences their coordination behaviour towards transition metals. Especially interesting in this regard are the coordination properties of electrophilic fluorophosphonium cations, since these types of ligands have the potential to act as ambidentate Z-type ligands.

Therefore, **F-12-NSI** was reacted with iron(II) triflate in THF in a 2 : 1 stoichiometric reaction. Due to the paramagnetic character of the solution, NMR spectroscopic analysis could not reveal whether coordination occurred. Since no crystals could be isolated from this mixture, the solution was exposed to air, and a few yellow crystals of $[Fe(OTf)_2\{O=P(NEt_2)_2(2\text{-py})\}_2]$ (**32**) were subsequently obtained (Scheme 5.7). Colourless crystals of diethylammonium diphenylsulfonimide, which result from ligand decomposition, were also isolated from the mixture. Within complex **32**, the iron(II) cation is coordinated in an octahedral fashion by two phosphine oxide ligands **O=12** *via* the oxygen atoms and the pyridyl-nitrogen donor atoms. In addition, two triflate anions are coordinated to the Fe^{2+} cation in the axial positions, whereas the diethylamino groups of the ligand are not involved in any coordination.

Since no coordination of the fluorophosphonium salt **F-12-NSI** occurred with iron(II), the reaction mixture of **F-12-NSI** with $NiBr_2$ was heated to reflux in THF, using a 1 : 1 stoichiometry. A green solution from which it was not possible to isolate any pure material was formed. However, $^{31}P\{^1H\}$ NMR spectroscopy suggests the formation of a nickel(II) complex in which the fluorophosphonium cation, rather than the phosphine oxide, is involved in coordination. In the $^{31}P\{^1H\}$ NMR, a shift of the doublet from the cationic ligand, which appears at 44.5 ppm ($CDCl_3$), to a doublet at 71.6 ppm (in THF) is observed. This downfield shift is probably due to decreased shielding of the P bridgehead caused by electron-donation from the ligand to the nickel(II) cation. This observation points towards the conclusion that the fluorophosphonium salt does not act as Z-type ligand within the nickel(II) complex, since in this case an upfield shift should be observed in the phosphorus NMR due to the electron-donation from the metal into the ligand (σ*) orbital.[293] However, since no single-crystals could be isolated from the reaction mixture, no further conclusions can be drawn about the coordination mode of the ligand. The diamagnetic character of the complex, however, points towards a square-planar coordination geometry of the complex. In addition to the doublet in the $^{31}P\{^1H\}$ NMR spectrum, a triplet appeared at around 60 ppm, which indicates the unexpected presence of the corresponding difluorophosphorane.

Further coordination studies focused on copper(I), another late 3d transition metal, since no coordination complexes could be isolated using the very electron-deficient fluorophosphonium salt **F-12-NSI** and iron(II) and nickel(II). Therefore, **F-12-NSI** was reacted with $[Cu(MeCN)_4]PF_6$ in THF in a 2 : 1 stoichiometric reaction (Scheme 5.7). *In-situ* $^{31}P\{^1H\}$ NMR and $^{19}F\{^1H\}$ NMR spectroscopy indicated no coordination, since only the starting material was observed in solution. However, it was found that air exposure leads to the oxidation of the fluorophosphonium cation **F-12**$^+$ and the oxidation of the copper(I) cation to afford the air-stable copper(II) phosphine oxide complex **33**. The oxidation of the copper(I) cation is not surprising, since Cu^I is highly susceptible to disproportionation to Cu^{II} and Cu^0, and the oxidation of the fluorophosphonium salt **F-12-NSI** has also been observed previously. Within the complex $[Cu(THF)_2\{O=P(NEt_2)_2(2\text{-py})\}_2](PF_6)_2$ (**33**), the copper(II) cation is coordinated in an octahedral fashion, similar to that observed for the iron(II) complex **32**, by two ligands *via* their oxygen and pyridyl-nitrogen atoms. In the axial positions, two THF molecules can be found. The diethylamino groups are again not involved in any coordination. The blue colour of the complex as well as its paramagnetic nature confirmed the +2 oxidation state of the metal centre.

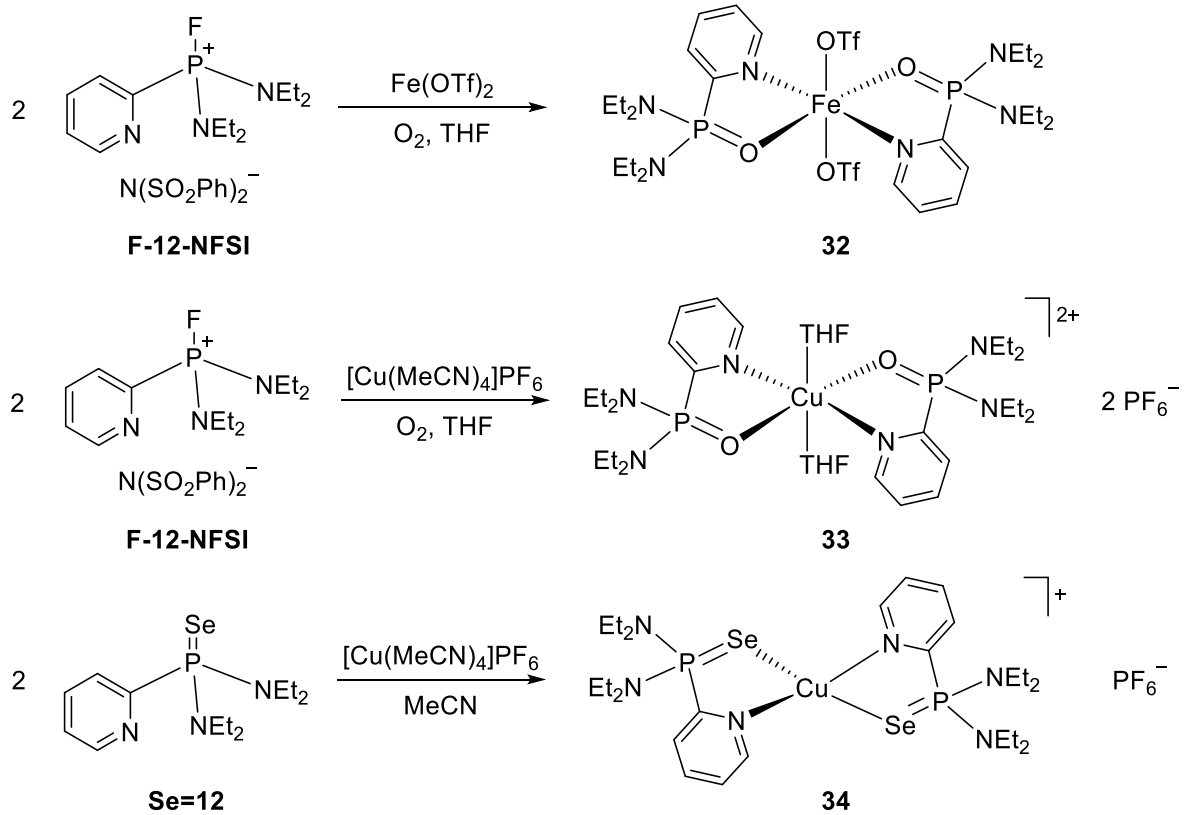

Scheme 5.7: *Synthesis of transition metal complexes **32**–**34** of the bridgehead-modified 2-pyridyl-phosphines.*

In order to investigate the influence of the nature of the bridgehead on the metal coordination, the heavier analogue $Se=P(NEt_2)_2(2\text{-py})$ (**Se=12**) was reacted with $[Cu(MeCN)_4]PF_6$ in acetonitrile. The mixture immediately turned bright yellow. Attempts to crystallise the compound from THF in

order to provide reaction conditions similar to those used in the isolation of the phosphine oxide complex **33** failed. However, layering a saturated DCM solution with diethyl ether resulted in the formation of yellow crystals of complex **34**, which were found to be a tetrahedral copper(I) complex in which two ligand molecules coordinate to the copper(I) cation *via* the selenium atoms and the pyridyl-nitrogen atoms. As observed previously, the diethylamino groups are not involved in the coordination. The diamagnetic complex was analysed by NMR spectroscopy and exhibits a singlet at 77.1 ppm in the $^{31}P\{^{1}H\}$ NMR spectrum with selenium satellites and a one-bond coupling of $^{1}J_{PSe}$ = 692.1 Hz (CD_3CN). Interestingly, the chemical shift of the signal is almost identical with that of the free ligand **12** (71.6 ppm, $CDCl_3$), whereas the $^{1}J_{PS}$ in the free ligand is approximately 70 Hz greater ($^{1}J_{PSe}$ = 760.0 Hz) than that of the complex. The formation of a tetrahedral copper complex with the selenide **Se=12**, rather than an octahedral complex like that observed for the oxide **O=12**, is probably due to the +1 oxidation state of the copper centre.

Since no higher oxidation state 3d transition metal complexes of the fluorophosphonium cation **F-12**$^{+}$ could be isolated, its coordination chemistry towards Mo^{0} was examined. $Mo(CO)_6$ was selected as the precursor, due to the high electron density of the metal in the stable, low-oxidation state (which makes it more likely to exhibit backdonation to the P-centre). Furthermore, the CO ligands of molybdenum hexacarbonyl are quite labile and should be easily replaceable by other ligands at elevated temperatures. Thus, $Mo(CO)_6$ was brought to reflux with **F-12-NSI** in THF overnight. A colour change from colourless to deep brown was observed and indicated complexation. After workup, only a very viscous oil was obtained, but NMR spectroscopic analysis confirmed the presence of a Mo fluorophosphonium complex. In contrast to the Ni^{II} complex, an upfield shift of the doublet in the $^{31}P\{^{1}H\}$ NMR from 44.5 ppm for the free ligand ($^{1}J_{PF}$ = 1050.1 Hz, $CDCl_3$) to 17.8 ppm ($^{1}J_{PF}$ = 1039.6 Hz, $CDCl_3$) was observed. This upfield shift may result from electron-donation from the metal to the ligand, causing greater shielding of the phosphorus atom. Consequently, the presence of some kind of Z-type interaction can be assumed, since such a strong shift in the $^{31}P\{^{1}H\}$ NMR was recorded (Figure 5.6).

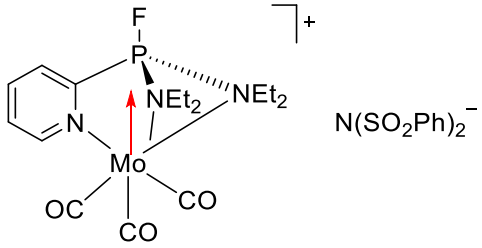

Figure 5.6: *Proposed fluorophosphonium molybdenum complex with electron-donation from the metal to the ligand.*

If the only electronic interaction between the molybdenum centre and the ligand was coordination *via* the pyridyl- or amino-nitrogen donor atoms, only a small shift of the phosphorus magnetic resonance would be expected, such as that observed for the molybdenum tris-2-pyridyl-phosphine complex [{P(2-py)$_3$}Mo(CO)$_3$], for which a shift in the $^{31}P\{^1H\}$ NMR spectrum from –1.0 ppm ($CDCl_3$) of the free ligand to –3.2 ppm ($CDCl_3$) is observed upon coordination.[61]

IR spectroscopic analysis of the reaction mixture was not unambiguous and more structural information is needed in order to provide a clearer picture of the proposed Mo fluorophosphonium complex and the presence of Z-type interactions.

5.4.1 Solid State Structures of the Transition Metal Complexes

The solid state structures of the new copper and iron (amino)-2-pyridyl-phosphine complexes [Fe(OTf)$_2${O=P(NEt$_2$)$_2$(2-py)}$_2$] (**32**), [Cu(THF)$_2${O=P(NEt$_2$)$_2$(2-py)}$_2$](PF$_6$)$_2$ (**33**) and [Cu{Se=P(NEt$_2$)$_2$(2-py)}$_2$]PF$_6$ (**34**) were determined by single-crystal X-ray crystallography, and selected bond lengths and angles are given in Table 5.2.

Table 5.2: *Selected bond lengths (Å) and angles (°) in the transition metal complexes **32**–**34** (M = Fe, Cu, X = O, Se).*

	32	**33**	**34**
P(1)–C$_{py}$	1.824(3)–1.827(3)	1.826(4)	1.836(3)–1.847(2)
P(1)–N$_{Amino}$	1.627(2)–1.641(2)	1.610(4)–1.619(3)	1.640(2)–1.656(3)
P(1)=X	1.498(2)–1.500(2)	1.510(0)	2.1294(8)–2.1319(7)
M–X	2.042(2)–2.054(2)	1.967(2)	2.4063(5)–2.4171(6)
M–N$_{py}$	2.148(2)–2.153(2)	2.011(3)	2.038(3)–2.092(2)
M–OTf/OTHF	2.205(2)–2.320(2)	2.426(3)	-
P(1)–C$_{py}$–N$_{py}$	113.4(2)–113.8(2)	113.0(3)	113.4(2)–117.2(2)
N$_{py}$–M–X	82.79(8)–82.96(8)	86.9(1)	95.26(7)–96.04(7)

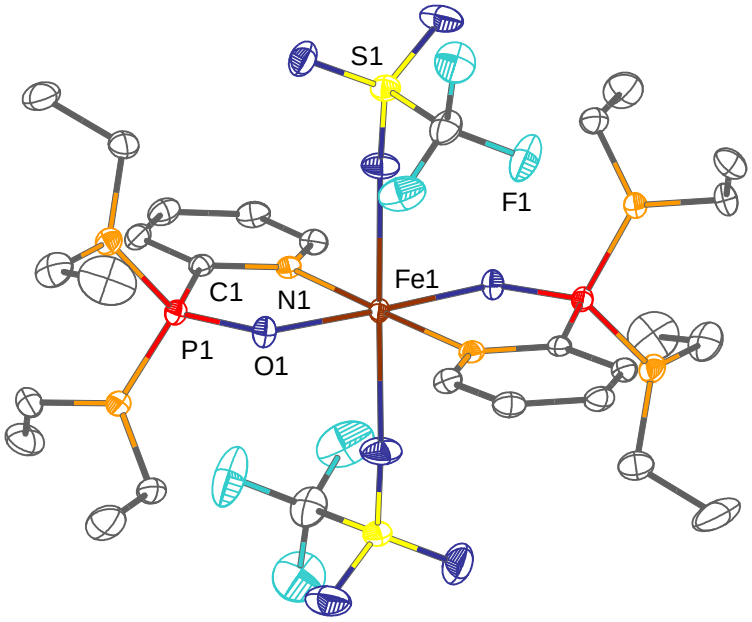

Figure 5.7: *Structure of [Fe(OTf)$_2${O=P(NEt$_2$)$_2$(2-py)}$_2$] (**32**). Only one molecule in the asymmetric unit is depicted. Hydrogen atoms are omitted for clarity. Displacement ellipsoids are drawn at the 30 % probability level.*

The solid state structure of **32** is shown in Figure 5.7. It is that of an octahedral iron(II) complex, in which two phosphine oxide ligands **O=12** coordinate to the metal cation in a *trans* fashion with their oxygen and pyridyl-nitrogen donor atoms. The Fe–O bond lengths are in the range of 2.042(2)–2.054(2) Å, whereas the Fe–N_{py} bond lengths are found to be slightly longer (2.148(2)–2.153(2) Å). Very similar Fe–N_{py} bond lengths (2.109(3)–2.117(2) Å) were found in the high-spin tris-2-pyridyl-phosphine iron(II) complex [{P(6-Me-2-py)$_3$}FeCl$_2$]·toluene (**6**·toluene). This observation is consistent with the paramagnetic character of complex **32** and points towards a high-spin $t_{2g}^4e_g^2$ configuration of the Fe^{II} centre. In the axial positions of the complex, two triflate anions coordinate to the iron centre with Fe–OTf bond lengths of 2.205(2)–2.320(2) Å. A slight distortion of the octahedral coordination geometry is evidenced by the N_{py}–Fe–O bond angles of 82.79(8)–82.96(8)°, which deviate slightly from 90°.

The very similar complex **33** is obtained with copper(I) hexafluorophosphate (Figure 5.8). It is again an octahedral complex, in which the phosphine oxide **O=12** coordinates to the metal with the oxygen of the bridgehead and the pyridyl-nitrogen atoms. The Cu–O bond lengths are 1.967(2) Å and the Cu–N_{py} bond lengths are found to be 2.011(3) Å. These bond lengths are about 0.1 Å shorter than those observed in the iron(II) complex. In the axial position of the complex, two THF solvent molecules are coordinated to the metal centre. The elongated Cu–OTHF bonds of 2.426(3) Å point towards a Jahn-Teller distortion along the z-axis, which is typical of a d^9 electronic configuration. This distortion along the z-axis also leads to the shorter equatorial bond lengths discussed previously.[307] Again, the octahedral coordination geometry around the copper(II) centre is slightly

distorted by the small bite of the chelate ligands, as indicated by the N_{py}–Cu–O bond angles of 86.9(1)°.

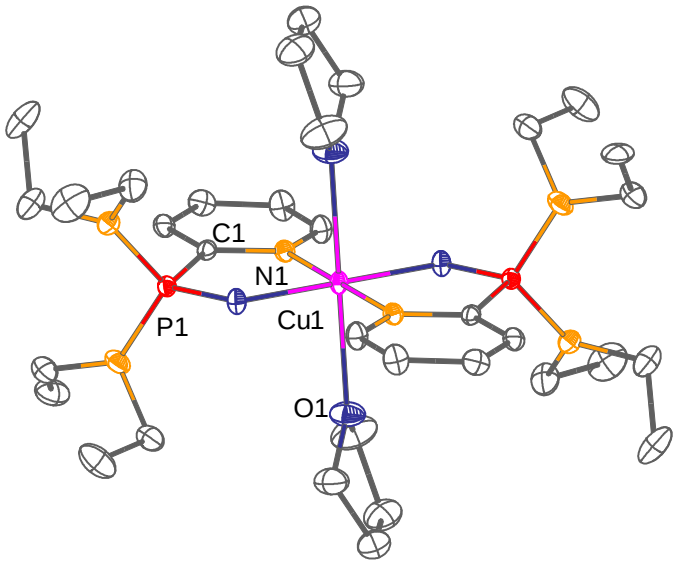

Figure 5.8: *Structure of the cation of [Cu(THF)$_2${O=P(NEt$_2$)$_2$(2-py)}$_2$](PF$_6$)$_2$ (**33**). Hydrogen atoms and PF$_6^-$ counterions are omitted for clarity. Displacement ellipsoids are drawn at the 30 % probability level.*

The tetrahedral copper(I) phosphine selenide complex **34** is shown in Figure 5.9. The copper cation is coordinated by two selenium atoms and two pyridyl-nitrogen atoms of the two **Se=12** ligand molecules. The Cu–N_{py} bond lengths of 2.038(3)–2.092(2) Å are longer than those in the copper complex **33**, despite the reduction in the coordination number. The latter observation is consistent with the differences in the oxidation states of the two copper complexes **33** and **34** (*i.e.*, ionic radii Cu^+ 0.77 Å *vs.* Cu^{2+} 0.70 Å). The N_{py}–Cu–Se bond angles are in the range 95.26(7)–96.04(7)° and indicate a distorted tetrahedral coordination geometry.

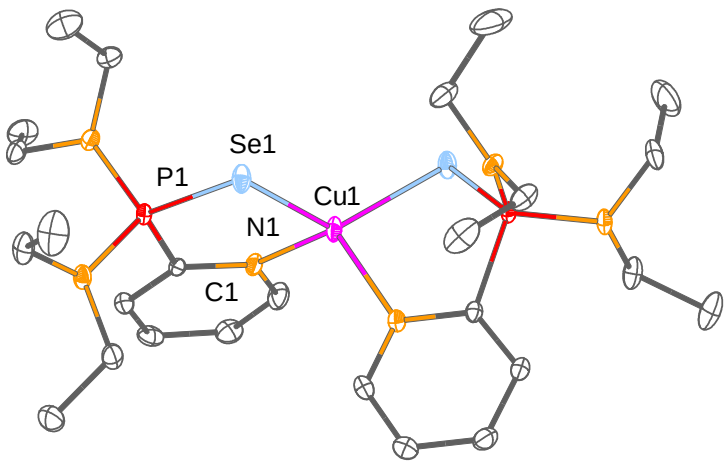

Figure 5.9: *Structure of the cation of [Cu{Se=P(NEt$_2$)$_2$(2-py)}$_2$]PF$_6$ (**34**). Hydrogen atoms and PF$_6^-$ counterions are omitted for clarity. Displacement ellipsoids are drawn at the 30 % probability level.*

5.5 Concluding Remarks

In addition to the alteration of the ligand backbone of phosphines and the introduction of electron-donating or electron-withdrawing substituents, bridgehead modifications are an obvious way to tune the electronic properties of phosphorus compounds. One approach in this regard is the oxidation of the phosphorus bridgehead position with chalcogenides to afford air- and moisture-stable phosphorus(V) compounds. As part of this study, a variety of oxidised phosphorus(V) compounds of tris-2-pyridyl-phosphines and unsymmetrical derivatives were isolated and structurally characterised. It has been shown that the introduction of substituents into the 6-position of tris-2-pyridyl-phosphines or the implementation of additional donor functionalities, such as amino groups, do not affect the synthetic oxidation protocol.

Beside oxidation with chalcogenides, more recently, the fluorination of phosphorus compounds has been the focus in the synthesis of Lewis-acidic P^V cations.[285–288] Since usually, only fluorophosphonium cations containing phenyl substituents (*e.g.* C_6F_5) with limited coordination abilities[286,289,290,301] were focused upon, the aim of this study was to extend this concept to multidentate 2-pyridyl-phosphine ligand sets. Additionally, the presence of pyridyl groups within the ligand framework has been shown to be beneficial, due to the possibility to form pyridinium fluorophosphonium dications, for example, by methylation of the pyridyl moiety, in order to enhance the Lewis acidity.[248,303] Thus, it was shown that the fluorination of tris-2-pyridyl-phosphines $P(2\text{-py})_3$ (**1**) and $P(6\text{-Me-2-py})_3$ (**2**) using xenon difluoride leads to the formation of difluorophosphoranes $F_2P(2\text{-py})_3$ (**F_2-1**) and $F_2P(2\text{-py})_3$ (**F_2-2**), besides the corresponding phosphine oxides **O=1** and **O=2**. The difluorophosphoranes **F_2-1** and **F_2-2** can be converted into the corresponding fluorophosphonium cations by fluoride abstraction. A novel one-step procedure for the synthesis of fluorophosphonium salts was also developed. Treatment of the (amino)-2-pyridyl-phosphine $(Et_2N)_2P(2\text{-py})$ (**12**) with the bench-stable fluorinating reagent NFSI leads to the selective formation of the fluorophosphonium salt $[FP(NEt_2)_2(2\text{-py})][N(SO_2Ph)_2]$ (**F-12-NSI**).

The coordination chemistry of the fluorophosphonium cations towards a variety of transition metals was investigated. From the reaction of the (amino)-2-pyridyl fluorophosphonium cation (**F-12$^+$**) with iron and copper salts, only the corresponding octahedral phosphine oxide complexes **32** and **33** could be isolated. However, such phosphorus(V) compounds have received a great deal of attention in homogeneous transition metal catalysis due to their air- and moisture-stability.[283,284] Coordination studies with Mo^0 were very promising, since a Z-type interaction in which the fluorophosphonium cation acts as σ-donor was indicated by NMR spectroscopy. However, more structural information is needed in order to confirm the actual bonding situation within the molybdenum complex.

6 Iron 2-Pyridyl-phosphines Complexes in Homogeneous Catalysis

6.1 Preamble

In recent years, there has been a great deal of research into the development of Earth-abundant transition metal catalysts, since such metals can be excellent alternatives to rare precious metals regarding sustainability.[308] As one of the most abundant elements on Earth, iron offers long-term availability, which is superior to most other transition metals and it benefits from its low toxicity, environmentally friendliness and its low price.[309] So far, a broad range of hydrofunctionalisation reactions of simple alkenes have been developed using iron catalysts in a variety of oxidation states.[310] The kinetically and thermodynamically accessible oxidation states of iron and its variable coordination geometries provide the basis for new reactivity and consequently novel catalytic mechanisms with unique substrate scope.

When the iron centre is present in a high-oxidation state (+2 and +3), the catalysts act either as a Lewis acid or as a mediator of radical processes.[311] During Lewis acid-catalysed reactions the coordination of an alkene to iron causes them to be more susceptible towards attack from nucleophiles, such as amines, alcohols, carboxylic acid, thiols, alkenes, alkynes and arenes (Scheme 6.1a).[311] In low-valent iron-catalysed hydrofunctionalisation reactions of alkenes, the Fe centre is present in a formal oxidation state of less than +2. Often such iron complexes are highly reactive species, which are air- and moisture-sensitive, and therefore frequently generated *in-situ* through the reduction of more stable Fe^{II} or Fe^{III} pre-catalysts.[312,313] Low-oxidation state iron-catalysed hydrofunctionalisations proceed commonly by the coordination of the alkene to the iron centre and subsequent bond activation of the substrate by σ-bond coordination or oxidative addition (Scheme 6.1b).

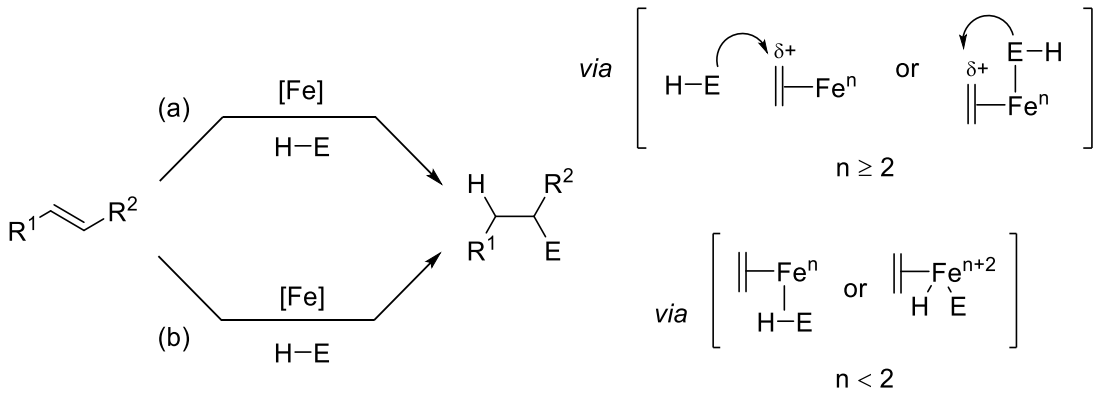

Scheme 6.1: *(a) High-oxidation state iron catalysts acting as Lewis acid catalysts and (b) low-oxidation state iron catalyst in hydrofunctionalisation reactions.*

In particular, industrially important hydrogenation reactions of alkenes have been intensively investigated due to their high atom economy and the potential for hydrogen storage in small molecules.[314] P. J. Chirik and co-workers developed highly active and selective bis(imino)pyridine dinitrogen iron(0) complexes[312,315] for the hydrogenation of unactivated, unfunctionalised terminal alkenes (Scheme 6.2).[316] The iron(0) species can be obtained from the reduction of iron(II) dihalide precursors using sodium amalgam[317,318] or $NaHBEt_3$[315] (Scheme 6.2). Since the pyridine(diamine) ligand acts a "non-innocent" ligand, with π-accepting properties, the iron centre can best be described as resonance hybrid between Fe^0 and Fe^{II}.[319]

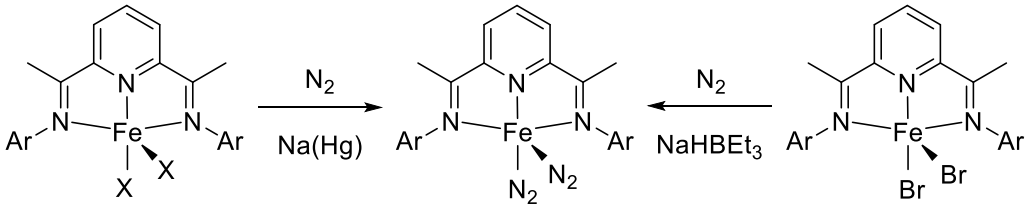

X = Cl, Br

Ar = 2,6-^{i}Pr$_2$-C$_6$H$_3$

***Scheme 6.2**: Reduction of the iron(II) dihalide complexes with sodium amalgam or sodium triethylborohydride under 1 atm of dinitrogen.* [315]

The hydrogenation of alkenes using bis(imino)pyridine dinitrogen iron(0) complexes probably occurs *via* the loss of the two nitrogen molecules, followed by olefin coordination and oxidative addition of hydrogen. The formally 18 valence-electron olefin dihydride complex then undergoes alkene insertion and alkane reductive elimination (Scheme 6.3).[315]

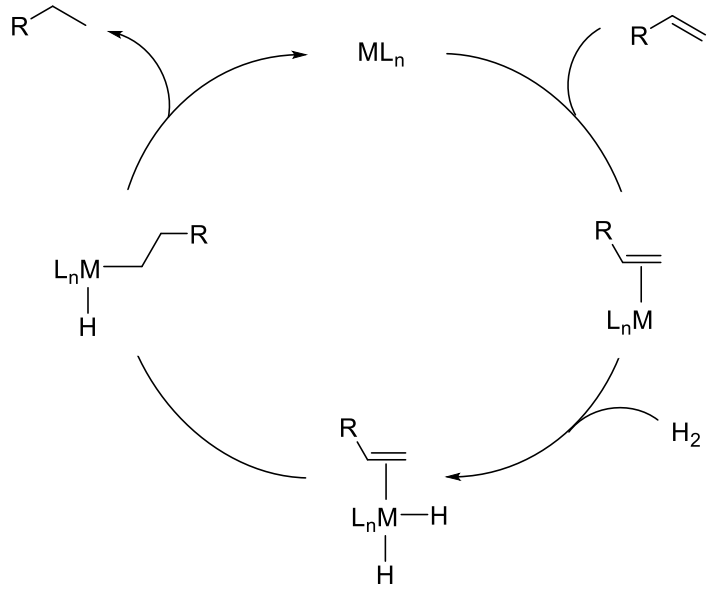

***Scheme 6.3**: Simplified scheme of the transition metal catalysed hydrogenation of alkenes.*

Besides P. J. Chirik's work on bis(imino)pyridine complexes, bis(arylimidazol-2-ylidene)pyridine,[316] bis(phosphino)amine[320] pincer complexes and $[Fe(\eta^4\text{-anthracene})_2]^-$ complexes[321,322] (among others) have been employed for the hydrogenation of various alkenes under mild conditions (Figure 6.1).

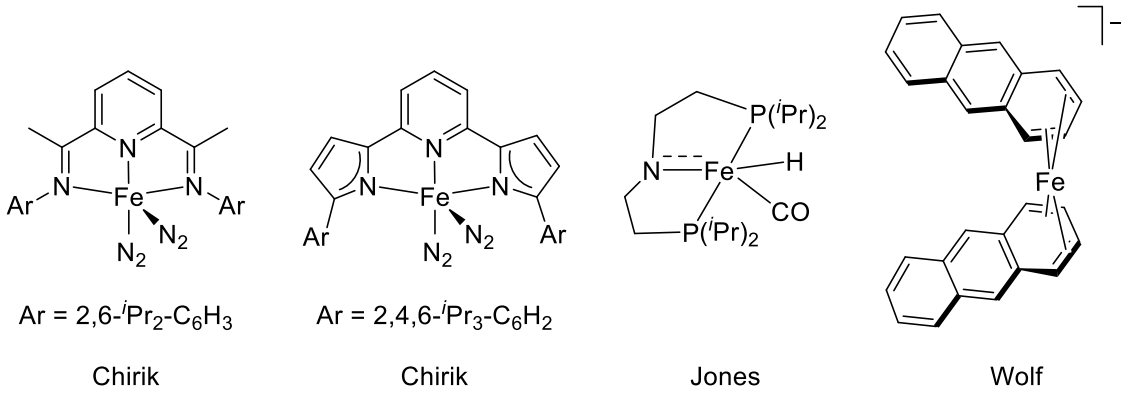

Figure 6.1: *Selected examples of iron catalysts used for the hydrogenation of alkenes.*

In addition to hydrogenation reactions, hydrosilylations of olefins rank among the most industrially used catalytic reactions, providing access to various organosilicon compounds.[323] The first example of an iron-catalysed hydrosilylation was already reported in the 1970s and utilised $Fe(CO)_5$ as the catalyst. Since this reaction required high reaction temperatures and did not show good selectivity,[324] platinum-based catalysts (*e.g.* Speier's and Karstedt's catalysts) have dominated the area for a long time.[325,326] However, recently much progress was made in the development of cheaper iron catalysts and, for example, P. J. Chirik and co-workers were able to achieve very high activities and selectivities using the aforementioned bis(imino)pyridine dinitrogen iron(0) complexes and bis(imino)pyridine iron dialkyl complexes.[315,327] Moreover, H. Nakazawa applied terpyridine iron(II) complexes, which can be reduced *in-situ* using $NaHBEt_3$, in alkene hydrosilylation,[328] and T. Ritter and co-workers reported the use of benzylamine-based Fe catalysts for the regio- and stereoselective 1,4-hydrosilylation of 1,3-dienes (Figure 6.2).[329]

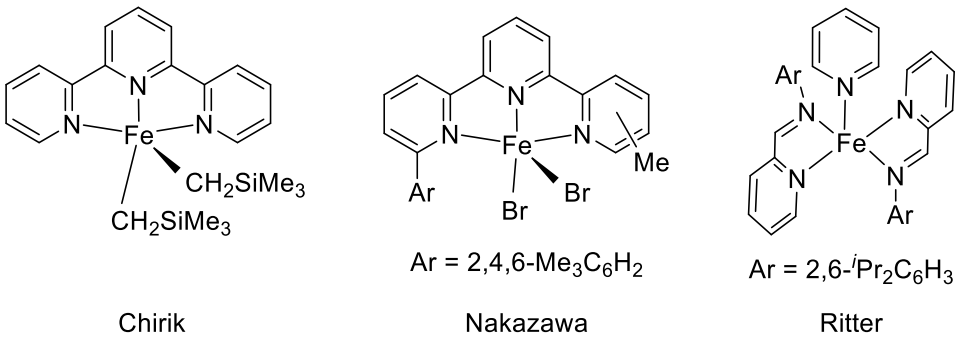

Figure 6.2: *Selected examples of iron catalysts for the hydrosilylation of alkenes.*

The mechanism of transition metal-catalysed hydrosilylation was first proposed by A. J. Chalk and J. F. Harrod (Scheme 6.4).[330,331] Here, the oxidative addition of the silane to the metal centre is followed by the alkene insertion. Reductive elimination of the carbon–silicon bond results in the formation of the hydrosilylation product. However, this mechanism does not explain often-observed dehydrosilylation and hydrogenation side-products. Therefore, M. S. Wrighton and co-workers proposed a "modified Chalk-Harrod" mechanism, in which the alkene insertion into an Fe–Si bond is followed by reductive elimination of the C–H bond.[332,333] Depending on the insertion of the alkene into either the Fe–H or Fe–Si bond, respectively, Markovnikov or classic anti-Markovnikov products can be obtained.

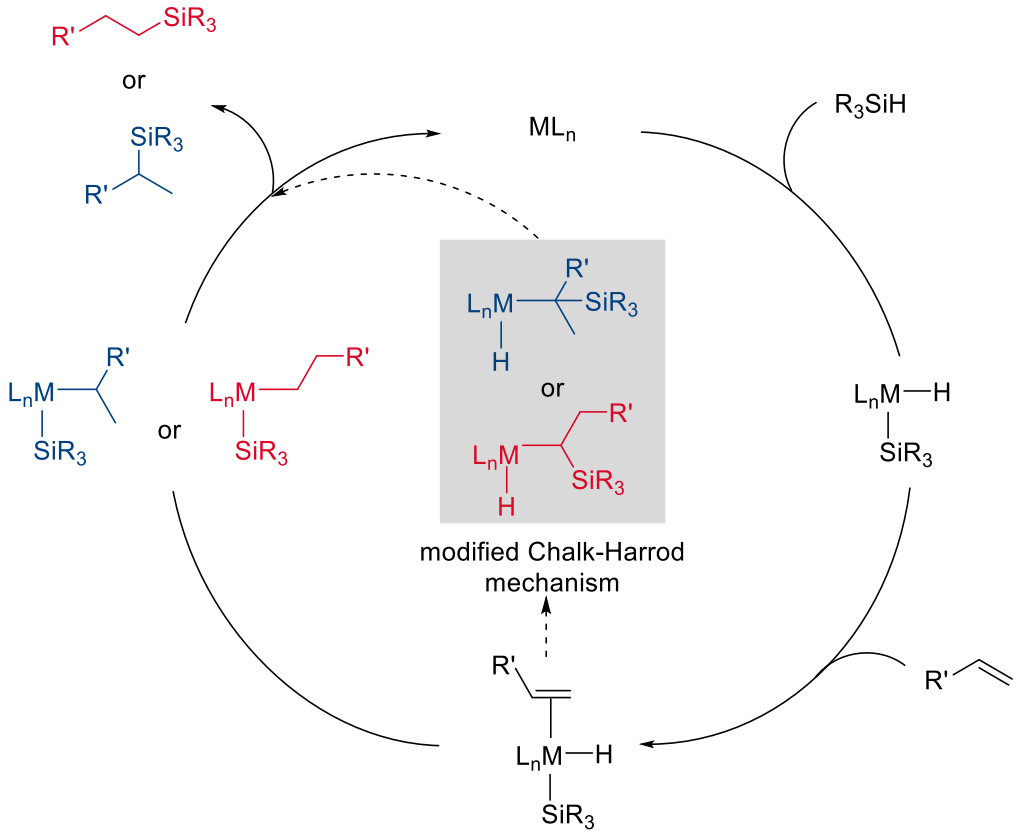

***Scheme 6.4**: Chalk Harrod and modified Chalk-Harrod mechanism for the hydrosilylation of alkenes.*

Although pyridine-containing P,N ligands have found wide applications in catalysis, like the examples illustrated before, 2-pyridyl-phosphines have been largely overlooked and their applications in homogeneous catalysis remains an area with excellent potential for further expansion. Especially, bearing in mind that the catalysts can potentially be separated from reaction media *via* protonation of the pyridyl-nitrogen atoms and subsequent phase separation. In order to examine the catalytic activity of the synthesised iron half-sandwich complexes [{P(2-py)$_3$}FeCl$_2$] (**6**) and [{P(2-py)$_3$}FeCl(OTf)] (**7**), hydrogenation and hydrosilylation reactions of styrene were carried out. In the following sections, these two complexes are described as catalysts, although the true nature of the catalytically active species in reactions could not be revealed. Further substrates

beside styrene were not examined as part of this thesis, since we were only interested in a proof of principle at this stage.

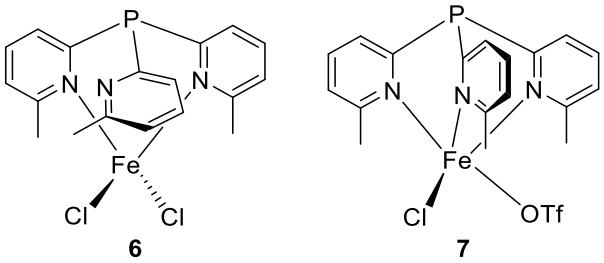

Figure 6.3: *Iron tris-2-pyridyl-phosphine complexes* ***6*** *and* ***7****, which were in the centre of interest.*

6.2 Hydrogenation

In order to develop new simple metal catalysts, the tris-2-pyridyl-phosphine iron(II) complexes **6** and **7** were applied in catalytic hydrogenation reactions of styrene (**35**) to obtain ethylbenzene (**36**). Each catalytic reaction was conducted using a 0.7 mol·L^{-1} solution of styrene in toluene and 10 mol% of the catalysts in either toluene (**6**) or THF (**7**, due to solubility issues) in Teflon-lined high pressure vessels (Scheme 6.5).

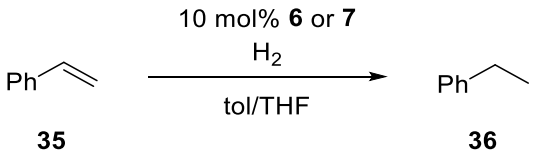

Scheme 6.5: *Hydrogenation of styrene using the iron(II) 2-pyridyl-phosphine complexes* ***6*** *and* ***7****.*

The hydrogenation reactions were carried out using different hydrogen pressures (between 5 and 30 bar) and reaction temperatures (rt and 60 °C). The reactions were performed for 18 h in the absence of a reducing agent, oxygen and water, and conversion was determined *via* GC-MS using an internal standard (*n*-decane). The results of the catalytic hydrogenation reactions are contained in Table 6.1.

Under the given conditions, styrene was not completely hydrogenated to ethylbenzene applying the iron catalysts **6** and **7**. Looking at the results from catalyst **6**, a maximum conversion of only 23 % at 10 bar hydrogen pressure at room temperature was observed. Higher hydrogen pressures and reaction temperatures did not result in enhanced catalytic activity.

Hydrogenation reactions employing catalyst **7** proceed to a maximum of 14 % conversion at room temperature and 40 % conversion at 60 °C. In the case of complex **7**, an increase in hydrogen pressure leads to a slightly enhanced catalytic activity, although at 60 °C the optimum pressure was found to be 10 bar.

Table 6.1: *Hydrogenation of styrene using 10 mol% of the tris-2-pyridyl iron(II) complexes* ***6*** *and* ***7****.*

Entry	mol %	Catalyst	p [bar]	T [°C]	Conversion [%]
1	10	**6**	5	rt	22
2	10	**6**	10	rt	23
3	10	**6**	30	rt	2
4	10	**6**	5	60	16
5	10	**6**	10	60	0
6	10	**6**	30	60	0
7	10	**7**	5	rt	6
8	10	**7**	10	rt	9
9	10	**7**	30	rt	14
10	10	**7**	5	60	23
11	10	**7**	10	60	40
12	10	**7**	30	60	25

Since quantitative conversions of styrene (**35**) to ethylbenzene (**36**) were not obtained from the previous reactions, $NaHBEt_3$ (two equivalents with respect to the catalysts) in toluene was added to the reaction mixture (Scheme 6.6). This should lead to an *in-situ* reduction of the iron(II) centre to form low-valent iron species, which could then potentially be active catalysts for hydrogenation reactions. This idea was inspired by P. J. Chirik's work on bis(imino)pyridine dinitrogen iron(0) complexes, which were obtained from the reduction of the corresponding dibromo or dichloro iron(II) precursors.[315,317,319]

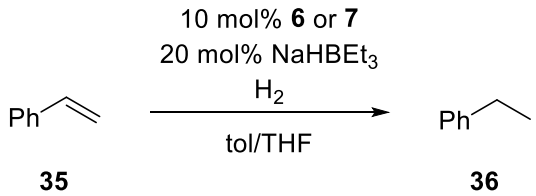

Scheme 6.6: *Hydrogenation of styrene using the iron(II) 2-pyridyl-phosphine complexes* ***6*** *and* ***7*** *and* $NaHBEt_3$ *as additive.*

The results of the hydrogenation reactions with the addition of 10 mol% of the catalysts **6** or **7** and 20 mol% of $NaHBEt_3$ as reducing agent are listed in Table 6.2. The mixtures were again stirred for 18 h.

Table 6.2: *Hydrogenation of styrene using 10 mol% of the tris-2-pyridyl iron(II) complexes* ***6*** *and* ***7*** *and 20 mol% of* $NaHBEt_3$.

Entry	mol %	Catalyst	Additive	p [bar]	T [°C]	Conversion [%]
1	10	**6**	20 mol% $NaHBEt_3$	5	rt	46
2	10	**6**	20 mol% $NaHBEt_3$	10	rt	50
3	10	**6**	20 mol% $NaHBEt_3$	30	rt	10
4	10	**6**	20 mol% $NaHBEt_3$	5	60	6
5	10	**6**	20 mol% $NaHBEt_3$	10	60	40
6	10	**6**	20 mol% $NaHBEt_3$	30	60	23
7	10	**7**	20 mol% $NaHBEt_3$	5	rt	92
8	10	**7**	20 mol% $NaHBEt_3$	10	rt	100
9	10	**7**	20 mol% $NaHBEt_3$	30	rt	100
10	10	**7**	20 mol% $NaHBEt_3$	5	60	11
11	10	**7**	20 mol% $NaHBEt_3$	10	60	100
12	10	**7**	20 mol% $NaHBEt_3$	30	60	25

The comparison with the hydrogenation reactions without additive shows a clear increase of the conversion of styrene to ethylbenzene. In the case of catalyst **6** the optimum hydrogen pressure under these conditions is 10 bar and conversions of 50 and 40 % at room temperature and 60 °C, respectively, are obtained.

When the iron(II) complex **7** is used instead, quantitative conversions can already be achieved at 10 bar hydrogen pressure and room temperature. Even at a hydrogen pressure of 5 bar at room temperature, 92 % conversion was witnessed. This is a significantly enhanced catalytic activity compared to the hydrogenation reactions without the addition of sodium triethylborohydride, Although P. J. Chirik and co-workers already obtained full conversion of styrene to ethylbenzene using one of their bis(imino)pyridine dinitrogen iron(0) complexes within 12 min and 0.3 % catalyst loading,[315] this work illustrates the first example of iron 2-pyridyl-phosphine complexes applied in catalytic hydrogenation reactions.

Interestingly, from the previous results it is obvious that elevated temperatures are not beneficial for the hydrogenation reaction. This observation could probably be ascribed to the formation of catalytically inactive iron-arene complexes (*e.g.* iron styrene complexes, Figure 6.4). P. J. Chirik and co-workers already reported the competitive irreversible formation of η^6-aryl iron complexes at elevated temperatures, which has been shown to serve as a major catalyst deactivation pathway.

The low catalytic activity of such coordinatively saturated iron(0) arene complexes can be attributed to their 18 valence-electron configuration.[317,318]

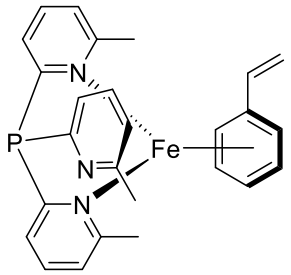

Figure 6.4: *Possible catalyst deactivation pathway at elevated reaction temperatures for the iron(II) complexes* ***6*** *and* ***7*** *after the reduction with* $NaHBEt_3$.

6.2.1 Investigation of the Catalytically Active Iron Species

In order to investigate the active low-valent iron species, which potentially forms after the addition of sodium triethylborohydride to the iron(II) compounds, complexes **6** and **7** were treated with two equivalents of $NaHBEt_3$ in toluene at –80 °C without the addition of styrene and hydrogen. The mixtures turned dark brown immediately after the addition of the reducing agent and no precipitate formation was observed. Also applying a magnet to the sample did not result in the deposition of any nanomaterial (*e.g.* Fe nanoparticles). Unfortunately, despite several crystallisation attempts no products could be isolated, and also NMR spectroscopy gave no indication about whether an iron(0) species had been formed due to the paramagnetic character of the mixtures. Therefore, no conclusions about the homogeneous or heterogeneous nature of the catalytically active species can be made at this stage, although visual inspection is consistent with a homogeneous mechanism. Nevertheless, the unambiguous distinction between homogeneous and heterogeneous catalysts is intricate under reducing conditions and further hydrogenation poisoning experiments have to be carried out in the presence of mercury or dibenzo[*a*,*e*]cyclooctatetraene.[334] The question at this point is also to what extend the definition of a well-defined catalyst is necessary, since research at the frontier between homogeneous and heterogeneous catalysis has shown that the formation of an active low-valent homogeneous catalyst, from $FeCl_3$ and $LiAlH_4$, followed by degeneration into a heterogeneous catalyst can occur without major loss of catalytic activity.[335]

In order to gain further insight in the formation of possible low-valent iron species, the reaction mixtures were analysed after the hydrogenation reactions. This has proven to be problematic, since the solutions could not be recovered from the reaction vessels without exposure to air. The air-sensitivity of the mixtures is demonstrated by the isolation of crystals of an octahedrally coordinated iron(II) complex $[Fe\{O=P(6\text{-Me-2-py})_3\}_4][Fe_2Cl_6(\mu\text{-}O)]$ (**37**) from a hydrogenation reaction, employing catalyst **6** (Figure 6.5). In complex **37** the metal centre is coordinated by four phosphine

oxide ligands (**O=2**). Two of the ligands coordinate the metal *via* their pyridyl-nitrogen atoms and their oxygen atom in the equatorial positions, and two ligands coordinate the metal only *via* their oxygen donor atom in the axial positions. The anion comprises two Fe^{III} atoms, which are connected by a bridging oxide. Each Fe^{III} centre is also coordinated by three Cl atoms. The isolation of this compound illustrates the need for air- and moisture-free conditions during the hydrogenation reactions.

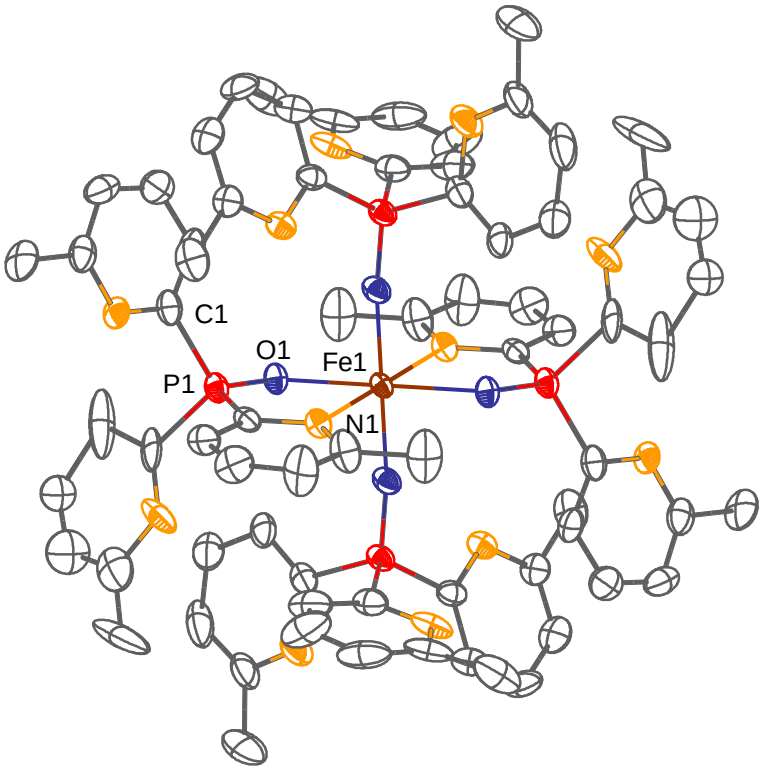

Figure 6.5: *Structure of the dication $[Fe(\{O=P(6\text{-}Me\text{-}2\text{-}py)\}_4]^{2+}$ (**37**). Hydrogen atoms are omitted for clarity. Displacement ellipsoids are drawn at the 30 % probability level.*

6.2.2 Blind Tests

To show that styrene is not already hydrogenated in the absence of a metal catalyst, hydrogenation reactions of the substrate itself at different H_2 pressures and temperatures were conducted (Table 6.3). Under these conditions a maximum conversion of 36 % was reached.

Likewise blind tests were conducted using only iron(II) chloride and iron(II) triflate with or without the addition of $NaHBEt_3$ (Table 6.3). Interestingly, iron(II) chloride itself and in combination with $NaHBEt_3$ at room temperature shows catalytic activity for the hydrogenation of styrene. An almost quantitative conversion was obtained at high hydrogen pressures of 30 bar. In comparison, with catalyst **7** comparable conversion was already obtained at 5 bar H_2 using a similar loading.

Table 6.3: *Hydrogenation of styrene using no catalyst or 10 mol% iron(II) chloride or iron(II) triflate. In some reactions 20 mol% of the reducing agent $NaHBEt_3$ was added.*

Entry	mol %	Additive	p [bar]	T [°C]	Conversion [%]
1	-	-	5	rt	2
2	-	-	10	rt	0
3	-	-	30	rt	0
4	-	20 mol% $NaHBEt_3$	5	rt	36
5	-	20 mol% $NaHBEt_3$	10	rt	36
6	-	20 mol% $NaHBEt_3$	30	rt	18
7	$FeCl_2$	-	30	rt	81
8	$FeCl_2$	20 mol% $NaHBEt_3$	5	rt	39
9	$FeCl_2$	20 mol% $NaHBEt_3$	30	rt	96
10	$Fe(OTf)_2$	-	30	rt	34
11	$Fe(OTf)_2$	20 mol% $NaHBEt_3$	5	rt	57
12	$Fe(OTf)_2$	20 mol% $NaHBEt_3$	30	rt	32

The catalytic activity of iron(II) chloride in conjunction with a reducing agent can probably be attributed to the *in-situ* formation of iron nanoparticles under the given conditions.[336] Interestingly, some rare examples of iron nanoparticle-catalysed hydrogenation reactions are reported in the literature. For example, J. G. de Vries described the catalytic hydrogenation of alkenes and alkynes under moderate conditions using Fe nanoparticles, which were prepared from the reduction of $FeCl_3$ with EtMgBr in THF or Et_2O.[337,338] M. Beller also reported the use of ultra-small Fe^0 nanoparticles, obtained from the decomposition of $[Fe(N\{Si(CH_3)_3\}_2)_2]_2$ under three bar of hydrogen at elevated temperatures, and their application in the hydrogenation of C–C multiple bonds under mild conditions.[339]

To verify the formation of iron particles, $FeCl_2$ was reacted with one equivalent of $NaHBEt_3$ in toluene in the absence of styrene. The mixture turns dark immediately and a ferromagnetic precipitate is formed, which could be separated from the reaction mixture using a magnet. SEM analyses of the solid has shown the formation of small particles in the range of 100–200 nm (Figure 6.6). During the measurement, uniform particles and no crystalline contents (such as NaCl) were witnessed, although transmission electron microscopy is required to obtain a more detailed look at the nature of the particles.

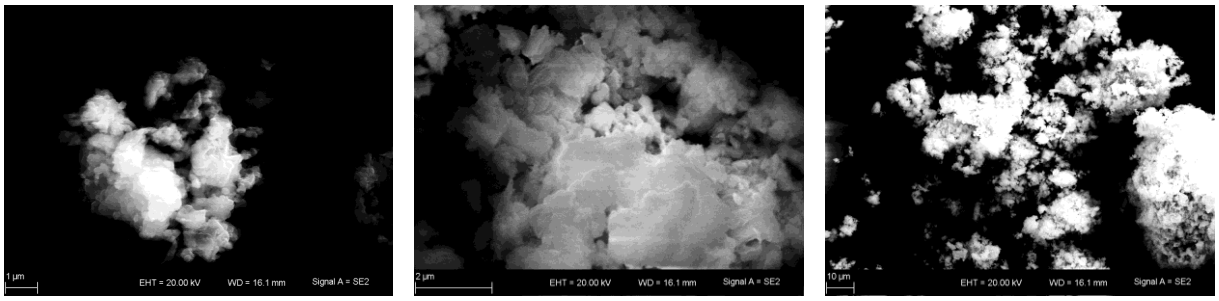

Figure 6.6: *SEM images of the iron particles at different resolutions.*

From energy dispersive X-ray spectroscopy measurements (EDX) an elemental composition of 10.5 % iron, 20.7 % chlorine, 30.6 % sodium and 38.2 % oxygen can be obtained (Figure 6.7). The high oxygen content can be attributed to the sample preparation, which was carried out quickly under air. However, interesting is the chlorine content of the sample, which comes from the reduction of the iron chloride. In what way the chlorine content influences the reactivity must be further examined with Cl-free iron nanoparticles.

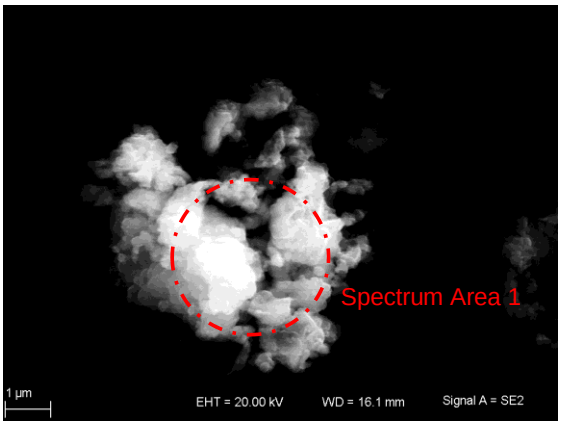

Element	m %
O	23.18
Na	26.69
Cl	27.79
Fe	22.34

Figure 6.7: *SEM image of the iron particles and mass percentages of the given area as determined by EDX.*

Since iron(II) chloride and the complexes **6** and **7** have shown different activities for the hydrogenation of styrene under reducing conditions, it can be concluded that the 2-pyridyl-phosphine ligand has an influence on the metal centre and its catalytic activity. Whereas for $FeCl_2$ a heterogeneous mechanism is most likely, the fact that from the reaction of complexes **6** and **7** with $NaHBEt_3$ no precipitate formation could be witnessed, suggests a homogeneous reaction path. However, colloidal iron nanoparticles could still be present and further poisoning experiments and kinetic studies have to be carried out in order to investigate the reaction mechanism further.

6.3 Hydrosilylation

The hydrosilylation of alkenes ranks among the most important industrial applications of homogeneous catalysis and has attracted a great deal of research in the past decade or so.[323] Recently, much progress was made in the development of iron catalysts for catalytic

hydrosilylations, which led predominantly to the formation of industrially viable anti-Markovnikov products (Scheme 6.7).[312,313,315–318] However, selective Markovnikov silylations, especially asymmetric versions, have become an important aim in the development of new catalytic systems.[340] Apart from the formation of the desired silylated products **38** and **39**, side-products, such as dehydrosilylation **40** and hydrogenation **36** products,[333] as well as double- or triple-silylated species **41**,[341] have frequently been observed (Scheme 6.7). The appearance of dehydrosilylation and hydrogenation side-products can be explained by a modified Chalk-Harrod mechanism, in which alkene insertion into a M–Si bond is assumed (Scheme 6.4).[332,333]

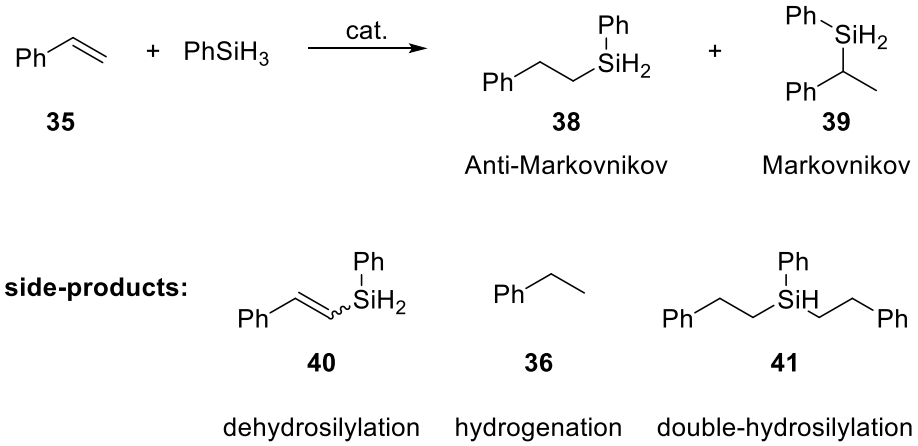

Scheme 6.7: *Hydrosilylation of styrene and the formation of Anti-Markovnikov and Markovnikov products as well as certain side-products.*

For the investigation of the tris-2-pyridyl-phosphine iron(II) complexes **6** and **7** as catalysts in hydrosilylation reactions, styrene (0.7 mol·L^{-1} of toluene) was reacted with one equivalent phenylsilane in the presence of 5 mol% of the catalysts in toluene (**6**) or in THF (**7**). Complex **7** was dissolved in THF, due to the low solubility in toluene. The catalytic reactions were carried out under air- and moisture-free conditions at room temperature or at elevated temperatures (60 °C for THF reactions, 100 °C for toluene reactions). The reaction progress was monitored by GC-MS analyses with respect to the internal standard *n*-decane. Unfortunately, both complexes did not show any catalytic activity for the hydrosilylation of styrene even after 5 days at elevated temperatures.

Therefore, reducing agents (two equivalents with respect to the catalyst) were added to the mixtures in the hope of forming catalytically active low-valent iron species,[342–344] analogously to the results obtained for the hydrogenation reactions. Based on literature reports $NaHBEt_3$,[315,317,328,345,346] $LiAlH_4$[343,347] and EtMgBr[313] were selected and a colour change from pale yellow to brown was observed in all cases after the addition to the complexes **6** and **7**. Unfortunately, as was seen before, no low-oxidation state iron compounds could be isolated from the reactions of the iron(II) complexes with the different reducing agents.

Table 6.4: *Hydrosilylation of styrene using 5 mol% of the tris-2-pyridyl iron(II) complexes **6** and **7** and 10 mol% of a reducing agent.*

Entry	mol %	Catalyst	Additive	T [°C]	Conversion [%]	Product
1	5	**6**	10 mol% $NaHBEt_3$	rt	3	**39**
2	5	**6**	10 mol% $NaHBEt_3$	100	76	**39**
3	5	**6**	10 mol% $LiAlH_4$	rt	3	**39**
4	5	**6**	10 mol% $LiAlH_4$	100	10	**39**
5	5	**6**	10 mol% EtMgBr	rt	0	-
6	5	**6**	10 mol% EtMgBr	100	0	-
7	5	**7**	10 mol% $NaHBEt_3$	rt	21	**36**
8	5	**7**	10 mol% $NaHBEt_3$	60	18	**36**
9	5	**7**	10 mol% $LiAlH_4$	rt	0	-
10	5	**7**	10 mol% $LiAlH_4$	60	14	**36**
11	5	**7**	10 mol% EtMgBr	rt	5	**36**
12	5	**7**	10 mol% EtMgBr	60	15	**36**

Under the given conditions, only 3 % conversion could be obtained using complex **6** in conjunction with $NaHBEt_3$ at room temperature. When the reaction temperature was increased to 100 °C, 76 % conversion could be achieved over the course of six days. Although harsh conditions and long reaction times were required, the exclusive formation of the Markovnikov product **39** was observed. This is a remarkable observation, since the first examples of iron-catalysed Markovnikov selective hydrosilylations,[348] and asymmetric versions,[349] were only reported in 2018. S.-F. Zhu and co-workers have attributed the origin of the Markovnikov regioselectivity to an aryl-directed effect or more specifically π-π interactions between the ligand backbone and the aromatic styrene.[348] In contrast, the hydrosilylation of styrene using bis(imino)pyridine dinitrogen iron(0) complexes, developed by P. J. Chirik and co-workers, proceeded within 90 min at room temperature and resulted only in the formation of the anti-Markovnikov product **38**.[315]

Remarkably, Markovnikov regioselectivity was also obtained from the hydrosilylation of styrene with sodium triethylborohydride as catalyst itself. The reaction proceeds with phenylsilane and 10 mol% $NaHBEt_3$ at 60 °C in 24 hours.[350] For this reaction an anionic reaction mechanism was proposed, in which the first step involves the addition of the Na–H bond to the alkene. The formation of an internal carbanion, which explains the regioselectivity of the hydrosilylation and the need for resonance-stabilised alkenes, is then followed by the reaction with the silane to give potentially a pentacoordinate silylated species. In the final step of the catalytic cycle a hydride is

abstracted from this species by free triethylborane under regeneration of the catalyst.[350] Since the $NaHBEt_3$-catalysed hydrosilylation of styrene proceeds much faster than the reaction using complex **6** in conjunction with $NaHBEt_3$, a different reaction mechanism is assumed.

When complex **7** with $NaHBEt_3$ as reducing agent was used as catalyst for the hydrosilylation of styrene, very similar conversions of around 20 % at room temperature and at 60 °C were achieved after 6 days. This time, however, the hydrogenation product ethylbenzene (**36**) is formed instead of any silylated product. This finding again indicates that $NaHBEt_3$ reacts first with the iron complexes, instead of catalysing the hydrosilylation on its own.

The hydrosilylation reactions in the presence of $LiAlH_4$ resulted only in conversions of 10 or 14 % using **6** and **7** at 100 or 60 °C, respectively. In the case of **6**, again the Markovnikov product **38** was detected, whereas catalyst **7** leads to the formation of ethylbenzene (**36**).

When the Grignard compound EtMgBr was used as the reducing agent no conversion was obtained for the iron complex **6** and only 15 % conversion at 60 °C for complex **7**. Again, ethylbenzene was obtained as the product from this reaction. Also, for all of the reactions employing EtMgBr, the formation of phenyl(diethyl)silane (**42**) was observed as a side-product (Scheme 6.8).

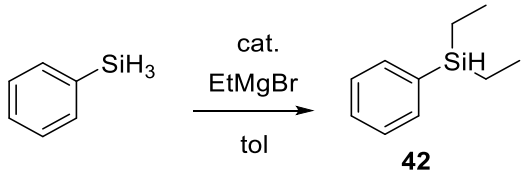

42

Scheme 6.8: *Side-reaction from the catalytic reaction employing the Grignard reagent EtMgBr.*

6.4 Concluding Remarks

In this current study the catalytic activities of the iron(II) tris-2-pyridyl-phosphine complexes **6** and **7** were examined in hydrogenation and hydrosilylation reactions of styrene.

The use of complexes **6** and **7** as catalysts for the hydrogenation of styrene has shown that only maximum conversions of 23 % (rt, 10 bar H_2) and 40 % (60 °C, 10 bar H_2), respectively, could be obtained. In the case of **6**, an increase in reaction temperature did not lead to enhanced catalytic activity, whereas for **7**, an increase in reaction temperature led to a slightly enhanced catalytic activity.

The addition of the reducing agent $NaHBEt_3$ did lead to enhanced catalytic activity in hydrogenation reactions, probably due to the formation of low-valent iron species. This *in-situ* reduction approach prevents the challenging preparation and storage of low-oxidation state iron complexes. For complex **6**, a maximum conversion of 50 % at room temperature and a hydrogen pressure of 10 bar

was achieved in the presence of $NaHBEt_3$. In the case of complex **7**, the enhanced catalytic activity was much more drastic. 100 % conversion of styrene to ethylbenzene was already obtained at room temperature and 10 bar hydrogen. Elevated temperatures were not beneficial for both catalysts in the presence of $NaHBEt_3$, probably due to the formation of catalytically inactive iron-arene complexes. Since no low-valent iron species could be isolated from the reactions of catalysts **6** and **7** with sodium triethylborohydride, the question of whether a homogeneous or heterogeneous catalyst is present remains unanswered. However, the absence of any precipitation by visual inspection points towards homogeneous catalysis.

Interestingly, blind tests have shown that styrene can almost be quantitatively hydrogenated at room temperature and 30 bar hydrogen pressure using iron(II) chloride and $NaHBEt_3$ as catalytic system. This finding can probably be explained by the formation of catalytically active iron nanoparticles.

The investigation of the tris-2-pyridyl-phosphine iron complexes **6** and **7** in hydrosilylation reactions has shown no conversion to any silylated product without the presence of an external reducing agent. Through the addition of $NaHBEt_3$ to complex **6**, 76 % conversion to the Markovnikov silylation product **39** could be witnessed. The same regioselectivity but with far higher reactivity was obtained with sodium triethylborohydride as catalyst on its own. Of course, $NaHBEt_3$ would provide an inexpensive and commercially available catalyst, but its use is limited to the hydrosilylation of resonance-stabilised alkenes.[350] In the case of complex **7** and $NaHBEt_3$, only the formation of 21 % of the hydrogenation product ethylbenzene (**36**) was detected. No enhancement of the catalytic activities was achieved by using $LiAlH_4$ or EtMgBr as reducing agents. Although the overall catalytic activity of the iron complexes **6** and **7** with or without reducing agent was quite low in hydrosilylation reactions, the formation of different products for the two iron(II) complexes was observed. Whereas **6** leads to the formation of the Markovnikov product **39**, **7** causes the hydrogenation product **36** to be formed.

7 Conclusions and Future Work

The exploration of phosphorus-bridged 2-pyridyl-phosphines presented in this work highlights their potential as easily electronically and sterically modifiable ligands for transition metals.

The effects of substitution at the 6-position of the pyridyl rings in P-bridged tris-pyridyl ligands of the type $P(6\text{-}R\text{-}2\text{-}py)_3$ illustrate a simple but none-the-less important result that such substitution can influence the coordination of the ligands on steric and electronic grounds. The impact of this is seen in the comparison between the coordination behaviour of the unsubstituted ligand $P(2\text{-}py)_3$ (**1**) with the 6-methyl-substituted counterpart $P(6\text{-}Me\text{-}2\text{-}py)_3$ (**2**). Whereas **1** forms the sandwich cation $[\{P(2\text{-}py)_3\}_2Fe]^{2+}$ (**5**) with iron(II), the reaction of the methyl-substituted counterpart $P(6\text{-}Me\text{-}2\text{-}py)_3$ (**2**) with Fe^{II} results in the half-sandwich arrangements $[\{P(6\text{-}Me\text{-}2\text{-}py)_3\}FeCl_2]$ (**6**) and $[\{P(6\text{-}Me\text{-}2\text{-}py)_3\}FeCl(OTf)]$ (**7**). In contrast, the Br- and CN-functionalised ligand sets $P(6\text{-}Br\text{-}2\text{-}py)_3$ (**3**) and $P(6\text{-}CN\text{-}2\text{-}py)_3$ (**4**) do not bind to iron(II) at all, probably due to the reduced basicity of the pyridyl-nitrogen donor atoms. The access to the CN-substituted ligand $P(6\text{-}CN\text{-}2\text{-}py)_3$ (**4**) provides the possibility for further functionalisation and the introduction of chiral substituents, such as carboxylic acids or amines. Although limited studies of the isovalent Al-ligand $[MeAl(6\text{-}Me\text{-}2\text{-}py)_3]^-$ have been undertaken recently,[39,42] this current study is the first in which the steric influence of substituents has been explored in any family of P-bridged neutral tris-pyridyl ligands. The significance of this is that these ligand systems are far more robust and air stable than their metal-bridged counterparts and therefore easier to employ in Real-World settings.

As part of this thesis it was also shown that that the 2-pyridyl-phosphine ligand set can be extensively elaborated upon using a simple set of synthetic approaches. The (alkoxy)-2-pyridyl-phosphines $(RO)_xP(2\text{-}py)_{3-x}$ (x = 1, 2) are easily derived from (amino)-2-pyridyl-phosphines $(R_2N)_xP(2\text{-}py)_{3-x}$ (x = 1, 2) by direct reactions with alcohols. In addition, step-wise reaction of alcohols, depending on the nucleophilicity of the alcohol, with the amino-phosphines can be used to obtain multidentate alkoxy-amino-2-pyridyl-phosphines $(R_2N)(RO)P(2\text{-}py)$ (containing three different substituents). This synthetic approach for the easy modification of the 2-pyridyl-phosphine ligand framework provides the potential means for the introduction of chirality, by creating stereogenic P bridgeheads or through the introduction of chiral alkoxide groups. Although preliminary studies have shown that racemic mixtures of P-stereogenic alkoxy-amino-2-pyridyl-phosphines can be separated on an analytical scale, a preparative separation of the enantiomers, for further applications in the field of asymmetric homogeneous catalysis, is a target for future studies. Coordination studies of the (amino)- and (alkoxy)-2-pyridyl-phosphines with Cu^I reveal that ligands with two N donor atoms form dimeric arrangements, while $(PhO)_2P(2\text{-}py)$, incorporating only one

N donor atom, shows completely different coordination behaviour. The amino-phosphine $(Et_2N)_2P(2\text{-py})$ forms the A-frame complex $[Rh_2Cl_2(\mu\text{-CO})\{(Et_2N)_2P(2\text{-py})\}_2]$ (**25**) with Rh^I, in which a Rh–Rh bond is present. An unexpected *in-situ* reduction and the formation of the nickel(0) complex $[\{(MeO)_2P(2\text{-py-H})\}_2\{(MeO)_2P(2\text{-py})\}_2Ni](BF_4)_2$ (**26**) was observed from the reaction of the bis(methoxy)-2-pyridyl-phosphine **17** with $[Ni(MeCN)_6](BF_4)_2$. NMR spectroscopic analysis of the reaction mixture provides some evidence for a fluoride-assisted redox reaction. Since similar nickel bis-phosphine complexes with non-coordinating pendant amine bases within the ligand backbone have found applications in electrocatalytic hydrogen oxidation and proton reduction reactions,[255–258] the electrocatalytic behaviour of **26** in the presence of hydrogen or a proton source should be investigated. A drawback in this regard could be the instability of **26** towards acids.

In order to compare the 2-pyridyl-phosphines to the classical tertiary phosphines used in homogeneous transition metal catalysis, Tolman electronic parameters were derived from experimental and computational data. It was shown that the synthesis of molybdenum and tungsten complexes, including only metal–P coordination, is problematic due to the presence of a variety of donor atoms and the resulting coordination modes that can be adopted. However, two suitable Mo^0 complexes, $[Mo(CO)_5\{P(6\text{-Me-2-py})_3\}]$ (**30**) and *cis*-$[Mo(CO)_4\{P(6\text{-Br-2-py})_3\}_2]$ (**31**), could be isolated, and conversion of the carbonyl stretching frequencies into the corresponding Tolman electronic parameters has shown that the introduction of the substituents into the 6-position has indeed an influence on the overall donor strength of the phosphines. This finding was supported by the calculation of the Tolman electronic parameter by DFT methods. The calculations also enabled the comparison of the donor strength of all synthesised 2-pyridyl-phosphines with PPh_3 and $P(^tBu)_3$.

In addition to modification of the ligand backbone, bridgehead modification was also investigated as part of this thesis. Through oxidation of the P bridgehead, air-stable phosphorus(V) chalcogenides and difluorophosphoranes were synthesised. The difluorophosphoranes were synthesised from the reaction of the 2-pyridyl-phosphines and xenon difluoride. Through fluoride abstraction, these compounds can then be converted into the corresponding fluorophosphonium cations. As part of this thesis a novel one-step procedure for the synthesis of fluorophosphonium salts was also developed. Treatment of the (amino)-2-pyridyl-phosphine $(Et_2N)_2P(2\text{-py})$ (**12**) with the bench-stable fluorinating reagent NFSI leads to the selective formation of the fluorophosphonium salt $[FP(NEt_2)_2(2\text{-py})][N(SO_2Ph)_2]$ (**F-12-NSI**). With this method, the use of the very reactive xenon difluoride can be avoided. Unfortunately, the coordination chemistry of the fluorophosphonium cations towards a variety of transition metals only led to the isolation of phosphine oxide complexes. Coordination studies with Mo^0 revealed that $[FP(NEt_2)_2(2\text{-py})]^+$ can potentially act as Z-type ligand, in which the phosphine acts as σ-acceptor. However, since no such Mo complex could be isolated, further structural evidence is needed.

Catalytic studies of the hydrogenation and hydrosilylation of styrene using the iron(II) complexes **6** and **7** were carried out and have shown that the addition of reducing agents is necessary to form catalytically active low-valent iron species. In the case of **7**, complete conversion of styrene to ethylbenzene was achieved at room temperature and 10 bar H_2 pressure over the course of 18 h in the presence of $NaHBEt_3$. It was shown that increased reaction temperatures do not result in a higher catalytic activity of the complexes, probably due to the formation of catalytically inactive iron-arene complexes. In hydrosilylation reactions similar findings were made. The presence of $NaHBEt_3$ led to slightly enhanced catalytic activity, although no quantitative conversions could be achieved. Whereas complex **6** leads to the formation of the Markovnikov silylation product **39**, ethylbenzene (**36**) was formed from reactions utilising complex **7**. For both catalytic reactions the identification of the active iron catalyst species remains a major goal. This would help answering the question whether a homogeneous or heterogeneous catalyst is formed under reducing conditions.[334] For this investigation, poisoning experiments and kinetic studies have to be carried out. Since only styrene was used as the substrate and the solvent choice was very limited, there is a lot of room for further reaction optimisations. Especially, the use of aliphatic alkenes in hydrosilylation reactions is very interesting to see whether again a Markovnikov selectivity can be achieved. Also, only high catalyst loadings of 5 and 10 mol% have been used so far and the use of lower catalyst amounts in hydrogenation reactions should be investigated.

Now that this thesis has laid the foundation, the next stage of the research would be to look at the broader range of coordination sites and electronic properties within the ligand family. Potential candidates are shown in Figure 7.1 and could be based on 2,2'-bipyridyl-phosphine derivatives. Although $P(2,2'\text{-bipy})_3$ was already reported by R. H. Holm in 1972,[351] the concept of the introduction of amino and alkoxy groups could be extended towards bipyridine-based systems and chiral 2,2-bipyridyl-phosphines could be obtained *via* the introduction of chiral amino and alkoxy groups or the formation of P-stereogenic centres.

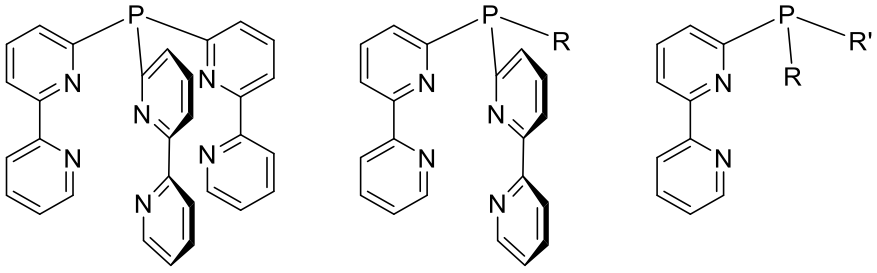

Figure 7.1: *2,2'-Bipyridine based phosphine ligands and unsymmetrical 2,2'-bipyridyl-phosphine derivatives (R = amino or alkoxy group).*

Further work could also move towards the direction of supramolecular chemistry. Since 3-pyridyl- and 4-pyridyl-phosphines have already successfully been applied as ligands,[352–354] the potential of

2-pyridyl-phosphines as building blocks could be investigated in the future. The reactions of diols and triols with two or three equivalents of (amino)-bis-2-pyridyl-phosphines could be utilised to obtain a range of new ligands, like those shown in Figure 7.2.

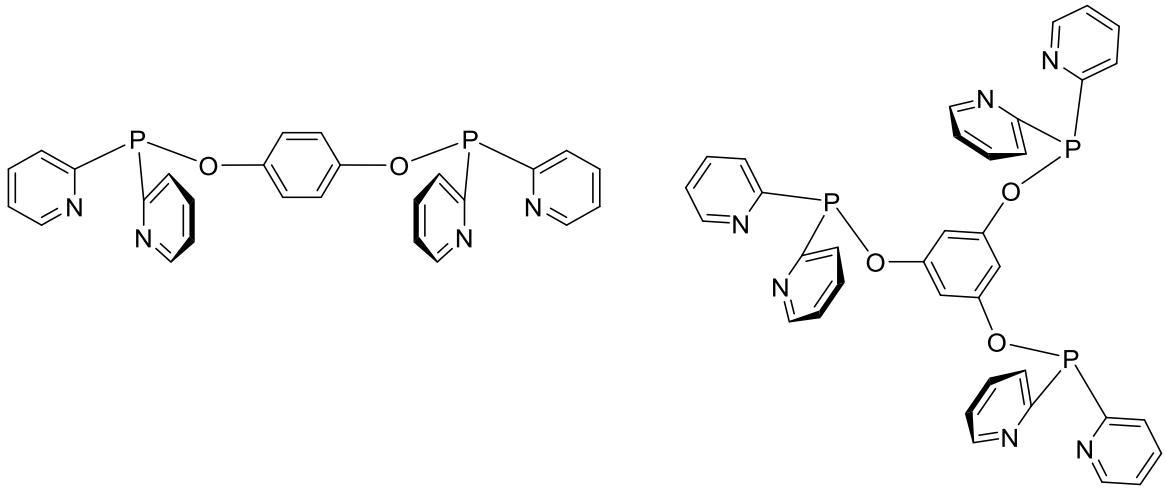

Figure 7.2: *(Alkoxy)-2-pyridyl-phosphine building blocks. Designed for future applications in the field of supramolecular chemistry.*

Depending on the choice of transition metal, different coordination motifs could be adopted. With gold, for example, macrocycles could potentially be formed *via* the coordination of the soft P bridgehead to the metal centre, similar to those reported for flexible bis-phospholane ligands (Figure 7.3).[355]

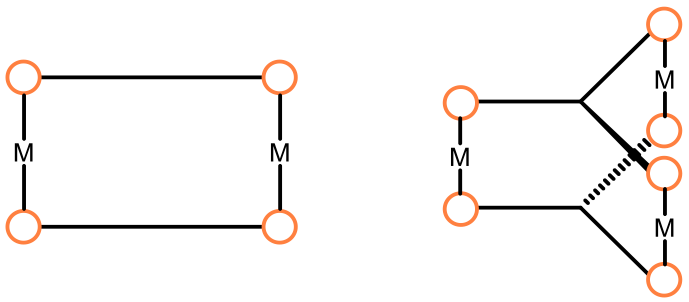

Figure 7.3: *Potential formation of gold macrocycles with (alkoxy)-2-pyridyl-phosphines as templates.*

The ability for these ligand sets to employ a combination of their P, O and pyridyl-N atoms should give rise to interesting coordination chemistry and supramolecular assemblies.

8 Experimental Details

8.1 General Working Techniques

All experiments were carried out on a Schlenk-line under a dry, oxygen-free nitrogen or argon atmosphere or with the aid of a N_2-filled glove box (Saffron type α or MBraun lab star 50). Dry ice/acetone or nitrogen/ethyl acetate mixtures were used as cooling baths to obtain temperatures of around –78 °C.

8.2 Solvents and Starting Materials

All solvents were freshly distilled over appropriate drying agents under nitrogen or taken from a solvent purification system (SPS-800, MBraun). Solvents were subsequently stored over molecular sieves. Deuterated solvents were dried over P_2O_5 or CaH_2, when necessary, or over molecular sieves. All pyridine derivatives were distilled from calcium hydride and dried over molecular sieves before use. Phosphorus trichloride was distilled and phenol was sublimed prior to use. $(Me_2N)PCl_2$,[173] $(Et_2N)PCl_2$,[174] $(Et_2N)_2PCl$,[178] $(Et_2N)PhPCl$,[179] $[Ni(MeCN)_6](BF_4)_2$[356] and $[M(CO)_5(MeCN)]$ (M = Mo, W)[265] were prepared according to literature procedures. All other reagents were purchased from the supplier and used without any further purification.

8.3 Analytical Techniques

Nuclear Magnetic Resonance Spectroscopy: NMR spectra were recorded on a Bruker Avance DRX 400, a 400 MHz Avance III HD Smart Probe Spectrometer, a 400 MHz Avance III HD Spectrometer or a Bruker Avance III HD 500MHz Smart Probe spectrometer at room temperature (298 K), unless otherwise indicated. All spectra were recorded in dry $CDCl_3$, CD_3COCD_3, CD_3CN, D_8-THF or D_8-tol with $SiMe_4$ (^1H) as an internal standard. ^1H and ^{13}C NMR spectra were referenced to TMS, whereas all other heteronuclei were referenced to TMS *via* the Ξ scale.[357] Unambiguous assignments of the NMR resonances were made on the basis of 2D NMR experiments (^1H-^1H COSY, ^1H-^1H NOESY, ^1H-^{13}C HMQC, ^1H-^{13}C HSQC, ^1H-^{13}C HMBC and ^1H-^{31}P HMBC experiments). Some *in-situ* NMR experiments were carried out without deuterated solvent and without a lock. Scheme 8.1 shows the labelling scheme for the NMR assignments used in the experimental section.

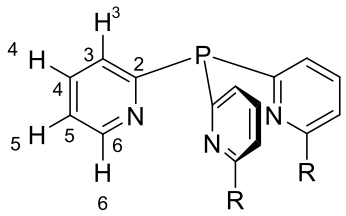

Scheme 8.1: *Atom labelling scheme used in the NMR studies for the 2-pyridyl-phosphine ligands.*

Simulations of spectra were carried out with SpinWorks.[204] Data from the literature were used to determine the algebraic sign of the coupling constants.

Infrared Spectroscopy: A Perkin-Elmer FT IR instrument with an ATR sample setting was used for the IR measurements of the solid compounds, whereas IR measurements of the KBr pellets were obtained using a Perkin Elmer FT IR Spectrum 2000 or Bruker Tensor 27 spectrometer.

Ultraviolet-Visible Spectroscopy: UV-Vis spectroscopy was performed on a Varian Cary 50 UV spectrometer or on a Perkin Elmer Lambda 900 UV-Vis-NIR spectrometer.

Elemental Analysis: The carbon, hydrogen and nitrogen contents of the compounds were determined using an Exeter Analytical CE-440 Elemental Analyser or a Heraeus Vario el Analyser. Highly air-sensitive samples were sealed inside pre-weighed aluminium capsules under an inert atmosphere in a glovebox.

Melting Point: Melting points and decomposition temperatures were obtained using a standard melting point apparatus and are uncorrected.

High-Resolution Mass Spectrometry: HR ESI MS measurements were carried out in positive or negative ion mode under electrospray ionisation on a Bruker Impact II and Esquire 3000 Plus or a ThermoFinnigan Orbitrap Classic. EI MS measurements were recorded on a Thermo Fischer Scientific Mat 8230.

Gas Chromatography-Mass Spectrometry: GC-MS measurements were performed on a Shimadzu GCMS-QP2010 system. A Varian Chirasil-L-Dex column (25 m x 0.25 mm) was used for all analyses. Internal standard calibrations were carried out before the analyses of the catalytic reactions. For these, a known amount of an internal standard (*n*-decane) was added to the substrate (styrene) before injection. The mixtures were then analysed by GC-MS and the peak areas of the substrate *vs.* the standard were compared to the theoretically calculated molar ratios (Table 8.1). Through this procedure, the response factor could be obtained by normalisation of the response of the substrate with respect to the response of the standard (Figure 8.1). This response factor (1.09753 for styrene/*n*-decane) was taken into consideration for the evaluation of all GC-MS results, and the internal standard was added prior to the reaction.

Table 8.1: *Calibration of the substrate styrene vs. the internal standard n-decane.*

Entry	Molar ratio styrene/*n*-decane	Integral ratio styrene/*n*-decane
1	0.25	0.268
2	0.25	0.203
3	0.25	0.296
4	0.50	0.594
5	0.50	0.537
6	0.50	0.512
7	0.71	0.783
8	0.71	0.754
9	1.00	1.105
10	1.00	1.121

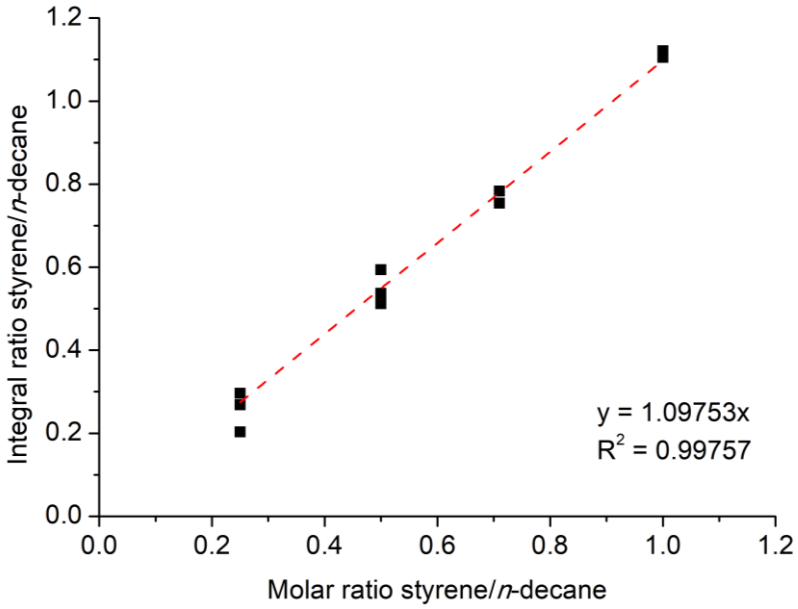

Figure 8.1: *Calibration of the substrate styrene with respect to an internal standard (n-decane).*

Chiral High-Performance Liquid Chromatography: The chiral HPLC screening was carried out by the company Phenomenex. The BH_3-protected phosphines **BH_3-13** and **BH_3-18** were tested on seven different stationary phases in reverse phase and polar organic conditions. Both racemates could be separated on a cellulose-based column (Cellulose-3), which has a cellulose-methyl benzoate phase (Figure 8.2).

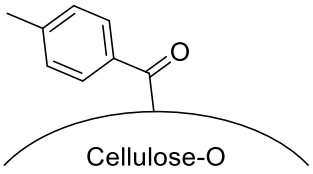

Figure 8.2: *Lux Cellulose-3 column material from the company Phenomenex.*

Satisfactory results were obtained in reverse phase conditions with a mixture of ammonium bicarbonate, acetonitrile and diethylamine in a 40:60:0.1 ratio for **BH_3-13** and a 46:54:0.1 ratio in the case of **BH_3-18**. UV-Vis measurements at a wavelength of 254 nm were used for detection.

Scanning Electron Microscopy: SEM images were collected on a Zeiss LEO 1530 Gemini with a secondary electron detector. To obtain good conductivity, the samples were coated with carbon.

Single-crystal X-ray Diffraction: Single-crystal X-ray crystallography was carried out with a Bruker D8-Quest Photon-100 diffractometer using an Incoatec IμS Cu microsource (Cu-Kα λ = 1.5418 Å), a Nonius Kappa CCD diffractometer (Mo-Kα, λ = 0.71073 Å) or an Oxford Xcalibur S CCD diffractometer (Mo-Kα, λ = 0.71073 Å). For the Bruker machine, data collection and reduction were carried out using the APEX2/APEX3 and SAINT packages,[358] whereas for the Nonius machine the HKL Denzo and Scalepack programs[359] were used. For the Oxford Xcalibur diffractometer data were collected and processed with CrysAlis Pro.[360] Structures were solved by direct methods using SHELXS[361] or SHELXT[362] and refined using full-matrix least squares on F^2 (SHELXL-2014[363] and the graphical interface shelXle[364]) For **2** and **3**, the absolute structures were determined from intensity quotients.[365] Absorption effects were corrected on the basis of multiple equivalent reflections using SADABS[366] or SCALE3 ABSPACK.[367] In general, carbon-bound hydrogen atoms were included in idealised positions and refined using a riding model. Pictures were generated in Diamond.[368] Crystallographic details are given in Chapter 8.7, page 153 and the colour code for the solid state structures is depicted in the beginning of the thesis (page IX). CCDC numbers: 1431706 (**2**), 1431707 (**3**), 1431708 (**5**), 1431709 (**6**·toluene), 1431710 (**7**·2THF), 1431711 (**8**), 1505955 ([**14**·LiCl]$_2$), 1505956 (**22**), 1505957 ([**10**(LiCl)$_3$·2THF]$_2$), 1505958 (**24**·2THF), 1505959 (**21**·MeOH), 1505960 ([**15**·LiCl]$_2$), 1505961 (**23**·3THF), 1505962 (**20**).

8.4 Computational Details

All calculations, except the NBO analyses, were carried out with the ORCA package (version 4.0.0.1) in the gas phase.[369,370] For all ORCA calculations, atom-pairwise dispersion corrections with the Becke-Johnson damping scheme (D3BJ) were utilised.[371,372] Density fitting techniques, also called resolution-of-identity approximation (RI), were used for GGA calculations, whereas the RIJCOSX[373] approximation was used for hybrid and double-hybrid calculations. NBO

analyses[374,375] were computed using Gaussian 09 (Revision D.01).[376] Molecular orbitals were visualised with IboView.[207,208] The given plotting-threshold (X %) of the molecular orbitals denotes the iso-surface that encloses X % of the orbital's electron density. Since various methods, functionals and basis sets, were employed throughout this thesis, in the following paragraphs more detailed information about the DFT studies is given.

8.4.1 Calculations Conducted in Chapter 2

Calculation of Protonation Energies of Tripodal Tris-2-pyridyl-phosphine ligands

Geometry optimisations and frequency analyses, to prove the absence of imaginary frequencies, of the tris-2-pyridyl phosphines **1**–**3** and their protonated counterparts were carried out in the gas phase at the BP86,[136–138] def2-TZVP[139,140] level of theory. From these, the free enthalpies were extracted, and the first protonation energies were calculated. In order to confirm the observed trend, single point calculations on a higher level of theory, employing the PWPB95[185] functional and the def2-QZVP[139,140] basis set, were used to calculate the first protonation energies. The double-hybrid functional was chosen, since it has shown excellent performance in large benchmark studies for a variety of main group and organic chemistry.[377,378] Both methods result in the same trend and therefore the protonation energies from the obtained Gibbs energies were discussed, since entropic effects are included in these calculations. The charge distribution within the ligands was examined employing CHELPG charges (charges from electrostatic potentials using a grid-based method) developed by C. M. Breneman and K. B. Wiberg.[141]

Table 8.2: *Protonation energies of the tris-2-pyridyl-phosphines **1**–**3**.*

Compound	First Free Protonation Enthalpy from Frequency Analysis [kcal·mol^{-1}]	First Protonation Energy from Single Point Calculations [kcal·mol^{-1}]
1	–248.40	–254.17
2	–253.38	–258.46
3	–239.30	–245.62

8.4.2 Calculations Conducted in Chapter 3

Investigation of the Electronic Properties of (Amino)-2-pyridyl-phosphines

To investigate the electronic situation in the (amino)-2-pyridyl-phosphines, geometry optimisations and frequency analysis of the ligands **11**, [**11**·LiCl]$_2$ and **12** were carried out employing the BP86[136–138] functional in conjunction with the def2-TZVP[139,140] basis set. CHELPG charges were calculated on the same level of theory.[141]

Calculations of the Inversion Barriers of 2-Pyridyl-phosphines

Geometry optimisations and frequency analysis to prove the absence of imaginary frequencies of the tetrahedral phosphines **13** and **18** were obtained employing the BP86[136–138] functional in conjunction with the def2-TZVP[139,140] basis set. For the inversion process of the phosphines, relaxed surface scans at the same level of theory were utilised to find approximate transition state geometries. The presence of transition states was confirmed by frequency analyses after optimisation to a saddle point. For the calculation of reliable energies, single point calculations employing the PWPB95[185] functional and the def2-QZVP[139,140] basis were used.

Investigation of the Bonding Situation in the Rhodium Complex 25

In order to investigate the bonding situation in complex **25**, especially the nature of the Rh–Rh bond, a geometry optimisation and frequency analysis were carried out using the BP86[136–138] functional in conjunction with the old-ZORA-def2-TZVP[139,140] basis set and the auxiliary basis sets def2/J (decontracted, for C, H, N, O, P, Cl)[140] and SARC/J[379–382] (for Rh) for Coulomb fitting. This functional was selected since it showed the best agreement with the experimentally obtained CO stretching frequency (Table 8.3, IR, KBr, ν [cm^{-1}] = 1786, CO stretch).

Table 8.3: *Different programmes and functionals for the determination of the CO stretching band in* ***25****.*

Programme and Functional	νCO [cm^{-1}]
Gaussian09, M062X	1941
Gaussian09, B3LYP	1859
Gaussian09, B3P86	1880
ORCA4, M06	1921
ORCA4, BP86	**1786**
ORCA4, TPSS	1794

Investigation of the Bonding Situation in the Nickel Complex 26·MeOH

To determine the NH stretching frequency of **26**·MeOH, geometry optimisation and frequency analysis of the dication $[\{(MeO)_2P(2\text{-py-H})\}_2\{(MeO)_2P(2\text{-py})\}_2Ni]^{2+}$ were carried out on the TPSS,[244] def2-TZVP[139,140] level of theory.

8.4.3 Calculations Conducted in Chapter 4

Investigation of the Donor Strengths

Geometry optimisation of the [Ni(CO)$_3$L] and the Mo complexes **30** and **31** were carried out employing the TPSS[244] functional in conjunction with the def2-TZVP[139,140] basis set. Frequency calculations of the optimised structure at the same level of theory were utilised to prove the absence of imaginary frequencies and to determine the carbonyl stretching frequencies. A relativistic pseudopotential was applied for Mo (def2-ECP).[383] The meta-GGA functional was chosen, since it showed excellent agreement of the symmetric A_1 CO stretch in [Ni(CO)$_3${P(^{t}Bu)$_3$}] with that reported in the literature (ν [cm^{-1}] = 2056, CO stretch, Table 8.4).[261]

Table 8.4: *Different functionals for the determination of the symmetric carbonyl stretching frequency in [Ni(CO)$_3${P(^{t}Bu)$_3$}].*

Functional	νCO [cm^{-1}]
TPSS	**2042**
BP86	2029
revPBE	2018
M06	2157

8.4.4 Calculations Conducted in Chapter 5

Investigation of the Lewis-Acidity of F-12$^+$

The structure of the cation **F-12$^+$** was optimised and a frequency analysis was carried out, employing the BP86[136–138]functional in conjunction with the def2-TZVP[139,140] basis set.

8.5 Synthetic Protocols

8.5.1 Synthesis of Tris-2-pyridyl-phosphine Ligands

Synthesis of P(2-py)$_3$ (1)

Tris-2-pyridyl-phosphine was prepared using a modified procedure from the literature.[74] 2-Bromopyridine (1.90 mL, 20.00 mmol) in 25 mL of diethyl ether was added dropwise over a period of 40 min to an ^{n}BuLi solution (12.50 mL, 20.00 mmol, 1.60 mol·L^{-1} in *n*-hexane) at –78 °C. The dark red mixture was stirred for 3 h. Afterwards PCl_3 (0.58 mL, 6.66 mmol) in 10 mL of diethyl ether was added slowly. The brown mixture was warmed up to room temperature overnight. The pale brown suspension was then extracted with degassed sulfuric acid (2 mol·L^{-1}, 1 x 20 mL, 1 x

10 mL). The aqueous phase was separated from the organic phase and the pH of the aqueous layer was adjusted with degassed aqueous sodium hydroxide solution (pH 8–9). A higher pH value resulted only in the formation of an orange oil and lowered the yield of the reaction significantly. The resulting precipitate was filtered off, washed with *n*-hexane and dried under vacuum. Yield: 0.93 g, 3.50 mmol, 53 %. ^{1}H NMR ($CDCl_3$, 500.20 MHz), δ [ppm] = 8.75 (3H, d, J_{HH} = 4.6 Hz, H6), 7.67–7.62 (3H, m, H4), 7.44 (3H, d, J_{HH} = 7.7 Hz, H3), 7.26–7.22 (3H, m, H5). ^{31}P{^{1}H} NMR ($CDCl_3$, 202.48 MHz), δ [ppm] = –1.0 (s). ^{13}C{^{1}H} NMR ($CDCl_3$, 125.78 MHz), δ [ppm] = 161.6 (d, J_{CP} = 2.7 Hz, C2), 150.3 (d, J_{CP} = 11.9 Hz, C6), 135.9 (d, J_{CP} = 4.1 Hz, C4), 129.3 (d, J_{CP} = 20.1 Hz, C3), 122.8 (s, C5). Elemental analysis, calcd. for $P(2\text{-py})_3$, C 67.92, H 4.56, N 15.84; found C 66.97, H 4.66, N 15.49. ATR-IR, $\tilde{\nu}$ [cm^{-1}] = 1571 (s), 1559 (m), 1450 (s), 1421 (m), 1414 (m), 1277 (m), 1147 (m), 1147 (m), 1085 (w), 1046 (w), 988 (s), 961 (w), 908 (w), 897 (w), 772 (s), 764 (s), 722 (w). M. p.: 108–110 °C.

Synthesis of $P(6\text{-Me-2-py})_3$ (2)

2-Bromo-6-methylpyridine (2.28 mL, 20.00 mmol) was dissolved in 30 mL of diethyl ether. This solution was added dropwise to ^{n}BuLi (12.50 mL, 20.00 mmol, 1.60 mol·L^{-1} in *n*-hexane) at –78 °C. The resulting dark orange solution was stirred for 3 h at –78 °C. PCl_3 (0.58 mL, 6.66 mmol) was added dropwise to the dark red lithiated species. The resulting brown mixture was allowed to warm up to room temperature. After stirring overnight, a pale yellow solution with a light brown precipitate was formed. The mixture was extracted with degassed H_2SO_4 (2.0 mol·L^{-1}, 1 x 20 mL, 1 x 10 mL) and the two phases were separated. Afterwards the pH of the aqueous layer was adjusted to pH 8–9 with degassed aqueous NaOH solution and the product precipitated. The resulting pale brown powder was filtered off, washed with *n*-hexane and dried under vacuum. Yield: 1.34 g, 3.09 mmol, 62 %. Colourless crystals were obtained from layering a saturated toluene solution with *n*-hexane. ^{1}H NMR ($CDCl_3$, 500.20 MHz), δ [ppm] = 7.47 (3H, td, J_{HH} = 2.0 Hz, 7.7 Hz, H4), 7.08–7.02 (6H, m, H3,5), 2.57 (9H, s, CH_3). ^{31}P{^{1}H} NMR ($CDCl_3$, 202.48 MHz), δ [ppm] = –3.2 (s). ^{13}C{^{1}H} NMR ($CDCl_3$, 125.78 MHz), δ [ppm] = 161.5 (d, J_{CP} = 5.1 Hz, C2), 158.7 (d, J_{CP} = 13.7 Hz, C6), 135.7 (d, J_{CP} = 2Hz, C4), 125.7 (d, J_{CP} = 13.9 Hz, C3/5), 122.1 (s, C3/5), 24.6 (s, CH_3). Elemental analysis, calcd. for $P(6\text{-Me-2-py})_3$, C 70.33, H 5.91, N 13.68; found C 70.00, H 5.80, N 12.40. ATR-IR, $\tilde{\nu}$ [cm^{-1}] = 1577 (m), 1558 (m), 1445 (s), 1382 (w), 1371 (w), 1247 (m), 1178 (m), 1141 (m), 1099 (m), 1032 (w), 996 (m), 978 (w), 854 (w), 784 (s), 738 (m). M. p.: 101–103 °C.

Synthesis of $P(6\text{-Br-2-py})_3$ (3)

The ligand was prepared using a modified procedure from the literature.[384] 2,6-Dibromopyridine (4.74 g, 20.00 mmol) was dissolved in 40 mL of diethyl ether and cooled down to –60 °C. To this white slurry a solution of ^{n}BuLi (12.50 mL, 20.00 mmol, 1.60 mol·L^{-1} in *n*-hexane) was added

dropwise. Afterwards the solution was allowed to warm up to –40 °C for 20 min until a clear yellow solution was formed. This mixture was then cooled down to –78 °C and PCl_3 (0.58 mL, 6.66 mmol) in 5 mL of diethyl ether was added dropwise with stirring. The mixture slowly reached room temperature overnight. The precipitate was filtered off and washed with degassed water and *n*-hexane. Afterwards the pale brown precipitate was dried under vacuum. Yield: 1.80 g, 3.60 mmol, 54 %. Colourless crystals were grown from a saturated toluene/THF solution. ^{1}H NMR (CD_3COCD_3, 500.20 MHz), δ [ppm] = 7.81–7.76 (3H, m, H4), 7.64 (3H, d, J_{HH} = 8.0 Hz, H3/5), 7.51–7.47 (3H, m, H3/5). ^{31}P{^{1}H} NMR (CD_3COCD_3, 202.48 MHz), δ [ppm] = –0.9 (s). ^{13}C{^{1}H} NMR was not recorded due to the low solubility of **3**. Elemental analysis, calcd. for P(6-Br-2-py)$_3$, C 35.89, H 1.81, N 8.37; found C 35.16, H 1.93, N 7.93. ATR-IR, $\tilde{\nu}$ [cm^{-1}] = 1558 (m), 1541 (m), 1413 (s), 1375 (m), 1237 (w), 1175 (m), 1133 (w), 1111 (m), 1085 (m), 987 (w), 979 (m), 785 (s), 749 (m), 725 (m). M. p.: 220 °C.

Synthesis of P(6-CN-2-py)$_3$ (4)

P(6-CN-2-py)$_3$ was synthesised according to a literature procedure.[142] P(6-Br-2-py)$_3$ (0.50 g, 1.00 mmol) was added to copper cyanide (0.49 g, 5.00 mmol) in 20 mL of dry pyridine with stirring. The mixture was brought to reflux overnight, turning from yellow to dark red. The dark slurry was then cooled with an ice bath and an aqueous sodium cyanide (1.44 g, 29.00 mmol in 5 mL H_2O) solution was added. The mixture was stirred for another 4 h at this temperature. The brown precipitate was filtered off and washed with water until the washings were colourless. The product was dried under vacuum. Yield: 0.23 g, 0.68 mmol, 70 %. ^{1}H NMR ($CDCl_3$, 500.05 MHz), δ [ppm] = 7.88–7.83 (3H, m, H4), 7.82–7.79 (3H, m, H3), 7.71–7.68 (3H, m, H5). ^{31}P{^{1}H} NMR ($CDCl_3$, 161.98 MHz), δ [ppm] = –1.3 (s). ^{13}C{^{1}H} NMR ($CDCl_3$, 125.74 MHz), δ [ppm] = 162.3 (d, J_{CP} = 2.7 Hz, C2), 136.9 (d, J_{CP} = 4.7 Hz, C4), 134.6 (d, J_{CP} = 11.1 Hz, C6), 132.8 (d, J_{CP} = 23.9 Hz, C3), 128.1 (s, C5), 116.8 (s, CN). Elemental analysis, calcd. for P(6-CN-2-py)$_3$, C 63.53, H 2.67, N 24.70; found C 62.09, H 2.94, N 23.07.

8.5.2 Synthesis of Transition Metal Complexes Tris-2-pyridyl-phosphine Ligands

Synthesis of [{P(2-py)$_3$}$_2$Fe](OTf)$_2$ (5)

Ligand **1** (0.53 g, 2.00 mmol) and Fe(OTf)$_2$ (0.36 g, 1.00 mmol) were dissolved in 30 mL of acetonitrile affording a dark red solution immediately. The mixture was stirred for 16 h and then filtered over Celite. Complete evaporation of the solvent resulted in a red powder. Yield: 0.64 g, 0.74 mmol, 73 %. Through layering of a saturated methanol solution with diethyl ether dark red crystals could be obtained. Crystalline yield: 35 mg, 0.40 mmol, 4 %. ^{1}H NMR (CD_3COCD_3, 500.20 MHz), δ [ppm] = 8.65–8.60 (3H, m, H3), 8.20–8.16 (3H, m, H4), 7.72 (3H, dd, J_{HH} = 0.7 Hz,

5.8 Hz, H6), 7.33–7.29 (3H, m, H5). $^{31}P\{^{1}H\}$ NMR (CD_3COCD_3, 202.48 MHz), δ [ppm] = –9.0 (s). $^{13}C\{^{1}H\}$ NMR (CD_3COCD_3, 100.61 MHz), δ [ppm] = 161.6 (s, C6), 161.5 (s, C2), 137.6 (d, J_{CP} = 15.2 Hz, C4), 133.9 (d, J_{CP} = 52.2 Hz, C3), 126.9 (s, C5). Elemental analysis, calcd. for $[\{P(2\text{-py})_3\}_2Fe](OTf)_2$, C 43.45, H 2.74, N 9.50; found C 41.41, H 2.51, N 8.83. ATR-IR, $\tilde{\nu}$ [cm^{-1}] = 1586 (w), 1456 (m), 1430 (m), 1282 (m), 1255 (s), 1222 (m), 1126 (s), 1091 (m), 1026 (s), 911 (w), 865 (w), 776 (s), 720 (m), 668 (w).

Synthesis of [{P(6-Me-2-py)$_3$}FeCl$_2$]·toluene (6·toluene)

Ligand **2** (0.31 g, 1.00 mmol) and $FeCl_2$ (0.13g, 1.00 mmol) were dissolved in 30 mL toluene. The resulting pale yellow solution was then refluxed for 16 h affording a bright yellow suspension. The mixture was filtered over Celite and some solvent was removed *in vacuo*. Yield: 246 mg, 0.47 mmol, 47 % (on the basis of **6**·toluene). Storage of the filtrate at –14 °C gave pale yellow crystals of **6**·toluene. Crystalline yield: 30 mg, 0.06 mmol, 6 % (on the basis of **6**·toluene). Due to the paramagnetic iron(II) centre NMR data could not be obtained. Satisfactory elemental analysis could not be obtained. ATR-IR, $\tilde{\nu}$ [cm^{-1}] = 1591 (m), 1554 (m), 1495 (w), 1445 (s), 1380 (w), 1262 (w), 1238 (w), 1184 (m), 1133 (m), 1102 (m), 1014 (s), 859 (w), 8.3 (s), 798 (s), 783 (m), 742 (s), 734 (s), 697 (m), 669 (w).

Synthesis of [{P(6-Me-2-py)$_3$}FeCl(OTf)]·2THF (7·2THF)

Compound **2** (0.15 g, 0.50 mmol), iron(II) triflate (0.18 g, 0.50 mmol) and lithium chloride (0.02 g, 0.50 mmol) were dissolved in 25 mL THF. The solution turned yellow and was brought to reflux for a few minutes. The mixture was stirred for 16 h and then filtered through Celite. The solvent was removed completely, and the resulting solid was washed with *n*-hexane. A very air-sensitive yellow/orange powder was obtained after drying under vacuum. Yield: 0.13 g, 0.21 mmol, 38 % (on the basis of **7**·2THF). Yellow crystals could be grown from the THF reaction mixture. Due to the paramagnetic iron(II) centre NMR data could not be obtained. Elemental analysis, calcd. for $[\{P(6\text{-Me-2-py})_3\}FeCl(OTf)]\cdot THF$, C 44.56, H 4.23, N 6.78; found C 44.19, H 4.15, N 6.82. ATR-IR, $\tilde{\nu}$ [cm^{-1}] = 3498 (w, br), 1632 (w), 1596 (m), 1559 (w), 1451 (m), 1312 (m), 1262 (s), 1171 (s), 1100 (w), 1041 (1019 (m), 861 (w), 791 (m), 768 (m), 741 (w).

Synthesis of [(MeCN)$_3$Cu{P(6-Me-2-py)$_3$}Cu(MeCN)](PF$_6$)$_2$ (8)

Ligand **2** (0.30 g, 1.00 mmol) and tetrakis(acetonitrile) copper(I) hexafluorophosphate (0.75 g, 2.00 mmol) gave a yellow solution in 30 mL of acetonitrile. The mixture was stirred for 16 h and then filtered over Celite. The solvent was removed completely, resulting in a yellow precipitate. Yield: 0.60 g, 0.67 mmol, 68 %. Crystals could be obtained from layering a saturated DCM solution with diethyl ether. Crystalline yield: 90 mg, 0.10 mmol, 10 %. ^{1}H NMR (CD_3CN, 400.13 MHz), δ

[ppm] = 8.27–8.17 (3H, m, H3), 7.99–7.92 (3H, m, H4), 7.55 (3H, d, J_{HH} = 7.9 Hz, H5), 2.86 (9H, s, CH_3), 1.99 (MeCN solvent residual signal overlaps with the signal of the coordinated MeCN molecules). $^{31}P\{^1H\}$ NMR (CD_3CN, 202.48 MHz), δ [ppm] = –15.3 (s, br), –244.6 (sep, J_{PF} = 705.6 Hz, PF_6). $^{13}C\{^1H\}$ NMR (CD_3CN, 125.78 MHz), δ [ppm] = 162.7 (d, J_{CP} = 4.9 Hz, C6), 151.7 (d, J_{CP} =33.6 Hz, C2), 139.4 (d, J_{CP} = 15.8 Hz, C4), 133.9 (d, J_{CP} = 48.7 Hz, C3), 128.1 (s, C5), 118.4 (s, CN from MeCN, overlapping with solvent residual signal), 25.9 (s, CH_3), 1.3 (sep, CH_3 from MeCN, overlapping with solvent residual signal). Elemental analysis, calcd. for $[(MeCN)_3Cu\{P(6\text{-}Me\text{-}2\text{-}py)_3\}Cu(MeCN)](PF_6)_2 \cdot 2DCM$, C 31.77, H 3.24, N 9.26; found C 32.32, H 3.39, N 7.39. ATR-IR, $\tilde{\nu}$ [cm^{-1}] = 1591 (w), 1447 (m), 1385 (w), 1260 (w), 1180 (w), 1098 (w), 1037 (w), 1011 (w), 830 (s), 795 (m), 740 (m), 701 (w).

Synthesis of $[\{P(6\text{-}Me\text{-}2\text{-}py)_3\}NiCl]BF_4 \cdot DCM$ (9·DCM)

The iron complex **5** in acetonitrile (stock solution in MeCN, 14 mmol·L^{-1}, V = 2 mL) was added to $[Ni(MeCN)_6](BF_4)_2$ resulting in an orange solution. The mixture was stirred overnight at room temperature and a brown precipitate was obtained after the solvent was removed. A few red crystals could be obtained from layering a saturated DCM solution with *n*-hexane. Compound **9**·DCM could not be characterised by NMR spectroscopy due to its paramagnetic character.

Synthesis of $[\{P(2\text{-}py)_3\}W(CO)_4] \cdot DCM$ (28·DCM) and *cis*-$[W(CO)_4\{P(2\text{-}py)_3\}_2]$ (29)

A mixture of $P(2\text{-}py)_3$ (50 mg, 0.19 mmol) and 5 ml of acetonitrile was treated with $[W(CO)_5(MeCN)]$ (0.30 ml, 0.19 mmol). The reaction mixture was stirred for 6 days at room temperature. The resulting red brown solution was filtered, and the solvent was removed *in vacuo*. Small dark red crystals and colourless crystals (of **28**·DCM and **29**, respectively) were grown from layering a DCM solution with *n*-hexane at –25 °C for 6 days. Compounds **28**·DCM and **29** could not be characterised completely due to their inseparability. $^{31}P\{^1H\}$ NMR ($CDCl_3$, 161.99 MHz), δ [ppm] = 33.5 (s, $^1J_{PW}$ = 118.3 Hz, **29**), –8.2 (s, **28**).

Synthesis of $[Mo(CO)_5\{P(6\text{-}Me\text{-}2\text{-}py)_3\}]$ (30)

Me_3NO (24 mg, 0.33 mmol) and $[Mo(CO)_6]$ (86 mg, 0.33 mmol) were dissolved in 8 ml of acetonitrile and stirred for 30 min at room temperature. **2** (0.10 g, 0.33 mmol) in 3 ml of acetonitrile was added to this resulting bright yellow solution. Stirring for 3 days led to an orange brown suspension. The precipitate was filtered off, resulting in a red brown solution. Crystals could be obtained from the acetonitrile solution at –25 °C. Crystalline yield: 33 mg, 0.61 mmol, 18 %. ^1H NMR (CD_3CN, 400.16 MHz), δ [ppm] = 7.53 (3H, td, J_{HH} = 7.8 Hz, 3.3 Hz, H4), 7.18 (3H, dd, J_{HH} = 7.8 Hz, 2.5 Hz, H5), 6.93 (3H, dd, J_{HH} = 7.8 Hz, 2.5 Hz, H3), 2.46 (9H, s, CH_3). $^{31}P\{^1H\}$ NMR (CD_3CN, 161.99 MHz), δ [ppm] = 45.3 (s). $^{13}C\{^1H\}$ NMR (CD_3CN, 100.63 MHz), δ [ppm]

= 211.8 (d, J_{CP} = 26 Hz, *trans*-CO), 206.3 (d, J_{CP} = 9.2 Hz, *cis*-CO), 159.4 (d, J_{CP} = 17.7 Hz, C2), 157.6 (d, J_{CP} = 59.7 Hz, C6), 136.4 (d, J_{CP} = 5.1 Hz, C4), 124.7 (d, J_{CP} = 15.0 Hz, C3), 123.6 (d, J_{CP} = 1.7 Hz, C5), 23.2 (s, CH_3). Elemental analysis, calcd. for $[Mo(CO)_5\{P(6\text{-Me-2-py})_3\}]$, C 50.84, H 3.34, N 7.73; found C 50.83, H 3.23, N 8.23. ATR-IR, $\tilde{\nu}$ [cm^{-1}] = 3441 (br), 3054 (w), 2926 (w), 2070 (s, CO stretch), 1991 (s, CO stretch), 1931 (br, CO stretch), 1913 (s, CO stretch), 1579 (m), 1559 (m), 1444 (s), 1375 (w), 1248 (w), 1174 (w), 1135 (w), 1092 (w), 1038 (w), 984 (w), 899 (w), 865 (w), 785 (m), 735 (m). MS (ESI, +) m/z: 825.1407, calcd. 825.1406 (0.12 ppm error), $[M+P(6\text{-Me-2-py})_3]^+$.

Synthesis of *cis*-$[Mo(CO)_4\{P(6\text{-Br-2-py})_3\}_2]$ (31·2 *n*-hexane)

A mixture of $[Mo(CO)_6]$ (0.11 g, 0.40 mmol) and Me_3NO (30 mg, 0.40 mmol) in 3 ml of acetonitrile was stirred for 30 min at room temperature. Ligand **3** (0.20 g, 0.40 mmol) in 7 ml of acetonitrile was added to the yellow solution. The resulting brown solution with white precipitate was stirred for 5 days. The precipitate was filtered off and crystals were grown overnight from the saturated MeCN solution. Yield: 64 mg, 0.53 mmol, 13 %. ^{1}H NMR ($CDCl_3$, 400.16 MHz), δ [ppm] = 7.66 (3H, d, J_{HH} = 7.5 Hz, H5), 7.43–7.37 (3H, m, H4), 7.27 (3H, d, J_{HH} = 8.0 Hz, H3). $^{31}P\{^1H\}$ NMR ($CDCl_3$, 161.99 MHz), δ [ppm] = 50.3 (s). $^{13}C\{^1H\}$ NMR ($CDCl_3$, 100.63 MHz), δ [ppm] = 208.2 (s, CO), 160.19 (d, J_{CP} = 51.7 Hz, C2), 141.5 (t, J_{CP} = 7.4 Hz, C6), 137.8 (s, C4), 128.4 (t, J_{CP} = 9.8 Hz, C5), 128.0 (s, C3). Elemental analysis, calcd. for *cis*-$[Mo(CO)_4\{P(6\text{-Br-2-py})_3\}_2]$, C 33.70 H 1.50, N 6.93; found C 33.98, H 1.49, N 7.11. ATR-IR, $\tilde{\nu}$ [cm^{-1}] = 3437 (br), 3082 (w), 2920 (w), 2361 (w), 2029 (s, CO stretch), 1923 (s, CO stretch), 1880 (s, CO stretch), 1544 (s), 1415 (s), 1379(m), 1168 (m), 1112 (s), 1080 (m), 980 (m), 905 (w), 790 (m), 760 (m), 727 (m). MS (ESI, +) m/z: 1236.4835, calcd.1236.4856 (–1.7 ppm error), $[M+Na]^+$.

8.5.3 Synthesis of (Amino)- and (Alkoxy)-2-pyridyl-phosphines

Synthesis of $(Me_2N)P(2\text{-py})_2$ ($[10(LiCl)_3\cdot 2THF]_2$)

2-Bromopyridine (1.53 mL, 2.53 g, 16.00 mmol) in 20 mL of diethyl ether was added dropwise over a period of 30 min to a solution of ^{n}BuLi (10.00 mL, 16.99 mmol, 1.60 mol·L^{-1} in *n*-hexane) at −78 °C. The resulting dark orange solution was stirred for 3 h at −78 °C. To this dark red mixture, $(Me_2N)PCl_2$ (0.92 mL, 1.17 g, 8.00 mmol) in 15 mL of diethyl ether was added. After the addition, the suspension was allowed to warm to room temperature overnight. The formed pale orange solution, containing a brown precipitate, was filtered and the solid was dried *in vacuo*. The solid consists of a mixture of **1** and other P-containing products (86 % product, 14 % side products according to $^{31}P\{^1H\}$ NMR) as well as LiCl (m_{total} = 1.70 g). Layering of a saturated THF solution with *n*-hexane resulted in the crystallisation of $[\{(Me_2N)P(2\text{-py})_2\}(LiCl)_3\cdot 2THF]_2$. ^{1}H NMR

(D_8-THF, 400.13 MHz), δ [ppm] = 8.71–8.67 (2H, m, H6), 7.72–7.65 (4H, m, H3,4), 7.22–7.16 (2H, m, H5), 3.69–3.63 (8H, m, THF, OCH_2), 2.82 (6H, d, J_{PH} = 9.0 Hz, CH_3), 1.85–1.78 (8H, m, THF, CH_2). $^{31}P\{^1H\}$ NMR (D_8-THF, 161.98 MHz), δ [ppm] = 60.1 (s). $^{7}Li\{^1H\}$ NMR (D_8-THF, 155.51 MHz), δ [ppm] = 0.35 (s). $^{13}C\{^1H\}$ NMR (D_8-THF, 100.61 MHz), δ [ppm] = 165.7 (d, J_{CP} = 1.9 Hz, C2), 150.3 (d, J_{CP} = 10.4 Hz, C6), 135.5 (d, J_{CP} = 2.1 Hz, C3/4), 126.5 (d, J_{CP} = 17.7 Hz, C3/4), 122.3 (s, C5), 68.0 (s, THF, OCH_2), 43.0 (d, J_{CP} = 14.5 Hz, CH_3), 26.2 (s, THF, CH_2). Elemental analysis, calcd. for $[\{(Me_2N)P(2\text{-py})_2\}(LiCl)_3\cdot 2THF]_2$, C 47.75, H 6.02, N 8.36; found C 46.83, H 6.09, N 7.88.

Synthesis of $(Et_2N)P(2\text{-py})_2$ ([11·$(LiCl)_2$)

2-Bromopyridine (1.90 mL, 3.16 g, 20.00 mmol) was dissolved in 30 mL of diethyl ether. This solution was added dropwise to a solution of ^{n}BuLi (12.50 ml, 20.00 mmol, 1.60 mol·L^{-1} in *n*-hexane) at –78 °C. The resulting dark orange solution was stirred for 3 h at –78 °C. $(Et_2N)PCl_2$ (1.46 mL, 1.74 g, 10 mmol) was added dropwise to the lithiated species. The resulting brown mixture was allowed to warm to room temperature. After stirring overnight, a pale orange solution with a brown precipitate was formed. The solution was filtered and the solid dried *in vacuo* to yield [**11**·LiCl]$_2$, other P-containing products and LiCl (m_{total} = 2.31 g) as a light brown powder. The powder could be purified by crystallisation from THF/*n*-hexane in very small yields. ^1H NMR (CD_3COCD_3, 400.13 MHz), δ [ppm] = 8.71 (2H, d, J_{HH} = 4.7 Hz, H2), 7.79–7.74 (2H, m H4), 7.63 (2H, dd, J_{HH} = 1.0 Hz, 7.8 Hz, H5), 7.29–7.26 (2H, m, H3), 3.24–3.16 (4H, m, CH_2), 1.08 (6H, t, J_{HH} = 7.1 Hz, CH_3). $^{31}P\{^1H\}$ NMR (CD_3COCD_3, 161.98 MHz), δ [ppm] = 58.2 (s). $^{13}C\{^1H\}$ NMR ($CDCl_3$, 100.63 MHz), δ [ppm] = 165.0 (s, C_q), 150.0 (d, J_{CP} = 12.1 Hz, C2), 135.4 (d, J_{CP} = 2.0 Hz, C4), 126.8 (d, J_{CP} = 18.2 Hz, C5), 122.1 (s, C3), 45.0 (d, J_{CP} = 14.1 Hz, CH_2), 14.5 (d, J_{CP} = 3.0 Hz, CH_3).

Synthesis of $(Et_2N)_2P(2\text{-py})$ (12)

2-Bromopyridine (1.90 mL, 20.00 mmol) in 25 mL of diethyl ether was added dropwise over a period of 30 min to a solution of ^{n}BuLi (12.50 mL, 20.00 mmol, 1.6 mol·L^{-1} in *n*-hexane) at –78 °C. The resulting dark orange solution was stirred for 2 h at –78 °C. $(Et_2N)_2PCl$ (4.20 mL, 20.00 mmol) was added dropwise, resulting in a dark brown mixture. After stirring overnight (over which time the reaction reached rt), a dark solution with a precipitate was formed. This solution was then filtered to remove the solid. The solvent was removed *in vacuo* and fractional distillation of the resulting dark brown oil under reduced pressure (b. p. 82 °C, 0.1 mbar) gave a yellow oil. Yield: 2.87 g, 11.30 mmol, 57 %. ^1H NMR ($CDCl_3$, 400.13 MHz), δ [ppm] = 8.70–8.68 (1H, m, H6), 7.61–7.56 (1H, m, H4), 7.56–7.51 (1H, m, H3), 7.06–7.02 (1H, m, H5), 3.16–3.07 (8H, m, CH_2), 1.14 (12H, t, J_{HH} = 7.1 Hz, CH_3). $^{31}P\{^1H\}$ NMR ($CDCl_3$, 161.98 MHz), δ [ppm] = 93.9 (s). $^{13}C\{^1H\}$

NMR ($CDCl_3$, 100.63 MHz), δ [ppm] = 165.9 (d, J_{CP} = 16.3 Hz, C2), 150.1 (d, J_{CP} = 7.6 Hz, C6), 135.0 (s, C4), 126.5 (d, J_{CP} = 22.3 Hz, C3), 121.1 (s, C5), 43.5 (d, J_{CP} = 16.3 Hz, CH_2), 14.5 (d, J_{CP} = 2.3, CH_3). Elemental analysis, calcd. for $(Et_2N)_2P(2\text{-py})$, C 61.64, H 9.55, N 16.59; found C 61.67, H 9.82, N 16.11. HR-MS (ESI, +) m/z: 254.1772, calcd. 254.1781 (–3.5 ppm error), $[M]^+$.

Synthesis of $Ph(Et_2N)P(2\text{-py})$ (13)

2-Bromopyridine (1.90 mL, 20.00 mmol) in 25 mL of diethyl ether was added dropwise over a period of 40 min to an ^{n}BuLi solution (12.50 mL, 2.000 mmol, 1.60 mol·L^{-1} in *n*-hexane) at –78 °C. The dark red mixture was stirred for 3 h and then $(Et_2N)PhPCl$ (4.31g, 20.00 mmol) in 5 mL of diethyl ether was added dropwise. The resulting dark brown mixture was warmed to room temperature overnight, resulting in an orange solution with a pale brown precipitate. The solvent was removed, and 10 mL of DCM was added. After the mixture was filtered over degassed silica, the solvent was removed, affording a crimson oil (m = 2.84 g). The dark red oil was distilled twice under reduced pressure to afford **13** as a yellow oil. Yield: 1.73 g, 4.10 mmol, 33 %. ^{1}H NMR ($CDCl_3$, 500.20 MHz), δ [ppm] = 8.71 (1H, d, J_{HH} = 4.7 Hz, H6), 7.67–7.62 (1H, m, H4), 7.54–7.51 (1H, m, H3), 7.45–7.41 (2H, m, Ph-H-*ortho*), 7.37–7.29 (3H, m, Ph-H-*meta/para*), 7.18–7.14 (1H, m, H5), 3.21–3.08 (4H, m, CH_2), 0.99 (6H, t, J_{HH} = 7.1 Hz, CH_3). $^{31}P\{^1H\}$ NMR ($CDCl_3$, 161.98 MHz), δ [ppm] = 59.7 (s). $^{13}C\{^1H\}$ NMR ($CDCl_3$, 125.78 MHz), δ [ppm] = 165.8 (d, J_{CP} = 16.3 Hz, C2), 149.9 (d, J_{CP} = 11.0 Hz, C6), 139.3 (d, J_{CP} =13.8 Hz, Ph-C_q), 135.2 (d, J_{CP} = 2.2 Hz, C4), 132.3 (d, J_{CP} = 20.1 Hz, Ph-C-*ortho*), 128.3 (s, Ph-C-*meta/para*), 128.0 (d, J_{CP} = 6.2 Hz, Ph-C-*meta/para*), 126.4 (d, J_{CP} = 18.1 Hz, C3), 121.7 (s, C5), 44.6 (d, J_{CP} = 15.4 Hz, CH_2), 14.4 (d, J_{CP} = 3.0 Hz, CH_3). Elemental analysis, calcd. for $(Et_2N)PhP(2\text{-py})$, C 69.73, H 7.42, N 10.85; found C 70.27, H 7.49, N 10.87. MS (ESI, +) m/z: 259.1362, calcd. 259.1359 (1.16 ppm error), $[M]^+$.

Synthesis of $(BH_3)P(NEt_2)Ph(2\text{-py})$ (BH_3-13)

1.73 g (6.70 mmol) of the phosphine $(Et_2N)PhP(2\text{-py})$ (**13**) were dissolved in 30 mL diethyl ether and 1.15 equivalents of borane dimethylsulfide (3.85 mL, 7.70 mmol, 2.00 mol·L^{-1} in THF) were added. The mixture was stirred for 45 min and degassed water was added to quench the additional borane dimethylsulfide. The borane-protected phosphine was then extracted with ethyl acetate and purified by column chromatography (*n*-hexane/diethyl ether; 5 : 1, v/v, R_f = 0.61). **BH_3-13** was obtained as colourless oil. Yield: 1.71 g, 6.28 mmol, 94 %. ^{1}H NMR ($CDCl_3$, 400.16 MHz), δ [ppm] = 8.76 (1H, d, J_{HH} = 4.7 Hz, H6), 8.17–7.89 (1H, m, H3), 7.82–7.75 (1H, m, H4), 7.57–7.49 (2H, m, Ph-H), 7.49–7.34 (4H, m, Ph-H, H5), 3.28 (4H, dq, J_{HH} = 10.6 Hz, 7.1 Hz, CH_2), 1.41–0.56 (br, BH_3), 0.97 (6H, t, J_{HH} = 7.1 Hz, CH_3).$^{31}P\{^1H\}$ NMR ($CDCl_3$, 161.99 MHz), δ [ppm] = 65.7–63.6 (m). $^{11}B\{^1H\}$ NMR ($CDCl_3$, 128.38 MHz), δ [ppm] = –37.6 (d, J_{BP} = 68.5 Hz). $^{13}C\{^1H\}$ NMR ($CDCl_3$, 100.63 MHz), δ [ppm] = 157.0 (d, J_{CP} = 77.9 Hz, C2), 150.0 (d, J_{CP} = 13.1 Hz, C6), 136.0

(d, J_{CP} = 9.5 Hz, C4), 132.0 (d, J_{CP} = 10.2 Hz, Ph-C), 131.3 (s, Ph-C_q), 130.8 (s, Ph-C), 128.9 (d, J_{CP} = 26.3 Hz, C3), 128.3 (d, J_{CP} = 10.4 Hz, C5), 124.7 (s, Ph-C), 41.2 (s, CH_2), 13.9 (s, CH_3). Elemental analysis, calcd. for $BH_3P(NEt_2)(Ph)(2\text{-py})$, C 66.20, H 8.15, N 10.29; found: C 66.41, H 8.07, N 10.14. MS (EI) m/z: 272.2 $[M]^+$.

Synthesis of (MeO)P(2-py)$_2$ ([14·LiCl]$_2$)

The crude precipitate of $(Me_2N)P(2\text{-py})_2$·LiCl + LiCl (1.00 g, 3.18 mmol) was stirred in MeOH (40 mL) overnight, resulting in a clear orange solution. After the solvent was removed *in vacuo*, the product was obtained as a brown oil, which could be crystallised as $[\{(MeO)P(2\text{-py})_2\}LiCl]_2$ from a THF solution at –14 °C. Crystalline yield: 0.22 g, 0.84 mmol, 27 %. ^{1}H NMR ($CDCl_3$, 400.13 MHz), δ [ppm] = 8.78 (2H, d, J_{HH} = 4.8 Hz, H6), 7.68–7.64 (4H, m, H3,4), 7.23–7.18 (2H, m, H5), 3.89 (3H, d, J_{PH} = 13.5 Hz, CH_3). $^{31}P\{^1H\}$ NMR ($CDCl_3$, 161.98 MHz), δ = 99.5 (s). $^7Li\{^1H\}$ NMR ($CDCl_3$, 155.51 MHz), δ [ppm] = 2.33 (s). $^{13}C\{^1H\}$ NMR ($CDCl_3$, 100.61 MHz), δ [ppm] = 164.3 (d, J_{CP} = 8.3 Hz, C2), 150.6 (d, J_{CP} = 10.4 Hz, C6), 136.1 (d, J_{CP} = 4.1 Hz, C4), 125.0 (d, J_{CP} = 21.1 Hz, C3), 123.4 (s, C5), 58.2 (d, J_{CP} = 21.2 Hz, CH_3). Elemental analysis, calcd. for $[\{(MeO)P(2\text{-py})_2\}LiCl]_2$·LiCl, C 43.56, H 3.66, N 9.24; found C 44.72, H 3.87, N 9.87.

Synthesis of (2-BuO)P(2-py)$_2$ ([15·LiCl]$_2$)

The crude compound $(Me_2N)P(2\text{-py})_2$·LiCl + LiCl (1,36 g, 4.30 mmol) and 2 equivalents of racemic 2-butanol (0.79 mL, 8.70 mol) were heated overnight at 90 °C in 15 mL of toluene. The mixture was filtered over Celite and the solvent was removed, resulting in 0.79 g of a brown oil with a purity of 80 % according to $^{31}P\{^1H\}$ NMR spectroscopy. Colourless single-crystals of $[\{(2\text{-BuO})P(2\text{-py})_2\}LiCl]_2$ could be obtained from layering a saturated THF solution with *n*-hexane. Crystalline yield: 70 mg, 0.23 mmol, 5 %. ^{1}H NMR ($CDCl_3$, 400.13 MHz), δ [ppm] = 8.83 (2H, d, J_{HH} = 5.0 Hz, H6), 7.76–7.67 (4H, m, H3,4), 7.25–7.20 (2H, m, H5), 4.24–4.14 (1H, m, OCH), 1.93–1.81 (1H, m, CH_2), 1.78–1.65 (1H, m, CH_2), 1.41 (3H, d, J_{HH} = 6.4 Hz, $OCHCH_3$), 0.98 (3H, t, J_{HH} = 7.5 Hz, CH_2CH_3). $^{31}P\{^1H\}$ NMR ($CDCl_3$, 161.98 MHz), δ [ppm] = 88.1 (s). $^7Li\{^1H\}$ NMR ($CDCl_3$, 155.51 MHz), δ [ppm] = 2.51 (s). $^{13}C\{^1H\}$ NMR ($CDCl_3$, 100.61 MHz), δ [ppm] = 164.9 (d (br), J_{CP} = 35.8 Hz, C2), 150.8 (d, J_{CP} = 10.1 Hz, C6), 136.5 (d, J_{CP} = 4.0 Hz, C3/4), 124.9–124.5 (m, C3/4), 123.4 (d, J_{CP} = 2.5 Hz, C5), 80.9 (d, J_{CP} = 20.8 Hz, OCH), 31.1 (d, J_{CP} = 5.6 Hz, CH_2), 21.8 (d, J_{CP} = 5.6 Hz, $OCHCH_3$), 10.1 (s, CH_2CH_3). Elemental analysis, calcd. for $[\{(2\text{-BuO})P(2\text{-py})_2\}LiCl]_2$, C 55.56, H 5.66, N 9.26; found C 55.80, H 5.83, N 9.03.

Synthesis of (*S*)-(2-BuO)P(2-py)$_2$ ([15-*S*·LiCl]$_2$)

Crystals of $[\{(Me_2N)P(2\text{-py})_2\}(LiCl)_3\cdot 2THF]_2$ (17mg, 0.034 mmol) were reacted with (*S*)-(+)-2-butanol (6.3 µL, 0.068 mmol) in 0.6 mL of D_8-toluene in a Young NMR tube. The mixture

was heated overnight at 85 °C. The phosphine **5**-*S* was obtained in 91 % yield according to $^{31}P\{^{1}H\}$ NMR spectroscopy. ^{1}H NMR (D_8-tol, 400.13 MHz), δ [ppm] = 8.66–8.57 (2H, m, H6), 7.69–7.63 (2H, m, H3), 7.10–7.04 (2H, m, H4), 6.63–6.56 (2H, m, H5), 4.11–4.01 (1H, m, OCH), 1.79–1.69 (1H, m, CH_2), 1.59–1.52 (1H, m, CH_2), 1.28 (3H, d, J_{HH} = 6.3 Hz, $OCHCH_3$), 0.88 (3H, t, J_{HH} = 3.7 Hz, CH_2CH_3). $^{31}P\{^{1}H\}$ NMR (D_8-tol, 161.98 MHz), δ [ppm] = 93.1 (s).

Synthesis of (*R*)-(2-BuO)P(2-py)$_2$ ([15-*R*·LiCl]$_2$)

Crystals of $[\{(Me_2N)P(2\text{-}py)_2\}(LiCl)_3\cdot 2THF]_2$ (15mg, 0.030 mmol) were reacted with enantiomerically pure (*R*)-(–)-2-butanol (5.5 µL, 0.060 mmol) in 0.6 mL of D_8-toluene in a Young NMR tube. The mixture was heated overnight at 85 °C. The enantiomerically pure phosphine **5**-*R* was obtained in 94 % yield according to $^{31}P\{^{1}H\}$ NMR spectroscopy. ^{1}H NMR (D_8-tol, 400.13 MHz), δ [ppm] = 8.66–8.61 (2H, m, H6), 7.69–7.63 (2H, m, H3), 7.10–7.04 (2H, m, H4), 6.63–6.56 (2H, m, H5), 4.11–4.01 (1H, m, OCH), 1.82–1.68 (1H, m, CH_2), 1.58–1.50 (1H, m, CH_2), 1.28 (3H, d, J_{HH} = 6.3 Hz, $OCHCH_3$), 0.88 (3H, t, J_{HH} = 7.4 Hz, CH_2CH_3). $^{31}P\{^{1}H\}$ NMR (D_8-tol, 161.98 MHz), δ [ppm] = 92.8 (s).

Synthesis of (MeO)$_2$P(2-py) (17)

A mixture of **12** (0.67 g, 2.63 mmol) and 30 mL MeOH was heated overnight at 50 °C. The mixture was dried under vacuum, resulting in a clear pale yellow oil. Yield: 0.35 g, 2.05 mmol, 73 %. ^{1}H NMR ($CDCl_3$, 400.13 MHz), δ [ppm] = 8.81–8.78 (1H, m, H6), 7.77–7.69 (2H, m, H3,4), 7.28–7.23 (1H, m, H5), 3.65 (6H, d, J_{PH} = 10.6 Hz, CH_3). $^{31}P\{^{1}H\}$ NMR ($CDCl_3$, 161.98 MHz), δ [ppm] = 150.1 (s). $^{13}C\{^{1}H\}$ NMR ($CDCl_3$, 100.62 MHz), δ [ppm] = 163.7 (d, J_{CP} = 6.0 Hz, C2), 150.3 (d, J_{CP} = 11.4 Hz, C6), 135.6 (s, C4), 125.1 (d, J_{CP} = 15.9 Hz, C3), 123.9 (s, C5), 53.8 (d, J_{CP} = 9.2 Hz, CH_3). Elemental analysis, calcd. for $(MeO)_2P(2\text{-py})$, C 49.13, H 5.89, N 8.18; found C 49.59, H 6.04, N 8.44. HR-MS (ESI, +) m/z: 172.0518, calcd. 172.0522 (–2.32 ppm error), $[M]^+$.

Synthesis of (Et$_2$N)(PhO)P(2-py) (18)

12 (0.86 g, 3.40 mmol) and PhOH (0.32 g, 3.40 mmol) were brought to reflux in toluene (20 mL) overnight. After the solvent was removed *in vacuo* the product was obtained as a yellow oil. Yield: 0.81 g, 2.93 mmol, 86 %. ^{1}H NMR ($CDCl_3$, 400.13 MHz), δ [ppm] = 8.81–8.79 (1H, m, H6), 7.96–7.92 (1H, m, H3), 7.76 (1H, tt, J_{HH} = 7.6 Hz, 2.0, H4), 7.36–7.30 (2H, m, Ph-H-*meta*), 7.28–7.25 (1H, m, H5), 7.17 - 7.13 (m, 2H, Ph-H-*ortho*), 7.09–7.04 (1H, m, Ph-H-*para*), 3.22–3.05 (4H, m, CH_2), 1.00 (6H, t, J_{HH} = 7.3 Hz, CH_3). $^{31}P\{^{1}H\}$ NMR ($CDCl_3$, 161.98 MHz), δ [ppm] = 120.2 (s). $^{13}C\{^{1}H\}$ NMR ($CDCl_3$, 100.61 MHz), δ [ppm] = 164.7 (d, J_{CP} = 11.6 Hz, C2), 156.7 (d, J_{CP} = 8.3 Hz, Ph-C_q), 150.2 (d, J_{CP} = 13.2 Hz, C6), 135.9 (s, C4), 129.6 (s, Ph-C-*meta*), 126.1 (d, J_{CP} = 14.7 Hz, C3), 123.2 (s, C5), 122.4 (d, J_{CP} = 1.6 Hz, Ph-C-*para*), 119.9 (d, J_{CP} = 9.4 Hz, Ph-C-*ortho*),

43.2 (s, CH_2), 15.0 (d, J_{CP} = 3.8 Hz, CH_3). Elemental analysis, calcd. for $(Et_2N)(PhO)P(2\text{-py})$, C 65.68, H 7.98, N 10.21; found C 65.30, H 7.16, N 10.05. HR-MS (ESI, +) m/z: 275.1310, calcd. 275.1308 (0.73 ppm error), $[M]^+$.

Synthesis of $(BH_3)P(NEt_2)(OPh)(2\text{-py})$ (BH_3-18)

The (amino)(alkoxy)-2-pyridyl-phosphine **18** (0.69 g, 2.53 mmol) was reacted with 1.15 equivalents of borane dimethylsulphide (1.46 mL, 2.91 mmol, 2mol·L^{-1} in THF) in 15 mL THF. The mixture was stirred for two hours, and degassed water was then added to quench the excess $BH_3{\cdot}SMe_2$. The borane-protected phosphine was extracted with ethyl acetate and purified by column chromatography (*n*-hexane/ethyl acetate; 4 : 1, v/v, R_f = 0.42). **BH_3-18** was obtained as a pure oil. Yield: 0.57 g, 1.98 mmol, 78 %, over two steps. ^{1}H NMR ($CDCl_3$, 400.16 MHz), δ [ppm] = 8.85 (1H, d, J_{HH} = 4.7 Hz, H6), 8.07–8-00 (1H, m, H3), 7.87–7.78 (1H, m, H4), 7.43–7.37 (1H, m, H5), 7.37–7.31 (2H, m, Ph-H-*meta*), 7.26–7.21 (2H, m, Ph-H-*ortho*), 7.20–7.14 (1H, m, H Ph-H-*para*), 3.38–3.23 (2H, m, CH_2), 3.23–3.09 (2H, m, CH_2), 1.38 – 0.30 (br, BH_3), 0.95 (6H, t, J_{HH} = 7.1 Hz, CH_3). $^{31}P\{^1H\}$ NMR ($CDCl_3$, 161.99 MHz), δ [ppm] = 109.6–106.6 (m). $^{11}B\{^1H\}$ NMR ($CDCl_3$, 128.38 MHz), δ [ppm] = –39.5 (d, J_{BP} = 72.2 Hz). $^{13}C\{^1H\}$ NMR ($CDCl_3$, 100.63 MHz), δ [ppm] = 155.8 (d, J_{CP} = 118.0 Hz, C2), 151.8 (d, J_{CP} = 5.7 Hz, Ph-C_q), 150.4 (d, J_{CP} = 18.1 Hz, C6), 136.2 (d, J_{CP} = 8.2 Hz, C4), 129.3 (s, Ph-C-*para*), 127.7 (d, J_{CP} = 21.8 Hz, C3), 125.1 (s, C5), 124.7 (s, Ph-C-*para*), 121.7 (d, J_{CP} = 3.8 Hz, Ph-C-*ortho*), 40.2 (s, CH_2), 13.8 (s, CH_3). Elemental analysis, calcd. for $BH_3P(NEt_2)(OPh)(2\text{-py})$, C 62.53, H 7.70, N 9.72; found: C 63.00, H 7.68, N, 9.53. MS (EI) m/z: 288.2 $[M]^+$.

Synthesis of $(PhO)_2P(2\text{-py})$ (19)

A mixture of **12** (0.84 g, 3.30 mmol) and two equivalents of PhOH (0.62 g, 6.61 mmol) was brought to reflux for 41 h in toluene (18 mL). After which the solvent was removed *in vacuo* the resulting pale yellow oil was purified by vacuum distillation and then heated at 100 °C (to remove the excess PhOH) for 2 h to afford **19** in 96 % purity (according to $^{31}P\{^1H\}$ NMR spectroscopy). Yield: 0.43 g, 1.46 mmol, 44 %. ^{1}H NMR (CD_3CN, 400.13 MHz), δ [ppm] = 8.88 (1H, d, J_{HH} = 4.7 Hz, H6), 7.98–7.94 (1H, m, H3), 7.86 (1H, tt, J_{HH} = 7.7 Hz, 16, H4), 7.47–7.42 (1H, m, H5), 7.37–7.31 (4H, m, Ph-H-*meta*), 7.17–7.12 (4H, m, Ph-H-*ortho/para*). $^{31}P\{^1H\}$ NMR (CD_3CN, 161.98 MHz), δ [ppm] = 142.8 (s). $^{13}C\{^1H\}$ NMR (CD_3CN, 100.63 MHz), δ [ppm] = 162.5 (d, J_{CP} = 5.0 Hz, C2), 155.0 (d, J_{CP} = 4.2 Hz, Ph-C_q), 150.1 (d, J_{CP} = 15.8 Hz, C6), 136.3 (s, C4), 129.7 (s, Ph-*meta*), 125.0 (s, C5), 124.6 (d, J_{CP} = 12.9 Hz, C3), 124.0 (d, J_{CP} = 1.1 Hz, Ph-C-*ortho/para*), 120.1 (d, J_{CP} = 7.6 Hz, Ph-C-*ortho/para*). Elemental analysis, calcd. for $(PhO)_2P(2\text{-py})$, C 69.15, H 4.78, N 4.74; found C 69.57, H 4.95, N 4.52. HR-MS (ESI, +) m/z: 296.0842, calcd. 296.0835 (2.36 ppm error), $[M]^+$.

8.5.4 Synthesis of Transition Metal Complexes of (Amino)- and (Alkoxy)-2-pyridylphosphines

Synthesis of [(MeCN)Cu{(Et$_2$N)$_2$P(2-py)}]$_2$(PF$_6$)$_2$ (20)

12 (0.01g, 0.4 mmol) and [Cu(MeCN)$_4$]PF$_6$ (0.15g, 0.40 mmol) were reacted in MeCN (20 mL). The bright yellow mixture was stirred overnight, and the solvent was removed completely under vacuum. Colourless crystals of the complex could be grown from layering a saturated DCM solution with *n*-hexane. Crystalline yield: 74 mg, 0.074 mmol, 19 %. ^{1}H NMR (CD$_3$COCD$_3$, 400.14 MHz), δ [ppm] = 8.75 (1H, s (br), py-H), 8.10–7.31 (3H, m, py-H), 3.25–2.88 (8H, m, CH$_2$), 1.99 (3H, s, MeCN), 1.13 (12H, t, J_{HH} = 6.7 Hz, CH$_3$). ^{31}P{^{1}H} NMR (CD$_3$COCD$_3$, 161.98 MHz), δ [ppm] = 84.0 (s, br), –144.6 (sep, J_{PF} = 707.1 Hz, PF$_6$). ^{13}C{^{1}H} NMR spectrum could not be obtained due to extensive line broadening. Elemental analysis, calcd. for [(MeCN)Cu{(Et$_2$N)$_2$P(2-py)}]$_2$(PF$_6$)$_2$, C 35.81, H 5.41, N 11.14; found C 35.06, H 5.25, N 10.63.

Synthesis of [ClCu{(MeO)P(2-py)$_2$}]$_2$·MeOH (21·MeOH)

91 mg [{(MeO)P(2-py)$_2$}LiCl]$_2$ ([**14**·LiCl]$_2$) (0.35 mmol) and [Cu(MeCN)$_4$]PF$_6$ (0.13 g, 0.35 mmol) were brought to reflux in 15 mL of THF. After the solvent was removed, MeOH was added and the mixture was filtered over Celite. A few colourless crystals of **11**·MeOH could be grown from a saturated MeOH solution at –14 °C.

Synthesis of [(MeCN)Cu{(Et$_2$N)(PhO)P(2-py)}]$_2$(PF$_6$)$_2$ (22)

18 (0.25 g, 0.90 mmol) and [Cu(MeCN)$_4$]PF$_6$ (0.34 g, 0.90 mmol) in MeCN (15 mL) were brought to reflux for 2 h. The yellow solution was filtered over Celite, and the solvent was removed under reduced pressure, resulting in a yellow oil. Colourless crystals could be obtained from a saturated DCM solution at –14 °C after two days. Crystalline yield: 50 mg, 0.048 mmol, 5 %. ^{1}H NMR (CD$_3$CN, 400.14 MHz), δ [ppm] = 8.77–8.73 (1H, m, H6), 8.01–7.94 (1H, m, H3), 7.94–7.86 (1H, m, H4), 7.47–7.42 (1H, m, H5), 7.42–7.36 (2H, m, Ph-H), 7.20–7.13 (3H, m, Ph-H), 3.22–3.07 (4H, m, CH$_2$), 1.96 (MeCN solvent residual signal partially overlaps with the signal of the coordinated MeCN molecules), 0.98 (6H, t, J_{HH} = 7.1 Hz, CH$_3$). ^{31}P{^{1}H} NMR (CD$_3$CN, 161.98 MHz), δ [ppm] = 107.8 (s, br), –144.6 (sep, J_{PF} = 705.9 Hz, PF$_6$). ^{13}C{^{1}H} NMR (CD$_3$CN, 100.61 MHz), δ [ppm] = 160.3 (d, J_{CP} = 76.5 Hz, C2), 155.4 (s, Ph-C$_q$), 151.3 (d, J_{CP} = 17.3 Hz, C6), 137.5 (s, C4), 130.5 (s, Ph-C), 126.6 (d, J_{CP} = 18.0 Hz, C3), 125.5 (s, C5), 124.9 (s, Ph-C), 121.9 (d, J_{CP} = 6.2 Hz, Ph-C), 118.2 (s, MeCN), 42.8 (d, J_{CP} = 11.0 Hz, CH$_2$), 14.7 (s, CH$_3$), 0.76 (s, MeCN). Elemental analysis, calcd. for [(MeCN)Cu{(Et$_2$N)(PhO)P(2-py)}]$_2$(PF$_6$)$_2$, C 38.98, H 4.23, N 8.03; found C 38.70, H 4.29, N 7.98.

Synthesis of [(MeCN)Cu$_2${(PhO)$_2$P(2-py)}$_3$](PF$_6$)$_2$·3THF (23·3THF)

(PhO)$_2$P(2-py) (**19**, 0.103 g, 0.035 mmol) and [Cu(MeCN)$_4$]PF$_6$ (87 mg, 0.023 mmol) in MeCN (10 mL) were brought to reflux overnight. The solvent was removed under reduced pressure, resulting in an orange oil, which was washed with *n*-hexane. Yield: 0.10 g, 0.074 mmol, 64 %. A few colourless crystals could be grown from layering a saturated THF solution with diethyl ether. ^{1}H NMR (CD$_3$CN, 400.13 MHz), δ [ppm] = 8.73 (3H, s (br), H6), 7.95–7.84 (6H, m, H3,4), 7.50 (3H, s (br), H5), 7.39–7.30 (12H, m, Ph-H), 7.24–7.10 (18H, m, Ph-H), 1.99 (MeCN solvent residual signal partially overlaps with the signal of the coordinated MeCN molecules). ^{31}P{^{1}H} NMR (CD$_3$CN, 161.98 MHz), δ [ppm] = 120.7 (s, br), –144.6 (sep, J_{PF} = 705.6 Hz, PF$_6$). ^{13}C{^{1}H} NMR (CD$_3$CN, 100.63 MHz), δ [ppm] = 154.04 (s, Ph-C$_q$), 151.4 (d, J_{CP} = 18.9 Hz, C6), 137.9 (s, C3/4), 130.8 (s, Ph-C), 127.2 (s (br),C5), 127.1 (s (br), C3/4), 126.2 (s, Ph-C), 121.9 (d, J_{CP} = 5.2 Hz, Ph-C), 117.3 (MeCN), 1.32 (MeCN). Correct elemental analysis could not be obtained due to the presence of free PhOH as a contaminant.

Synthesis of [{OP(O)(H)(2-py)}Cu$_2${(PhO)$_2$P(2-py)}$_2$]$_2$(PF$_6$)$_2$ ·2THF (24·2THF)

The reaction of 0.12 g of (PhO)$_2$P(2-py) (**19**, 0.41 mmol) and [Cu(MeCN)$_4$]PF$_6$ (0.10 g, 0.28 mmol) in 12 mL MeCN was stirred overnight at room temperature, resulting in a pale yellow solution. After the solvent was removed, colourless crystals of **24**·2THF could be grown from a saturated THF solution at –14 °C. Crystalline yield: 48 mg, 4 %. In the following NMR assignment the ligand **19** will be referred to as **L1**, whereas [OP(O)(H)(2-py)]$^-$ will be denoted as **L2**. ^{1}H NMR (CD$_3$CN, 400.13 MHz), δ [ppm] = 8.84 (1H, d, J_{HH} = 4.7 Hz, py-H, L2), 8.81 (2H, d, J_{HH} = 4.2 Hz, py-H, L1), 8.02–7.89 (6H, m, py-H, L1, L2), 7.77 (1H, d, J_{PH} = 597.2 Hz, PH, L2), 7.65–7.60 (1H, m, py-H, L2), 7.56–7.51 (2H, m, L1), 7.43–7.35 (8H, m, Ph-H, L1), 7.20–7.17 (12H, m, Ph-H, L1). ^{31}P{^{1}H} NMR (CD$_3$CN, 161.98 MHz), δ [ppm] = 119.8 (s, br, L1), 21.6 (s, L2), –144.6 (sep, J_{PF} = 706.5 Hz, PF$_6$). ^{31}P NMR (CD$_3$CN, 161.98 MHz), δ [ppm] = 119.8 (s, br, L1), 21.6 (d, J_{PH} = 597.2 Hz, PH, L2), –144.6 (sep, J_{PF} = 706.5 Hz, PF$_6$). ^{13}C{^{1}H} NMR spectrum could not be obtained due to extensive line broadening. Elemental analysis, calcd. for [{OP(O)(H)(2-py)}Cu$_2${(PhO)$_2$P(2-py)}$_2$]$_2$(PF$_6$)$_2$·2THF, C 46.23, H 4.08, N 4.15; found C 46.47, H 3.71, N 4.10.

Synthesis of [Rh$_2$Cl$_2$(μ-CO){(Et$_2$N)$_2$P(2-py)}$_2$] (25)

Bis(diethylamino)-2-pyridyl-phosphine (**12**) (0.15 g, 0.60 mmol) in 4 mL DCM was added to [RhCl(CO)$_2$]$_2$ (0.12 g, 0.30 mmol) in 4 mL DCM. The mixture immediately turned brown, and gas formation could be observed. After stirring overnight, the brown solution was layered with *n*-hexane, affording brown crystals. Crystalline yield: 97 mg, 0.12 mmol, 40 %. ^{1}H NMR (CDCl$_3$, 400.16 MHz), δ [ppm] = 9.37 (2H, s, br, H6), 7.80–7.64 (2H, m, H3,4), 7.38 (1H, t, J_{HH} = 6.2 Hz,

H5), 3.70–3.52 (8H, m, CH_2), 3.21–3.00 (8H, m, CH_2), 1.29 (12H, t, J_{HH} = 7.1 Hz, CH_3), 0.96 (12H, t, J_{HH} = 7.1 Hz, CH_3). $^{31}P\{^1H\}$ NMR ($CDCl_3$, 161.99 MHz), δ [ppm] = 113.9–112.2 (m). $^{13}C\{^1H\}$ NMR ($CDCl_3$, 100.63 MHz), δ [ppm] = 230.6–229.2 (m, CO), 163.7 (d, J_{CP} =78.4 Hz, C2), 153.5–153.3 (m, C6), 136.2 (s, C3/4), 125.6 (s, C5), 124.4–124.2 (m, C3/4), 40.6 (m, CH_2), 13.5 (d, J_{CP} =84.0 Hz, CH_3). Elemental analysis, calcd. for $[Rh_2Cl_2(\mu\text{-}CO)\{(Et_2N)_2P(2\text{-}py)\}_2]$, C 39.97, H 5.96, N 10.36; found C 40.00, H 5.96, N 10.36. IR (KBr), $\tilde{\nu}$ [cm^{-1}] = 3547 (m), 3068 (m), 2966 (s), 2875 (s), 1786 (s, CO stretch), 1745 (m), 1583 (s), 1454 (s), 1378 (s), 1342 (m), 1286 (m), 1241 (w), 1178 (s). MS (ESI, +) m/z: 775.1156, calcd. 775.1158 (–0.26 ppm error), [M–Cl^+].

Synthesis of $[\{(MeO)_2P(2\text{-}py\text{-}H)\}_2\{(MeO)_2P(2\text{-}py)\}_2Ni](BF_4)_2\cdot MeOH$ (26·MeOH)

$(MeO)_2P(2\text{-}py)$ (**17**) (0.16 g, 0.95 mmol) in 3 mL acetonitrile was added to $[Ni(MeCN)_6](BF_4)_2$ (76 mg, 0.16 mmol) in 3 mL acetonitrile. The mixture turned brown/red immediately and was stirred overnight. Then the solvent was removed *in vacuo*, and the nickel complex **26**·2MeOH was crystallised from a saturated methanol solution at –20 °C. Crystalline yield: 55 mg, 0.058 mmol, 37 %. ^1H NMR (CD_3CN, 400.16 MHz), δ [ppm] = 8.88 (1H, d, J_{HH} = 5.3 Hz, H6), 8.31 (1H, t, J_{HH} = 7.9 Hz, H4), 8.03 (1H, t, J_{HH} = 7.9 Hz, H3), 7.83–7.77 (1H, m, H5), 3.06 (6H, s, br, CH_3), N–H cannot be unambiguously assigned. $^{31}P\{^1H\}$ NMR (CD_3CN, 161.99 MHz), δ [ppm] = 154.5 (s). $^{11}B\{^1H\}$ NMR (CD_3CN, 128.38 MHz), δ [ppm] = –1.2 (s). $^{19}F\{^1H\}$ NMR (CD_3CN, 376.50 MHz), δ [ppm] = –151.9 (s). $^{13}C\{^1H\}$ NMR (CD_3CN, 100.63 MHz), δ [ppm] = 159.5 (s, C2), 145.2 (s, C6), 142.3 (s, C4), 127.2 (s, C3), 125.9 (s, C5), 52.0 (s, CH_3). ATR-IR, $\tilde{\nu}$ [cm^{-1}] = 3427 (br, m), 2946 (w), 2839 (w), 2039 (br, w), 1641 (w), 1602 (m), 1493 (w), 1472 (w), 1443 (m), 1058 (s), 1034 (s), 1001 (s), 764 (s). Elemental analysis, calcd. for $[\{(MeO)_2P(2\text{-}py\text{-}H)\}_2\{(MeO)_2P(2\text{-}py)\}_2Ni](BF_4)_2$, C 36.67, H 4.61, N 6.10; found C 36.12, H 4.24, N 6.18. HR-MS (ESI, –) m/z: 1005.1412, calcd. 1005.1400 (1.2 ppm error), $[M+BF_4]^-$.

8.5.5 Synthesis of Bridgehead-modified 2-Pyridyl-phosphines

Synthesis of $O{=}P(6\text{-}Me\text{-}2\text{-}py)_3$ (O=2)

$P(6\text{-}Me\text{-}2\text{-}py)_3$ (0.10 g, 0.33 mmol) and *N*-fluorobenzenesulfonimide (0.10 g, 0.33 mmol) were reacted in 10 mL of THF. Subsequently, 0.1 mL of water was added. The mixture was filtered, and the solvent was removed *in vacuo*. Layering of a saturated DCM solution with *n*-hexane resulted in the formation of colourless crystals. Crystalline yield: 30 mg, 0.09 mmol, 29 %. ^1H NMR ($CDCl_3$, 500.20 MHz), δ [ppm] = 8.04–7.99 (3H, m, H3/5), 7.81–7.74 (3H, m, H4), 7.38–7.34 (3H, m, H3/5), 2.67 (9H, s, CH_3). $^{31}P\{^1H\}$ NMR ($CDCl_3$, 202.49 MHz), δ [ppm] = 11.8 (s). $^{13}C\{^1H\}$ NMR ($CDCl_3$, 125.78 MHz), δ [ppm] = 159.1 (s, br, C2), 141.9 (s, C6), 136.8 (d, J_{CP} = 9.9 Hz, C4), 131.6 (s, C3/5), 127.0 (s, C3/5), 24.2 (s, CH_3). Satisfactory elemental analysis could not be obtained.

Synthesis of S=P(6-Br-2-py)$_3$ (S=3)

P(6-Br-2-py)$_3$ (0.54 g, 1.10 mmol) was brought to reflux overnight with 3 equivalents of sulphur (0.10 g, 3.30 mmol) in 20 mL of toluene. The pale yellow mixture was filtered over Celite and the solvent was removed *in vacuo*, resulting in a pale yellow powder. Colourless crystals were obtained from layering a DCM solution with *n*-hexane. Crystalline yield: 0.24 g, 0.45 mmol, 42 %. ^{1}H NMR ($CDCl_3$, 500.20 MHz), δ [ppm] = 8.21 (1H, t, J_{HH} = 6.6 Hz, H3), 7.74–7.67 (1H, m, H4), 7.61–7.57 (1H, m, H5). ^{31}P{^{1}H} NMR ($CDCl_3$, 202.48 MHz), δ [ppm] = 33.3 (s). ^{13}C{^{1}H} NMR ($CDCl_3$, 125.78 MHz), δ [ppm] = 155.7 (d, J_{CP} =114.1 Hz, C2), 142.2 (d, J_{CP} = 21.0 Hz, C6), 138.3 (d, J_{CP} =10.3 Hz, C4), 130.2 (d, J_{CP} =2.6 Hz, C5), 128.0 (d, J_{CP} = 23.5 Hz, C3). Elemental analysis, calcd. for S=P(6-Br-2-py)$_3$, C 33.74, H 1.70, N 7.87; found C 33.76, H 1.80, N 8.14.

Synthesis of Se=P(6-Br-2-py)$_3$ (Se=3)

P(6-Br-2-py)$_3$ (0.10 g, 0.20 mmol) was brought to reflux overnight with 1.3 equivalents of grey selenium powder (0.02 g, 0.26 mmol) in 15 mL of toluene. The black mixture was then filtered over Celite, resulting in a pale yellow clear solution. The solvent was removed under reduced pressure, giving a yellow precipitate. Yield: 75 mg, 0.13 mmol, 65 %. Yellow crystals could be grown from layering a saturated DCM solution with *n*-hexane. ^{1}H NMR ($CDCl_3$, 400.13 MHz), δ [ppm] = 8.27–8.22 (1H, m, H3), 7.74–7.67 (1H, m, H4), 7.60–7.56 (1H, m, H5). ^{31}P{^{1}H} NMR ($CDCl_3$, 161.98 MHz), δ [ppm] = 27.7 (s, J_{PSe} = 771.5 Hz). ^{13}C{^{1}H} NMR ($CDCl_3$, 100.61 MHz), δ [ppm] = 154.6 (d, J_{CP} =105.0 Hz, C2), 142.1 (d, J_{CP} = 20.5 Hz, C6), 138.4 (d, J_{CP} = 10.6 Hz, C4), 130.2 (d, J_{CP} = 2.7 Hz, C5), 128.6 (d, J_{CP} = 24.5 Hz, C3). Elemental analysis, calcd. for Se=P(6-Br-2-py)$_3$, C 31.01, H 1.56, N 7.23; found C 31.83, H 1.31, N 7.00.

Synthesis of Se=P(NEt$_2$)$_2$(2-py) (Se=12)

(Et$_2$N)$_2$P(2-py) (0.31 g, 1.20 mmol) and grey selenium powder (0.13g, 1.60 mmol) were brought to reflux overnight in toluene (15 mL). The yellow mixture was filtered over Celite to remove the excess selenium and the solvent was removed under reduced pressure, resulting in a yellow oil. Yield: 90 mg, 0.27 mmol, 22 %. ^{1}H NMR ($CDCl_3$, 400.13 MHz), δ [ppm] = 8.70–8.68 (1H, m, H6), 8.61 (1H, tt, J_{HH} = 8.0 Hz, 1.0 Hz, H4), 7.84 - 7.76 (1H, m, H3), 7.34–7.30 (1H, m, H5), 3.34–3.10 (8H, m, CH_2), 1.06 (12H, t, J_{HH} = 7.2 Hz, CH_3). ^{31}P{^{1}H} NMR (CDCl3, 161.98 MHz), δ [ppm] = 71.6 (s, J_{PSe} = 760.0 Hz). ^{13}C{^{1}H} NMR ($CDCl_3$, 100.61 MHz), δ [ppm] = 158.6 (d, J_{CP} =138.0 Hz, C2), 148.7 (d, J_{CP} = 17.9 Hz, C6), 136.0 (d, J_{CP} = 12.3 Hz, C3), 129.5 (d, J_{CP} = 30.7 Hz, C4), 124.4 (d, J_{CP} = 3.4 Hz, C5), 39.7 (d, J_{CP} = 4.6 Hz, CH_2), 13.2 (d, J_{CP} = 3.7 Hz, CH_3). Elemental analysis, calcd. for Se=P(NEt$_2$)$_2$(2-py), C 46.97, H 7.28, N 12.65; found C 47.36, H 7.38, N 12.11.

Synthesis of $F_2P(NEt_2)(2\text{-py})$ (F_2-12)

Bis(diethylamino)-2-pyridyl-phosphine (**12**) (0.74 g, 2.91 mmol) in 5 mL of DCM was added slowly to XeF_2 (0.49 g, 2.91 mmol) in 5mL of DCM at –78 °C. The mixture was stirred at this temperature for 10 min and then for 30 min at room temperature before the solvent was removed under reduced pressure. The compound was washed with *n*-hexane and **F_2-12** was then obtained as a pale yellow oil. Yield: 0.60 g, 2.06 mmol, 71 %. ^{1}H NMR ($CDCl_3$, 400.13 MHz), δ [ppm] = 8.68 (1H, d, J_{HH} = 4.8 Hz, H6), 7.72–7.64 (1H, m, H3), 7.57–7.51 (1H, m, H4), 7.26–7.19 (1H, m, H5), 3.21–3.09 (8H, m, CH_2), 1.17 (12H, t, J_{HH}= 6.9 Hz, CH_3). ^{31}P{^{1}H} NMR ($CDCl_3$, 161.98 MHz), δ [ppm] = –61.6 (t, J_{PF} = 730.0 Hz). ^{19}F{^{1}H} NMR ($CDCl_3$, 99.74 MHz), δ [ppm] = –52.3 (d, J_{PF} = 730.0 Hz). ^{13}C{^{1}H} NMR ($CDCl_3$, 100.61 MHz), δ [ppm] = 163.4 (dt, J_{CP} = 301.4 Hz, J_{CF} = 51.6 Hz, C2), 149.0 (d, J_{CP} =19.6 Hz, C6), 135.3 (d, J_{CP} = 15 Hz, C4), 123.7 (dt, J_{CP} = 31.7 Hz, J_{CF} = 4.2 Hz, C3), 122.9 (d, J_{CP} = 4.7 Hz, C5), 44.2–43.9 (m, CH_2), 15.7 (s, CH_3). Elemental analysis, calcd. for $F_2P(NEt_2)(2\text{-py})$, C 53.58, H 8.31, N 14.43; found C 53.57, H 8.48, N, 14.95.

Synthesis of $[(Et_2N)PF(2\text{-py})][N(SO_2Ph)_2]$ (F-12-NSI)

N-Fluorobenzenesulfonimide (0.12g, 0.40 mmol) in 5mL of THF was added to **12** (98 mg, 0.40 mmol) in 5 mL of THF. The mixture was stirred for 10 min before the solvent was removed under reduced pressure, resulting in a colourless oil. Yield: 0.20 g, 0.35 mmol, 90 %. ^{1}H NMR ($CDCl_3$, 400.13 MHz), δ [ppm] = 8.76 (1H, d, J_{HH} = 4.6 Hz, H6), 8.16–8.11 (1H, m, H3), 8.09–8.03 (1H, m, H4), 7.72 (4H, t, J_{HH} = 7.3 Hz, Ph-H-*ortho*), 7.69–7.63 (1H, m, H5), 7.19 (2H, t, J_{HH} = 7.3 Hz, Ph-H-*para*), 7.12 (4H, t, J_{HH} = 7.3 Hz, Ph-H-*meta*), 3.19 - 3.08 (8H, m, CH_2), 1.06 (12H, t, J_{HH} = 7.2 Hz, CH_3). ^{31}P{^{1}H} NMR ($CDCl_3$, 161.98 MHz), δ [ppm] = 44.5 (d, J_{PF} = 1050.1 Hz). ^{19}F{^{1}H} NMR ($CDCl_3$, 99.74 MHz), δ [ppm] = –91.0 (d, J_{PF} = 1050.1 Hz). ^{13}C{^{1}H} NMR ($CDCl_3$, 100.61 MHz), δ [ppm] = 152.0 (dd, J_{CP} =25.8 Hz, J_{CF} = 3.1 Hz, C6), 142.4 (dd, J_{CP} = 213.0 Hz, J_{CF} = 31.3 Hz, C2), 138.9 (d, J_{CP} = 13.0 Hz, C4), 130.9 (d, J_{CP} = 27.9 Hz, C3), 129.9 (s, C5), 129.9 (s, Ph-C-*para*), 129.6 (s, Ph-C_q) 127.6 (s, Ph-C-*meta*), 126.6 (Ph-C-*ortho*), 41.4 (d, J_{CP} = 4.2 Hz, CH_2), 13.6, s, CH_3). Elemental analysis, calcd. for $[(Et_2N)PF(2\text{-py})][N(SO_2Ph)_2]$, C 52.80, H 6.03, N 9.86; found C 50.47, H 6.05, N 9.20.

8.5.6 Synthesis of Iron and Copper Complexes of Bridgehead-modified 2-Pyridyl-phosphines

Synthesis of $[Fe(OTf)_2\{O{=}P(NEt_2)_2(2\text{-py})\}_2]$ (32)

$Fe(OTf)_2$ (83 mg, 0.24 mmol) in 5 mL of THF was added to $[FP(NEt_2)(2\text{-py})][N(SO_2Ph)_2]$ (0.13 g, 0.47 mmol) in 5 mL of THF. The solution turned yellow-orange and was stirred overnight. The saturated THF solution was exposed to air overnight then layered with *n*-hexane, and after 2 days a

few orange crystals could be grown. Due to the paramagnetic iron (II) centre, NMR spectroscopic data could not be obtained. Sufficient elemental analysis could not be obtained.

Synthesis of $[Cu(THF)_2\{O=P(NEt_2)_2(2\text{-}py)\}_2](PF_6)_2$ (33)

85 mg (0.34 mmol) of $(Et_2N)_2P(2\text{-}py)$ (**12**) in 2 mL DCM were added to NFSI (0.11 g, 0.34 mmol) in 1 mL DCM. The mixture was stirred for one hour, after which the solvent was removed under reduced pressure. $[Cu(MeCN)_4]PF_6$ in 3 mL THF was added to the resulting oil. The yellow solution was stirred overnight and then left open to air over 2 days. From this solution, blue crystals were isolated. Crystalline yield: 26 mg, 0.06 mmol, 17 %. Compound **33** could not be characterised by NMR spectroscopy due to its paramagnetic character. Elemental analysis, calcd. for $[Cu(THF)\{O=P(NEt_2)_2(2\text{-}py)\}_2](PF_6)_2$, C 37.35, H 5.86, N 8.72; found C 37.34, H 5.51, N 8.54.

Synthesis of $[Cu\{Se=P(NEt_2)_2(2\text{-}py)\}_2]PF_6$ (34)

$Se=P(NEt_2)_2(2\text{-}py)$ (73 mg, 0.22 mmol) in 5 mL MeCN was added to $[Cu(MeCN)_4]PF_6$ (41 mg, 0.11 mmol) in 5 mL acetonitrile. The bright yellow solution was stirred overnight. A saturated DCM solution was layered with diethyl ether, resulting in the formation of yellow crystals. Crystalline Yield: 49 mg, 0.05 mmol, 51 %. ^{1}H NMR (CD_3CN, 500.20 MHz), δ [ppm] = 8.59 (1H, d, J_{HH} = 4.6 Hz, H6), 8.10–8.05 (1H, m, H3), 8.04–8.00 (1H, m, H4), 7.70–7.63 (1H, m, H5), 3.35–3.24 (4H, m, CH_2), 3.18–3.07 (4H, m, CH_2), 1.06 (12H, t, J_{HH} = 7.12, CH_3). $^{31}P\{^1H\}$ NMR (CD_3CN, 202.48 MHz), δ [ppm] = 77.1 (s, J_{PSe} = 692.1 Hz), –144.6 (sep, J_{PF} = 706.5 Hz, PF_6). $^{13}C\{^1H\}$ NMR (CD_3CN, 125.78 MHz), δ [ppm] = 152.3 (d, J_{CP} = 150.1 Hz, C2), 151.1 (d, J_{CP} = 19.7 Hz, C6), 137.7 (d, J_{CP} = 7.5 Hz, C3), 127.4 (d, J_{CP} = 3.0 Hz, C5), 126.3 (d, J_{CP} = 18.8 Hz, C4), 39.4 (d, J_{CP} = 4.2 Hz, CH_2), 12.1 (d, J_{CP} = 3.1 Hz, CH_3). Elemental analysis, calcd. for $[Cu\{Se=P(NEt_2)_2(2\text{-}py)\}_2]PF_6$, C 35.75, H 5.54, N 9.63; found C 35.67, H 5.50, N 9.48.

8.6 Homogeneous Catalysis

8.6.1 Hydrogenation Reactions

Catalytic hydrogenation reactions were carried out using the liquid phase reactor system SPR16 Generation2, developed by Amtec GmbH. The autoclaves (volume ≈ 20 mL) of the reactor system were equipped with Teflon insets and Teflon stir bars. For the reactions, stock solutions of compound **6** in toluene and **7** in THF (c = 0.0233 mol·L^{-1}) were prepared. Styrene was used as the substrate of choice and *n*-decane as the internal standard (c = 0.7 mol·L^{-1} in toluene). 0.5 mL of the styrene/*n*-decane solution, 1.5 mL of a solution of the iron complexes (10 mol% with respect to the substrate), and eventually 0.07 mL of $NaHBEt_3$ (c = 1 mol·L^{-1} in toluene, 20 mol% with respect to the substrate) were injected into the Teflon-lined autoclaves, which were purged with argon for two

minutes beforehand. Hydrogen gas was introduced, stirring (1500 rpm) and heating in some cases was initiated. After 18 h the pressure was released, and conversions were determined by GC-MS analyses with respect to the internal standard *n*-decane. All reactions were run as duplicates and the conversions are obtained from average values. Products were identified with comparison to authentic samples, analysed by NMR spectroscopy.

GC-MS Analysis: t_R = 4.9 min (ethylbenzene), t_R = 6.0 min (styrene), t_R = 8.3 min (*n*-decane), temperature programme: 50 °C, 5 min / 10 °C·min^{-1} / 90°C, 1 min.

8.6.2 Hydrosilylation Reactions

Catalytic hydrosilylation reactions were carried out in Schlenk flasks with Teflon stir bars under air- and moisture-free conditions. For the reactions, stock solutions of compound **6** in toluene and **7** in THF (c = 0.0233 mol·L^{-1}) were prepared. Styrene was used as the substrate and *n*-decane as the internal standard (c = 0.7 mol·L^{-1} in toluene). The catalyst stock solutions (5 mol% with respect to the substrate) were added to a solution of styrene and *n*-decane in toluene (c = 0.7 mol·L^{-1}). The reducing agents $NaHBEt_3$ (c = 1 mol·L^{-1} in toluene, 10 mol% with respect to the substrate) or EtMgBr (c = 3 mol·L^{-1} in diethyl ether, 10 mol% with respect to the substrate) and phenylsilane (one equivalent with respect to the substrate) were added to this mixture. In the case of $LiAlH_4$, the reducing agent (10 mol% with respect to the substrate) was added first to the Schlenk flask, which was then evacuated to remove any air from the system. The reaction mixtures were stirred at room temperature, 60 °C (THF reactions) or 100 °C (toluene reactions) and samples were taken periodically for GC-MS measurements. Conversions were determined by GC-MS analyses with respect to the internal standard *n*-decane. Products were identified with comparison to authentic samples, analysed by NMR spectroscopy.

GC-MS Analysis: t_R = 4.9 min (ethylbenzene), t_R = 6.00 min (styrene), t_R = 9.2 min (*n*-decane), t_R = 23.0 min (Markovnikov product), temperature programme: 50 °C, 5 min / 5 °C·min^{-1} / 100 °C, 1 min / 10 °C·min^{-1} / 190 °C, 2 min.

8.7 Crystallographic Data

8.7.1 Additional Information about the Refinements

P(6-Me-2-py)$_3$ (2) and P(6-Br-2-py)$_3$ (3): The structures of **2** and **3** are very similar. However, **2** appears to adopt a superstructure with a unit-cell volume four times that of **3**. While **3** contains only ⅓ of a molecule in the asymmetric unit, **2** contains 1+⅓. The structure of **2** contains local translations that amount to C-centring (½,½,0) in the reported R-centred cell. If these translations

are considered to be real, the structure can be described with a subcell essentially identical to **3**. However, reconstructed precession images show clearly that the additional diffraction peaks are present, and that the supercell is appropriate (Table 8.5). For **3**, there is no sign of any additional diffraction peaks to indicate a larger cell. Thus, we conclude that the supercell structure for **2** is genuine, at least for the crystal examined. Refining **2** in the smaller cell analogous to **3** does produce a satisfactory refinement, but with somewhat elongated displacement ellipsoids, especially for the methyl group (of which there is only one unique in that representation) (Figure 8.3).

Table 8.5: *Reconstructed precession images for **2**, showing the consistency between the diffraction pattern and the reported supercell description indicated by the predicted reflection positions (green circles). No such additional spots appear in the diffraction pattern of **3**.*

1*kl*	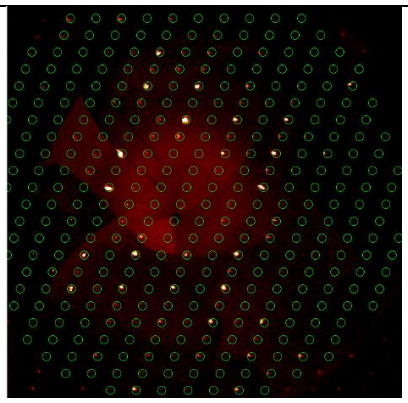	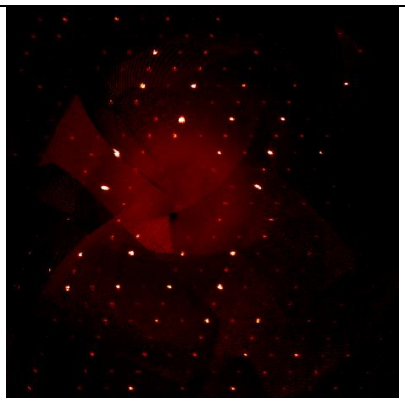
*h*0*l*	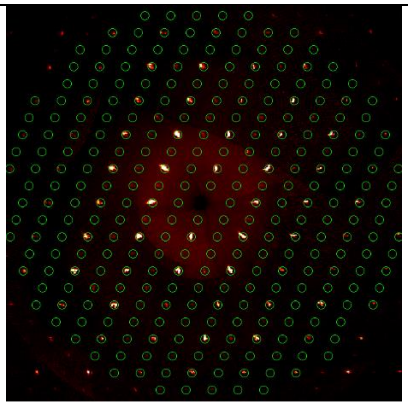	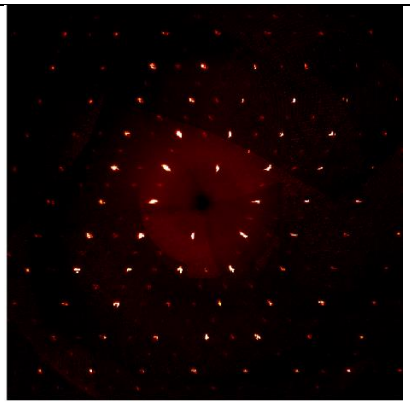
*h*1*l*	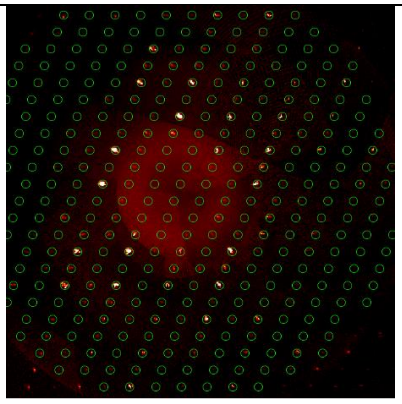	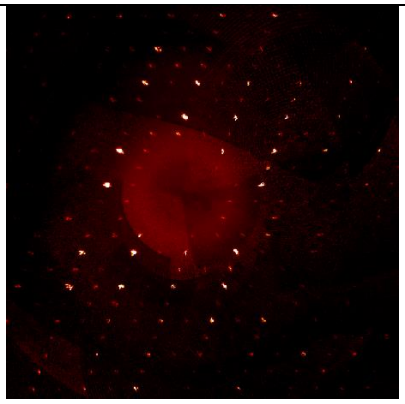

*hk*0	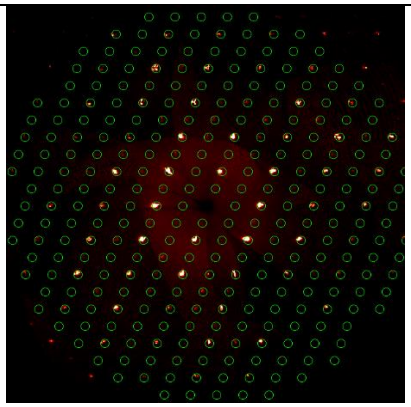	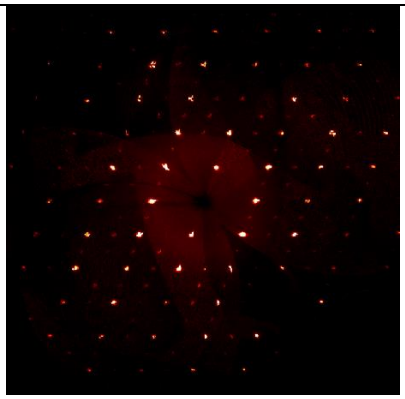
*hk*1	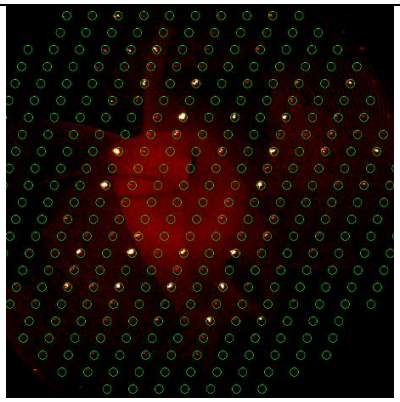	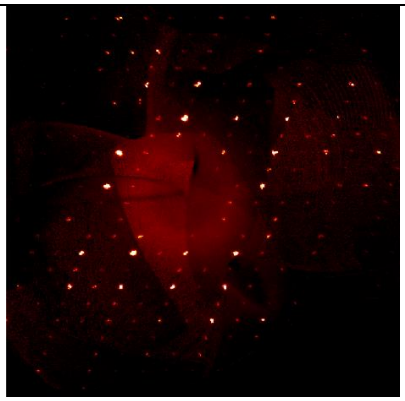

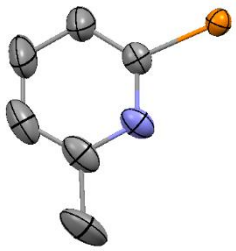

Figure 8.3: *Displacement ellipsoid plot for the asymmetric unit of **2** in the subcell analogous to **3**.*

$Et_2NP(2\text{-}py_2)$ $([11{\cdot}LiCl]_2)$: The crystal was non-merohedrally twinned, and the structure was solved and refined using the programmes APEX2,[358] Cell Now, Twinabs and shelxle.[364] The diffraction pattern was indexed on the basis of two orientation matrices related by the twin law (0 1 1) [-2 4 3]. The twin scale factor (BASF) refined to 0.41796. Both domains were integrated simultaneously, and data based on both domains were used for the refinement.

$(2\text{-}BuO)P(2\text{-}py)_2$ $([15{\cdot}LiCl]_2)$: The 2-butoxide groups were modelled in two orientations, with the terminal C atoms in the two orientations (C2/C4) constrained to lie at the same position. To control the geometry, the bond distances and 1,3-distances were restrained to standard values. All of the (non-H) atoms were refined anisotropically, but with the application of ISOR restraints.

[(MeCN)Cu$_2${(PhO)$_2$P(2-py)}$_3$](PF$_6$)$_2$·3THF (23·3THF): One PF_6^- anion was modelled as disordered over two orientations with a common P atom position. The other PF_6^- anion did not seem to exhibit the same degree of rotational disorder and was modelled with a single orientation. All P–F distances in both anions were restrained to a common refined value. A reasonable octahedral geometry was maintained without restraints on the F...F distances. All F atoms were refined anisotropically with the application of ISOR restraints. Three solvent THF molecules are present, one of which is disordered about an inversion centre. All of the bond distances were restrained to standard values, and all of the non-H atoms were refined anisotropically with ISOR restraints. For one THF site, a superimposed diethyl ether molecule was clearly visible and included with all bond distances and 1,3-distances restrained to standard values. All atoms were refined anisotropically with ISOR restraints.

[{OP(O)(H)(2-py)}Cu$_2${(PhO)$_2$P(2-py)}$_2$]$_2$(PF$_6$)$_2$·2THF (24·2THF): One PF_6^- anion was modelled as disordered over two orientations with a common P atom position. All P–F distances were restrained to a common refined value, but restraints on F...F distances were not applied. All F atoms were refined anisotropically with the application of ISOR restraints. Two solvent THF molecules are present. All of the bond distances were restrained to standard values, and all of the non-H atoms were refined anisotropically with ISOR restraints.

[{(MeO)$_2$P(2-py-H)}$_2${(MeO)$_2$P(2-py)}$_2$Ni](BF$_4$)$_2$·MeOH (26·MeOH): One of the methoxide groups was modelled as disordered over two positions and the MeOH solvent molecule was modelled over two orientations. Hydrogen atoms, beside the hydrogens attached to the pyridyl nitrogen atoms (H31 and H32) were calculated on idealised positions. The hydrogen atoms H31 and H32 (attached to N1 and N3) were detected as significant residual electron density maxima and were refined with only restrained distance:

		x	y	z	sof	U	Peak	Distances to nearest atoms (including eq.)	
Q4	1	1.0825	-0.0008	0.2482	1.00000	0.05	0.92	0.84	N3
Q9	1	0.7447	0.5293	0.2555	1.00000	0.05	0.65	0.93	N1

Exchanging the scattering factors of the *ortho*-atoms within the pyridyl rings (nitrogen and carbon) leads to significant drop of the R values and generates several errors with CheckCif.

***cis*-[Mo(CO)$_4${P(6-Br-2-py)$_3$}$_2$]·2 *n*-hexane (31·2 *n*-hexane)**

The unit cell contains two heavily disordered *n*-hexane molecules, which have been treated as a diffuse contribution to the overall scattering without specific atom positions by squeeze/Platon.[385,386] The solvent accessible void was found to be in the position (–0.004, 0.000,

0.500) with a volume of 332.3 $Å^3$ and 103.2 electrons. The calculated number of electrons matches the electron count of two *n*-hexane molecules. A disordered N-C-Br unit within one ligand was refined over two positions. All of the non-H atoms were refined anisotropically, but with the application of ISOR restraints in the case of the disordered pyridyl moiety.

$[Cu(THF)_2\{O=P(NEt_2)_2(2\text{-}py)\}_2](PF_6)_2$ (33): The ethyl groups were modelled in two orientations, with the terminal C atoms in the two orientations constrained to lie at the same position. The THF molecule was modelled over two positions. All of the (non-H) atoms were refined anisotropically, but with the application of SIMU and DELU restraints.

8.7.2 Overview of Crystallographic Data

Table 8.6: *Single-crystal X-ray crystallographic data of* ***2***, ***3***, ***O=2***, ***S=3*** *and* ***Se=3****.*

Compound reference	**2**	**3**	**O=2**	**S=3**	**Se=3**
CCDC number	1431706	1431707			
Chemical formula	$C_{18}H_{18}N_3P$	$C_{15}H_9Br_3N_3P$	$C_{18}H_{18}N_3PO$	$C_{15}H_9N_3PSBr_3$	$C_{15}H_9N_3PSeBr_3$
Formula mass	307.32	501.95	323.32	534.01	580.91
Crystal system	trigonal	trigonal	monoclinic	monoclinic	monoclinic
a/Å	30.7488(8)	15.7876(6)	13.3242(7)	19.2901(5)	19.4971(9)
b/Å	30.7488(8)	15.7876(6)	8.6350(4)	8.6439(2)	8.6792(4)
c/Å	11.8199(4)	11.1637(5)	14.4440(8)	21.5148(7)	21.473(1)
α/°	90	90	90	90	90
β/°	90	90	95.383(2)	92.400(1)	91.667(2)
γ/°	120	120	90	90	90
Unit cell volume/Å^3	9678.3(6)	2409.7(2)	1654.5(2)	3584.3(2)	3632.0(3)
Temperature/K	180	180	180	180	180
Space group	*R*3*c*	*R*3*c*	$P2_1/n$	*C*2/*c*	*C*2/*c*
Z	24	6	4	8	8
Radiation type	CuKα	CuKα	CuKα	MoKα	CuKα
Absorption coefficient, μ/mm^{-1}	1.495	10.247	1.531	6.959	11.377
No. of reflections measured	35814	7384	21939	11829	54428
No. of independent reflections	3769	941	2911	4026	3224
R_{int}	0.036	0.062	0.0347	0.0521	0.1118
Final R1 values (I > 2σ(I))	0.028	0.033	0.0339	0.0450	0.0480
Final wR(F^2) values (I > 2σ(I))	0.072	0.061	0.1123	0.0813	0.1372
Final R1 values (all data)	0.031	0.039	0.0389	0.0753	0.0497
Final wR(F^2) values (all data)	0.074	0.062	0.1175	0.0918	0.1391
Goodness of fit on F^2	1.05	1.09	0.959	1.051	1.127
Flack x [(I+)-(I-)]/[(I+)+(I-)]	0.03(1)	–0.01(3)			

Table 8.7: *Single-crystal X-ray crystallographic data of* ***5*****–****9***.

Compound reference	**5**	**6**·toluene	**7**·2THF	**8**	**9**·DCM
CCDC number	1431708	1431709	1431710	1431711	
Chemical formula	$C_{32}H_{24}N_6P_2O_6S_2F_6Fe$	$C_{25}H_{26}N_3PCl_2Fe$	$C_{19}H_{18}N_3PO_3SF_3ClFe{\cdot}2C_4H_8O$	$C_{26}H_{30}N_7P_3F_{12}Cu_2$	$C_{19}H_{20}N_3PBF_4Cl_3Ni$
Formula mass	884.48	526.21	619.80	888.56	573.22
Crystal system	monoclinic	triclinic	monoclinic	triclinic	monoclinic
a/Å	17.6327(9)	8.0155(3)	13.7879(4)	8.2686(5)	13.1342(5)
b/Å	20.011(1)	10.7101(4)	8.6473(2)	14.9441(9)	9.0768(4)
c/Å	19.809(1)	15.0458(6)	22.5638(6)	14.9496(8)	20.4667(9)
α/°	90	98.595(2)	90	78.976(2)	90
β/°	91.836(2)	99.108(2)	95.033(1)	80.942(2)	106.295(4)
γ/°	90	91.742(2)	90	84.159(2)	90
Unit cell volume/Å^3	6986.1(6)	1259.09(8)	2679.9(1)	1785.7(2)	2342.0(2)
Temperature/K	180	180	180	180	130
Space group	$P2_1/n$	$P\bar{1}$	$P2/c$	$P\bar{1}$	$P2_1/n$
Z	8	2	4	2	4
Radiation type	CuKα	CuKα	CuKα	CuKα	MoKα
Absorption coefficient, μ/mm^{-1}	6.234	7.489	7.225	3.598	1.284
No. of reflections measured	103989	14375	32629	45856	17899
No. of independent reflections	12364	4367	4745	6267	5533
R_{int}	0.054	0.042	0.036	0.031	0.0672
Final R1 values (I > 2σ(I))	0.039	0.045	0.036	0.049	0.0546
Final wR(F^2) values (I > 2σ(I))	0.094	0.092	0.088	0.126	0.0886
Final R1 values (all data)	0.052	0.059	0.042	0.054	0.1114
Final wR(F^2) values (all data)	0.102	0.098	0.094	0.130	0.1043
Goodness of fit on F^2	1.02	1.06	1.07	1.03	1.015

Table 8.8: *Single-crystal X-ray crystallographic data of* ***10****–****15*** *and* ***20****.*

Compound reference	[**10**$(LiCl)_3$·2THF]$_2$	[**11**·LiCl]$_2$	[**14**·LiCl]$_2$	[**15**·LiCl]$_2$	**20**
CCDC number	1505957		1505955	1505960	1505962
Chemical formula	$C_{40}H_{60}N_6P_2O_4Cl_6Li_6$	$C_{14}H_{18}N_3PClLi$	$C_{22}H_{22}N_4P_2O_2Cl_2Li_2$	$C_{28}H_{34}N_4P_2O_2Cl_2Li_2$	$C_{30}H_{54}N_8P_4F_{12}Cu_2$
Formula mass	1005.22	301.67	521.15	605.31	1005.77
Crystal system	triclinic	triclinic	monoclinic	monoclinic	monoclinic
a/Å	10.9913(3)	8.1048(5)	9.6580(3)	19.142(1)	11.0995(5)
b/Å	11.7487(3)	9.9978(5)	13.2919(4)	8.0771(6)	9.0222(5)
c/Å	12.2632(4)	10.5302(6)	10.1121(3)	22.268(2)	21.487(1)
α/°	105.486(1)	77.619(2)	90	90	90
β/°	99.106(1)	86.643(2)	98.764 (1)	104.894(4)	94.122(2)
γ/°	115.139(1)	68.411(2)	90	90	90
Unit cell volume/Å^3	1312.84(7)	774.76(8)	1282.97(7)	3327.3(4)	2146.2(2)
Temperature/K	180	180	180	180	180
Space group	$P\bar{1}$	$P\bar{1}$	$P2_1/n$	$I2/a$	$P2_1/c$
Z	1	2	2	4	2
Radiation type	CuKα	CuKα	CuKα	CuKα	CuKα
Absorption coefficient, μ/mm^{-1}	3.894	3.076	3.670	2.896	3.406
No. of reflections measured	36815	16796	17882	33730	36582
No. of independent reflections	4628	2736	2262	2405	3796
R_{int}	0.053	-	0.036	0.101	0.040
Final R1 values (I > 2σ(I))	0.046	0.0390	0.037	0.072	0.043
Final wR(F^2) values (I > 2σ(I))	0.115	0.1162	0.103	0.177	0.111
Final R1 values (all data)	0.063	0.0407	0.042	0.109	0.050
Final wR(F^2) values (all data)	0.125	0.1182	0.106	0.204	0.115
Goodness of fit on F^2	1.05	1.137	1.07	1.06	1.04

Table 8.9: *Single-crystal X-ray crystallographic data of* ***21****–* ***25****.*

Compound reference	**21**·MeOH	**22**	**23**·3THF	**24**·2THF	**25**
CCDC number	1505959	1505956	1505961	1505958	
Chemical formula	$C_{24}H_{30}N_4P_2O_4Cl_2Cu_2$	$C_{34}H_{44}N_6P_4O_2F_{12}Cu_2$	$C_{63}H_{65.64}N_4P_5O_{8.5}F_{12}Cu_2$	$C_{94}H_{96}N_6P_8O_{164}F_{12}Cu$	$C_{27}H_{48}N_6P_2OCl_2Rh_2$
Formula mass	698.44	1047.71	1524.77	2295.68	811.37
Crystal system	triclinic	monoclinic	triclinic	monoclinic	orthorhombic
a/Å	8.9283(5)	10.3510(2)	14.9241(5)	13.4157(4)	12.8542(2)
b/Å	9.4929(6)	10.4256(2)	15.6614(5)	18.3267(6)	17.2047(2)
c/Å	9.5208(6)	20.5378(4)	15.8894(5)	20.2257(6)	31.2368(4)
α/°	108.092(3)	90	96.511(2)	90	90
β/°	109.909(2)	92.868(1)	105.792(2)	91.545(2)	90
γ/°	91.050(3)	90	99.492(2)	90	90
Unit cell volume/Å^3	714.22(8)	2213.57(7)	3475.4(2)	4971.0(3)	6908.1(2)
Temperature/K	180	180	180	180	130
Space group	$P\bar{1}$	$P2_1/c$	$P\bar{1}$	$P2_1/n$	$Pbca$
Z	1	2	2	2	8
Radiation type	CuKα	CuKα	CuKα	CuKα	MoKα
Absorption coefficient, μ/mm^{-1}	4.938	3.358	2.607	2.950	1.233
No. of reflections measured	18128	24637	90535	52568	50217
No. of independent reflections	2529	3921	12274	8723	11328
R_{int}	0.046	0.036	0.045	0.067	0.0308
Final R1 values (I > 2σ(I))	0.032	0.029	0.049	0.074	0.0301
Final wR(F^2) values (I > 2σ(I))	0.085	0.071	0.128	0.159	0.0551
Final R1 values (all data)	0.037	0.036	0.067	0.105	0.0413
Final wR(F^2) values (all data)	0.089	0.076	0.141	0.179	0.0587
Goodness of fit on F^2	1.09	1.02	1.02	1.06	1.078

Table 8.10: *Single-crystal X-ray crystallographic data of* ***26, 28–31****.*

	26·MeOH	**28**·DCM	**29**	**30**	**31**·2 *n*-hexane
Chemical formula	$C_{29}H_{46}B_2F_8N_4NiO_9P_4$	$C_{20}H_{14}N_3PO_4Cl_2W$	$C_{34}H_{24}N_6P_2O_4W$	$C_{23}H_{18}N_3PO_5Mo$	$C_{34}H_{18}N_6P_2O_4Br_6Mo$
Formula mass	950.91	646.06	826.38	543.31	1211.88
Crystal system	triclinic	triclinic	orthorhombic	monoclinic	triclinic
a/Å	8.9718(3)	10.5568(3)	17.0942(2)	10.4126(3)	10.7277(6)
b/Å	14.0281(4)	14.7613(5)	10.2626(1)	22.0156(5)	11.7959(5)
c/Å	17.3940(6)	15.4570(4)	17.9547(2)	10.8107(3)	19.1179(7)
α/°	81.344(3)	105.255(3)	90	90	79.702(3)
β/°	82.327(3)	108.189(3)	90	109.128(3)	84.994(4)
γ/°	74.196(3)	92.397(3)	90	90	65.607(5)
Unit cell volume/Å^3	2072.5(1)	2187.4(1)	3149.81(6)	2341.4(1)	2167.5(2)
Temperature/K	130	130	130	130	130
Space group	$P\bar{1}$	$P\bar{1}$	$Pna2_1$	$P2_1/n$	$P\bar{1}$
Z	2	4	4	4	2
Radiation type	MoKα	MoKα	MoKα	MoKα	MoKα
Absorption coefficient, μ/mm^{-1}	0.711	5.631	3.819	0.667	5.949
No. of reflections measured	41003	35979	75112	20609	27582
No. of independent reflections	16682	14346	13030	7736	14088
R_{int}	0.0282	0.0338	0.0260	0.0270	0.0375
Final R1 values (I > 2σ(I))	0.0505	0.0281	0.0177	0.0332	0.0449
Final wR(F^2) values (I > 2σ(I))	0.1248	0.0504	0.0360	0.0649	0.0961
Final R1 values (all data)	0.0725	0.0455	0.0203	0.0463	0.0788
Final wR(F^2) values (all data)	0.1384	0.0551	0.0369	0.0698	0.1064
Goodness of fit on F^2	1.019	1.033	1.103	1.028	1.032
Flack x [(I+)-(I-)]/[(I+)+(I-)]			-0.0194(15)		

Table 8.11: *Single-crystal X-ray crystallographic data of* ***32****–****34****,* ***37*** *and diethylammonium diphenylsulfonimide.*

Compound reference	**32**	**33**	**34**	**37**	Diethylammonium diphenylsulfon-imide
Chemical formula	$C_{28}H_{48}N_6P_2O_8S_2F_6Fe$	$C_{34}H_{64}N_6P_4O_4F_{12}Cu$	$C_{26}H_{48}N_6P_3Se_2F_6Cu$	$C_{72}H_{74}Cl_6Fe_3N_{12}O_5P_4$	$C_{32}H_{44}N_4O_8S_4$
Formula mass	892.63	1036.33	837.07	1691.56	740.95
Crystal system	monoclinic	monoclinic	triclinic	triclinic	orthorhombic
a/Å	9.3923(2)	9.1652(2)	9.1602(3)	13.5190(4)	9.7114(2)
b/Å	53.537(1)	13.0060(3)	14.7850(4)	14.0732(5)	11.6171(2)
c/Å	12.2009(3)	19.7334(5)	14.9391(4)	14.2776(4)	32.6347(5)
α/°	90	90	66.927(1)	105.085(3)	90
β/°	104.157(1)	97.308(1)	85.910(1)	99.074(3)	90
γ/°	90	90	79.606(1)	111.332(3)	90
Unit cell volume/Å^3	5948.7(2)	2333.16(9)	1830.86(9)	2344.9(1)	3681.8(1)
Temperature/K	180	182	180	130	180
Space group	$P2_1/n$	$P2_1/c$	$P\bar{1}$	$P\bar{1}$	*Pbca*
Z	6	2	2	1	4
Radiation type	CuKα	CuKα	CuKα	MoKα	CuKα
Absorption coefficient, μ/mm^{-1}	5.518	2.770	4.862	0.744	2.815
No. of reflections measured	90857	22522	51993	23526	24275
No. of independent reflections	10509	4115	6453	10845	3240
R_{int}	0.0452	0.0605	0.0438	0.0393	0.0366
Final R1 values (I > 2σ(I))	0.0429	0.0556	0.0352	0.1297	0.0312
Final wR(F^2) values (I > 2σ(I))	0.0995	0.1303	0.0897	0.3681	0.0777
Final R1 values (all data)	0.0466	0.0689	0.0380	0.1785	0.0371
Final wR(F^2) values (all data)	0.1011	0.1364	0.0921	0.4046	0.0816
Goodness of fit on F^2	1.129	1.121	1.101	1.382	1.049

9 References

[1] C. Moberg, *Angew. Chem. Int. Ed.* **1998**, *37*, 248–268.

[2] J. L. Fillol, A. Kruckenberg, P. Scherl, H. Wadepohl, L. H. Gade, *Chem. Eur. J.* **2011**, *17*, 14047–14062.

[3] A. Petuker, K. Merz, C. Merten, U. P. Apfel, *Inorg. Chem.* **2016**, *55*, 1183–1191.

[4] S. Trofimenko, *J. Am. Chem. Soc.* **1967**, *89*, 3170–3177.

[5] S. Trofimenko, in *Prog. Inorg. Chem.* (Ed.: S. J. Lippard), John Wiley & Sons, **1986**.

[6] J. C. Calabrese, S. Trofimenko, J. S. Thompson, *J. Chem. Soc., Chem Commun.* **1986**, *530*, 1122–1123.

[7] S. Trofimenko, *Chem. Rev.* **1993**, *93*, 943–980.

[8] N. Kitajimaj, W. B. Tolman, in *Prog. Inorg. Chem.* (Ed.: K. D. Karlin), John Wiley & Sons, **1995**.

[9] L. F. Szczepura, L. M. Witham, K. J. Takeuchi, *Coord. Chem. Rev.* **1998**, *174*, 5–32.

[10] A. G. Blackman, *Polyhedron* **2005**, *24*, 1–39.

[11] J. E. Richman, T. J. Atkins, *J. Am. Chem. Soc.* **1974**, *96*, 2268–2270.

[12] C. Bianchini, A. Meli, M. Peruzzini, F. Vizza, P. Frediani, J. A. Ramirez, *Organometallics* **1990**, *9*, 226–240.

[13] W. H. Hohman, D. J. Kountz, D. W. Meek, *Inorg. Chem.* **1986**, *25*, 616–623.

[14] M. J. Burk, J. E. Feaster, R. L. Harlow, *Organometallics* **1990**, *9*, 2653–2655.

[15] M. J. Burk, *J. Am. Chem. Soc.* **1991**, *113*, 8518–8519.

[16] M. J. Burk, R. L. Harlow, *Angew. Chem. Int. Ed.* **1990**, *29*, 1462–1464.

[17] M. J. Burk, *Acc. Chem. Res.* **2000**, *33*, 363–372.

[18] D. L. Jameson, J. K. Blaho, K. T. Kruger, K. A. Goldsby, *Inorg. Chem.* **1989**, *28*, 4312–4314.

[19] J. P. Wibaut, G. L. C. La Bastide, *Recl. Trav. Chim. Pay-B* **1933**, *52*, 493–498.

[20] A. Tlili, F. Monnier, M. Taillefer, *Chem. Commun.* **2012**, *48*, 6408–6410.

[21] W. C. Davies, F. G. Mann, *J. Chem. Soc.* **1944**, 276–283.

[22] E. Plazek, R. Tyka, *Chem. Abstr.* **1958**, *52*, 20156c.

[23] E. Plazek, R. Tyka, *Zesz. Nauk. Politech, Wroclaw. Chem.* **1957**, *4*, 79–88.

[24] R. T. Jonas, T. D. P. Stack, *Inorg. Chem.* **1998**, *37*, 6615–6629.

[25] R. K. Boggess, D. A. Zatko, *J. Coord. Chem.* **1975**, *4*, 217–224.

[26] G. Kurtev, K. Ribola, D. Jones, R. A. Cole-Hamilton, D. J. Wilkinson, *J. Chem. Soc., Dalton Trans.* **1980**, 55–58.

[27] B. A. Trofimov, A. V. Artem'ev, S. F. Malysheva, N. K. Gusarova, N. A. Belogorlova, A. O. Korocheva, Y. V. Gatilov, V. I. Mamatyuk, *Tetrahedron Lett.* **2012**, *53*, 2424–2427.

[28] B. A. Trofimov, N. K. Gusarova, A. V. Artem'ev, S. F. Malysheva, N. A. Belogorlova, A. O. Korocheva, O. N. Kazheva, G. G. Alexandrov, O. A. Dyachenko, *Mendeleev Commun.* **2012**, *22*, 187–188.

[29] T. Gneuß, M. J. Leitl, L. H. Finger, N. Rau, H. Yersin, J. Sundermeyer, *Dalton Trans.* **2014**, *44*, 8506–8520.

[30] A. J. Plajer, A. L. Colebatch, F. J. Rizzuto, P. Pröhm, A. D. Bond, R. García-Rodríguez, D. S. Wright, *Angew. Chem. Int. Ed.* **2018**, *57*, 1–6.

[31] F. G. Mann, J. Watson, *J. Org. Chem.* **1948**, 502–531.

[32] C. K. Ingold, F. R. Shaw, *J. Chem. Soc.* **1927**, 2918–2926.

[33] W. C. Davies, W. P. G. Lewis, *J. Chem. Soc.* **1934**, 1599–1604.

[34] J. P. Wibaut, A. P. de Jonge, H. G. P. van der Voort, P. P. H. L. Otto, *Recl. Trav. Chim. Pay.-B.* **1951**, *70*, 1054–1066.

[35] D. L. White, J. W. Faller, *Inorg. Chem* **1982**, *21*, 1–19.

[36] H. Adolfsson, K. Warnmark, C. Moberg, *J. Chem. Soc., Chem. Commun.* **1992**, 1054–1055.

[37] R. García-Rodríguez, S. Kopf, D. S. Wright, *Dalton Trans.* **2018**, *47*, 2232–2239.

[38] R. García-Rodríguez, D. S. Wright, *Chem. Eur. J.* **2015**, *21*, 14949–14957.

[39] R. García-Rodríguez, T. H. Bullock, M. McPartlin, D. S. Wright, *Dalton Trans.* **2014**, *43*, 14045–14053.

[40] C. S. Alvarez, F. García, S. M. Humphrey, A. D. Hopkins, R. A. Kowenicki, M. McPartlin, R. A. Layfield, R. Raja, M. C. Rogers, A. D. Woods, D. S. Wright, *Chem. Commun.* **2005**, 198–200.

[41] R. García-Rodríguez, S. Hanf, A. D. Bond, D. S. Wright, *Chem. Commun.* **2017**, *53*, 1225–1228.

[42] R. García-Rodríguez, H. R. Simmonds, D. S. Wright, *Organometallics* **2014**, *33*, 7113−7117.

[43] Á. García-Romero, A. J. Plajer, L. Álvarez-Miguel, A. D. Bond, D. S. Wright, R. García-Rodríguez, *Chem. Eur. J.* **2018**, *24*, 1–9.

[44] M. A. Beswick, C. J. Belle, M. K. Davies, M. A. Halcrow, P. R. Raithby, A. Steiner, D. S. Wright, *Chem. Commun.* **1996**, *19*, 2619–2620.

[45] D. Morales, J. Pérez, L. Riera, V. Riera, D. Miguel, *Organometallics* **2001**, *20*, 4517–4523.

[46] F. García, A. D. Hopkins, S. M. Humphrey, M. McPartlin, M. C. Rogers, D. S. Wright, *Dalton Trans.* **2004**, *0*, 361–362.

[47] M. A. Beswick, M. K. Davies, P. R. Raithby, A. Steiner, D. S. Wright, *Organometallics* **1997**, *1*, 1109–1110.

[48] F. Reichart, M. Kischel, K. Zeckert, *Chem. Eur. J.* **2009**, *15*, 10018–10020.

[49] K. Zeckert, S. Zahn, B. Kirchner, *Chem. Commun.* **2010**, *46*, 2638–2640.

[50] K. Zeckert, *Organometallics* **2013**, *32*, 1387–1393.

[51] K. Zeckert, J. Griebel, R. Kirmse, M. Weiß, R. Denecke, *Chem. Eur. J.* **2013**, *19*, 7718–7722.

[52] I. Schrader, K. Zeckert, S. Zahn, *Angew. Chem. Int. Ed.* **2014**, *53*, 13698–13700.

[53] F. García, A. D. Hopkins, R. A. Kowenicki, M. McPartlin, M. C. Rogers, D. S. Wright, *Organometallics* **2004**, *23*, 3884–3890.

[54] R. García-Rodríguez, D. S. Wright, *Dalton Trans.* **2014**, *43*, 14529–14532.

[55] J. E. Parks, B. E. Wagner, R. H. Holm, *J. Organomet. Chem.* **1973**, *56*, 53–66.

[56] A. J. Plajer, A. L. Colebatch, M. Enders, Á. García-Romero, A. D. Bond, R. García-Rodríguez, D. S. Wright, *Dalton Trans.* **2018**, *47*, 7036–7043.

[57] K. Zeckert, *Inorganics* **2016**, *4*, 19.

[58] K. Zeckert, *Dalton Trans.* **2012**, *41*, 14101–14106.

[59] F. R. Keene, M. R. Snow, E. R. T. Tiekink, *Acta Crystallogr. C* **1988**, *44*, 757–758.

[60] A. Steiner, D. Stalke, *Organometallics* **1995**, *14*, 2422–2429.

[61] C.-Y. Y. Kuo, Y.-S. S. Fuh, J.-Y. Y. Shiue, S. J. Yu, G.-H. Lee, S.-M. Peng, *J. Organomet. Chem.* **1999**, *588*, 260–267.

[62] A. N. Kharat, B. T. Jahromi, A. Bakhoda, *Transition Met. Chem.* **2011**, *37*, 63–69.

[63] W. Huber, R. Linder, J. Niesel, U. Schatzschneider, B. Spingler, P. C. Kunz, *Eur. J. Inorg. Chem.* **2012**, 3140–3146.

[64] A. V. Artem'ev, A. V. Kashevskii, A. S. Bogomyakov, A. Y. Safronov, A. O. Sutyrina, A. A. Telezhkin, I. V. Sterkhova, *Dalton Trans.* **2017**, *46*, 5965–5975.

[65] K. R. Adam, P. A. Anderson, T. Astley, I. M. Atkinson, J. M. Charnock, C. D. Garner, J. M. Gulbis, T. W. Hambley, M. A. Hitchman, F. R. Keene, E. R. T. Tiekink, *J. Chem. Soc., Dalton Trans.* **1997**, 519–530.

[66] M. D. Le Page, B. O. Patrick, S. J. Rettig, B. R. James, *Inorg. Chim. Acta* **2015**, *431*, 276–288.

[67] A. Bakhoda, N. Safari, V. Amani, H. R. Khavasi, M. Gheidi, *Polyhedron* **2011**, *30*, 2950–2956.

[68] J. G. Woollard-Shore, J. P. Holland, M. W. Jones, J. R. Dilworth, *Dalton Trans.* **2010**, *39*, 1576–1585.

[69] T. Astley, H. Headlam, M. A. Hitchman, F. R. Keene, J. Pilbrow, H. Stratemeier, E. R. T. Tiekink, Y. C. Zhong, *J. Chem. Soc., Dalton Trans.* **1995**, 3809–3818.

[70] R. Gregorzik, J. Wirbser, H. Vahrenkamp, *Chem. Ber.* **1992**, *125*, 1575–1581.

[71] F.-W. Lee, M. Chi-Wang Chan, K.-K. Cheung, C.-M. Che, *J. Organomet. Chem.* **1998**, *563*, 191–200.

[72] G. Zhang, J. Zhao, G. Raudaschl-Sieber, E. Herdtweck, F. E. Kühn, *Polyhedron* **2002**, *21*, 1737–1746.

[73] S. A. Saucedo Anaya, A. Hagenbach, U. Abram, *Polyhedron* **2008**, *27*, 3587–3592.

[74] F. R. Keene, M. R. Snow, P. J. Stephenson, E. R. T. Tiekink, *Inorg. Chem.* **1988**, *27*, 2040–2045.

[75] R. P. Schutte, S. J. Rettig, B. R. James, *Can. J. Chem.* **1996**, *2072*, 2064–2072.

[76] R. P. Schutte, S. J. Rettig, A. M. Joshi, B. R. James, *Inorg. Chem.* **1997**, *36*, 5809–5817.

[77] K. Wajda, F. Pruchnik, T. Lis, *Inorg. Chim. Acta* **1980**, *40*, 207–211.

[78] C. J. L. Lock, M. A. Turner, *Acta Crystallogr. C* **1987**, *43*, 2096–2099.

[79] A. V. Artem'ev, N. K. Gusarova, S. F. Malysheva, O. N. Kazheva, G. G. Alexandrov, O. A. Dyachenko, B. A. Trofimov, *Mendeleev Commun.* **2012**, *22*, 260–262.

[80] M. D. Le Page, B. O. Patrick, S. J. Rettig, B. R. James, *Inorg. Chim. Acta* **2015**, *425*, 198–210.

[81] S. Hanf, R. García-Rodríguez, A. D. Bond, E. Hey-Hawkins, D. S. Wright, *Dalton Trans.* **2016**, *45*, 276–283.

[82] Y. U. N. Xie, Y. Yang, J. Rettig, R. James, *Can. J. Chem.* **1992**, *70*, 751–762.

[83] A. Steiner, D. Stalke, *Angew. Chem. Int. Ed.* **1995**, *34*, 1752–1755.

[84] A. Steiner, D. Stalke, *Organometallics* **1995**, *14*, 2422–2429.

[85] A. Steiner, D. Stalke, *J. Chem. Soc., Chem Commun.* **1993**, *6*, 444–446.

[86] P. Espinet, K. Soulantica, *Coord. Chem. Rev.* **1999**, *193–195*, 499–556.

[87] S. Hanf, R. García-Rodríguez, S. Feldmann, A. D. Bond, E. Hey-Hawkins, D. S. Wright, *Dalton Trans.* **2017**, *46*, 814–824.

[88] Z. Zhang, H. Cheng, *Coord. Chem. Rev.* **1996**, *147*, 1–39.

[89] G. R. Newkome, *Chem. Rev.* **1993**, *93*, 2067–2089.

[90] A. Suzuki, *Angew. Chem. Int. Ed.* **2011**, *50*, 6723–6733.

[91] R. Noyori, *Angew. Chem. Int. Ed.* **2002**, *41*, 2008–2022.

[92] E. I. Negishi, *Angew. Chem. Int. Ed.* **2011**, *50*, 6738–6764.

[93] I. Ojima, *Catalytic Asymmetric Synthesis*, John Wiley & Sons, **2008**.

[94] D. Steinborn, *Fundamentals of Organometallic Catalysis*, Wiley-VCH, **2011**.

[95] C. A. Tolman, *Chem. Soc. Rev.* **1972**, *1*, 337–353.

[96] B. M. Trost, *Proc. Natl. Acad. Sci. USA* **2004**, *101*, 5348–5355.

[97] M. Breuer, K. Ditrich, T. Habicher, B. Hauer, M. Keßeler, R. Stürmer, T. Zelinski, *Angew. Chem. Int. Ed.* **2004**, *43*, 788–824.

[98] R. Noyori, *Chem. Soc. Rev.* **1989**, *18*, 187–208.

[99] J. R. Khusnutdinova, D. Milstein, *Angew. Chem. Int. Ed.* **2015**, *54*, 12236–12273.

[100] J. C. Jeffrey, T. B. Rauchfuss, *Inorg. Chem* **1979**, *18*, 2658–2666.

[101] W. S. Knowles, *Angew. Chem. Int. Ed.* **2002**, *41*, 1998–2007.

[102] R. H. Grubbs, *Adv. Synth. Catal.* **2007**, *349*, 34–40.

[103] P. W. N. M. van Leeuwen, P. C. J. Kamer, Eds., *Phosphorus (III) Ligands in Homogeneous Catalysis Design and Synthesis*, John Wiley & Sons, **2012**.

[104] A. G. Orpen, N. G. Connelly, *Organometallics* **1990**, *9*, 1206–1210.

[105] W. Strohmeier, F.-J. Müller, *Chem. Ber.* **1967**, *100*, 2812–2821.

[106] C. A. Tolman, *Chem. Rev.* **1977**, *77*, 313–348.

[107] T. L. Brown, K. J. Lee, *Coord. Chem. Rev.* **1993**, *128*, 89–116.

[108] D. Woska, A. Prock, W. P. Giering, *Organometallics* **2000**, *19*, 4629–4638.

[109] T. P. Yoon, E. N. Jacobsen, *Science* **2003**, *299*, 1691–1693.

[110] B. D. Vineyard, W. S. Knowles, G. L. Bachman, D. J. Weinkauff, *J. Am. Chem. Soc.* **1977**, *99*, 5946–5952.

[111] E. J. Bergner, K. Ebel, T. Johann, O. Löber, *Method for the Production of Menthol*, **2010**, EP2398755A1.

[112] T. Johann, O. Löber, E. J. Bergner, K. Ebel, K. Harth, C. Walsdorff, *Method for Producing Optically Active Carbonyl Compounds*, **2008**, US7468463.

[113] J. K. Whitesell, *Chem. Rev.* **1989**, *89*, 1581–1590.

[114] M. Farina, C. Morandi, *Tetrahedron* **1974**, *30*, 1819–1831.

[115] A. S. C. Chan, J. J. Pluth, J. Halpern, *J. Am. Chem. Soc.* **1980**, *102*, 5952–5954.

[116] J. M. Brown, P. A. Chaloner, *J. Am. Chem. Soc.* **1980**, *102*, 3040–3048.

[117] S. E. Gibson, M. P. Castaldi, *Chem. Commun.* **2006**, 3045–3062.

[118] K. Inoguchi, S. Sakuraba, K. Achiwa, *Synlett* **1992**, 169–178.

[119] A. Buhling, P. C. J. Kamer, P. W. N. M. Van Leeuwen, J. W. Elgersma, *J .Mol. Catal. A* **1997**, *116*, 297–308.

[120] P. Von Matt, A. Pfaltz, *Angew. Chem. Int. Ed.* **1993**, *32*, 566–568.

[121] J. Sprinz, G. Helmchen, *Tetrahedron Lett.* **1993**, *34*, 1769–1772.

[122] G. Helmchen, A. Pfaltz, *Acc. Chem. Res.* **2000**, *33*, 336–345.

[123] F. E. Hahn, M. C. Jahnke, *Angew. Chem. Int. Ed.* **2008**, *47*, 3122–3172.

[124] H. Yang, M. Alvarez, N. Lugan, R. Mathieu, *J. Chem. Soc., Chem Commun.* **1995**, 1721–1722.

[125] J. M. Brown, D. I. Hulmes, T. P. Layzell, *J. Chem. Soc., Chem. Commun.* **1993**, *0*, 1673–1674.

[126] M.-P. A. Lyle, A. A. Narine, P. D. Wilson, *J. Org. Chem.* **2004**, *69*, 5060–5064.

[127] D. H. Woodmansee, M. Neuburger, A. Pfaltz, *Chem. Sci.* **2010**, *1*, 72–78.

[128] G. Chelucci, G. Orru, G. A. Pinna, *Tetrahedron* **2003**, *59*, 9471–9515.

[129] G. H. Lee, A. S. C. Chan, C.-C. Chen, R. Cao, M.-R. Lee, S.-M. Peng, *Organometallics* **1997**, *16*, 3469–3473.

[130] B. Fell, G. Papadogianakis, *J. Mol. Catal.* **1991**, *66*, 143–154.

[131] I. R. Baird, M. B. Smith, B. R. James, *Inorg. Chim. Acta* **1995**, *235*, 291–297.

[132] C. Abu-Gnim, I. Amer, *J. Chem. Soc., Chem Commun.* **1994**, 115–117.

[133] E. Drent, P. Arnoldy, P. H. M. Budzelaar, *J. Organomet. Chem.* **1993**, *455*, 247–253.

[134] D. Camp, I. D. Jenkins, *Austr. J. Chem.* **1988**, *41*, 1835–1839.

[135] F. Xiao-Yuan, S. Shu-Jun, *Int. J. Quantum Chem.* **1981**, *20*, 197–200.

[136] A. D. Becke, *Phys. Rev. A* **1988**, *38*, 3098–3100.

[137] J. P. Perdew, *Phys. Rev. B* **1986**, *33*, 8822–8824.

[138] J. P. Perdew, *Phys. Rev. B* **1986**, *34*, 7406.

[139] F. Weigend, R. Ahlrichs, *Phys. Chem. Chem. Phys.* **2005**, *7*, 3297–3305.

[140] F. Weigend, *Phys. Chem. Chem. Phys.* **2006**, *8*, 1057–1065.

[141] C. M. Breneman, K. B. Wiberg, *J. Comput. Chem.* **1990**, *11*, 361–373.

[142] W.-J. Peng, D. A. Aguilar, *MRI Contrast Agents and Ligands*, **1998**, WO98/22148.

[143] R. Gregorzik, J. Wirbser, H. Vahrenkamp, *Chem. Ber.* **1992**, *125*, 1575–1581.

[144] R. S. Brown, J. Huguet, *Can. J. Chem.* **1980**, *58*, 889–901.

[145] J. E. Huheey, E. A. Keiter, R. L. Keiter, *Inorganic Chemistry: Principles of Structure and Reactivity*, Prentice Hall, **1997**.

[146] A. Bakhoda, H. R. Khavasi, N. Safari, *Cryst. Growth Des.* **2011**, *11*, 933–935.

[147] P. A. Anderson, T. Astley, M. A. Hitchman, F. R. Keene, B. Moubaraki, K. S. Murray, B. W. Skelton, E. R. T. Tiekink, H. Toftlund, A. H. White, *J. Chem. Soc., Dalton Trans.* **2000**, 3505–3512.

[148] F. Baier, Z. Fei, H. Gornitzka, A. Murso, S. Neufeld, M. Pfeiffer, I. Rüdenauer, A. Steiner, T. Stey, D. Stalke, *J. Organomet. Chem.* **2002**, *661*, 111–127.

[149] I. Objartel, N. A. Pott, M. John, D. Stalke, *Organometallics* **2010**, *29*, 5670–5675.

[150] I. Objartel, D. Leusser, F. Engelhardt, R. Herbst-Irmer, D. Stalke, *Z. Anorg. Allg. Chem.* **2013**, *639*, 2005–2012.

[151] M. M. Olmstead, A. Maisonnat, J. P. Farr, A. L. Balch, *Inorg. Chem* **1981**, *20*, 4060–4064.

[152] T. Zhang, C. Ji, K. Wang, D. Fortin, P. D. Harvey, *Inorg. Chem.* **2010**, *49*, 11069–11076.

[153] J. A. Casares, P. Espinet, J. M. Martín-Álvarez, V. Santos, *Inorg. Chem* **2006**, *45*, 6628–6636.

[154] A. N. Kharat, B. Tamaddoni Jahromi, A. Bakhoda, A. Abbasi, *J. Coord. Chem.* **2010**, *63*, 3783–3791.

[155] A. Nemati Kharat, A. Bakhoda, S. Foroutannejad, C. Foroutannejad, *Z. Anorg. Allg. Chem.* **2011**, *637*, 2260–2264.

[156] M. J. Calhorda, C. Ceamanos, O. Crespo, M. C. Gimeno, A. Laguna, C. Larraz, P. D. Vaz, M. D. Villacampa, *Inorg. Chem.* **2010**, *49*, 8255–8269.

[157] X. K. Wan, Z. W. Lin, Q. M. Wang, *J. Am. Chem. Soc.* **2012**, *134*, 14750–14752.

[158] K. Nishide, S. Ito, M. Yoshifuji, *J. Organomet. Chem.* **2003**, *682*, 79–84.

[159] M. N. Birkholz, N. V. Dubrovina, H. Jiao, D. Michalik, J. Holz, R. Paciello, B. Breit, A. Börner, *Chem. Eur. J.* **2007**, *13*, 5896–5907.

[160] S. Kuang, Z. Zhang, K. Chinnakali, H. Fun, T. C. W. Mak, *Inorg. Chim. Acta* **1999**, *293*, 106–109.

[161] M. Driess, F. Franke, K. Merz, *Eur. J. Inorg. Chem.* **2001**, 2661–2668.

[162] S. Wingerter, M. Pfeiffer, A. Murso, C. Lustig, T. Stey, V. Chandrasekhar, D. Stalke, *J. Am. Chem. Soc.* **2001**, *123*, 1381–1388.

[163] A. Murso, M. Straka, M. Kaupp, R. Bertermann, D. Stalke, *Organometallics* **2005**, *24*, 3576–3578.

[164] I. Objartel, H. Ott, D. Stalke, *Z. Anorg. Allg. Chem.* **2008**, *634*, 2373–2379.

[165] A. Murso, D. Stalke, *Dalton Trans.* **2004**, 2563–2569.

[166] N. Kocher, D. Leusser, A. Murso, D. Stalke, *Chem. Eur. J.* **2004**, *10*, 3622–3631.

[167] A. Murso, D. Stalke, *Eur. J. Inorg. Chem.* **2004**, 4272–4277.

[168] N. M. Imukhametov, M. N. Garifzyanova, G. G. Azancheev, V. A. Al'fonsov, *Russ. J. Gen. Chem.* **1999**, *69*, 1965–1966.

[169] S. D. Stamatov, S. A. Ivanov, *Phosphorus, Sulfur Silicon Relat. Elem.* **1989**, *45*, 73–79.

[170] K. Skopek, J. A. Gladysz, *J. Organomet. Chem.* **2008**, *693*, 857–866.

[171] E. E. Nifantiev, A. I. Zavalishina, E. I. Smirnova, *Phosphorus, Sulfur Silicon Relat. Elem.* **1981**, *10*, 261–266.

[172] C. Kölmel, C. Oehsenfeld, R. Ahlrichs, *Theor. Chim. Acta* **1991**, *82*, 271–284.

[173] D. Hobuß, A. Baro, K. V. Axenov, S. Laschat, W. Frey, *Eur. J. Inorg. Chem.* **2011**, 384–392.

[174] L. E. Bowen, M. Charernsuk, T. W. Hey, C. L. McMullin, A. G. Orpen, D. F. Wass, *Dalton Trans.* **2010**, *39*, 560–567.

[175] X. Chen, H. Zhu, T. Wang, C. Li, L. Yan, M. Jiang, J. Liu, *J. Mol. Catal. A* **2016**, *414*, 37–46.

[176] E. J. Amigues, C. Hardacre, G. Keane, M. E. Migaud, *Green Chem.* **2008**, *10*, 660–669.

[177] A. E. Reed, F. Weinhold, *J. Chem. Phys.* **1985**, *83*, 735–746.

[178] P. Wucher, J. B. Schwaderer, S. Mecking, *ACS Catal.* **2014**, *4*, 2672–2679.

[179] M. Oliana, F. King, P. N. Horton, M. B. Hursthouse, K. K. Hii, *J. Org. Chem.* **2006**, *71*, 2472–2479.

[180] J. Wieland, B. Breit, *Nat. Chem.* **2010**, *2*, 832–837.

[181] B. Breit, W. Seiche, *J. Am. Chem. Soc.* **2006**, *78*, 249–256.

[182] C. C. Levin, *J. Am. Chem. Soc.* **1975**, *97*, 5649–5655.

[183] R. G. Pearson, *J. Mol. Struct.-Theochem.* **1983**, *103*, 25–34.

[184] A. Rauk, L. C. Allen, K. Mislow, *Angew. Chem. Int. Ed.* **1970**, *9*, 400–414.

[185] L. Goerigk, S. Grimme, *J. Chem. Theory Comput.* **2011**, *7*, 291–30.

[186] J. S. Harvey, V. Gouverneur, *Chem. Commun.* **2010**, *46*, 7477–7485.

[187] A. Grabulosa, J. Granell, G. Muller, *Coord. Chem. Rev.* **2007**, *251*, 25–90.

[188] K. M. Pietrusiewicz, M. Zablocka, *Chem. Rev.* **1994**, *94*, 1375–1411.

[189] E. I. Musina, A. V Shamsieva, I. D. Strelnik, T. P. Gerasimova, D. B. Krivolapov, I. E. Kolesnikov, E. V Grachova, S. P. Tunik, C. Bannwarth, S. Grimme, S. A. Katsyuba, A. A. Karasik, O. G. Sinyashin, *Dalton Trans.* **2016**, *45*, 2250–2260.

[190] D. M. Zink, M. Bächle, T. Baumann, M. Nieger, M. Kühn, C. Wang., W. Klopper, U. Monkowius, T. Hofbeck, H. Yersin, S. Bräse, *Inorg. Chem.* **2013**, *52*, 2292−2305.

[191] D. Volz, D. M. Zink, T. Bocksrocker, J. Friedrichs, M. Nieger, T. Baumann, U. Lemmer, S. Bräse, *Chem. Mater.* **2013**, *25*, 3414–3426.

[192] V. J. Catalano, J. M. López-de-Luzuriaga, M. Monge, M. E. Olmos, D. Pascual, *Dalton Trans.* **2014**, *43*, 16486–16497.

[193] J.-J. Cid, J. Mohanraj, M. Mohankumar, M. Holler, G. Accorsi, L. Brelot, I. Nierengarten, O. Moudam, A. Kaeser, B. Delavaux-Nicot, N. Armaroli, J.-F. Nierengarten, *Chem. Commun.* **2013**, *49*, 859–861.

[194] J. R. White, A. E. Cameron, *Phys. Rev.* **1948**, *74*, 991–1000.

[195] D. Redmore, *J. Org. Chem.* **1970**, *35*, 4114–4117.

[196] G. U. Spiegel, O. Stelzer, *Chem. Ber.* **1990**, *123*, 989–993.

[197] S. I. Noro, Y. Hijikata, M. Inukai, T. Fukushima, S. Horike, M. Higuchi, S. Kitagawa, T. Akutagawa, T. Nakamura, *Inorg. Chem.* **2013**, *52*, 280–285.

[198] S. M. Kuang, Z.-Z. Zhang, Q.-G. Wang, T. C. W. Mak, *J. Organomet. Chem.* **1998**, *558*, 131–138.

[199] J. P. Farr, M. M. Olmstead, A. L. Balch, *J. Am. Chem. Soc.* **1980**, *102*, 6654–6656.

[200] F. E. Wood, M. M. Olmstead, A. L. Balch, *J. Am. Chem. Soc.* **1983**, *105*, 6332–6334.

[201] J. P. Farr, M. M. Olmstead, A. L. Balch, *Inorg. Chem.* **1983**, *22*, 1229–1235.

[202] C. P. Kubiak, R. Eisenberg, *J. Am. Chem. Soc.* **1977**, *99*, 6129–6131.

[203] T. Murahashi, H. Kurosawa, *Coord. Chem. Rev.* **2002**, *231*, 207–228.

[204] SpinWorks, Version 4.2, K. Marat, University of Manitoba, Winnipeg, Manitoba, Canada, **2015**.

[205] S. Bauer, I. Maulana, P. Coburger, S. Tschirschwitz, P. Lönnecke, E. Hey-Hawkins, *Chem. Select.* **2017**, *2*, 7407–7416.

[206] G. Aullón, G. Ujaque, A. Lledós, S. Alvarez, P. Alemany, *Inorg. Chem.* **1998**, *37*, 804–813.

[207] G. Knizia, *J. Chem. Theory Comput.* **2013**, *9*, 4834–4843.

[208] G. Knizia, J. E. M. N. Klein, *Angew. Chem. Int. Ed.* **2015**, *54*, 5518–5522.

[209] A. E. Reed, R. B. Weinstock, F. Weinhold, *J. Chem. Phys.* **1985**, *83*, 735–746.

[210] J. Foster, F. Weinhold, *J. Am. Chem. Soc.* **1980**, *102*, 7211–7218.

[211] W. C. Lu, C. Z. Wang, M. W. Schmidt, L. Bytautas, K. M. Ho, K. Ruedenberg, *J. Chem. Phys.* **2004**, *120*, 2629–2637.

[212] M. Aresta, C. F. Nobile, A. Sacco, *Inorg. Chim. Acta* **1975**, *12*, 167–178.

[213] O. Kühl, P. C. Junk, E. Hey-Hawkins, *Z. Anorg. Allg. Chem.* **2000**, *626*, 17–20.

[214] P. Le Floch, L. Ricard, F. Mathey, A. Jutand, C. Amatore, *Inorg. Chem.* **1995**, *34*, 11–12.

[215] T. Tanase, H. Takahata, Y. Yamamoto, *Inorg. Chim. Acta* **1997**, *264*, 5–9.

[216] J. Mautz, K. Heinze, H. Wadepohl, G. Huttner, *Eur. J. Inorg. Chem.* **2008**, *2*, 1413–1422.

[217] R. S. Vinal, L. T. Reynolds, *Inorg. Chem* **1964**, *3*, 1062–1063.

[218] M. Meier, F. Basolo, in *Inorg. Syn.* (Ed.: R.J. Angelici), John Wiley & Sons, **1990**.

[219] T. M. Balthazor, R. C. Grabiak, *J. Org. Chem.* **1980**, *45*, 5425–5426.

[220] M. R. Mason, J. G. Verkade, *Organometallics* **1992**, *11*, 2212–2220.

[221] C. Amatore, A. Jutand, A. Thuilliez, *Organometallics* **2001**, *20*, 3241–3249.

[222] L. Malatesia, M. Angoletta, *J. Chem. Soc.* **1957**, 1186–1188.

[223] S. J. Berners-Price, R. K. Johnson, C. K. Mirabelli, L. F. Faucette, F. L. McCabe, P. J. Sadler, *Inorg.*

Chem. **1987**, *26*, 3383–3387.

[224] W. D. McGhee, T. Foo, F. J. Hollander, R. G. Bergman, *J. Am. Chem. Soc.* **1988**, *110*, 8543–8545.

[225] M. R. Mason, J. G. Verkade, *Organometallics* **1990**, *9*, 864–865.

[226] M. Ioele, G. Ortaggi, M. Scarsella, G. Sleiter, *Polyhedron* **1991**, *10*, 2475–2476.

[227] N. Y. Kozitsyna, A. M. Ellern, M. Y. Antipin, Y. T. Struchkov, ll'a I. Moiseev, *Mendeleev Commun.* **1991**, *1*, 92–94.

[228] I. Pryjomska, H. Bartosz-Bechowski, Z. Ciunik, A. M. Trzeciak, J. J. Ziółkowski, *Dalton Trans.* **2006**, *0*, 213–220.

[229] P. A. McLaughlin, J. G. Verkade, *Organometallics* **1998**, *17*, 5937–5940.

[230] V. V. Grushin, *Chem. Rev.* **2004**, *104*, 1629–1662.

[231] R. F. Jordan, W. E. Dasher, S. F. Echols, *J. Am. Chem. Soc.* **1986**, *108*, 1718–1719.

[232] J. Reedijk, *Comment. Inorg. Chem.* **1982**, *1*, 379–389.

[233] T. R. Musgrave, T. S. Lin, *J. Coord. Chem.* **1973**, *2*, 323–324.

[234] C. G. van Kralingen, J. Reedijk, *J. Chem. Soc., Chem. Commun.* **1976**, 533.

[235] J. Verbiest, J. A. C. Van Ooijen, J. Reedijk, *J. Inorg. Nuc. Chem.* **1980**, *42*, 971–975.

[236] R. W. M. Ten Hoedt, J. Reedijk, *Inorg. Chim. Acta* **1981**, *51*, 23–27.

[237] J. C. Jansen, H. Van Konigsveld, J. Reedijk, *Nature* **1977**, *269*, 318–319.

[238] S. Smit, W. L. Groeneveld, *Inorg. Nucl. Chem. Lett.* **1975**, *11*, 277–282.

[239] J. Y. Yang, R. M. Bullock, W. J. Shaw, B. Twamley, K. Fraze, M. R. DuBois, D. L. DuBois, *J. Am. Chem. Soc.* **2009**, *131*, 5935–5945.

[240] J. Y. Yang, S. E. Smith, T. Liu, W. G. Dougherty, W. A. Hoffert, W. S. Kassel, M. R. DuBois, D. L. DuBois, R. M. Bullock, *J. Am. Chem. Soc.* **2013**, *135*, 9700–9712.

[241] A. Cryst, B. Y. C. Glidewell, H. D. Holden, *Acta Cryst. B.* **1982**, 667–669.

[242] M. Carnes, D. Buccella, J. Y.-C. Chen, A. P. Ramirez, N. J. Turro, C. Nuckolls, M. Steigerwald, *Angew. Chem. Int. Ed.* **2009**, *48*, 290–294.

[243] A. Novak, in *Hydrogen Bonding in Solids Correlation of Spectroscopic and Crystallographic Data*, **1974**, pp. 177–216.

[244] J. Tao, J. P. Perdew, V. N. Staroverov, G. E. Scuseria, *Phys. Rev. Lett.* **2003**, *91*, 146401-1-146401–4.

[245] D. M. Roundhill, R. F. Sperline, W. B. Beaulied, *Coord. Chem. Rev.* **1978**, *26*, 263–279.

[246] M. R. J. Vallée, P. Majkut, I. Wilkening, C. Weise, G. Müller, C. P. R. Hackenberger, *Org. Lett.* **2011**, *13*, 5440–5443.

[247] J. Hynek, P. Brázda, J. Rohlíček, M. G. S. Londesborough, J. Demel, *Angew. Chem. Int. Ed.* **2018**, *57*, 5016–5019.

[248] J. M. Bayne, M. H. Holthausen, D. W. Stephan, *Dalton Trans.* **2016**, *45*, 5949–5957.

[249] M. Westerhausen, T. Bollwein, P. Mayer, H. Piotrowski, A. Pfitzner, *Z. Anorg. Allg. Chem.* **2002**, *628*, 1425–1432.

[250] B. Lippert, in *Prog. Inorg. Chem.* (Ed.: K.D. Karlin), John Wiley & Sons, **2005**.

[251] T. A. Ateşin, T. Li, S. Lachaize, W. W. Brennessel, J. J. García, W. D. Jones, *J. Am. Chem. Soc.* **2007**, *129*, 7562–7569.

[252] J. J. Garcia, N. M. Brunkan, W. D. Jones, *J. Am. Chem. Soc.* **2002**, *124*, 9547–9555.

[253] M. E. Evans, T. Li, W. D. Jones, *J. Am. Chem. Soc.* **2010**, *132*, 16278–16284.

[254] E. S. Wiedner, J. Y. Yang, S. Chen, S. Raugei, W. G. Dougherty, W. S. Kassel, M. L. Helm, R. M. Bullock, M. R. DuBois, D. L. DuBois, *Organometallics* **2012**, *31*, 144–156.

[255] J. Y. Yang, R. Morris Bullock, W. G. Dougherty, W. S. Kassel, B. Twamley, D. L. DuBois, M. R. DuBois, *Dalton Trans.* **2010**, *39*, 3001–3010.

[256] B. R. Galan, J. Schöffel, J. C. Linehan, C. Seu, A. M. Appel, J. A. S. Roberts, M. L. Helm, U. J. Kilgore, J. Y. Yang, D. L. DuBois, C. P. Kubiak, *J. Am. Chem. Soc.* **2011**, *133*, 12767–12779.

[257] R. Tatematsu, T. Inomata, T. Ozawa, H. Masuda, *Angew. Chem. Int. Ed.* **2016**, *55*, 5247–5250.

[258] S. Lense, M.-H. Ho, S. Chen, A. Jain, S. Raugei, J. C. Linehan, J. A. S. Roberts, A. M. Appel, W. Shaw, *Organometallics* **2012**, *31*, 6719–6731.

[259] D. G. Gusev, *Organometallics* **2009**, *28*, 763–770.

[260] D. R. Anton, R. H. Crabtree, *Organometallics* **1983**, *2*, 621–627.

[261] O. Kühl, *Coord. Chem. Rev.* **2005**, *249*, 693–704.

[262] G. Ciancaleoni, N. Scafuri, G. Bistoni, A. Macchioni, F. Tarantelli, D. Zuccaccia, L. Belpassi, *Inorg. Chem* **2014**, *53*, 9907–9916.

[263] D. W. Allen, B. F. Taylor, *J. Chem. Soc., Dalton Trans.* **1982**, 51–54.

[264] U. Beckmann, D. Süslüyan, P. C. Kunz, *Phosphorus, Sulfur Silicon Relat. Elem.* **2011**, *186*, 2061–2070.

[265] U. Koelle, *J. Organomet. Chem.* **1977**, *133*, 53–58.

[266] J. A. Casares, P. Espinet, R. Hernando, G. Iturbe, F. Villafañe, D. D. Ellis, A. G. Orpen, *Inorg. Chem.* **1997**, *36*, 44–49.

[267] P. Espinet, P. Gómez-Elipe, F. Villafañe, *J. Organomet. Chem.* **1993**, *450*, 145–150.

[268] A. L. Morris, J. T. York, *J. Chem. Educ.* **2009**, *86*, 1408–1411.

[269] F. R. Hartley, *Chem. Soc. Rev.* **1973**, 163–179.

[270] A. Kovacs, G. Frenking, *Organometallics* **2001**, *20*, 2510–2524.

[271] J. D. Atwood, T. L. Brown, *J. Am. Chem. Soc.* **1976**, *98*, 3160–3166.

[272] L. Hirsivaara, M. Haukka, J. Pursiainen, *Eur. J. Inorg. Chem.* **2001**, 2255–2262.

[273] L. Hirsivaara, M. Haukka, J. Pursiainen, *Inorg. Chem. Commun.* **2000**, *3*, 508–510.

[274] F. A. Cotton, D. J. Darensbourg, W. H. Ilsley, *Inorg. Chem* **1981**, *20*, 578–583.

[275] F. A. Cotton, D. J. Darensbourg, S. Klein, B. W. S. Kolthammer, *Inorg. Chem* **1982**, *21*, 294–299.

[276] T. F. Kemp, A. Wong, M. E. Smith, P. T. Bishop, N. Carthey, *Solid State Nucl. Magn. Reson.* **2008**, *34*, 224–227.

[277] S. Starosta, B. Bażanów, W. Barszczewski, *Dalton Trans.* **2010**, *39*, 7547–7555.

[278] V. N. Staroverov, G. E. Scuseria, J. Tao, J. P. Perdew, *J. Chem. Phys.* **2003**, *119*, 12129–12137.

[279] V. N. Staroverov, G. E. Scuseria, J. Tao, J. P. Perdew, *J. Chem. Phys.* **2004**, *121*, 11507.

[280] L. Perrin, E. Clot, O. Eisenstein, J. Loch, R. H. Crabtree, *Inorg. Chem.* **2001**, *40*, 5806–5811.

[281] M. Ohff, J. Holz, M. Quirmbach, A. Börner, *Synthesis* **1998**, 1391–1415.

[282] Q. Chen, J. Zeng, X. Yan, Y. Huang, Z. Du, K. Zhang, C. Wen, *Tetrahedron Lett.* **2016**, *57*, 3379–3381.

[283] T. M. Shaikh, C. Weng, F. Hong, *Coord. Chem. Rev.* **2012**, *256*, 771–803.

[284] A. G. Walden, A. J. M. Miller, *Chem. Sci.* **2015**, *6*, 2405–2410.

[285] K. M. Szkop, D. W. Stephan, *Dalton Trans.* **2017**, *46*, 3921–3928.

[286] C. B. Caputo, L. J. Hounjet, R. Dobrovetsky, D. W. Stephan, *Science* **2013**, *341*, 1374–1377.

[287] L. J. Hounjet, C. B. Caputo, D. W. Stephan, *Angew. Chem. Int. Ed.* **2012**, *51*, 4714–4717.

[288] K. F. Firth, J. Möbus, D. W. Stephan, *Chem. Commun.* **2016**, *52*, 13967–13970.

[289] M. Pérez, Z. W. Qu, C. B. Caputo, V. Podgorny, L. J. Hounjet, A. Hansen, R. Dobrovetsky, S. Grimme, D. W. Stephan, *Chem. Eur. J.* **2015**, *21*, 6491–6500.

[290] L. J. Hounjet, C. B. Caputo, R. Dobrovetsky, D. W. Stephan, *J. Am. Chem. Soc.* **2013**, *135*, 10–12.

[291] M. Mehta, M. H. Holthausen, I. Mallov, M. Pérez, Z. W. Qu, S. Grimme, D. W. Stephan, *Angew. Chem. Int. Ed.* **2015**, *54*, 8250–8254.

[292] M. L. H. Green, *J. Organomet. Chem.* **1995**, *500*, 127–148.

[293] A. Amgoune, D. Bourissou, *Chem. Commun.* **2011**, *47*, 859–871.

[294] H. Braunschweig, R. D. Dewhurst, *Dalton Trans.* **2011**, *40*, 549–558.

[295] E. J. Derrah, S. Ladeira, G. Bouhadir, K. Miqueu, D. Bourissou, *Chem. Commun.* **2011**, *47*, 8611–8613.

[296] C. Tan, P. Wang, H. Liu, X.-L. Zhao, Y. Lu, Y. Liu, *Chem. Commun.* **2015**, *51*, 10871–10874.

[297] R. J. Bowen, M. A. Fernandes, P. W. Gitari, M. Layh, *Acta Crystallogr. C* **2004**, *60*, o258-60.

[298] F. R. Keene, P. J. Stephenson, *Inorg. Chim. Acta* **1991**, *187*, 217–220.

[299] A. N. Kharat, A. Bakhoda, T. Hajiashrafi, A. Abbasi, *Phosphorus, Sulfur Silicon Relat. Elem.* **2010**, *185*, 2341–2347.

[300] N. Burford, B. W. Royan, R. E. H. Spence, T. S. Cameron, A. Linden, R. D. Rogers, *J. Chem. Soc., Dalton Trans.* **1990**, *1*, 1–8.

[301] L. J. Hounjet, C. B. Caputo, D. W. Stephan, *Dalton Trans.* **2013**, *42*, 2629–35.

[302] C. B. Caputo, D. Winkelhaus, R. Dobrovetsky, L. J. Hounjet, D. W. Stephan, *Dalton Trans.* **2015**, *44*, 12256–12264.

[303] S. Postle, V. Podgorny, D. W. Stephan, *Dalton Trans.* **2016**, *45*, 14651–14657.

[304] R. J. Bowen, M. A. Fernandes, P. W. Gitari, M. Layh, *Phosphorus, Sulfur Silicon Relat. Elem.* **2006**, *181*, 1403–1418.

[305] T. Liang, C. N. Neumann, T. Ritter, *Angew. Chem. Int. Ed.* **2013**, *52*, 8214–8264.

[306] P. A. Champagne, J. Desroches, J. D. Hamel, M. Vandamme, J. F. Paquin, *Chem. Rev.* **2015**, *115*, 9073–9174.

[307] I. Persson, P. Persson, M. Sandström, A.-S. Ullström, *J. Chem. Soc., Dalton Trans.* **2002**, 1256–1265.

[308] J. Loup, D. Zell, J. C. A. Oliveira, H. Keil, D. Stalke, L. Ackermann, *Angew. Chem. Int. Ed.* **2017**, *56*, 14197–14201.

[309] S. Enthaler, K. Junge, M. Beller, *Angew. Chem. Int. Ed.* **2008**, *47*, 3317–3321.

[310] M. D. Greenhalgh, A. S. Jones, S. P. Thomas, *ChemCatChem.* **2015**, *7*, 190–222.

[311] B. Plietker, Ed., *Iron Catalysis: Fundamentals and Applications*, Springer, **2011**.

[312] P. J. Chirik, *Acc. Chem. Res.* **2015**, *48*, 1687–1695.

[313] M. D. Greenhalgh, D. J. Frank, S. P. Thomas, *Adv. Synth. Catal.* **2014**, *356*, 584–590.

[314] T. Zell, R. Langer, *Recycl. Catal.* **2015**, *2*, 87–109.

[315] S. C. Bart, E. Lobkovsky, P. J. Chirik, *J. Am. Chem. Soc.* **2004**, *126*, 13794–13807.

[316] J. M. Darmon, G. W. Margulieux, Z. R. Turner, R. P. Yu, J. M. Hoyt, P. J. Chirik, *ACS Catal.* **2012**, *2*,

1760–1764.

[317] E. Lobkovsky, P. J. Chirik, A. M. Archer, M. W. Bouwkamp, M.-P. Cortez, *Organometallics* **2006**, *25*, 4269–4278.

[318] S. C. Bart, E. J. Hawrelak, E. Lobkovsky, P. J. Chirik, *Organometallics* **2005**, *24*, 5518–5527.

[319] B. M. Wile, R. J. Trovitch, S. C. Bart, A. M. Tondreau, E. Lobkovsky, C. Milsmann, E. Bill, K. Wieghardt, P. J. Chirik, *Inorg. Chem* **2009**, *48*, 4190–4200.

[320] R. Xu, W. D. Jones, H. Yuan, T. R. Cundari, S. M. Bellows, S. Chakraborty, *ACS Catal.* **2016**, *6*, 2127–2135.

[321] P. Büschelberger, D. Gärtner, E. Reyes-Rodriguez, F. Kreyenschmidt, K. Koszinowski, A. Jacobi von Wangelin, R. Wolf, *Chem. Eur. J.* **2017**, *23*, 3139–3151.

[322] B. R. Rad, R. Wolf, A. Welther, A. Jacobi von Wangelin, D. Gärtner, *Angew. Chem. Int. Ed.* **2014**, *53*, 3722–3726.

[323] D. Troegel, J. Stohrer, *Coord. Chem. Rev.* **2011**, *255*, 1440–1459.

[324] A. N. Nesmeyanov, R. K. Freidlina, E. C. Chukovskaya, R. G. Petrova, A. B. Belyavsky, *Tetrahedron* **1962**, *17*, 61–68.

[325] J. L. Speier, J. A. Webster, G. H. Barnes, *J. Am. Chem. Soc.* **1957**, *79*, 974–979.

[326] B. D. Karstedt, *Platinum Complexes of Unsaturated Siloxanes and Platinum Containing Organopolysiloxanes*, **1973**, US3775452.

[327] A. M. Tondreau, C. C. H. Atienza, J. M. Darmon, C. Milsmann, H. M. Hoyt, K. J. Weller, S. A. Nye, K. M. Lewis, J. Boyer, J. G. P. Delis, E. Lobkovsky, P. J. Chirik, *Organometallics* **2012**, *31*, 4886–4893.

[328] K. Kamata, A. Suzuki, Y. Nakai, H. Nakazawa, *Organometallics* **2012**, *31*, 3825–3828.

[329] J. Y. Wu, B. N. Stanzl, T. Ritter, *J. Am. Chem. Soc.* **2010**, *132*, 13214–13216.

[330] A. J. Chalk, J. F. Harrod, *J. Am. Chem. Soc.* **1965**, *87*, 16–21.

[331] J. F. Harrod, A. J. Chalk, *J. Am. Chem. Soc.* **1965**, *5*, 1133–1135.

[332] M. A. Schroeder, M. S. Wrighton, *J. Organomet. Chem.* **1977**, *128*, 345–358.

[333] C. L. Randolph, M. S. Wrighton, *J. Am. Chem. Soc.* **1986**, *108*, 3366–3374.

[334] J. A. Widegren, R. G. Finke, *J. Mol. Catal. A* **2003**, *198*, 317–341.

[335] T. N. Gieshoff, M. Villa, A. Welther, M. Plois, U. Chakraborty, R. Wolf, A. Jacobi Von Wangelin, *Green Chem.* **2015**, *17*, 1408–1413.

[336] V. H. Bönnemann, W. Brijoux, T. Joußen, *Angew. Chem. Int. Ed.* **1990**, *29*, 273–275.

[337] P. H. Phua, L. Lefort, J. A. F. Boogers, M. Tristany, J. G. De Vries, *Chem. Commun.* **2009**, 3747–3749.

[338] C. Rangheard, C. de Julià n Fernàndez, P.-H. Phua, J. Hoorn, L. Lefort, J. G. de Vries, *Dalton Trans.* **2010**, *39*, 8464–8471.

[339] V. Kelsen, B. Wendt, S. Werkmeister, K. Junge, M. Beller, B. Chaudret, *Chem. Commun.* **2013**, *49*, 3416–3418.

[340] M. Zaranek, P. Pawluc, *ACS Catal.* **2018**, *8*, 9865–9876.

[341] H. Brunner, *Angew. Chem. Int. Ed.* **2004**, *43*, 2749–2750.

[342] B. A. F. Le Bailly, M. D. Greenhalgh, S. P. Thomas, *Chem. Commun.* **2012**, *48*, 1580–1582.

[343] E. C. Ashby, J. J. Lin, *J. Org. Chem.* **1978**, *43*, 2567–2572.

[344] B. Bogdanović, M. Schwickardi, *Angew. Chem. Int. Ed.* **2000**, *39*, 4610–4612.

[345] X. Du, Y. Zhang, D. Peng, Z. Huang, *Angew. Chem. Int. Ed.* **2016**, *55*, 6671–6675.

[346] T. S. Carter, L. Guiet, D. J. Frank, J. West, S. P. Thomas, *Adv. Synth. Catal.* **2013**, *355*, 880–884.

[347] M. Kobayashi, M. Itoh, *Chem. Lett.* **2006**, *25*, 1013–1014.

[348] M.-Y. Hu, Q. He, S.-J. Fan, Z.-C. Wang, L.-Y. Liu, Y.-J. Mu, Q. Peng, S.-F. Zhu, *Nat. Commun.* **2018**, *9*, 221–232.

[349] B. Cheng, W. Liu, Z. Lu, *J. Am. Chem. Soc.* **2018**, *140*, 5014–5017.

[350] S. Witomska, V. Patroniak, P. Pawluc, *Chem. Commun.* **2017**, *53*, 5404–5407.

[351] E. Larsen, G. N. La Mar, B. E. Wagner, J. E. Parks, R. H. Holm, *Inorg. Chem.* **1972**, *11*, 2652–2668.

[352] L. Dubován, A. Pöllnitz, C. Silvestru, *Eur. J. Inorg. Chem.* **2016**, 1521–1527.

[353] V. Bocokić, A. Kalkan, M. Lutz, A. L. Spek, D. T. Gryko, J. N. H. Reek, *Nat. Commun.* **2013**, *4*, 2670–2679.

[354] A. W. Kleij, M. Lutz, A. L. Spek, P. W. N. M. van Leeuwen, J. N. H. Reek, *Chem. Commun.* **2005**, 3661–3663.

[355] M. Streitberger, A. Schmied, E. Hey-Hawkins, *Inorg. Chem.* **2014**, *53*, 6794–6804.

[356] A. Sen, T. W. Lai, R. R. Thomas, *J. Organomet. Chem.* **1988**, *358*, 567–588.

[357] R. K. Harris, E. D. Becker, S. M. Cabral De Menezes, R. Goodfellow, P. Granger, *Concepts Magn. Res.* **2002**, *14*, 326.

[358] APEX, SAINT, Bruker, Bruker AXS Inc., Madison, Wisconsin, USA, **2012**.

[359] Z. Otwinowski, W. Minor, *Meth. Enzymol.* **1997**, *276*, 307–326.

[360] CrysAlis PRO, Agilent, Agilent Technologies Ltd, Yarnton, Oxfordshire, England, **2014**.

[361] G. M. Sheldrick, *Acta Crystallogr. A* **2008**, *64*, 112–122.

[362] G. M. Sheldrick, *Acta Crystallogr. A* **2015**, *71*, 3–8.

[363] G. M. Sheldrick, *Acta Crystallogr. C* **2015**, *71*, 3–8.

[364] C. B. Hübschle, G. M. Sheldrick, B. Dittrich, *J. Appl. Cryst.* **2011**, *44*, 1281–1284.

[365] S. Parsons, H. D. Flack, T. Wagner, *Acta Crystallogr. B* **2013**, *69*, 249–259.

[366] SADABS, Bruker, Bruker AXS Inc., Madison, Wisconsin, USA, **2001**.

[367] SCALE3 ABSPACK, Oxford Diffraction, Oxford Diffraction Ltd, Abingdon, Oxfordshire, England, **2006**.

[368] Diamond-Crystal and Molecular Structure Visualization, H. Putz, K. Brandenburg, Crystal Impact GbR, Bonn, Nordrhein-Westfalen, Germany, **1999**.

[369] F. Neese, *WIREs Comput. Mol. Sci.* **2018**, *8*, e1327.

[370] F. Neese, *WIREs Comput. Mol. Sci.* **2012**, *2*, 73–78.

[371] S. Grimme, S. Ehrlich, L. Goerigk, *J. Comp. Chem.* **2011**, *32*, 1456–1465.

[372] S. Grimme, J. Antony, S. Ehrlich, H. Krieg, *J. Chem. Phys.* **2010**, *132*, 154104–154104.

[373] F. Neese, F. Wennmohs, A. Hansen, U. Becker, *Chem. Phys.* **2009**, *356*, 98–109.

[374] NBO, Version 3.1, E. D. Glendening, A. E. Reed, J. E. Carpenter, F. Weinhold, University of Wisconsin, Madison, Wisconsin, USA, **1995**.

[375] A. E. Reed, L. A. Curtiss, F. Weinhold, *Chem. Rev.* **1988**, *88*, 899–926.

[376] Gaussian 09, Revision D.01, M. J. Frisch, G. W. Trucks, H. B. Schlegel, G. E. Scuseria, M. A. Robb, G. Cheeseman, J. R. Scalmani, V. Barone, B. Mennucci, G. A. Petersson, H. Nakatsuji, M. Caricato, X. Li, H. P. Hratchian, A. F. Izmaylov, J. Bloino, G. Zheng, J. L. Sonnenberg, M. Hada, M. Ehara, K. Toyota, R. Fukuda, J. Hasegawa, M. Ishida, T. Nakajima, Y. Honda, O. Kitao, H. Nakai, T. Vreven, J. A.

Montgomery, Jr., J. E. Peralta, F. Ogliaro, M. Bearpark, J. J. Heyd, E. Brothers, K. N. Kudin, V. N. Staroverov, R. Kobayashi, J. Normand, K. Raghavachari, A. Rendell, J. C. Burant, S. S. Iyengar, J. Tomasi, M. Cossi, N. Rega, J. M. Millam, M. Klene, J. E. Knox, J. B. Cross, V. Bakken, C. Adamo, J. Jaramillo, R. Gomperts, R. E. Stratmann, O. Yazyev, A. J. Austin, R. Cammi, C. Pomelli, J. W. Ochterski, R. L. Martin, K. Morokuma, V. G. Zakrzewski, G. A. Voth, P. Salvador, J. J. Dannenberg, S. Dapprich, A. D. Daniels, Ö. Farkas, J. B. Foresman, J. V. Ortiz, J. Cioslowski, and D. J. Fox, Gaussian, Inc., Wallingford, Connecticut, USA, **2009**.

[377] L. Goerigk, S. Grimme, *Phys. Chem. Chem. Phys.* **2011**, *13*, 6670–6688.

[378] L. Goerigk, A. Hansen, C. A. Bauer, S. Ehrlich, A. Najibi, S. Grimme, *Phys. Chem. Chem. Phys.* **2017**, *19*, 32184–32215.

[379] D. A. Pantazis, F. Neese, *J. Chem. Theory Comput.* **2009**, *5*, 2229–2238.

[380] D. A. Pantazis, X. Y. Chen, C. R. Landis, F. Neese, *J. Chem. Theory Comput.* **2008**, *4*, 908–919.

[381] D. A. Pantazis, F. Neese, *Theor. Chem. Acc.* **2012**, *131*, 1292–1299.

[382] D. A. Pantazis, F. Neese, *J. Chem. Theory Comput.* **2011**, *7*, 677–684.

[383] D. Andrae, U. Haeussermann, M. Dolg, H. Stoll, H. Preuss, *Theor. Chim. Acta* **1990**, *77*, 123–141.

[384] Y. Uchida, M. R. K. Kimihiko, Y. Kawasaki, S. Oae, *Heteroat. Chem.* **1997**, *8*, 439–449.

[385] A. L. Spek, *Acta Crystallogr. C* **2015**, *71*, 9–18.

[386] A. L. Spek, *Acta Crystallogr. D* **2009**, *65*, 148–155.